



Contracts for field projects
and supporting research on . . .

78

Enhanced Oil Recovery

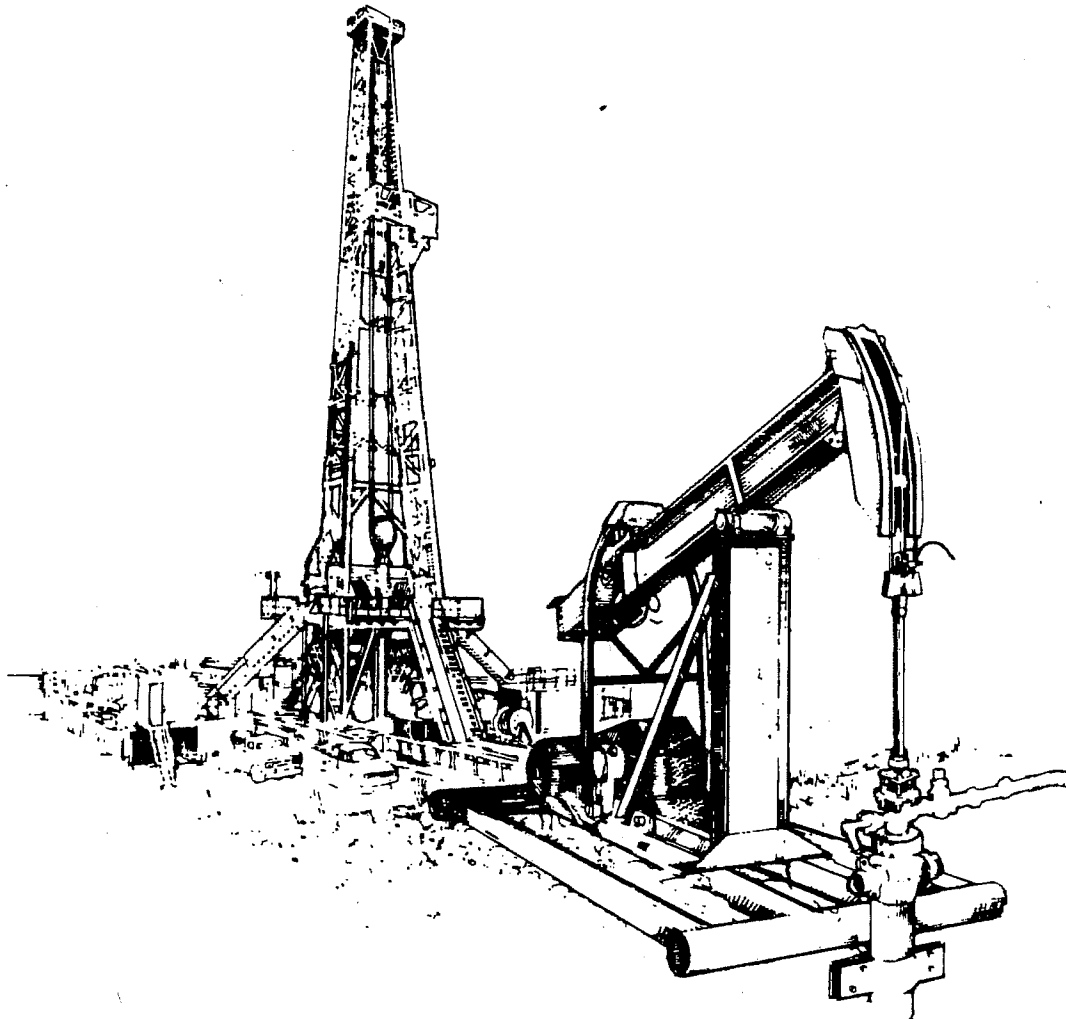
Reporting Period January–March 1994

DOE/BC-94/2

(DE95000126)

PROGRESS REVIEW

Quarter Ending March 31, 1994



United States Department of Energy

Office of Gas and Petroleum Technology
and Bartlesville Project Office

DISCLAIMER

This report was prepared as an account of work sponsored by an agency of the United States Government. Neither the United States Government nor any agency thereof, nor any of their employees, makes any warranty, express or implied, or assumes any legal liability or responsibility for the accuracy, completeness, or usefulness of any information, apparatus, product, or process disclosed, or represents that its use would not infringe privately owned rights. Reference herein to any specific commercial product, process, or service by trade name, trademark, manufacturer, or otherwise does not necessarily constitute or imply its endorsement, recommendation, or favoring by the United States Government or any agency thereof. The views and opinions of authors expressed herein do not necessarily state or reflect those of the United States Government or any agency thereof.

Available to DOE and DOE contractors from the Office of Scientific and Technical Information, P.O. Box 62, Oak Ridge, Tennessee 37831; prices available from (615) 576-8401.

Available to the public from the U.S. Department of Commerce, Technology Administration, National Technical Information Service, Springfield, Virginia 22161; prices available from (703) 487-4650.

U.S. Department of Energy
Washington, D.C. 20545

PATRICIA GODLEY
Assistant Secretary for Fossil Energy
Room 4G-084 Forrestal Building
Telephone Number 202-586-4695

REGINAL SPILLER
*Deputy Assistant Secretary for Gas
and Petroleum Technologies*

SANDRA WAISLEY
*Director for Oil and Gas Exploration
and Production*

Bartlesville Project Office
P.O. Box 1398
Bartlesville, Oklahoma 74005
Telephone No. 918-337-4401

THOMAS C. WESSON
Director

R. M. RAY
Deputy Director

BETTY J. FELBER
*Program Coordinator,
Enhanced Oil Recovery*

HERBERT A. TIEDEMANN
*Project Manager for
Technology Transfer*

DOE/BC--94/2
(DE95000126)
Distribution Category UC-122

PROGRESS REVIEW NO. 78

CONTRACTS FOR FIELD PROJECTS AND SUPPORTING RESEARCH ON ENHANCED OIL RECOVERY

Date Published - May 1995

UNITED STATES DEPARTMENT OF ENERGY

INDEX

COMPANIES AND INSTITUTIONS

	Page		Page
American Oil Recovery, Inc.		Stanford University	
Applications of Advanced Petroleum Production Technology and Water-Alternating-Gas Injection for Enhanced Oil Recovery—Mattoon Oil Field, Illinois	69	Productivity and Injectivity of Horizontal Wells	23
Colorado School of Mines		Scaleup of Miscible Flood Processes	11
Interdisciplinary Study of Reservoir Compartments	41	Surtek, Inc.	
Columbia University		Detailed Evaluation of the West Kiehl Alkaline-Surfactant-Polymer Field Project and Its Application to Mature Minnelusa Waterfloods	28
Dynamic Enhanced Recovery Technologies	74	Texaco Exploration and Production, Inc.	
Hughes Eastern Corporation		Postwaterflood CO ₂ Miscible Flood in Light Oil, Fluvial-Dominated Deltaic Reservoir	86
The Use of Indigenous Microbes to Selectively Plug the More Porous Zones to Increase Oil Recovery During Waterflooding	67	University of Alaska	
Illinois Institute of Technology		Study of Hydrocarbon Miscible Solvent Slug Injection Process for Improved Recovery of Heavy Oil from Schrader Bluff Pool, Milne Point Unit, Alaska	31
Surfactant-Enhanced Alkaline Flooding for Light Oil Recovery	1	University of Kansas	
Lawrence Berkeley Laboratory		Improved Oil Recovery in Fluvial-Dominated Deltaic Reservoirs of Kansas—Near Term Improving Reservoir Conformance Using Gelled Polymer Systems	88 4
Lawrence Berkeley Laboratory/Industry Heterogeneous Reservoir Performance Definition Project	52	University of Southern California	
Lawrence Livermore National Laboratory		Modification of Reservoir Chemical and Physical Factors in Steamfloods To Increase Heavy Oil Recovery	35
Multifrequency Electromagnetic Induction Oil Field Characterization and Process Monitoring Using Electromagnetic Methods	39 37	University of Southern Mississippi	
Lomax Exploration Company		Responsive Copolymers for Enhanced Petroleum Recovery	6
Green River Formation Waterflood Demonstration Project, Uinta Basin, Utah	75	University of Texas	
Louisiana State University		Revitalizing a Mature Oil Play: Strategies for Finding and Producing Unrecovered Oil in Frio Fluvial-Deltaic Reservoirs of South Texas	91
Assist in the Recovery of Bypassed Oil from Reservoirs in the Gulf of Mexico	64	University of Tulsa	
Maurer Engineering, Inc.		Application of Artificial Intelligence to Reservoir Characterization: An Interdisciplinary Approach	42
Horizontal Oil Well Applications and Oil Recovery Assessment	21	Integrated Approach Toward the Application of Horizontal Wells to Improve Waterflooding Performance	96
Michigan Technological University		University of Wyoming	
Visual Display of Reservoir Parameters Affecting Enhanced Oil Reservoirs	78	Anisotropy and Spatial Variation of Relative Permeability and Lithologic Character of Tensleep Sandstone Reservoirs in the Bighorn and Wind River Basins, Wyoming	50
Oklahoma Geological Survey			
Continued Support of the Natural Resources Information System for the State of Oklahoma	61		
Sierra Energy Company			
Enhanced Oil Recovery Utilizing High-Angle Wells in the Frontier Formation, Badger Basin Field, Park County, Wyoming	81		

Utah Geological Survey

Geological and Petrophysical Characterization of the Ferron Sandstone for Three-Dimensional Simulation of a Fluvial-Deltaic Reservoir	101
Increased Oil Production and Reserves from Improved Completion Techniques in the Bluebell Field, Uinta Basin, Utah	103

CONTENTS BY EOR PROCESS

Chemical Flooding—Supporting Research	1
Gas Displacement—Supporting Research	11
Thermal Recovery—Supporting Research	31
Geoscience Technology	41
Resource Assessment Technology	61
Microbial Technology	67
Field Demonstrations	69

**DOE Technical Project Officers for
Enhanced Oil Recovery**

DIRECTORY

Name	Phone number	Name of contractor
U. S. Department of Energy Gas and Petroleum Technology Oil and Gas Exploration and Production 3E-028/FORS Washington, D.C. 20585		
Bartlesville Project Office P. O. Box 1398 Bartlesville, Oklahoma 74005		
Edith Allison	918-337-4390	Columbia University Hughes Eastern Corporation Lomax Exploration Company Sierra Energy Company University of Texas Utah Geological Survey
Jerry Casteel	918-337-4412	Illinois Institute of Technology Stanford University University of Kansas University of Southern Mississippi
Robert Lemmon	918-337-4405	Colorado School of Mines Lawrence Berkeley Laboratory Michigan Technological University University of Tulsa University of Wyoming Utah Geological Survey
Rhonda Lindsey	918-337-4455	University of Kansas University of Tulsa
Chandra Nautiyal	918-337-4409	Texaco Exploration and Production, Inc.
R. Michael Ray	918-337-4403	Oklahoma Geological Survey
Thomas Reid	918-337-4233	Lawrence Livermore National Laboratory Maurer Engineering Inc. Stanford University Surtek, Inc. University of Alaska University of Southern California
Metairie Site Office 900 Commerce Road, East New Orleans, Louisiana 70123		
Gene Pauling	504-734-4131	American Oil Recovery, Inc. Louisiana State University

CHEMICAL FLOODING— SUPPORTING RESEARCH

SURFACTANT-ENHANCED ALKALINE FLOODING FOR LIGHT OIL RECOVERY

Contract No. DE-AC22-92BC14883

**Illinois Institute of Technology
Chicago, Ill.**

**Contract Date: Sept. 21, 1992
Anticipated Completion: Sept. 20, 1995
Government Award: \$150,000
(Current year)**

**Principal Investigator:
Darsh T. Wasan**

**Project Manager:
Jerry Casteel
Bartlesville Project Office**

Reporting Period: Jan. 1–Mar. 31, 1994

Objective

The overall objective of this project is to develop a cost-effective method for formulating a successful surfactant-enhanced alkaline flood by appropriately choosing mixed alkalis that form inexpensive buffers to obtain the desired pH

(between 8.5 and 12.0) for ultimate spontaneous emulsification and ultralow tension. In addition, the novel concept of pH gradient design to optimize floodwater conditions will be tested.

Summary of Technical Progress

From an investigation of the phase behavior and the regions wherein the middle phase occurs, the determination was made that the middle phase goes through a maximum with pH, sodium concentration, and surfactant concentration.¹ The optimum pH is about 12.0 to 13.5, the optimum sodium concentration is about 0.513 mol/L, and the optimum surfactant concentration is about 0.2%. The effect of surfactant type was also investigated, and Petrostep B-105 gave the most middle-phase production.

This quarter the contact angles of Long Beach oil, Adena oil, and a model oil on a solid glass surface in contact with an aqueous alkaline solution both with and without added pre-formed surfactant were studied. The contact angles with Long Beach and Adena oils showed oil-wet conditions, whereas the model oil showed both oil-wet and water-wet conditions, depending on the pH of the aqueous phase. When surfactant was added to the alkaline solution, the system was less oil-wet. Spreading of the oil on the glass surface was observed in all three systems.

Materials and Experiments

Two crude oils containing natural organic acids were contacted with an alkaline pH aqueous solution. One of the

crude oils used, a Long Beach crude oil obtained from THUMS Long Beach Co., has an acid number of 1.0, which was determined from ASTM procedure D-664, and an API gravity of 24.9. It was centrifuged at 40,000 g for 30 min to remove water and clays. The viscosity of the crude oil after centrifuging was 52 cP at 25 °C, and the interfacial tension (IFT) against deionized water was 24.5 mN/m. The other crude oil (Adena), obtained from SURTEK from Adena field located in Morgan County, Colo., is a light oil with an API gravity of 41.95, a viscosity of 3.75 cP at 25 °C, and an acid number less than 0.002. The IFT against deionized water is 39 mN/m. A model oil of oleic acid (99% pure) in decane (99+% pure) was also used.

The alkaline solutions are a mixture of sodium hydroxide (NaOH), sodium bicarbonate (NaHCO₃), and sodium chloride (NaCl). All alkalis were obtained from Fisher Scientific Co.

Two preformed surfactants, Petrostep B-105 (55% active) and Petrostep B-120, were added to the alkaline solution. The surfactants were obtained from Stepan Chemical Co., and the surfactant solutions were made on a 100% basis.

Throughout this study the solutions were made by diluting an equimolar ratio of NaHCO₃/NaOH (referred to as 20/20) with either the same molarity of NaHCO₃ plus NaCl to keep the total sodium constant or the same molarity of NaOH plus enough NaCl to keep the total sodium constant. By changing the ratio of NaHCO₃/NaOH, the pH is changed. Lower pH is obtained by adding the NaHCO₃ plus NaCl solution to the 20/20 mixture, or a higher pH is obtained by adding the NaOH plus NaCl solution to the 20/20 mixture. Note that 343 mol/m³ total sodium is about a 2.0 wt % NaHCO₃/NaOH mixture.

Two sets of experiments were conducted to determine the contact angle of an oil droplet on a glass coverslip. In the first set the oil droplet was placed on the coverslip before the coverslip was immersed in the alkaline solution. In the second set the coverslip was placed in the alkaline solution before the oil droplet contacted the coverslip; this created an initial aqueous film. The contact angle so measured is that angle taken inside the oil droplet. In all cases the systems were pre-equilibrated before measurements were made.

Long Beach Oil: Alkali Only

Figure 1 shows the contact angle as a function of the equilibrium pH of the solution for the Long Beach crude oil with varying sodium concentrations. In Fig. 1 no initial aqueous film was present. The contact angle goes through a minimum with pH. When the contact angle is zero, spreading of the oil droplet on the glass surface occurs.

Figure 2 shows the contact angle as a function of equilibrium pH when an initial aqueous film is present. When spreading occurs, the initial aqueous film drains and ruptures. Because of the presence of the aqueous film, the contact angles in Fig. 2 are greater than those in Fig. 1.

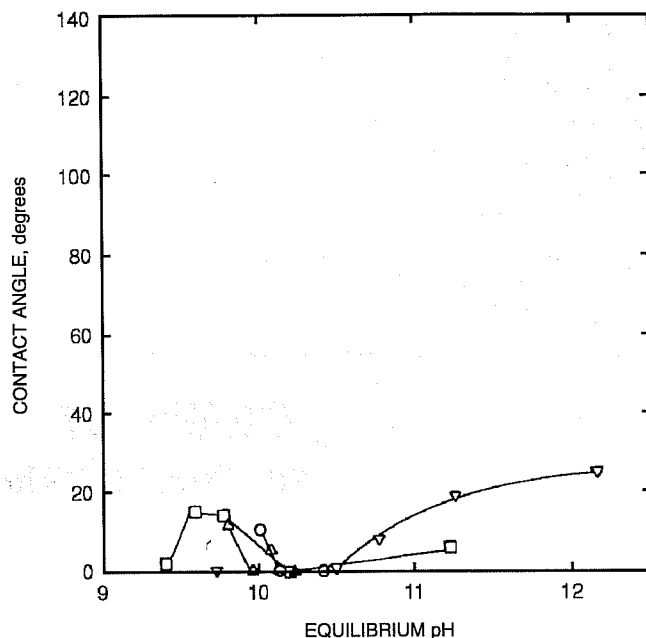


Fig. 1 Contact angle as a function of equilibrium pH for Long Beach crude oil with no initial aqueous film. Sodium concentrations: O, 0.086M, Δ, 0.171M, ∇, 0.343M, □, 1.0M.

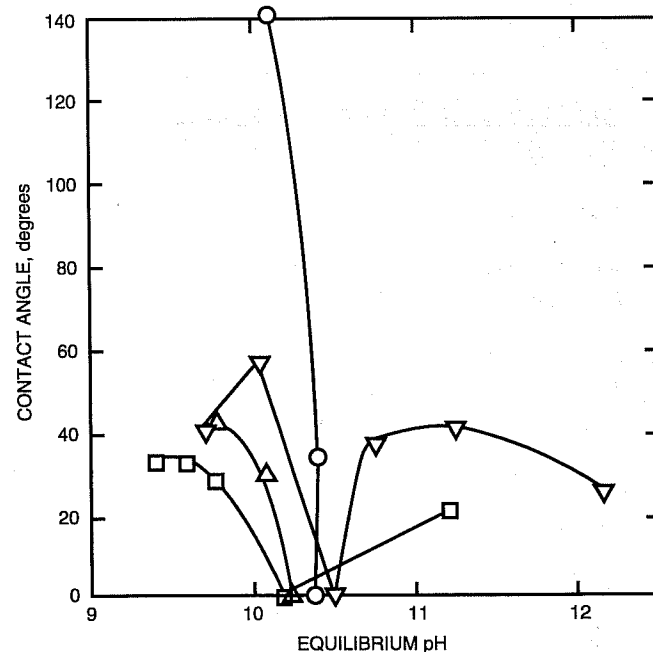


Fig. 2 Contact angle as a function of equilibrium pH for Long Beach crude oil with an initial aqueous film. Sodium concentrations: O, 0.086M, Δ, 0.171M, ∇, 0.343M, □, 1.0M.

Figure 3 shows the equilibrium IFT as a function of the equilibrium pH. The pK_a (disassociation constant of acid) of the system occurs at a pH of 10.6. The spreading observed in Figs. 1 and 2 takes place at and before the pK_a of the system.

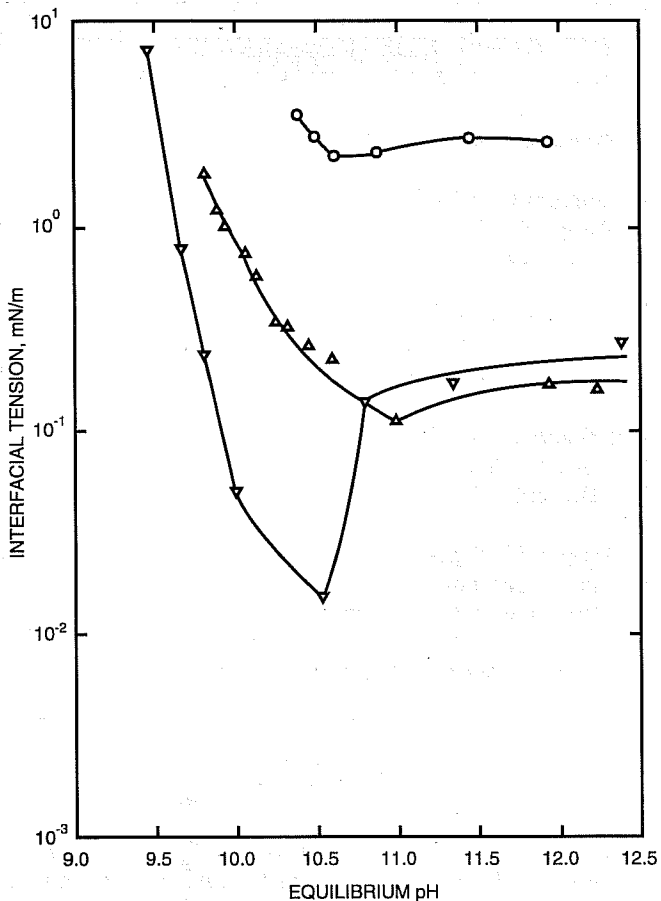


Fig. 3 Equilibrium interfacial tension as a function of equilibrium pH for Long Beach crude oil. Sodium concentrations: O, 0.171M. Δ , 0.343M. ∇ , 1.0M.

Model Oil: Alkali Only

Decane with 0.013M oleic acid was investigated against varying NaOH concentrations from 0.001 to 0.5% NaOH. The contact angle was determined when no initial aqueous film was present. The oil spread, giving zero contact angle, from 0.001 to 0.01% NaOH, and the contact angle was 175° from 0.01 to 0.5% NaOH. The pK_a of the system was approximately 0.01% NaOH (a pH of 10.6). Before the pK_a of the system, the concentration of un-ionized acid in the oil phase was high; after the pK_a of the system, the concentration of ionized acid in the aqueous phase was high. This means that the aqueous film between the oil droplet and the glass coverslip ruptures before the pK_a of the system because there is no surfactant in the aqueous phase to stabilize it; thus the system is oil-wet. After the pK_a of the system, the aqueous phase has ionized acid in it; thus the system is water-wet.

Long Beach Oil: Alkali + Added Surfactant

Figures 4 and 5 are the same as Figs. 1 and 2 except 0.1% surfactant was added in Figs. 4 and 5. When surfactant is added, the system becomes less oil-wet, and thus no spreading

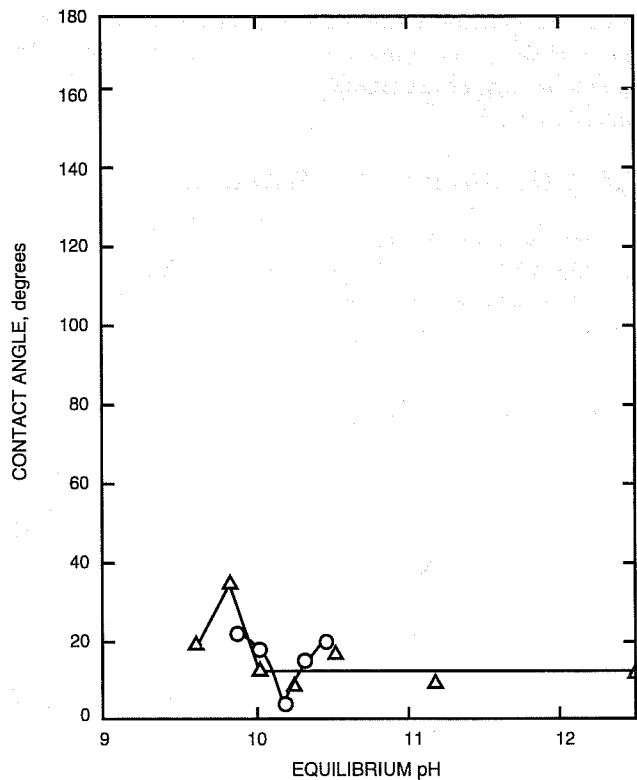


Fig. 4 Contact angle as a function of equilibrium pH for Long Beach crude oil with 0.1% Petrostep B-105 and without an initial aqueous film. Sodium concentrations: O, 0.086M. Δ , 1.0M.

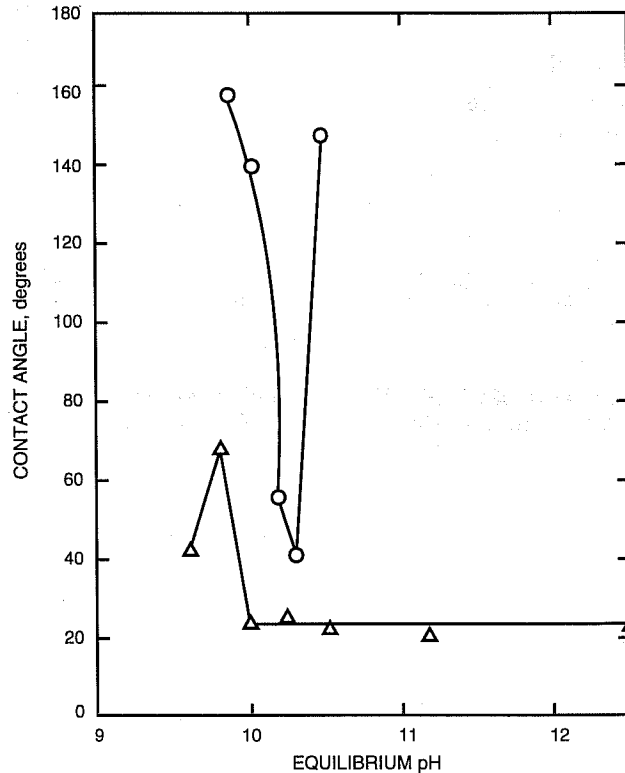


Fig. 5 Contact angle as a function of equilibrium pH for Long Beach crude oil with 0.1% Petrostep B-105 and with an initial aqueous film. Sodium concentrations: O, 0.086M. Δ , 1.0M.

occurs. In both cases, with and without an initial aqueous film, the 0.086M sodium sample went through a minimum. The minimum may be connected with the minimum in IFT observed in Fig. 6.

Adena Oil: Alkali + Added Surfactant

The Adena oil was also investigated against 0.2% Petrostep B-120 at 0.171 and 0.684M sodium with varying pH from 10.5 to 12.5. In all cases the oil spread on the glass coverslip, and thus the system became totally oil-wet.

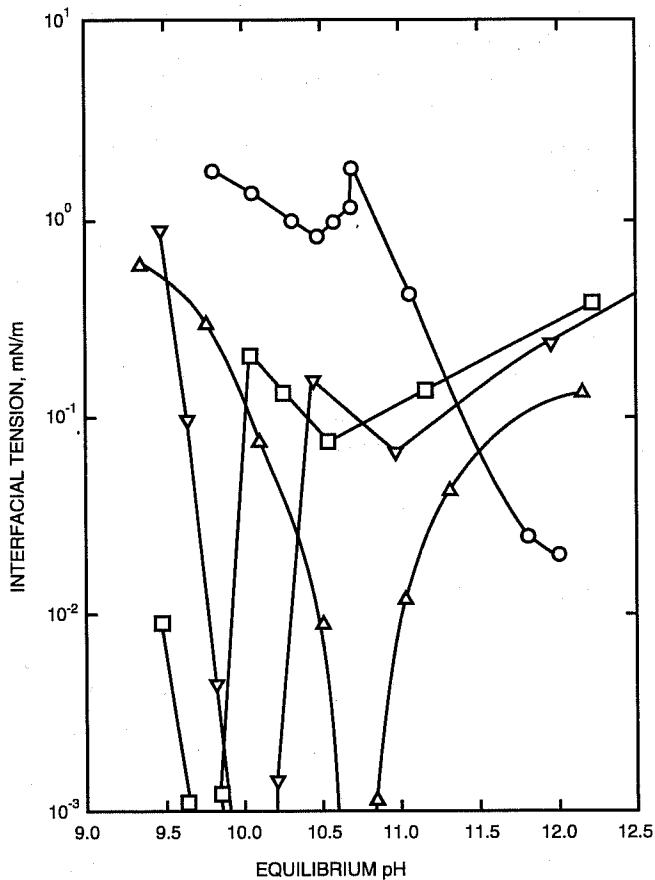


Fig. 6 Effect of pH and sodium on the equilibrium interfacial tension with 0.1% Petrostep B-105 for Long Beach crude oil. Sodium concentrations: O, 0.086M. Δ , 0.343M. ∇ , 0.684M. \square , 1.0M.

Reference

1. D. T. Wasan, Progress Report submitted to DOE for the period October 1–December 31, 1993.

IMPROVING RESERVOIR CONFORMANCE USING GELLED POLYMER SYSTEMS

Contract No. DE-AC22-92BC14881

University of Kansas
Center for Research
Lawrence, Kans.

Contract Date: Sept. 25, 1992
Anticipated Completion: Sept. 24, 1995
Government Award: \$707,123

Principal Investigators:
Don W. Green
G. Paul Willhite

Project Manager:
Jerry Casteel
Bartlesville Project Office

Reporting Period: Jan. 1–Mar. 31, 1994

Objectives

The general objectives of this research are to (1) identify and develop gelled polymer systems that have potential to improve reservoir conformance of fluid displacement processes, (2) determine the performance of these systems in bulk and in porous media, and (3) develop methods to predict the capability of these systems to recover oil from petroleum reservoirs.

This work focuses on three types of gel systems—an aqueous polysaccharide (KUSP1) system that gels as a function of pH, the chromium(III)–polyacrylamide system, and the aluminum citrate–polyacrylamide system. Laboratory research is directed at the fundamental understanding of the physics and chemistry of the gelation process in bulk form and in porous media. This knowledge will be used to develop conceptual and mathematical models of the gelation process. Mathematical models will then be extended to predict the performance of gelled polymer treatments in oil reservoirs.

Summary of Technical Progress

Development and Selection of Gelled Polymer Systems

Development of KUSP1 and Derivatives

The quality of the KUSP1 hydrogel (i.e., its ability to hold water) is diminished in the exopolysaccharide that is synthesized at late stages of the culture. This may be caused by production of extracellular (1 \rightarrow 3)- β -D-endoglucanase enzymes that can randomly hydrolyze the polysaccharide. The purification of an endoglucanase, which makes

oligosaccharides from the intact polymer, was previously reported. Such an enzyme is synthesized and excreted when *Cellulomonas flavigena* is grown in a medium that contains KUSP1. The presence of an enzyme that has exoglucanase activity (i.e., it liberates glucose units from the terminus of the polymer) was detected. The goal in this research is to determine how the activity of these enzymes (exoglucanase and endoglucanase) can be regulated, with the possible consequence of improving the quality of the hydrogels. The genes were cloned for the synthesis of the endoglucanase and exoglucanase into *Escherichia coli*, with the goal of improving understanding of how the activity of the enzymes can be modulated.

The Pierce bicinchoninic acid (BCA) reagent, which originally was developed for protein assays, is being used to determine the number of reducing groups in KUSP1. In this colorimetric procedure, a BCA-Cu⁺ complex is formed as a result of the oxidation of the reducing termini in KUSP1. The procedure is useful because it can be carried out under alkaline conditions in which KUSP1 is soluble. The procedure allows examination of the effects of growth conditions of *C. flavigena* upon the synthesis of KUSP1.

Physical and Chemical Characterization of Gel Systems

Rheological Characterization

The effect of shear deformation on the gelation of a polyacrylamide–chromium(III) system was investigated by subjecting samples to selected steady shear rates ranging from 0.47 to 14.88/s in a cone-and-plate geometry. Two sets of experiments were conducted, with and without superimposed oscillatory shear. Comparisons between these sets of data showed that the superimposed oscillatory shear did not significantly affect the viscosity–time data.

Steady shear viscosities as a function of time are shown in Fig. 1 for samples subjected to different shear rates. Significant increases in viscosity were observed between 1 and 3 h. After 5 h, the viscosity was lower in samples subjected to higher shear rates. Measurements after the viscosity increases (after 3 h) might be erroneous, particularly at the lower shear rates. Gel was observed when the sample was removed, which could compromise the velocity distribution assumptions required to calculate viscosity.

Oscillatory shear was superimposed on the steady shear for the experiments whose data are shown in Fig. 1. The storage moduli as a function of time are shown in Fig. 2. The data show that the applied shear rate affects the gelation process. Again, the data after the initial increases are suspect because of the reasons described previously.

Chemical Reaction Kinetics

The effects of anion type and anion concentration on the gelation of polyacrylamide–Cr(III) gels were studied. The anions studied were nitrate, perchlorate, chloride, sulfate, and acetate. Each anion system was prepared with chromium and

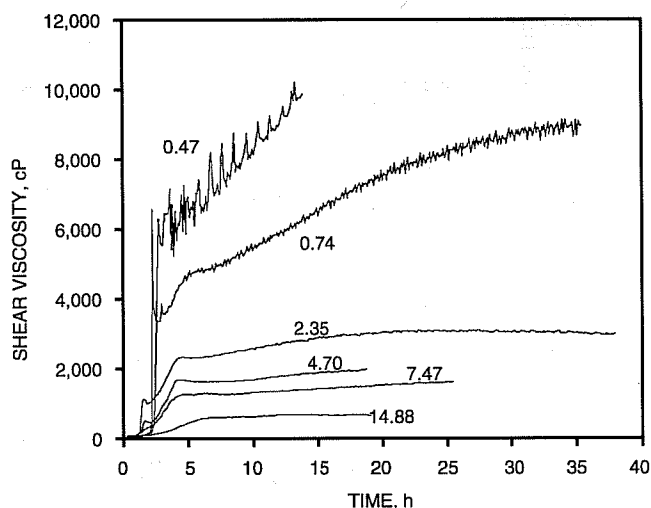


Fig. 1 Effect of shear on development of viscosity for a polyacrylamide–chromium(III) gel; 7500 ppm polyacrylamide, 100 ppm chromium, 2.0% sodium chloride (NaCl), initial pH = 5.0, 25 °C. Numbers are steady shear rates in 1/s units.

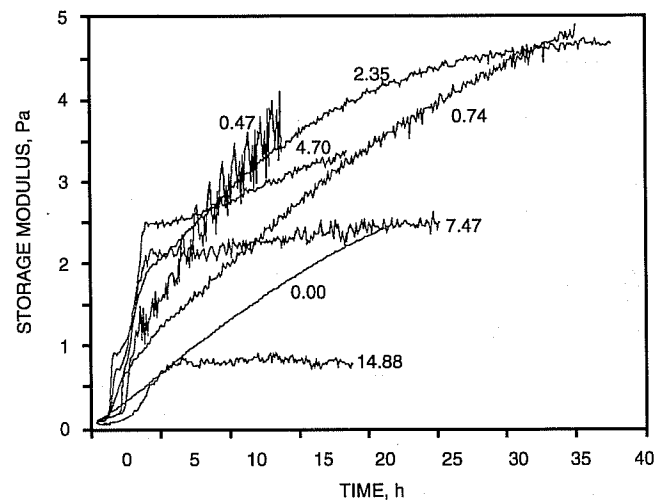


Fig. 2 Effect of shear on development of storage modulus for a polyacrylamide–chromium(III) gel; 7500 ppm polyacrylamide, 100 ppm chromium, 2.0% sodium chloride (NaCl), initial pH = 5.0, 25 °C. Numbers are steady shear rates in 1/s units.

sodium salts. For example, the nitrate system was prepared with chromium nitrate and sodium nitrate. Two methods were used to monitor gelation. Viscosity was measured on portions of the sample that were removed periodically. Gel time was defined as the time at which the viscosity increased sharply to values greater than 1000 cP. Gelation was also monitored using oscillatory shear measurements on a rheometer. The gel time for this method was the time the storage modulus, G' , equaled the loss modulus, G'' .

Gel times as a function of anion concentration are given in Fig. 3 using the viscosity method to monitor gelation. Figure 4 presents the $G' = G''$ data. Gel times were shorter for the method using viscosity than for the method using the

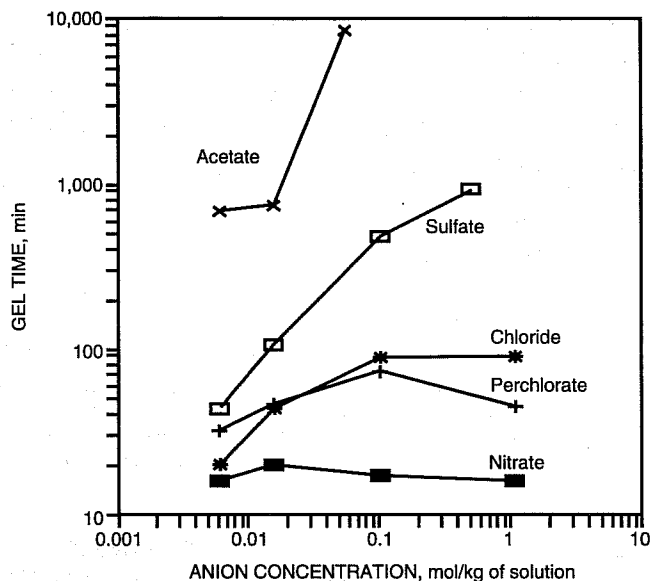


Fig. 3 Effect of anion type and concentration on gel time determined by viscosity measurements; 9000 ppm polyacrylamide, 100 ppm chromium, pH = 5.0. Viscosity greater than 1000 cP.

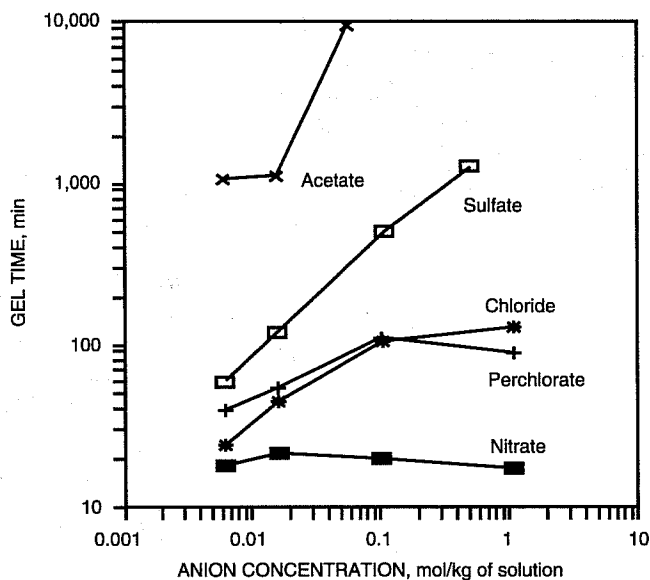


Fig. 4 Effect of anion type and concentration on gel time determined by oscillatory measurements; 9000 ppm polyacrylamide, 100 ppm chromium, pH = 5.0. Storage modulus, G' , equals loss modulus, G'' .

equality of storage and loss moduli. The anion type significantly affected the gel times. The nitrate system gelled most rapidly, followed by the perchlorate and chloride systems, followed by the sulfate system. Gels were formed the least rapidly with the acetate system.

Mechanisms of In Situ Gelation

Continuous pressure increases in the front sections of Berea sandstone cores were observed during the injection

of KUSP1 solutions. It was speculated that cell debris was filtering on the injection face of the core. A filtration procedure was developed for KUSP1 solutions that significantly improved the injectivity of KUSP1 solutions into Berea sandstone cores.

Flow experiments were conducted to determine if interactions between Berea sandstone and a 1.0N NaOH solution containing 1.0% KUSP1 would be sufficient to reduce the pH and cause gelation. A Berea core was saturated with the alkali polymer solution and allowed to soak. Small volumes of polymer solution were injected into the sandpack at selected times to test for gelation. Flow resistance in the sandpack had not increased, and the pH of the effluent had not decreased for up to 35 days of soaking. Thus, it does not appear that fluid-rock interactions will reduce the pH of the KUSP1 solution to levels where in situ gelation occurs.

RESPONSIVE COPOLYMERS FOR ENHANCED PETROLEUM RECOVERY

Contract No. DE-AC22-92BC14882

University of Southern Mississippi
Hattiesburg, Miss.

Contract Date: Sept. 22, 1992
Anticipated Completion: Sept. 21, 1995
Government Award: \$237,400
(Current year)

Principal Investigators:
Charles McCormick
Roger Hester

Project Manager:
Jerry Casteel
Bartlesville Project Office

Reporting Period: Jan. 1-Mar. 31, 1994

Objective

The overall objective of this research is the development of advanced water-soluble copolymers that rely on reversible microheterogeneous associations for mobility control and reservoir conformance for use in enhanced oil recovery (EOR).

Summary of Technical Progress

Advanced Copolymer Synthesis

Maleic anhydride (MA) does not homopolymerize by normal free radical polymerization but can readily form alternating copolymers with electron-donor monomers such as styrene,¹ vinyl ethers,² and vinyl acetate.³ *N*-vinylformamide (NVF), however, can homopolymerize and copolymerize to high molecular weight.^{4,5} The synthesis and characterization of the copolymers derived from MA and NVF are reported (Fig. 1). This class of copolymers is technologically important for EOR because hydrolysis yields polyelectrolyte or polyampholyte systems, depending on the solution pH.

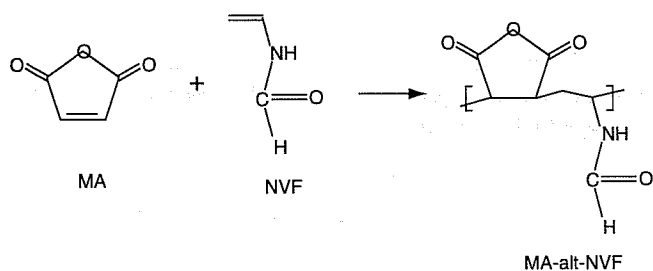


Fig. 1 Synthesis and characterization of monomer and copolymer structures [derived from maleic anhydride (MA) and *N*-vinylformamide (NVF)].

Monomer Purification and Copolymerization

Maleic anhydride was recrystallized from chloroform and vacuum dried at room temperature (melting point, 55 to 55.5 °C). *N*-vinylformamide, supplied by Air Products Inc., was distilled twice under reduced pressure before use (boiling point, 60 to 61 °C at 0.5 mm Hg). Azobisisobutyronitrile (AIBN) was recrystallized from ethanol. Tetrahydrofuran (THF), ether, and *N,N*-dimethylformamide (DMF) were used as received.

Maleic anhydride and NVF were copolymerized by free radical polymerization in THF under nitrogen at 65 to 67 °C using 0.1 mol % AIBN as the initiator. The feed ratio of NVF/MA was varied from 10/90 to 90/10 (Fig. 2). In a typical synthesis involving 60 mol % NVF in the feed, MA (8.06 g, 0.0822 mol), NVF (8.90 g, 0.125 mol), AIBN (0.0340 g, 2.07×10^{-4} mol), and THF (100 mL) were placed in a 250-mL flask equipped with magnetic stirrer, nitrogen inlet, and a

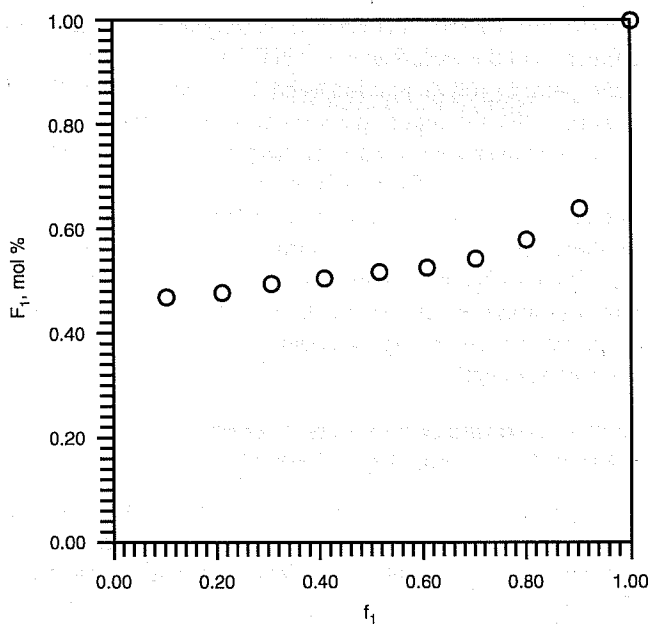


Fig. 2 *N*-vinylformamide (NVF) (F_1) (mol %) in the *N*-vinylformamide/maleic anhydride (NVF/MA) copolymer as a function of comonomer feed ratio (f_1).

condenser. The mixture was purged with prepurified nitrogen for 30 min and then immersed in an oil bath at 65 °C. Copolymerization was allowed to proceed to about 10% conversion. The copolymer was then precipitated in ether, filtered, purified by successive precipitations in ether from DMF, and then dried under vacuum at room temperature for 24 h.

Characterization of Molecular Structure

Nuclear magnetic resonance (NMR) spectra of ^1H and decoupled ^{13}C of the copolymer samples were recorded on Bruker 200- and 300-MHz instruments with dimethylsulfoxide (DMSO-d_6) as solvent. Distinct carbonyl resonances from MA and NVF occurred at 173 to 175 and 160 to 165 ppm, respectively, in ^{13}C NMR spectra and were useful for the estimation of copolymer composition. The mol fraction of each monomer in the respective copolymers was obtained by integration of the ^{13}C carbonyl resonances of MA and NVF. The reactivity ratios for NVF (M_1) and MA (M_2) were calculated by the graphical methods of Fineman-Ross⁶ and Kelen-Tudos⁷ and by a nonlinear least-square method.⁸ The results are summarized in Table 1.

TABLE 1

Reactivity Ratios of *N*-Vinylformamide and Maleic Acid

Method	r_1	r_2	$r_1 r_2$
Fineman-Ross	$2.2 \times 10^{-2} \pm 0.002$	-0.16 ± 0.01	
Kelen-Tudos	$4.1 \times 10^{-2} \pm 0.003$	$1.1 \times 10^{-2} \pm 0.001$	4.5×10^{-4}
Nonlinear least square	$2.8 \times 10^{-2} \pm 0.026$	$1.0 \times 10^{-2} \pm 0.025$	2.8×10^{-4}

The mole fraction of NVF in the copolymers was plotted as a function of the mole fraction of NVF in the feed to ascertain copolymer copolymerization behavior. The curve in Fig. 2 illustrates that the copolymers contain equimolar ratios of the monomers over a wide range of the composition of the feed, which suggests the formation of alternating structure. The alternating tendency of the comonomer pair is also indicated by their $r_1 r_2$ product, which approaches zero. Hydrolysis of the alternating copolymers yields water-soluble polymers with carboxylate and amine functionality. Their solution properties should be highly dependent on both solution pH and ionic strength.

Characterization of Polymers in Aqueous Solution by Dynamic Light Scattering

Polymer diffusion coefficients must be obtained in the limit of a zero scattering field vector, q , and also in the limit of zero polymer concentration. The dynamic light-scattering (DLS) field vector is defined by the light-scattering experimental conditions

$$q = 4 \pi n \sin\left(\frac{\theta}{2}\right) / \lambda_0 \quad (1)$$

where n and λ_0 are the solution refractive index and radiation wavelength in a vacuum, respectively. The low q values are required to eliminate DLS fluctuations because of internal motions of the macromolecules, which would be measured at higher scattering field vectors. The requirement of low polymer solution concentration minimizes interactions between individual macromolecular coils. Interactions of coils distort the DLS measurements and usually give a false indication of a larger coil size or smaller diffusional coefficient.

Analysis of DLS Experimental Data

Extrapolation to zero scattering field vector and zero concentration to find the true translational coefficient, D_{true} , can be accomplished by using a scattering equation, which expresses the apparent diffusion coefficient, D_{app} , as a linear function involving the polymer concentration, C , and the scattering angle, θ .

$$D_{\text{app}} = D_{\text{true}} + \alpha C + \beta \sin^2 \frac{\theta}{2} \quad (2)$$

In Eq. 1

$$\alpha = \kappa D_{\text{true}} [\eta] \quad (3)$$

$$\beta = \frac{q^2}{3 \sin^2(\theta/2)} D_{\text{true}} R_g^2 \quad (4)$$

where the polymer-solvent system constant κ is expected to have a value of 0.58 for random, nondraining, polymer coils;

R_g is the polymer coil mean square radius of gyration; and $[\eta]$ is the intrinsic viscosity of the polymer solution.

Multiple linear regression can be used with Eq. 2 to find D_{true} and the coefficients α and β when apparent diffusional coefficients are measured at several scattering angles and polymer concentration conditions. Thereafter the α and β values can be used to find the polymer radius of gyration, R_g , and system constant, κ . This can be accomplished by rearrangement of Eqs. 3 and 4.

$$\kappa = \frac{\alpha}{D_{\text{true}} [\eta]} \quad (5)$$

$$R_g = \frac{\lambda_0}{4 \pi n} (3\beta/D_{\text{true}})^{1/2} \quad (6)$$

If the true diffusional coefficient, D_{true} , is known, the Stokes-Einstein equation can be used to find the polymer coil average hydrodynamic radius, R_h .

$$R_h = \frac{kT}{6 \pi \eta_0 D_{\text{true}}} \quad (7)$$

In Eq. 7, k is the Boltzman constant, T is the absolute temperature, and η_0 is the solvent viscosity.

Plotting the DLS Scattering Equation With the Use of a Zimm Plot

The best-fit curve of the light-scattering equation and the DLS data can be compared with the use of a grid-plotting technique originally developed by Zimm for classical light scattering. The plot for DLS uses measurements of apparent diffusional coefficients, D_{app} , for a series of angles and polymer concentrations. The D_{app} are plotted versus $\sin^2(\theta/2)$. The points form a curve, which can be extrapolated to zero angle. Similar curves for several other polymer concentrations are plotted in the same way but are displaced from each other by use of a compound abscissa [$\sin^2(\theta/2) + kC$]. The value of k is arbitrarily selected to provide spacing between the curves. Each curve formed at each concentration can be extrapolated to give a point at zero angle. A second extrapolation of the curve formed from all zero angle points can be extrapolated to give points at zero concentration. A second extrapolation of all the zero concentration points will intersect the ordinate axis at the same point as the point previously described. This ordinate intercept of the zero angle curve and zero concentration curve is the true translation diffusion coefficient, D_{true} . The slope of the zero angle curve at the ordinate is the α value of Eq. 2, and the slope of the zero concentration is the β value of Eq. 2.

The Zimm plot is especially useful because the intersections of the angle and concentration lines are the fit values corresponding to the DLS data used in the regression analysis to find a best-fit light-scattering equation. Thus a visual comparison of the experimental data and the fit values predicted by the best-fit light-scattering equation can be quickly made.

A DLS Zimm plot of a polyacrylamide system is shown in Fig. 3. This plot shows that the true apparent diffusional coefficient is $3.36 \times 10^{-8} \text{ cm}^2/\text{s}$. This corresponds to a coil hydrodynamic radius, R_h , of 590 \AA . The coil radius of gyration, R_g , is calculated to be 670 \AA . The approximate Z average molecular weight can be determined from the following relationship:

$$M = \Phi \left[\frac{(6)^{1/2} \pi}{P} \right] \frac{R_h^3}{[\eta]} \quad (8)$$

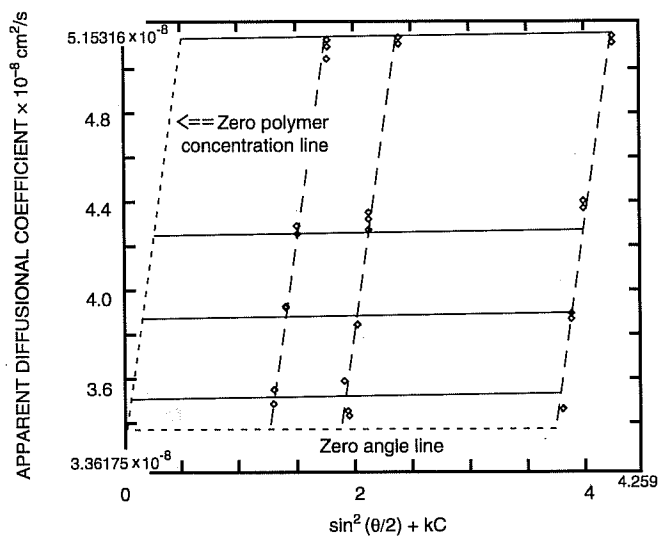


Fig. 3 Zimm plot of polyacrylamide in 0.5 M sodium chloride. Lines were produced using Eq. 2. Solid lines are lines of constant angle. Dashed lines are lines of constant concentration. Dynamic light scattering data were obtained at angles of $25, 45, 60,$ and 90° using polymer concentrations of $0.126, 0.189,$ and 0.379 g/L .

The draining parameter, P , for this polymer system is about 4.9 , and the measured intrinsic viscosity, $[\eta]$, is 2.4 dL/g . With the use of a Fox-Flory constant, Φ , of $2.07 \times 10^{21} / \text{mol}$, Eq. 8 gives a Zimm average molecular weight of $5.4 \times 10^6 \text{ g/mol}$.

Conclusions

The DLS characterization techniques described previously are being used routinely to characterize the polymers developed by the synthesis group. This characterization method is reasonably fast provided the polymer solutions can be filtered quickly to remove dust. The optimum filter pore size is about eight times the polymer hydrodynamic radius. This pore size will remove as much dust as possible without removing polymer from the solution. With very large polymer coils, filtration of dust becomes increasingly difficult. In this case, monomers and solvent must be cleaned before polymerization to ensure that clean polymer solutions can then be made for DLS analysis.

References

1. R. B. Seymour and D. P. Garner, *J. Coat. Technol.*, 48:41 (1976).
2. M. G. Baldwin, *J. Polym. Sci.*, A3: 703 (1965).
3. R. B. Seymour, D. P. Garner, and L. J. Sanders, *J. Macromol. Sci., Part A*, 13: 173 (1979).
4. S. Kondo, Y. Inagaki, M. Ozeki, and K. Tsuda, *J. Polym. Sci., Part A*, 27(10): 3383 (1989).
5. R. J. Badesso, T. W. Lai, R. K. Pinschmidt, D. J. Sagl, and B. R. Vijayendran, *Polym. Prepr., Am. Chem. Soc., Div. Polym. Chem.*, 32(2): 110 (1991).
6. M. Fineman and S. Ross, *J. Polym. Sci.*, 5(2): 259 (1950).
7. T. Kelen and F. Tudos, *J. Macromol. Sci., Part A*, 9: 1 (1975).
8. P. W. Tidwell and G. A. Mortimer, *J. Polym. Sci., Part A*, 3: 369 (1965).

GAS DISPLACEMENT— SUPPORTING RESEARCH

SCALEUP OF MISCIBLE FLOOD PROCESSES

Contract No. DE-FG22-92BC14852

**Stanford University
Stanford, Calif.**

**Contract Date: Sept. 30, 1992
Anticipated Completion: Sept. 30, 1995
Government Award: \$349,985**

**Principal Investigator:
Franklin M. Orr, Jr.**

**Project Manager:
Jerry Casteel
Bartlesville Project Office**

Reporting Period: Jan. 1–Mar. 31, 1994

Objective

The objective of this research is a systematic effort to quantify the relationships between process mechanisms that can lead to improved recovery from gas injection processes performed in heterogeneous fluvial-deltaic (Class 1) and

carbonate (Class 2) reservoirs. Research results will provide a rational basis for the design of displacement processes that take advantage of crossflow that results from capillary, gravity, and viscous forces to offset partially the adverse effects of heterogeneity. In effect, the high-permeability zones are used to deliver fluid by crossflow to zones that would otherwise be flooded only very slowly. The research effort is divided into five areas:

1. Development of miscibility in multicomponent systems.
2. Design estimates for nearly miscible displacements.
3. Design of miscible floods for fractured reservoirs.
4. Compositional flow visualization experiments.
5. Simulation of near-miscible flow in heterogeneous reservoirs.

Summary of Technical Progress

Work continued in the following areas:

1. *Development of Miscibility in Multicomponent Systems.* Progress is being made on the creation of a systematic theory of miscibility development in multicomponent systems. The dispersion-free theory developed previously at Stanford University shows that in any multicomponent displacement the recovery behavior is determined by a small number of key tie lines that include the tie lines that extend through the initial and injection compositions and one or more

crossover tie lines. If any of those tie lines is a critical tie line, then the displacement is multicontact miscible. Thus the key to determining minimum miscibility pressure (MMP) (or minimum enrichment for miscibility) is to find which tie line approaches the critical locus first as pressure (or enrichment) is increased. Efficient algorithms for calculation of the critical locus are being investigated. The next step is to develop an algorithm to determine which tie line lies closest to the critical locus. Once the key tie line for miscibility is so identified, it should be possible to develop an efficient algorithm to determine MMP for a multicomponent system. Work on the theory for systems with more than four components will begin next quarter. The goal is to develop a mathematical technique that will allow the solution of dispersion-free flow problems for systems with an arbitrary number of components.

2. *Design Estimates for Nearly Miscible Displacements.* The scaling theory developed previously has been extended to include the effects of layer ordering in scaling nearly miscible displacements in layered reservoirs. It was found that gravity forces can offset the adverse effects of high-permeability channels in some layered reservoirs if adequate vertical communication exists, a result that agrees with observations obtained in visualization experiments.¹ The combined effects of gravity and viscous forces on residual oil saturations (ROS) have also been studied.

3. *Design of Miscible Floods for Fractured Reservoirs.* The first stage of modifying the existing high-pressure pressure-volume-temperature (PVT) equipment to conduct high-pressure gravity drainage experiments is complete. In the first experiment, Means crude, whose phase behavior with carbon dioxide (CO₂) has been well studied in the Stanford University laboratory,² was used. A 2-ft-long by 2.5-in.-diameter sandstone core was saturated with 0.73 pore volume (PV) of crude oil and 0.27 PV of water before it was surrounded with liquid CO₂ at 900 psi and room temperature (about 22 °C). Preliminary results show that gravity drainage is rather efficient even at fairly low pressure (900 psi). A systematic study of gravity drainage in a pressure range from 900 to 1500 psi is being conducted to investigate the effects of miscibility development and consequent changes in interfacial tension (IFT) on gravity drainage rates and final oil recovery.

Progress has also been made in developing a theory of three-phase gravity drainage. Recent experimental and theoretical results suggest that zero ROS can be obtained in some parts of a reservoir if the reservoir is water wet and the system has a positive spreading coefficient.³

4. *Compositional Flow Visualization Experiments.* To understand more fully the visualization experimental results that have been obtained, a compositional simulator code is being modified to simulate the experiments. A subroutine for calculating the phase behavior of the fluid system used in the experiments is being written. The oil-water-alcohol systems used in the low-pressure experiments are not modeled accurately by cubic equations of state, and hence an approach based on excess free-energy models is being used.

5. *Simulation of Near-Miscible Flow in Heterogeneous Reservoirs.* Investigation continues on the streamtube approach as a numerical alternative to conventional finite-difference simulators to be used in predicting near-miscible gas injection in heterogeneous reservoirs. The streamtube approach has been applied to the two-phase immiscible case, which is assumed to be well understood and for which many reliable numerical methods have been developed. Results have provided new insight on the applicability of the streamtube approach and, particularly, on the novel idea that proposes to map a one-dimensional analytical solution (Riemann solution) along the streamtubes to obtain a two-dimensional (2-D) solution for a heterogeneous reservoir.⁴ In a dissertation titled "Viscous Fingering, Gravity Segregation and Permeability Heterogeneity in Two-Dimensional and Three-Dimensional Flows," the conclusions were reached that gravity could play a very important role in defining fluid distributions of flow in heterogeneous reservoirs and that when gravity, heterogeneity, and viscous instability are of comparable importance, 2-D flows are significantly different from three-dimensional (3-D) flows.⁵

Effects of Gravity and Viscous Forces on Residual Oil Saturation

Tertiary oil recovery or aquifer remediation processes attempt to recover oil that is trapped by capillary forces. Displacement of a hydrocarbon phase by water alone is an immiscible displacement that cannot completely recover oil from reservoirs because of the interplay of capillary forces with heterogeneities of the media. Two types of heterogeneities are commonly dealt with: pore-level heterogeneity and macroscopic heterogeneity. Pore-level heterogeneity, such as pore size (grain size) and pore-structure variations, controls the amount of oil left after the injected fluid has swept a zone, whereas macroscopic heterogeneity determines zones that the injected fluid sweeps. In numerical simulation of a displacement process, macroscopic heterogeneity can be represented directly by assigning different rock properties (permeability and porosity) to certain grid blocks, given knowledge of the detailed structure of the medium. Because of the complex nature of pore entrapment mechanisms, however, the effects of pore-level heterogeneity are represented by empirical correlations. One of the empirical correlations is the capillary desaturation curve (CDC), which defines the relationship between the ROS and the physical properties of a system. Accurate representation of the dependence of the CDC on fluid and rock properties is of great importance for simulations of enhanced oil recovery (EOR) and spilled oil cleanup processes because these processes must reduce the ROS to relatively low levels. This work describes theory and experiments that demonstrate the relative contributions of gravity and viscous and capillary forces in the correlation of ROS and the physical properties of water-wet systems.

The physical properties of a system are commonly represented by a capillary number, which is usually defined by one of the following equations

$$N_{c1} = \frac{\mu_w v}{\sigma} \quad (1)$$

$$N_{c2} = \frac{\nabla p k}{\sigma} \quad (2)$$

and a Bond number defined by

$$N_B = \frac{\Delta \rho g k}{\sigma} \quad (3)$$

or

$$B = \frac{\Delta \rho g R^2}{\sigma} \quad (4)$$

where μ_w = viscosity of the displacing phase

v = Darcy velocity

∇p = pressure gradient

k = permeability

R = radius of the grains composing the porous medium

$\Delta \rho$ = density differences between the fluids

σ = IFT of the system

According to Darcy's law, the capillary numbers (N_{c1} and N_{c2}) are related by $N_{c2} = N_{c1}/k_{rw}$, where k_{rw} is the relative permeability of the displacing phase. The use of N_{c1} or N_{c2} in the literature depends on the application to specific situations. N_{c1} , for example, is likely to be used to correlate results of experiments with constant injection rates, whereas N_{c2} may be used to describe flows with constant pressure drop. Even for processes with constant injection rates, N_{c2} is a more appropriate form to represent the ratio of viscous forces to capillary forces. The Bond numbers B and N_B are related by the correlation of the permeability (k) and the grain sizes (R) of a medium.

There are two CDCs for a displacement system, depending on the continuity of the displaced fluid.⁶⁻⁸ A discontinuous nonwetting phase is more difficult to displace from a medium than a continuous nonwetting phase.^{6,7} This work focuses attention on the displacement of a continuous nonwetting phase from a porous medium, which is commonly involved in oil recovery processes with an oil bank. The CDCs are generally obtained from laboratory measurements,^{7,9-11} although attempts have been made to predict CDCs by statistical¹² or deterministic theories.^{6,8,13} Studies of CDCs have been largely focused on the balance of capillary and viscous forces^{6,13,14} which is measured by the capillary number. Consequently, gravity effects are neglected in CDCs used in most simulators of EOR processes, even though some

studies^{7,15,16} have shown that gravity effects can be significant. This work examines the combined effects of gravity and viscous forces on oil entrapment in porous media and defines conditions under which gravity forces can be neglected or must be included in the analysis.

Entrapment Mechanisms

Entrapment mechanisms are first reviewed to identify the factors that influence oil entrapment during immiscible displacements. Mohanty et al.¹⁷ investigated the physics of oil entrapment in water-wet media and identified two entirely different entrapment mechanisms, namely, a snap-off process that traps oil in a pore and a bypass process caused by competition of flows between pores. From detailed experimental observations,¹⁸ the determination was made that approximately 80% of oil is entrapped by snap-off processes and 20% by bypassing processes for consolidated water-wet media.

Snap-off occurs in pores with large aspect ratios, the ratio of pore body and pore throat diameters. The large aspect ratio creates a significantly lower wetting phase pressure at the pore throat than that in the pore body. Hence the wetting phase flows toward the pore throat and forms a collar that grows and eventually breaks the nonwetting phase. Roof¹⁴ derived a static criterion for snap-off in noncircular capillary tubes on the basis of the capillary force balance at the pore throat and the pore body. A noncircular capillary tube was used as a model of the irregularities of pores and the roughness of solid surface of the medium. Ransohoff et al.¹⁹ extended Roof's static analysis to include the effects of viscous flow resistance in the water-filled corners of the capillary tube. For the system shown in part a of Fig. 1, the following static criterion for snap-off was obtained:

$$R_T \geq \frac{C_m R_c R_\lambda(0)}{R_\lambda(0) - R_c} \quad (5)$$

where C_m is a dimensionless interfacial curvature, which is a function of the cross-sectional geometries, and R_c and $R_\lambda(0)$ are the pore throat and pore body diameters, respectively.

To include the dynamic effects of viscous flow, Ransohoff et al.¹⁹ and Gauglitz et al.²⁰ calculated and experimentally measured the time required to transport enough fluid into the pore throat to have snap-off and compared it to the time for the nonwetting phase to flow through the pore throat. The ratio of these two times indicates whether snap-off can occur for a given system.

The random nature of the sizes and locations of pores in porous media incorporating the interconnections among the pores generates flow competitions among pores. The displacing fluid in the fast flow pores can trap oil in pores in which flows are slow. This mechanism is referred to as bypassing. Pore doublet models (PDM) have been used both theoretically^{6,18} and experimentally¹⁸ to demonstrate the bypass mechanism. The PDM is based on the assumption that well-developed Poiseuille flows compete in two parallel

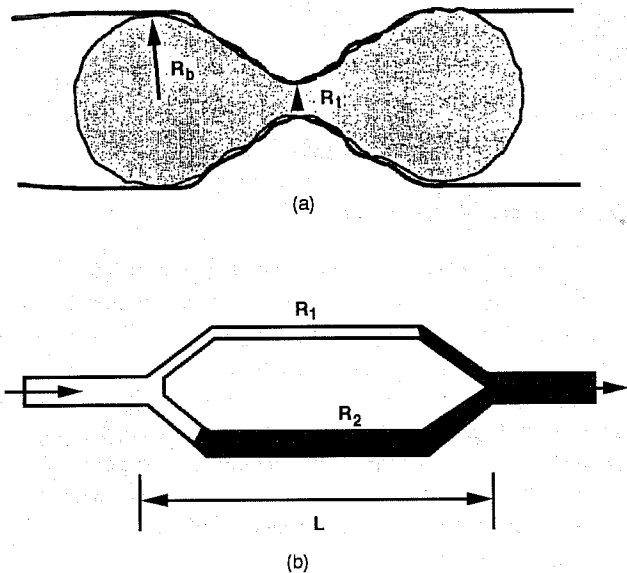


Fig. 1 Commonly used snap-off model (a) and pore doublet model (b).

flow paths (pores) with different sizes (see part b of Fig. 1). The flow velocity in each flow path can be obtained by combining Poiseuille's law and the Young-Laplace equation.⁶ The ratio of the velocities is an indication of the amount of fluid trapped in one pore. For an imbibition process, capillary forces draw the displacing phase into the smaller pore, whereas viscous forces make the fluid flow more rapidly in the larger pore. The result of this competition is that at low injection rate the oil in the large pore would be trapped. Chatzis and Morrow¹⁸ found experimentally, however, that little oil was trapped in their PDMs during free imbibitions, perhaps because capillary forces controlled the flow processes in their free imbibitions and curvatures at the junctions were larger than that of either tube. In reality, pores in the medium are not perfect capillary tubes but are irregularly shaped, and bypassing can cause entrapment. Chatzis and Morrow's observations¹⁸ from the combined model of capillary tube and neck-bulge-neck pore indicate that oil can be trapped there by the bypassing process.

Bypassing processes can also be represented by network models for studies of entrapment mechanisms in porous media.^{8,15,21-24} Network models represent porous media by networks of pores with different sizes and connectivities. Another approach, percolation theory, has also been used to represent the random nature of the porous media, in which the flow path is fully random. In its original form, percolation theory represented only two-phase displacements when capillary forces dominated the flow process, but it did not account for viscous or gravity forces. Invasion percolation theory was then introduced to include both the randomness of the medium and the continuity of the fluids. The following subsection reviews briefly effects of gravity in invasion percolation theory as well as the experimental results that demonstrate effects of gravity on residual nonwetting phase saturation.

Gravity Effects on Entrapment

The first theoretical investigation of gravity effects was reported by Wilkinson in an invasion percolation study.¹⁵ Wilkinson neglected the snap-off process and assumed that the nonwetting phase is entrapped by the bypassing process only. Correlation lengths for both viscous and buoyancy forces were introduced to measure the relative magnitudes of viscous and buoyancy forces compared with capillary forces in the medium. A viscous correlation length was defined as

$$\xi_v = \left(\frac{L_{\max}}{R} \right)_v \propto \left(\frac{N_{cl}}{k_w} \right)^{-v/(1+v)} \quad (6)$$

where L_{\max} is the maximum length of oil clusters in the system, R is the grain size (radius) of the medium, $k_w = k_{krw}/R^2$, and v is a percolation exponent ($v = 0.88$ for 3-D percolation). A gravity correlation length (ξ_G) is defined as

$$\xi_G = \left(\frac{L_{\max}}{R} \right)_G \propto B^{-v/(1+v)} \quad (7)$$

where B is the Bond number.^{7,15} For gravity-dominated flow, the ROS, S_{or} , was related to the gravity correlation length by

$$S_{or}^* - S_{or} \propto \left(\frac{1}{\xi_G} \right)^{(1+\beta)/v} \propto B^\lambda \quad (8)$$

where $\lambda = (1 + \beta)/(1 + v)$, which is a percolation constant ($\lambda = 0.77$ for 3-D percolation), S_{or}^* is the ROS at very low capillary number and Bond number, and β is also a percolation constant of 0.45 for 3-D percolation. For viscous-dominated cases, ROS was correlated as

$$S_{or}^* - S_{or} \propto \left(\frac{1}{\xi_v} \right)^{(1+\beta)/v} \propto \left(\frac{N_{cl}}{k_w} \right)^\lambda \quad (9)$$

For situations in which both viscous and gravity forces act, Wilkinson¹⁵ assumed that capillary and gravity forces were additive and that the ROS depends on $N_{cl} + (Bk_{krw}/R^2)$.

Blunt et al.²¹ used an effective correlation length for cases in which both viscous and gravity forces were involved. They defined the effective correlation length as

$$\frac{1}{\xi} = \frac{1}{L} + \frac{1}{\xi_v} + \frac{1}{\xi_G} \quad (10)$$

where L is the length of the system. For a porous medium of relatively large size, $1/L \approx 0$, and hence

$$\frac{1}{\xi} \approx \frac{1}{\xi_V} + \frac{1}{\xi_G} \quad (11)$$

In terms of capillary and Bond numbers, the residual nonwetting phase saturation is

$$S_{or}^* - S_{or} \propto [(Bk_{rw})^{\nu/(1+\nu)} + N_c^{\nu/(1+\nu)}]^{(1+\beta)/\beta} \quad (12)$$

Equation 12 indicates that the effective correlation length theory does not give a linear combination. With the percolation constants, however, the nonlinearity of Eq. 12 is weak.

An experimental study of gravity effects on ROS was conducted by Morrow and Songkran.⁷ They reported a substantial effect of gravity on residual nonwetting phase saturation in glass-bead packs. They used beads with different diameters to obtain a wide variation of Bond numbers. In all displacements IFT remained constant. The capillary number was varied by changing injection rates. They correlated their results against a linear combination of N_{cl} and B ,

$$S_{or} = f(N_{cl} + 0.001413B) \quad (13)$$

This correlation agrees well with Wilkinson's results, although Wilkinson's theory neglected the snap-off process. Blunt et al.²¹ demonstrated numerically that gravity forces (represented by the Bond number B) behave the same as viscous forces (N_{c2}). They did not obtain a linear combination of the two numbers, however. In the following sections, it is demonstrated both theoretically and experimentally that a linear combination of the dimensionless groups that represent capillary, viscous, and gravity forces gives an accurate correlation of the capillary desaturation curve.

Extended Representative Elemental Volume (REV)-Scale Models

Previously available models of snap-off and bypassing neglect the influence of gravity. This section extends such models to include gravity. In the following derivation of equations, it is assumed that the interface between oil and water phases is always in equilibrium so that the Young-Laplace equation can be used to represent the pressure difference across an interface. Flow of both phases is assumed to be well-developed Poiseuille flow, and therefore Poiseuille's law or Darcy's law is used to represent viscous pressure drops.

Snap-off Model

In past studies of snap-off processes, oil blob sizes were assumed to be smaller than the pore size. That assumption is known to be violated in displacements in real porous media; for example, Chatzis and Morrow¹⁸ observed that the blobs could be several pore sizes in extent. In this analysis, an oil blob is considered to occupy two pores in the vertical direction (see part b of Fig. 2). However, the analysis is not limited to

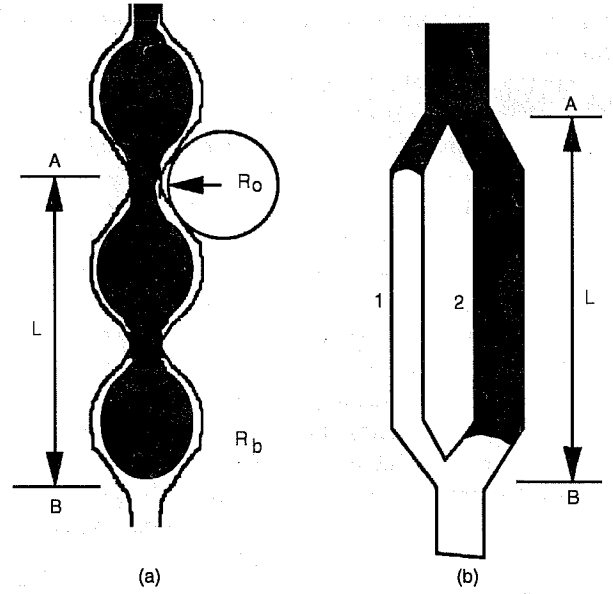


Fig. 2 Vertically oriented snap-off model (a) and pore doublet model (b).

two pore lengths and could be extended easily to multipore arrangements. Consider the situation shown in part b of Fig. 2. The pressures in both phases at the pore throat are

$$P_o = P_i + \frac{C_m \sigma}{R_b} - \Delta P_{ov} - \rho_o g L \quad (14)$$

and

$$P_w = P_i - \Delta P_{wv} - \rho_w g L \quad (15)$$

where R_b is the pore body radius, C_m is the dimensionless interfacial curvature in the pore body, and ΔP_{ov} and ΔP_{wv} are the viscous pressure drops of the oil and the wetting phases, respectively. Because of the continuity of the wetting phase, the wetting phase can reach the pore throat through other neighboring pores. Therefore Darcy's law is used to calculate the viscous pressure drops for both phases. ΔP_{ws} and ΔP_{ov} are then expressed as $\Delta P_{ws} = (\mu_w v L)/(k k_{rw})$ and $\Delta P_{ov} = (\mu_o v_o L)/(k k_{ro})$. Thus the difference between the two phases at the pore throat is

$$\Delta P_1 = (P_o - P_w)_1 = \frac{C_m \sigma}{R_b} + (\rho_w - \rho_o) g L + \frac{\mu_w v L}{k k_{rw}} - \frac{\mu_o v_o L}{k k_{ro}} \quad (16)$$

At the pore throat, the pressure difference between the two phases can also be obtained from the Young-Laplace equation,

$$\Delta P_2 = (P_o - P_w)_2 = \frac{\sigma}{R_t} - \frac{\sigma}{R_o} \quad (17)$$

where R_t is the pore throat radius and R_o is the radius of the pore neck.

Now consider the following situations: $\Delta P_2 > \Delta P_1$ and $\Delta P_2 < \Delta P_1$. When $\Delta P_2 > \Delta P_1$, the fluids would flow in such a way as to reduce ΔP_2 to keep the two forces in balance. In order to decrease ΔP_2 , the system would either increase R_t or decrease R_o . It is impossible to increase R_t further because of the solid pore structure. Thus the system would reduce R_o . To reduce the value of R_o , capillary forces pump the wetting phase into the pore throat. Consequently a wetting phase collar ring would form at the pore throat.¹⁹ The formation of the collar ring reduces the value of R_t and results in snap-off. When $\Delta P_2 < \Delta P_1$, however, the system becomes stable. To balance the pressure difference in this case, the system would either reduce R_t or increase R_o . Reducing R_t is impossible because the viscous pressure difference ΔP_1 pushes the interface outward to increase R_t . Thus increasing the effective value of R_o is the only solution. To increase the effective value of R_o , the capillary forces push the wetting phase away from the pore throat, and there is little wetting phase at the pore throat. Therefore there would be no snap-off. In summary, it is argued that the system would be stable if $\Delta P_2 < \Delta P_1$. The following stability condition is then obtained:

$$N_{c1} + \frac{k_{rw}}{a} N_B > \frac{kk_{rw}}{R_t L a} \left(1 - \frac{R_t}{R_o} - \frac{C_m R_t}{R_b} \right) \quad (18)$$

where $a = v_w/v_t - Mv_o/v_t$, v_t is the total flow velocity, and M is the mobility ratio at the trailing edge of the displacement front, $M = \mu_o k_{rw} / \mu_w k_{ro}$. The Bond number (N_B) is defined here in terms of permeability because permeability is the directly measurable property of the medium. Equation 18 shows that a linear combination of the capillary and Bond numbers arises naturally from a simple physical picture of a snap-off process. The relative magnitudes of gravity and viscous forces depend on values of the wetting phase relative permeability and the constant a . For an estimate of the value of a , consider the situation at the moment just before a drop of oil is trapped in the pores. The nonwetting phase is assumed to flow much more slowly than the wetting phase, so $v_w \gg v_o$. Therefore $v_w \approx v_t$, and the value of a is close to 1.

Hence the wetting phase relative permeability determines the relative contribution of the capillary and the Bond numbers, and

$$N_{c1} + k_{rw} N_B > k_{rw} \frac{k}{R_t L} \left(1 - \frac{R_t}{R_o} - \frac{C_m R_t}{R_b} \right) \quad (19)$$

Equation 19 suggests that mobility ratio would have minimal effect on the final residual nonwetting phase saturation, which agrees with experimental observations.^{11,25}

If $N_{c1} = 0$ and $N_B = 0$, Eq. 19 simplifies to

$$R_b > \frac{C_m R_t R_o}{R_o - R_t} \quad (20)$$

which is the same as Eq. 5.

Doublet Model

For vertically oriented doublet pores such as those shown in part b of Fig. 2, the pressure drops from point A to point B for each pore are written as (on the assumption that the tubes are cylindrical)

$$\Delta p_1 = \frac{8\mu_w v_1 L_1}{R_1^2} + \frac{8\mu_o v_1 (L - L_1)}{R_1^2} - \frac{2\sigma}{R_1} + L_1 \rho_w g + (L - L_1) \rho_o g \quad (21)$$

and

$$\Delta p_2 = \frac{8\mu_w v_2 L_2}{R_2^2} + \frac{8\mu_o v_2 (L - L_2)}{R_2^2} - \frac{2\sigma}{R_2} + L_2 \rho_w g + (L - L_2) \rho_o g \quad (22)$$

where R_i = radius of tube i

L_i = distance the displacing fluid flows in tube i

L = length of the tubes

v_i = flow velocity in tube i

Because the two pores are parallel, the pressure drops Δp_1 and Δp_2 must be equal, $\Delta p_1 = \Delta p_2$. Therefore the following expression is obtained in which the average velocity (v_a) of the doublet pores is $v_a = (R_1^2 v_1 + R_2^2 v_2) / (R_1^2 + R_2^2)$:

$$N_{c1} m + (\ell_1 - \ell_2) \frac{f}{1+f} N_B = \frac{2k}{R_1 L} \frac{f}{1+f} \left(1 - \frac{R_1}{R_2} \right) \quad (23)$$

where $\ell_i = L_i / L$

$\mu_r = \mu_o / \mu_w$

$f = R_2^2 / R_1^2$

$$m = (1 - \mu_r) \left[\left(1 + f - \frac{v_2}{v_a} f \right) \ell_1 f - \frac{v_2}{v_a} \ell_2 \right]$$

$$+ \mu_r \left[f \left(1 + f - \frac{v_2}{v_a} \right) - \frac{v_2}{v_a} \right] \quad (24)$$

The permeability of the PDM is defined as $(R_1^2 + R_2^2) / 8$ from Poiseuille's law.

To simplify the arguments, assume the radius of pore 1 is smaller than that of pore 2, $R_1 < R_2$. Capillary forces draw the wetting phase into the smaller pore (pore 1), and viscous forces make fluid flow more easily in the larger pore (pore 2). At the same time, gravity forces reduce the velocity difference between pores. The reduction of viscous forces slows the flow in the larger pore and thus results in more oil being trapped in

the larger pore. If the oil in pore 2 were completely trapped, the following parameters would have been obtained: $v_2 = 0$, $l_1 = 1$, $l_2 = 0$, and $m = f(1 + f)$. To avoid entrapment of the nonwetting phase in pore 2 completely, therefore, the system must have a value of m smaller than $f(1 + f)$. Thus rearrangement of Eq. 23 gives

$$N_{c1} + CN_B > C \frac{2k}{R_1 L} \left(1 - \frac{R_1}{R_2} \right) \quad (25)$$

where $C = 1/(1 + f)^2$.

For a given system, Eq. 25 indicates that the combined effects of gravity and capillary forces must be greater than a certain value to avoid oil entrapment in doublet pores. The relative magnitude of gravity forces and viscous forces depends on the value of C , which represents the heterogeneity of the system. $C = R_1^4 / (R_1^2 + R_2^2)^2$ is the relative permeability of the displacing phase (the wetting phase) and can be derived as

$$C = \frac{R^4}{(R_1^2 + R_2^2)^2} = \frac{k_1 R_1^2}{k(R_1^2 + R_2^2)} = \frac{Q_1}{Q_t} \quad (26)$$

where Q_1 and Q_t are the flow rate in pore 1 and the total flow rate in both pores. According to Darcy's law, $Q_1 = (Ak_{rw}k / \partial\Phi / \partial l) / \mu$ and $Q_t = (Ak / \partial\Phi / \partial l) / \mu$ for a given flow area A and potential gradient $\partial\Phi / \partial l$. Therefore

$$C = \frac{Q_1}{Q_t} = \frac{(Akk_{rw} / \mu)(\partial\Phi / \partial l)}{(Ak / \mu)(\partial\Phi / \partial l)} = k_{rw} \quad (27)$$

and

$$N_{c1} + k_{rw}N_B > k_{rw} \frac{2k}{R_1 L} \left(1 - \frac{R_1}{R_2} \right) \quad (28)$$

Thus Eq. 28 also suggests that a linear combination of the capillary and Bond numbers can be used to state a criterion for bypassing. Here again the coefficient of the Bond number is the wetting phase relative permeability.

Summary

In both snap-off and doublet models, criteria were obtained for the prevention of nonwetting phase entrapment in porous media in terms of linear combinations of capillary and Bond numbers. A comparison of Eqs. 19 and 28 indicates that they have similar forms. In both cases the relative contributions of capillary and Bond numbers are determined by the relative permeability of the displacing phase. With the use of the relationship of N_{c1} and N_{c2} , the following equations for snap-off and bypass processes are obtained:

$$N_{c2} + N_B > \frac{k}{R_1 L} \left(1 - \frac{R_t}{R_o} - \frac{2R_t}{R_b} \right) \quad (29)$$

and

$$N_{c2} + N_B > \frac{2k}{R_1 L} \left(1 - \frac{R_1}{R_2} \right) \quad (30)$$

The simplicity of Eqs. 29 and 30 suggests that N_{c2} is a more appropriate definition of capillary number than N_{c1} , even for processes with constant injection rates.

Experiments

Morrow and Songkran's experiments⁷ provide some evidence that a linear combination of capillary number and Bond number determines ROS. In their experiments, however, the Bond number was changed by varying the sizes of the beads used in packing columns. Results from experiments designed to examine whether use of the linear combination is reasonable if the Bond number is changed by the variation of IFT and density differences of the fluids are reported.

All displacements were conducted in the same sand-pack column. The Bond number was varied by using different IFTs and density differences of the fluids. Figure 3 is a schematic of the experimental apparatus. The high-pressure liquid chromatography (HPLC) pump provided constant injection rates ranging from 0.1 to 8.0 cm³/min. The length of the sand-packed porous medium was 119.0 cm and the diameter was 1.95 cm. The permeability was 48.5 darcys and the porosity was 0.256. A mixture of brine, isooctane (iC₈), and isopropanol (IPA) was used to generate fluid pairs of a wide range of IFT and density differences. This system has been well studied.⁷ Four tie lines were used to obtain IFTs varying from 0.1 to 38.1 mN/m and densities from 0.11 to 0.33 g/cm³, which correspond to a range of capillary and Bond numbers from 10⁻⁶ to 10⁻³ in this work.

All displacements were conducted with initial wetting phase saturations. They were established by injecting the

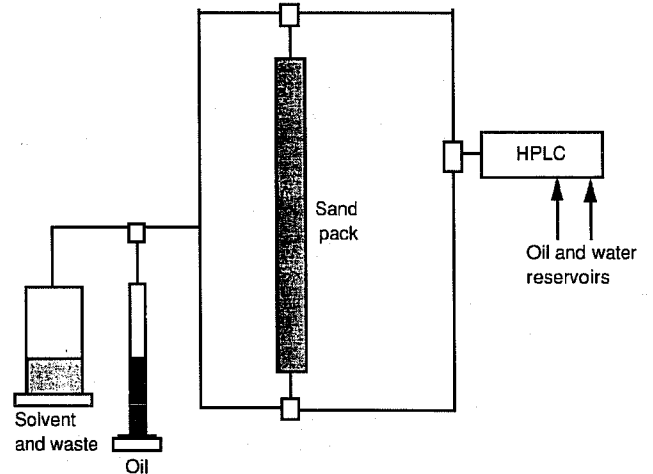


Fig. 3 Schematic diagram of the experimental setup. HPLC, high-pressure liquid chromatography.

nonwetting phase into the top of the column that was fully saturated with the wetting phase. The initial wetting phase saturation varied from 0.15 to 0.25 PV. The large variation of initial wetting phase saturations resulted from large variations in mobility ratios in different runs. In this range of initial wetting phase saturation, repeated experiments showed that this variation of initial wetting phase saturation did not influence the residual nonwetting phase saturation. Therefore the differences in the residual nonwetting phase saturation are the results of the capillary and Bond number variations. So that the directional effects of gravity forces could be studied, displacements were conducted by injecting the wetting phase from either the bottom or top of the column. Displacement from the bottom is referred to as gravity-favorable and that from the top as gravity-unfavorable because the gravity forces stabilize the displacements when the injected phase enters the column from the bottom.

In all the displacements, little additional recovery was observed shortly after the breakthrough, which is consistent with the idea that the sand pack was strongly water wet. Following the common practice, the final ROS was plotted against the capillary number alone for all displacements in Fig. 4. Apparently the experimental data cannot be reasonably correlated by the capillary number alone. The experimental results also indicate, therefore, that gravity forces and the flow directions affect the residual nonwetting phase saturations.

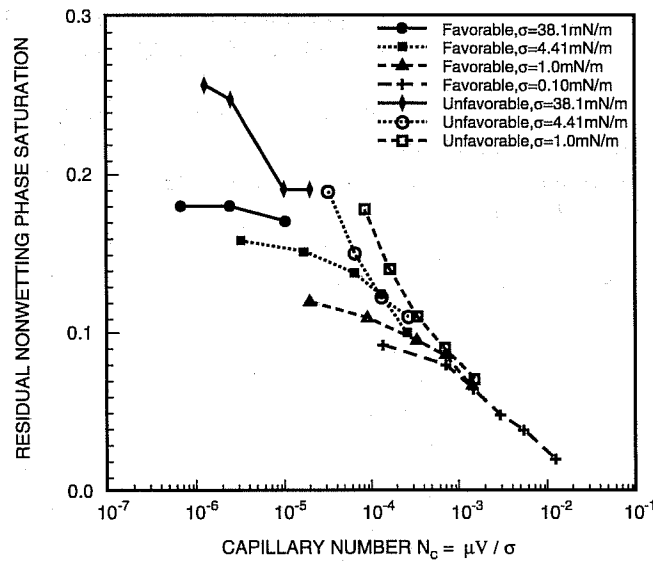


Fig. 4 Correlations of residual nonwetting phase saturation with the capillary number alone for all displacements.

Discussion

In the definitions of capillary number (N_{cl}) and Bond number N_B , five variables are involved: (1) the injection rates (v), (2) the IFT (σ), (3) the density difference ($\Delta\rho$), (4) the viscosity of the wetting phase (μ_w), and (5) the permeability of the medium (kk_{rw}). In the experiments described, IFT and

density differences as well as injection rates were varied to obtain a wide range of capillary and Bond numbers. To check the other parameters, the experimental results of Morrow and Songkran,⁷ who varied the capillary number and Bond number by changing different bead sizes and injection rates, were reviewed. Changing bead size changes the permeability of the bead pack. The permeability of a bead pack can be related to the bead size through the Kozeny–Carman equation

$$K = \frac{\phi^3}{k_z(1-\phi)^2 A_s^2} \quad (31)$$

where A_s is the specific surface area per unit solid volume, for spherical bead $A_s = 3/R$, K_z is the Kozeny constant, which is approximately equal to 5 for bead packings, and ϕ is the porosity of the packing, which is about 0.38 for bead packings. Therefore the permeability of a bead pack can be simply related to bead size as

$$k = 0.00317R^2 \quad (32)$$

Thus the correlation given by Morrow and Songkran⁷ can be rearranged in terms of N_B as

$$S_{or} = f(N_{cl} + 0.445N_B) \quad (33)$$

A comparison of Eq. 33 with the theoretical results indicates that the wetting phase relative permeability at the trailing edge of the displacement front is about 0.445, which is consistent with Morrow and Songkran's measurements ($k_{rw} = 0.5$).⁷

As did Morrow and Songkran,⁷ a least-square fit of ROSs was obtained from gravity-favorable displacements with an effective number defined as $N_e = N_{cl} + CN_B$. As Fig. 5 shows, a straight-line correlation on the semilog plot exists when $c = 0.5$ and $N_e > 10^{-5}$. According to Eqs. 18 and 28, the value of c_1 is the relative permeability of the wetting phase. This value is very close to the measured relative permeability by Morrow and Songkran.⁷ Again, these experiments suggest that a linear combination of the capillary and the Bond numbers correlates the ROSs, and the appropriate coefficient is the wetting phase relative permeability.

With the use of the same value of c , all experimental results were correlated, as Fig. 6 shows, for both gravity-favorable and gravity-unfavorable displacements. At high values of N_e , the correlation is excellent, whereas it is less satisfactory when N_e is small. The difference between the gravity-favorable and gravity-unfavorable displacements may result partly from the accuracy of the flow rate and permeability measurements because the subtraction of the two numbers enhanced the significance of the measurement error when these two values were comparable. In general, the correlation is good. The following correlation of the ROS was obtained with the capillary and the Bond numbers, when $N_e > 10^{-5}$:

$$S_{or} = 0.02 + 0.0505 \log \frac{0.01227}{N_{cl} + 0.5 N_B} \quad (34)$$

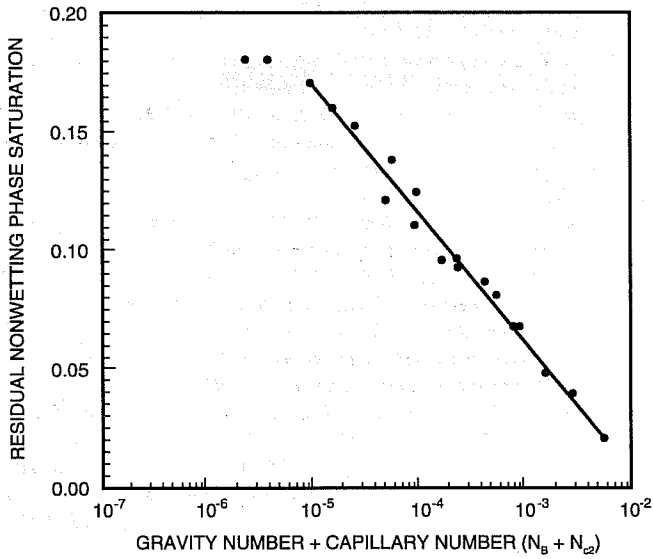


Fig. 5 Correlation of the residual oil saturations and the sum of the capillary and Bond numbers for gravity-favorable displacements. ●, experimental data. —, best-fit.

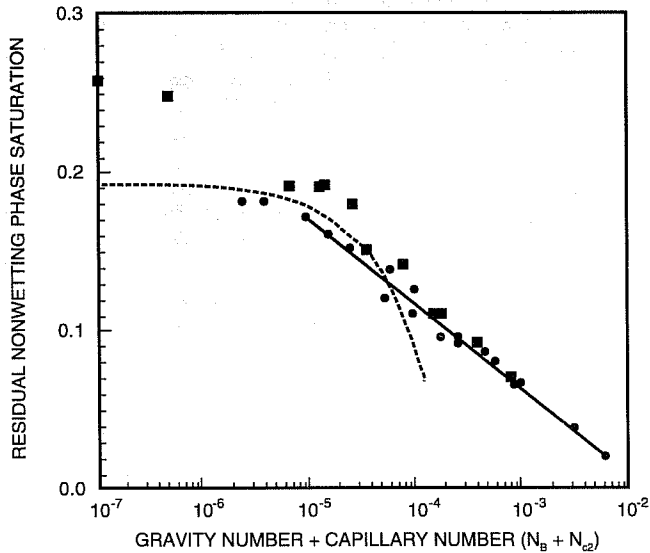


Fig. 6 Correlations of residual oil saturations and the sum of capillary and Bond numbers from percolation theory and best fit of the experimental data. ●, displacements from bottom. ■, displacements from top. —, correlation. . . . , percolation.

Figure 7 shows a comparison of the experimental data and the correlation given by Eq. 34. The agreement is very good except for gravity-unfavorable displacements at high IFTs. In these cases the displacements were no longer stable because the gravity forces were larger than the viscous forces (i.e., the value of $N_{c1} + 0.5 N_B$ is close to zero or negative). Therefore, for a system with gravity forces larger than or equal to the capillary forces, gravity-favorable displacements have much lower ROS than gravity-unfavorable displacements.

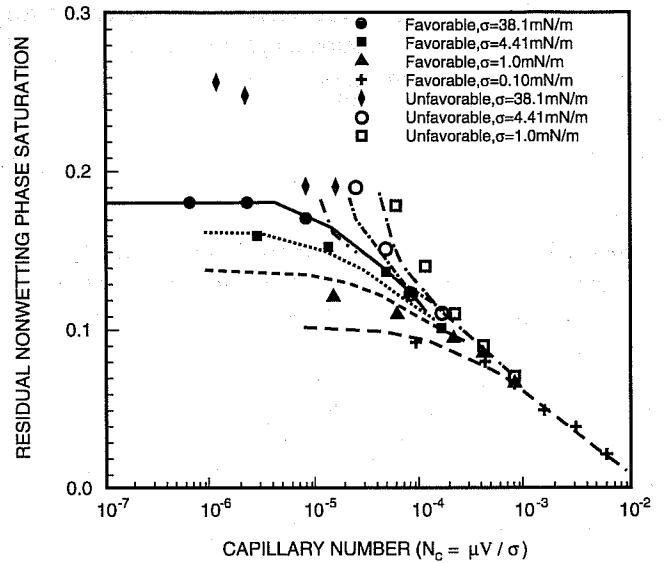


Fig. 7 Comparison of the correlation given by Eq. 34 with experimental data. Lines are correlations and dots are the experimental data.

For a given system, it would be useful to determine which forces are most important. Therefore the linear combination is rearranged to obtain

$$N_e = N_{c1} \left(1 + \frac{\Delta \rho g k k_{rw}}{\mu_w v} \right) \quad (35)$$

The relative magnitudes of N_{c1} and N_B in a system can be reflected by the gravity number

$$N_g = \frac{\Delta \rho g k k_{rw}}{\mu_w v} \quad (36)$$

When $N_g > 1$, the Bond number is the dominating factor, whereas when $N_g < 1$, the capillary number is the controlling parameter in determining the ROS.

Note that the gravity number (N_g) is proportional to the medium permeability. Thus flow in a high-permeability medium will have larger gravity effects than that in a low-permeability medium. For an illustration of this concept, compare typical oil-spill and oil-recovery situations. The permeability of a typical soil is about 100 darcys, water viscosity is around $10^{-3} \text{ N}\cdot\text{s}$ (1 cP), and the flow rate is about 1 ft/d, which is about $3.5 \times 10^{-6} \text{ m/s}$. It is also assumed that the density difference is about 300 kg/m^3 and the IFT is about $40 \times 10^{-3} \text{ N/m}$. The gravity number (N_g) is about 5 (i.e., the gravity forces are larger than the viscous forces in typical spilled-oil cleanup processes). For a waterflood oil-recovery process, however, the permeability is in the order of 100 mD. If the same fluid properties are used, the gravity number is about 5×10^{-3} . Thus gravity forces are less significant than viscous forces in determining final oil saturation in oil reservoirs.

From these results, an argument can be made for the concept of effective correlation length used by Blunt et al.²¹ The criterion for preventing oil entrapment is

$$N_e > \frac{a}{L} \quad (37)$$

where a is the parameter representing the heterogeneity of the medium and L is the length of the oil ganglion to be trapped. Therefore the length of an oil ganglion to be trapped in the system is

$$L \propto \frac{a}{N_e} = \frac{a}{N_{c2} + N_B} \quad (38)$$

By the same argument given by Blunt et al.,²¹ the following can be obtained:

$$\xi_e \propto N_e^{-v/(1+v)} \quad (39)$$

and

$$S_{or}^* - S_{or} \propto \left(\frac{1}{\xi_e} \right)^{(1+\beta)/v} \propto N_e^\lambda = (N_{c2} + N_B)^\lambda \quad (40)$$

where ξ_e is the effective correlation length. Thus gravity and viscous forces have similar effects on the effective correlation length of a displacement process. Figure 6 shows a comparison of the experimental data and the invasion percolation correlation. As one would expect, the agreements become less satisfactory at high value of N_e because that percolation is valid only for cases in which capillary forces dominate.

Conclusions

It has been demonstrated theoretically and experimentally that a linear combination of gravity and viscous forces can be used to correlate residual nonwetting phase saturations for both gravity-favorable and gravity-unfavorable displacements. When gravity forces are comparable to or larger than the viscous forces, gravity-unfavorable displacements have significantly higher residual nonwetting phase saturation than gravity-favorable displacements. Because soils have much higher permeabilities than oil reservoirs, gravity effects on residual nonwetting phase saturations are much more significant in spilled-oil cleanup than in oil-recovery processes. The effective correlation length for a percolation process can be related to a linear combination of the gravity and viscous forces.

References

1. D. Zhou, F. J. Fayers, and F. M. Orr, Jr., *Scaling Multiphase Flow in Simple Heterogeneous Porous Media*, paper SPE 27816 presented at

- the SPE/DOE Ninth Symposium on Improved Oil Recovery, Tulsa, Okla., April 17–20, 1994.
2. K. Hagedorn, *Component Partitioning in CO₂Crude Oil Mixtures*, Ph.D. dissertation, Stanford University, 1992.
3. M. J. Blunt, D. Fenwick, and D. Zhou, *What Determines Residual Oil Saturation in Three Phase Flow?* paper SPE 27816 presented at the SPE/DOE Ninth Symposium on Improved Oil Recovery, Tulsa, Okla., April 17–20, 1994.
4. M. R. Thiele, M. J. Blunt, and F. M. Orr, Jr., *A New Technique for Predicting Flow in Heterogeneous Systems Using Streamtubes*, paper SPE 27834 presented at the SPE/DOE Ninth Symposium on Improved Oil Recovery, Tulsa, Okla., April 17–20, 1994.
5. H. Tchelepi, *Viscous Fingering, Gravity Segregation and Permeability Heterogeneity in Two-Dimensional and Three-Dimensional Flows*, Ph.D. dissertation, Stanford University, 1994.
6. W. L. Lake, *Enhanced Oil Recovery*, first edition, Prentice Hall, Englewood Cliffs, N.J., 1989.
7. N. R. Morrow and B. Songkran, *Effects of Viscous and Buoyancy Forces on Nonwetting Phase Trapping in Porous Media*, in *Surface Phenomena in Enhanced Oil Recovery*, D. Shah (Ed.), pp. 387–411, Plenum Press, New York, 1982.
8. D. Zhou and H. E. Stenby, *Immiscible Displacement in a Porous Medium Simulated by a Statistical Model*, in *North Sea Oil and Gas Reservoirs-II*, 1990.
9. J. M. Garnes, A. M. Mathisen, A. Scheie, and A. Skauge, *Capillary Number Relations for Some North Sea Reservoir Sandstones*, paper SPE 20264 presented at the SPE/DOE Seventh Symposium on Enhanced Oil Recovery, Tulsa, Okla., April 22–25, 1990.
10. M. J. King, A. J. Falzone, W. R. Cook, J. W. Jennings, Jr., and W. H. Mills, *Simultaneous Determination of Residual Oil Saturation and Capillary Pressure Curves Utilizing Ultracentrifuge*, paper SPE 15595 presented at the SPE 61st Annual Technical Conference and Exhibition, New Orleans, La., October 5–8, 1986.
11. J. J. Taber and R. S. Seright, *Horizontal Injection and Production Wells for EOR or Waterflooding*, paper SPE 23952 presented at the SPE/DOE Eighth Symposium on Enhanced Oil Recovery, Tulsa, Okla., April 21–24, 1992.
12. G. L. Larson, H. T. Davis, and L. E. Scriven, *Displacements of Residual Non-wetting Fluid from Porous Media*, *Chem. Eng. Sci.*, 36: 75–81 (1981).
13. G. L. Stegemeier, *Relationship of Trapped Oil Saturation to Petrophysical Properties of Porous Media*, paper SPE 4754 presented at the SPE Improved Oil Recovery Symposium, Tulsa, Okla., April 21–24, 1974.
14. J. G. Roof, *Snap-Off of Oil Droplets in Water-Wet Pores*, *Soc. Pet. Eng. J.*, 85–90 (March 1970).
15. D. Wilkinson, *Percolation Effects in Immiscible Displacement*, *Phys. Rev. A*, 30(1): 520–531 (1984).
16. D. Wilkinson, *Percolation Effects in Immiscible Displacement*, *Phys. Rev. A*, 34(2): 1380–1385 (1986).
17. K. K. Mohanty, H. T. Davis, and L. E. Scriven, *Physics of Oil Entrapment in Water-Wet Rock*, *SPE Reserv. Eng.*, 2(1): 113–128 (February 1987).
18. I. Chatzis and N. R. Morrow, *Correlation of Capillary Number Relationships for Sandstone*, *Soc. Pet. Eng. J.*, 24(5): 555–562 (October 1984).
19. T. C. Ransohoff, P. A. Gauglitz, and C. J. Radke, *Snap-Off of Gas Bubbles in Smoothly Constructed Noncircular Capillaries*, *A.I.Ch.E.J.*, 33(5): 753–765 (1987).
20. P. A. Gauglitz, C. M. St. Laurent, and J. C. Radke, *Experimental Determination of Gas Bubble Breakup in a Constricted Cylindrical Capillary*, *Ind. Eng. Chem. Res.*, 17340: 27–31 (April 1988).
21. M. Blunt, M. J. King, and H. Scher, *Simulation and Theory of Two-Phase Flow in Porous Media*, *Phys. Rev. A*, 46(12): 7680–7698 (1992).
22. I. Fatt, *The Network Model of Porous Media I: Capillary Pressure Characteristics*, *Pet. Trans., AIME*, 207: 144–159 (1956).

23. I. Fatt, The Network Model of Porous Media II: Dynamic Properties of a Single Size Tube Network, *Pet. Trans., AIME*, 207: 160-163 (1956).
24. I. Fatt, The Network Model of Porous Media III: Dynamic Properties of Networks with Tube Radius Distribution, *Pet. Trans., AIME*, 207: 164-170 (1956).
25. A. Abrams, The Influence of Fluid Viscosity, Interfacial Tension, and Flow Velocity on Residual Oil Saturation Left by Waterflood, *Soc. Pet. Eng. J.*, 14: 927-935 (1975).

HORIZONTAL OIL WELL APPLICATIONS AND OIL RECOVERY ASSESSMENT

Contract No. DE-AC22-92BC14861

**Maurer Engineering, Inc.
Houston, Tex.**

**Contract Date: June 3, 1993
Anticipated Completion: June 2, 1994
Government Award: \$124,119**

**Principal Investigator:
William J. McDonald**

**Project Manager:
Thomas Reid
Bartlesville Project Office**

Reporting Period: Jan. 1–Mar. 31, 1994

Objective

The primary objective of this project is to examine factors affecting technical and economic successes of horizontal well applications. The goals of the project will be accomplished through five tasks designed to evaluate the technical and economic successes of horizontal drilling, highlight current limitations, and outline technical needs to overcome these limitations. Data describing experiences of the operators throughout the domestic oil and gas industry will be gathered and organized. Maurer Engineering Inc. (MEI) databases containing detailed horizontal case histories will also be used. All these data will be categorized and analyzed to assess the status of horizontal well technology and to estimate the impact of horizontal wells on present and future domestic oil recovery and reserves.

Summary of Technical Progress

Information Base on Horizontal Wells

A spreadsheet data file was constructed from well data describing domestic horizontal wells. Three principal forma-

tions are the focus of the majority of this activity: the Austin Chalk in Texas, the Bakken Shale in North Dakota, and the Niobrara in Colorado and Wyoming. Results from these fields are well known, and a large volume of published results is available. Given the objective of the present study, it was decided to limit the analyses to formations other than these three fractured carbonates. On the basis of domestic well data, over 430 horizontal wells have been completed in other formations.

About 180 operators drilled these other wells in a total of 112 formations. Questionnaires covering over 60% of the wells were returned.

Specialized Database for Horizontal Well Forecasting

A database for the data describing formations drilled horizontally was constructed in dBASE IV. Questionnaires have been received from several sources, including operators listed in the original well data file, participant companies in the DEA-44 Horizontal Well Technology joint industry project, attendees of the Horizontal Technology Forum held in Calgary during July 1993, and attendees of the Horizontal Technology Forum held in Houston, Tex., during September 1993.

Over 160 database records have been generated. Several questionnaires describing formations outside the scope of this study, including Austin Chalk wells and wells outside the United States, have been returned. These data may be evaluated at a later date.

Economic and Technical Trend Analysis

Multiple analyses have been performed on the database. Overview analyses were designed to determine the types and frequencies of the various applications of horizontal technology. Results are shown for 58 domestic formations in Fig. 1. Applications reported include (1) intersect natural fractures,

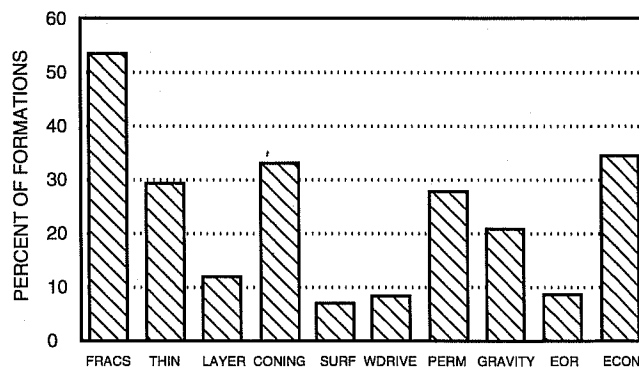


Fig. 1 Horizontal technology applications (58 formations). FRACS, intersect natural fractures; THIN, target thin formations; LAYER, layered or heterogeneous formations; CONING, water or gas coning; SURF, surface restrictions; WDRIVE, water drive–water injection; PERM, low permeability; GRAVITY, gravity drainage; EOR, extended oil recovery; and ECON, favorable economics.

(2) target thin formation, (3) layered or heterogeneous formation(s), (4) water or gas coning, (5) surface restrictions, (6) water drive–water injection, (7) low permeability, (8) gravity drainage, (9) enhanced oil recovery (EOR), and (10) favorable economics. Multiple responses were typical; therefore the results shown in the figure total more than 100%. The three most common applications include intersecting fractures (53%), delaying coning (33%), and economics (35%). Least-used applications include surface restrictions (7%) and water drive and EOR (each with less than 9%).

Operators were asked whether their horizontal applications in each field were technical and/or economic successes. Not unexpectedly, most programs were indicated as technically successful. Of 57 responses, 54 were reported to be technically successful, which represents an overall 95% success rate. This high rate of success suggests that horizontal technology has advanced to the point that most technical challenges to placing a well in the ground can and have been overcome.

According to the survey, economic success has not been as widespread as technical success. Of 56 responding formations, 28 were considered to be economic successes (50%) and 24 were considered to be economically unsuccessful (43%). An additional four formations (7%) had mixed economic results (i.e., multiple operators in a particular field reported both successful and unsuccessful projects).

When lithology is considered, the data suggest that carbonate applications have been slightly more technically successful than clastic: 100% vs. 91%. This difference may reflect the lack of experience with the larger variety of clastic formation types and applications rather than indicate inherent technical difficulties. Conversely, clastic applications were reported to be more economically successful than carbonates: 59% vs. 45%, respectively.

Horizontal Well Application Forecast

Another key parameter in the project data is the estimated increase in reserves as a result of implementing horizontal technology. Results from 47 questionnaires (Fig. 2) show that over half the operators have seen an increase of greater than 5%. Horizontal wells are expected to increase recoverable reserves through, for example, delaying the onset of water coning or accessing oil not economically recoverable with vertical wells.

Proven U.S. oil reserves amount to about 27 billion bbl according to the Tertiary Oil Recovery Information System (TORIS). This volume represents 5% of the total domestic original oil in place (OOIP) of 513 billion bbl. Increases in these reserves, as reported by survey respondents, ranged from 0 to 300%. The overall average increase is 24.6%. Extrapolated to the total U.S. reserves base, this represents an additional 6.6 billion bbl of reserves as the result of the widespread and appropriate application of horizontal technology.

A forecast of the number of horizontal wells to be drilled over the next several years is shown in Fig. 3. According to

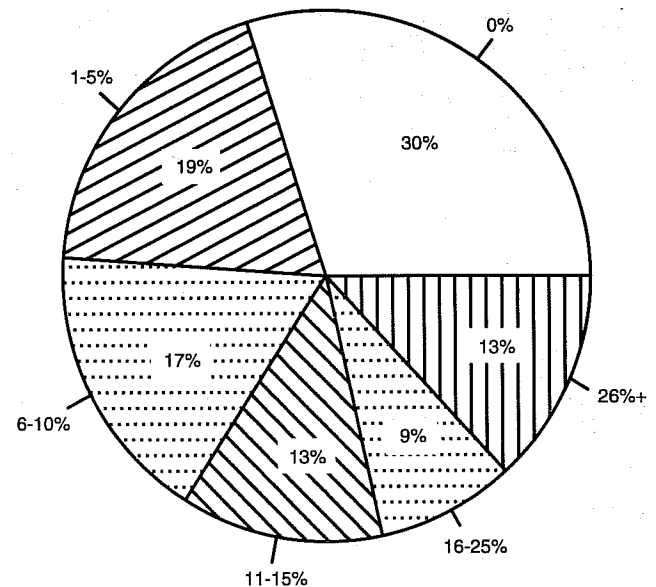


Fig. 2 Chart showing reserves increase with horizontal wells. (Average increase, 24.6%.)

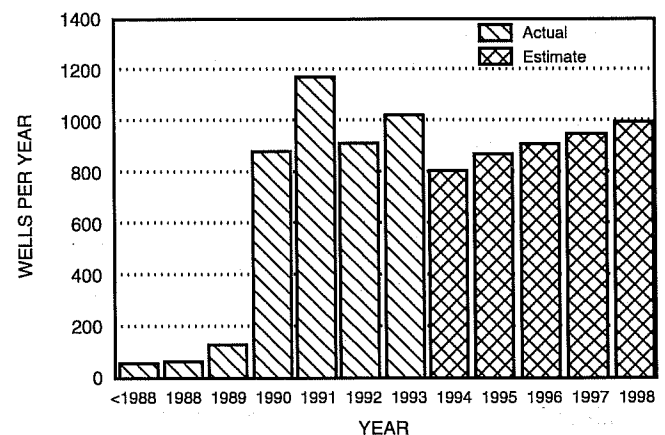


Fig. 3 Horizontal well forecast.

these data, which were obtained from Petroleum Information, American Petroleum Institute, and Spears and Associates, the number of wells drilled per year has been relatively constant in recent years and will remain at about the same level in the near future.

These data also show that the greatest application of horizontal technology was in 1991, with about 1160 horizontal wells completed. The next most active year was 1993, during which 1020 horizontal wells were completed in U.S. fields.

Technical developments are expected to continue to advance the application and improve the economics of horizontal technology. Chief among the industry's needs are tools to define reservoir characteristics and match them with horizontal well length, completion type, etc. Not all reservoirs are economic candidates for horizontal drilling. For example,

low-productivity horizontal wells that require gravel packing usually have a prohibitively high cost/benefit ratio. Other reservoirs may require a specific horizontal well length (longer is not always better) and completion to be economic.

Technical barriers and hindrances have been identified for which solutions are being or remain to be developed. Among these problems are the following:

1. *Wellbore location.* Tools need to be refined to assist in identifying the optimal wellbore location within the reservoir. Real-time geosteering (i.e., looking ahead of the bit and adjusting the wellpath on the basis of the geology encountered or about to be encountered) continues to be an important area of technical development.

2. *Completion design.* Advanced tools are needed to identify the optimal completion on the basis of the reservoir conditions actually encountered. Completion options for multibranch wells are also in need of development. Early versions did not allow for hydraulic isolation between the individual legs, but efforts continue to be directed toward solving this problem.

3. *Minimizing formation damage.* Improved operations and fluids are needed to minimize formation damage (skin damage). Longer horizontal sections allow damaging drilling fluids to be in contact with the formation for longer time periods. Fluid invasion can cause a significant reduction in effective permeability under these circumstances.

4. *Stimulation.* Wellbore stimulation is critical to the success of a horizontal well, both after drilling (if required) and during remedial workover operations. Operators and service companies are developing improved tools and chemicals for stimulation operations. Interesting areas in current development include the use of fracturing techniques (multiple minifrac) to overcome formation damage, hydraulic fracture design and control, and bypassing formation damage by drilling several short laterals.

5. *Workover technologies.* Improved water-gas identification and isolation tools and chemicals are needed for remedial operations. Chemical systems are being developed that can be injected into high-permeability zones to selectively block water influx.

6. *Field development.* New screening tools are needed to identify the optimal field development; horizontal wells in new and previously developed fields can be used for this procedure.

7. *Regulations.* Technical solutions are being developed for new and existing environmental and bureaucratic regulations.

Analysis of Canadian Horizontal Well Experience

On the basis of analyses of U.S. horizontal well data, it became apparent that the application of horizontal wells for domestic carbonate reservoirs producing light oil can be adequately documented and analyzed. Data describing clastic

reservoirs producing light or heavy oil are sparse, however, and applications of horizontal wells in these formations will be difficult to analyze on the basis of domestic data alone. A major objective of the project is to forecast the future application of horizontal technology in historically less popular formation types, including light and heavy oil in clastics.

Therefore the study has been expanded to include Canadian horizontal well application data. Canadian operators have exploited a wide variety of formation types with horizontal wells, including unconsolidated sands, fractured carbonates, tight reservoirs, and EOR projects (steam and miscible floods and bitumen production).

A listing of Canadian horizontal wells was obtained from Petroleum Information Canada. A total of 1422 wells was cited in four provinces: Saskatchewan (63%), Alberta (34%), British Columbia (3%), and Manitoba (<1%). These wells were drilled by about 140 operators.

Production surveys similar to those distributed to domestic operators were sent to most Canadian operators. Over 60 have been returned and are being analyzed by the project team. These data and results will be included in a separate section of the final report. Additionally, conclusions will be drawn from the Canadian experience with respect to lessons that can be applied effectively in the United States.

PRODUCTIVITY AND INJECTIVITY OF HORIZONTAL WELLS

Contract No. DE-FG22-93BC14862

**Stanford University
Stanford, Calif.**

**Contract Date: Mar. 10, 1993
Anticipated Completion: Mar. 10, 1998
Government Award: \$359,000
(Current year)**

**Principal Investigators:
F. John Fayers
Khalid Aziz
Thomas A. Hewett**

**Project Manager:
Thomas Reid
Bartlesville Project Office**

Reporting Period: Jan. 1-Mar. 31, 1994

Objectives

The project objectives include the following:

- *Modeling horizontal wells*—Establish detailed three-dimensional (3-D) methods of calculation that will successfully predict horizontal well performance under a range of reservoir and flow conditions, review both commercial simulators and simple inflow performance relationships used by the industry, investigate the sensitivity of various parameters on the performance of horizontal wells, and develop modeling techniques and computer codes based on generalized 3-D flexible gridding techniques that can be incorporated into reservoir simulators.

- *Reservoir characterization studies*—Investigate reservoir heterogeneity descriptions of interest to applications of horizontal wells, develop averaging techniques in three dimensions that will adequately compute effective single-phase and two-phase directional permeabilities within the variable gridding characteristics of the model developed in task 1, and perform sensitivity studies of the averaging technique to uncertainties in the heterogeneity distribution.

- *Experimental planning and interpretation*—Review technical literature on two-phase flow in pipes and the correlation of these results in terms of their relevance to horizontal wells; perform sensitivity studies to choose parameter spaces of interest for some typical field conditions using the advice of oil companies; plan key experiments to investigate sensitivity to parameter variation, including inflow distribution, completion variations, void fractions, etc.; perform data analysis, including flow pattern distribution, scaling, dependence on perforation intervals, confidence levels, etc.; and revise two-phase pressure drop in horizontal wells and incorporate this capability in the analytic solutions for critical rates task.

Summary of Technical Progress

Coning and cresting behavior in horizontal and vertical wells have been studied using the commercial simulator, Eclipse. The second quarterly report compared the predictions of five analytical methods for critical rates and presented the results in a table for a gas-cresting example problem.¹ This report contains the simulation results based on the same example problem for horizontal and vertical wells.

Critical Rates and Breakthrough Times in Horizontal and Vertical Wells— Simulation Results

Simulation results are presented for the coning and cresting critical rates for vertical and horizontal wells. The isotropic case of the gas coning example in Ref. 1 (also Example 8-7 of Ref. 2) with the same reservoir properties is used in the simulation runs. For the sake of completeness, the

parameters of the base example problem are repeated. The reservoir has a gas cap with a gas-oil contact 72 ft above a horizontal well length L of 1640 ft. Other parameters are a well radius (r) of 2640 ft, oil viscosity (μ_o) of 0.42 cP, oil formation factor (B_o) of 1.1 reservoir barrel (RB)/stock tank barrel (STB), finite density ($\Delta\rho$) of 0.48 g/cm³, well radius (r_w) of 0.328 ft, effective well radius (r_e) of 1489 ft, and permeability ($k_v = k_h$) of 70 mD. In the case of vertical wells, simulation results of critical rates are compared with four analytical solutions. The Wheatley analytical method³ agrees with the simulation results. The method of Meyer and Garder⁴ underestimates the critical coning rates, whereas the Chaperon method,⁵ which is only applicable to the case with the well at the bottom of the reservoir, overestimates the critical rate. The proposed method of Guo and Lee⁶ gives rates that are much higher than the simulation results (up to a factor of 14). It also predicts a maximum in the critical rate for a completion penetration fraction of about $1/3$. This feature of the Guo and Lee method is contrary to the simulation behavior as well as to the solution of the other three analytical methods.

Another important feature of horizontal wells is their ability to delay gas or water breakthrough into the well. Simulation runs were made to compare the breakthrough times of the crest into the horizontal well with the analytical results of Papatzacos et al.⁷ It is shown that horizontal wells can significantly postpone the breakthrough time of gas into the well in comparison with vertical wells.

Summary of Wheatley's Method

Wheatley³ presents an approximate analytical theory for the problem of water coning into a partially penetrating oil well. Figure 1 shows the schematic of the problem. The reservoir is taken to be homogeneous and bounded above by a horizontal impermeable barrier extending to the drainage

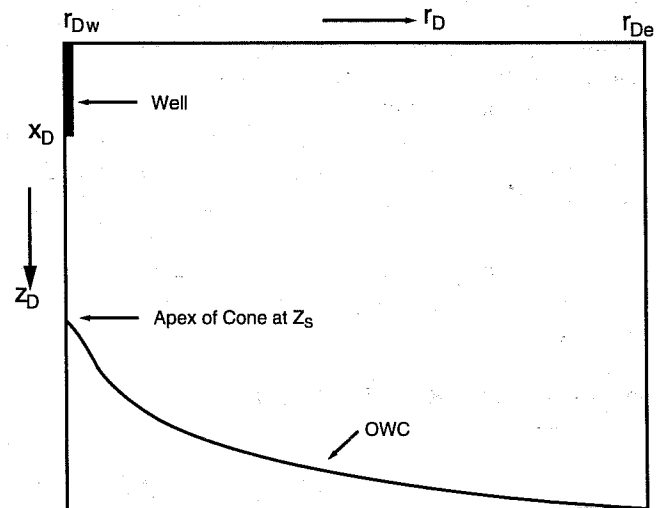


Fig. 1 Schematic of the water coning problem. Z_s , dimensionless depth. OWC, oil-water contact.

radius (r_{De}) from the well. The influx of oil at the drainage radius is assumed to be steady and radially symmetric. The flow region is bounded below by the oil–water contact (OWC), which is deformed toward the well as a result of the reduction in pressure near the well.

Wheatley defined the fluid potential, Φ , in the oil phase, parametrically, as follows:

$$\Phi = \frac{q}{aX_D - b} (A_1 + aA_2 + bA_3 - A_4) \quad (1)$$

where

$$A_1(r_D, Z_D) = 2 \ln r_D - g(r_D, Z_D - Y_D) + g(r_D, Z_D + Y_D) \quad (2)$$

$$A_2(r_D, Z_D) = g(r_D, Z_D - X_D) - g(r_D, Z_D + X_D) \quad (3)$$

$$A_3(r_D, Z_D) = f^{-1}(r_D, Z_D - X_D) + f^{-1}(r_D, Z_D + X_D) \quad (4)$$

$$A_4(r_{De}, 1) = A_1(r_{De}, 1) + aA_2(r_{De}, 1) + bA_3(r_{De}, 1) \quad (5)$$

$$f(r, z) = (r^2 + z^2)^{1/2} \quad (6)$$

$$g(r, z) = \ln [z + f(r, z)] \quad (7)$$

The dimensionless parameters and variables are the fractional completion penetration; $X_D = x/h$, the dimensionless radius $r_D = r(k_v/k_h)^{1/2}/h$, and the dimensionless depth $Z_D = z/h$; h is the thickness of oil column; and k_v and k_h are the vertical and horizontal permeabilities. Y_D is a dimensionless depth, to be determined for the start of a semi-infinite line source on the well axis.

Construction of the potential function in Eq. 1 is based on an ingenious combination of line and point source terms to satisfy the Laplace equation. In addition, the potential function in Eq. 1 satisfies exactly or nearly exactly all the boundary conditions of the problem:

- $\Phi = 0$ at r_{De} and $Z_D = 1$ and is approximately zero at r_{De} for $0 < Z_D < 1$.
- $\Phi = -\Delta p$, the maximum pressure drop across the reservoir at r_{Dw} and $Z_D = 0$. Φ is approximately constant at r_{Dw} for $0 < Z_D \leq X_D$.
- $\Phi = -\Delta p g h(1 - z)$ on the OWC, which is actually the streamline.
- $\partial\Phi/\partial z = 0$ on $Z_D = 0$ and $\partial\Phi/\partial r = 0$ on $r_D = 0$ and $Z_D > X_D$.

The line source strength q can be computed from

$$q = q_{DC} \Delta p g h(aX_D - b) \quad (8)$$

once q_{DC} , a , b , and Y_D have been determined. The unknown parameters are q_{DC} , the dimensionless critical rate; a and b , relative strengths of line and point sources, respectively; Y_D , the dimensionless depth of the line source; and Z_S , the dimensionless depth to the apex of the cone.

Wheatley³ has proposed an iterative procedure to determine these unknowns along with the critical oil rate. His procedure has been employed in obtaining the relevant results reported in the next section. A step-by-step outline of the procedure is given:

1. Choose an initial guess value of Z_S slightly less than one and set $Y_D = 1$.

2. Calculate a , b , and Y_D by iteration from:

$$aX_D - b = (r_{De} - Y_D)/(r_{De} - 1) \quad (9)$$

$$b/r_{Dw} = a \ln(r_{Dw}/X_D) - \ln(1 - X_D^2/Y_D^2) \quad (10)$$

$$Y_D^2 = Z_S^2 + \frac{Z_S(Z_S^2 - X_D^2)^2}{(aX_D - b)(Z_S^2 - X_D^2) - 2bX_D^2} \quad (11)$$

3. Calculate the dimensionless rate from

$$q_D = (Z_S - 1)/(A_1 + aA_2 + bA_3 - A_4) \quad (12)$$

where A_1 , A_2 , and A_3 are evaluated from Eqs. 2 to 7 at $r_D = 0$ and $Z_D = Z_S$.

4. Reduce the estimate for Z_S and recompute a , b , Y_D , and q_D .

5. Repeat step 4 until a maximum in q_D is obtained, above which self-consistent values of a , b , Y_D , and Z_S cannot be obtained.

6. Reduce Z_S , keeping a , b , and Y_D fixed, and recompute q_D using Eq. 12. Note that A_1 , A_2 , and A_3 are functions of Z_S .

7. Repeat step 6 until a new maximum $q_D = q_{DC}$ is obtained, where $Z_S = Z_{Smin}$.

8. Finally, compute the critical rate from

$$q_c = 6.145 \times 10^{-3} h^2 k_h \Delta p q_{DC} / \mu_o B_o \quad (13)$$

where q_c = critical oil production rate, STB/d

h = oil zone thickness, ft

k_h = horizontal permeability, mD

Δp = density difference, g/cm³

μ_o = oil viscosity, cP

B_o = oil formation volume factor, RB/STB

The same procedure can be used for the gas coning problem (as used here) by taking the origin of Z_D at the bottom of the oil zone. The resulting potential function has the same properties given above, where Δp in Eq. 8 becomes Δp_{og} .

Results and Discussion

Critical Rates

The analytical solutions for coning and cresting critical rates are all based on the assumption of a steady-state condition among other assumptions (see Ref. 1). Most commercial black oil simulators, like Eclipse (used here), do not provide the user with an easy option of specifying constant potential at the outer lateral boundaries of the reservoir. To set up such a boundary condition, oil injectors were used in the oil zone and gas injectors in the gas cap with specified bottomhole pressure controls to eventually achieve the steady-state condition in the reservoir. Care has to be taken in selecting a fine grid for a 3-D model. Advantage can be taken of symmetry, which allows one quarter of a square pattern area to be studied. It is also desirable to select relative permeabilities that will help development of a sharp interface. Determining a critical rate by simulation involves a number of iterative runs in which the oil production rate is varied until a maximum rate is found for which the gas-oil interface eventually reaches steady state before breaking through into the well. Sometimes breakthrough occurs after a very long period.

The simulation results for vertical wells are presented first. The same reservoir properties and parameters as those given in the previous section are used for a gas coning case. Figure 2 shows the variation of the critical rate with the completion penetration fraction X_D . It also compares the simulation results for critical coning rates with the analytical results from Wheatley,³ Meyer and Garder,⁴ Chaperon,⁵ and Guo and Lee.⁶ The coning critical rates from simulations agree with the predictions of Wheatley's method very well (within 5% difference). With the use of the Meyer and Garder method, known in the literature to underestimate critical rates, the critical rates for this example problem were underestimated also. Chaperon's equation, which is only applicable to the case where the well is at the bottom of the reservoir, overestimates the simulation result for that well location by 28%. The recently proposed model of Guo and Lee⁶ gives results much higher (up to a factor of 14) than the simulation results. In addition, it gives an optimum completion penetration fraction of about $1/3$, whereas all the other methods and the simulations predict a value of zero for the optimum completion penetration fraction (assuming that a constant total well rate is possible).

A simulation procedure similar to that described is employed to determine the critical rate for an infinite horizontal well and uses a two-dimensional (2-D) $x-z$ grid. Figure 3 displays a comparison between critical rates for vertical and horizontal wells. It is assumed that the completion interval of the vertical well is to the same height as the position of the horizontal well (with fixed length of 1640 ft). The results indicate a marginally higher critical rate for the horizontal well (about 25% higher). This seems to be a rather modest improvement over the vertical well, which might not justify the use of horizontal wells with their higher drilling costs in a field application. Figure 4 shows the effect of the reservoir horizontal dimension x_e on the critical rate of the horizontal well. These carefully executed simulations

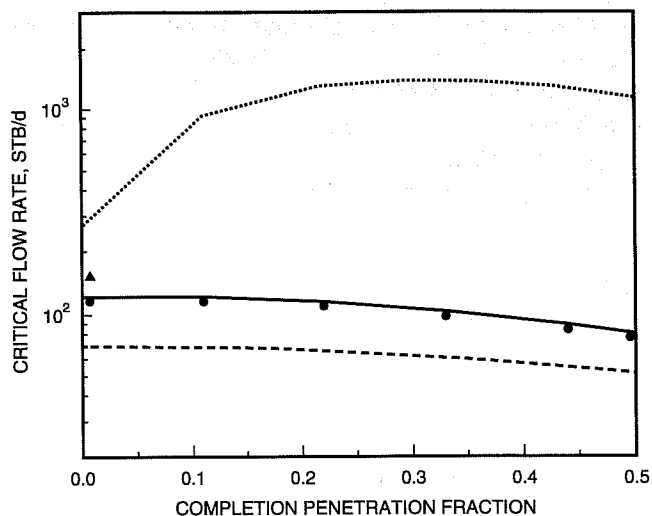


Fig. 2 Comparison of critical rates between simulation and analytical solutions for the vertical well at various completion penetration fractions. ●, simulation. —, Wheatley.³, Guo and Lee.⁶ ---, Meyer and Garder.⁴ ▲, Chaperon.⁵

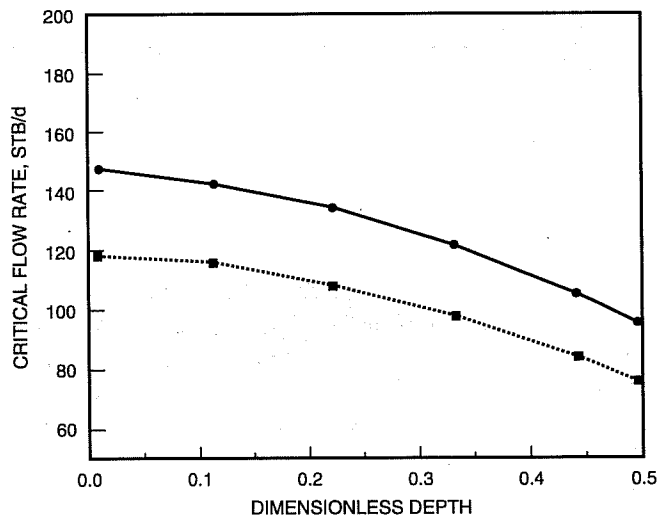


Fig. 3 Comparison of critical rates of horizontal (—●—) and vertical (.....) wells at various dimensionless depths from simulations.

show a sharp decrease in the critical cresting rate from high critical rates at close spacing followed by a long, slowly declining tail as the spacing increases. Note that Joshi's method² overestimates the simulation results by a factor of about 2.5. In fact, for an infinite reservoir, there is no critical rate and the true steady state condition is only possible for a zero rate (see Papatzacos et al.⁷ and references therein). This is consistent with the slow decrease of the critical rate toward zero as shown in Fig. 4. It is known that the interface behaves like a stretched elastic band so that when the anchor points at the reservoir boundary are far enough apart, the band readily deforms into the horizontal well. The major impact of horizontal wells derives from their ability to postpone the breakthrough of gas into the well.

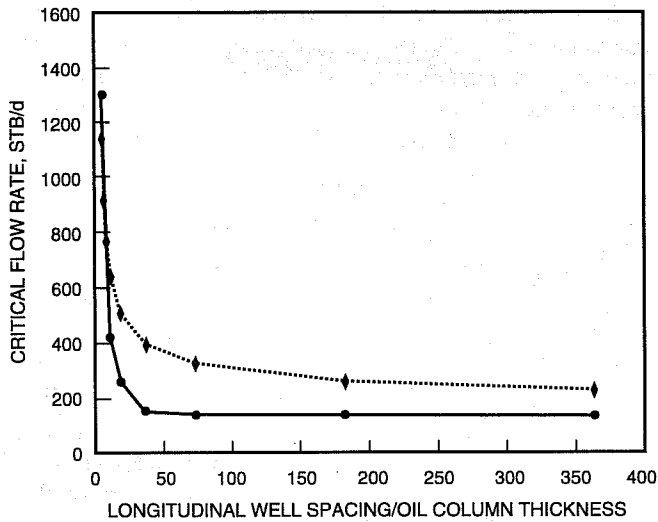


Fig. 4 Variation of the critical rate with the horizontal dimension of the reservoir for the horizontal well. —●—, simulation data.♦...., Joshi's solution.²

Breakthrough Times

Papatzacos et al.⁷ report semianalytical solutions for cone breakthrough times for horizontal wells. Their solutions are derived by a moving boundary method with assumption of either constant pressure or gravity equilibrium in the cone. Final results of that work are given here. Details can be found in Ref. 7 and references therein. Two types of conditions are used at the moving crest interface. One is the assumption of constant pressure at the moving boundary which results in the breakthrough time given by

$$t_{BtD} = \frac{1}{6q_D} \quad (14)$$

where the dimensionless oil rate and time are defined in consistent units by

$$q_D = \frac{\mu_o B_o}{2\pi(k_v k_h)^{1/2} h \Delta \rho g} q_o$$

$$t_{BtD} = \frac{\Delta \rho g k_v t}{h \phi \mu_o} \quad (15)$$

The second condition is the assumption of vertical equilibrium in the crest. The solution has been determined by the method of fast Fourier transform (FFT). For $q_D > 0.4$, researchers have been able to close the iteration procedure and explicitly find

$$t_{BtD} = 1 - (3q_D - 1) \ln[3q_D / (3q_D - 1)] \quad (16)$$

For large values of q_D , Eq. 14 becomes equal to Eq. 16. For values of $q_D \leq 1/3$, the FFT solution should be used. A simpler approach is to use instead a quadratic fit to the FFT solution given by Ref. 7,

$$\ln(t_{BtD}) = -1.7179 - 1.1633 U + 0.16308 U^2 - 0.046508 U^3 \quad (17)$$

where $U = \ln(q_D)$.

Figure 5 displays simulation results for breakthrough times for a horizontal well located at the bottom of the reservoir along with the results for a horizontal well 8 ft above the bottom of the reservoir. In both cases the distance between well and the gas-oil interface is fixed at 72 ft. At $t_{BtD} = 2.0$ in this problem, the corresponding real time is 252 d, and $q_D = 1.0$ is equivalent to a rate of 13715 STB/d. The predictions of the semianalytical results discussed previously are also shown. Simulation results are closer to the predictions based on the gravity equilibrium condition in Eq. 16 for values of $q_D < 0.3$. Sensitivity of the location of the well is more pronounced for lower flow rates as shown in Fig. 5.

A marginally higher critical rate was found for the horizontal well in comparison with the vertical well for the example problem. The important practical factor is not how much higher the critical rate of horizontal wells is relative to those of vertical wells, but rather how much longer a reservoir can be produced without breakthrough of a cone using horizontal wells in comparison with vertical wells. To address this issue one can produce the reservoir at supercritical rates by horizontal and vertical wells and determine the breakthrough times.

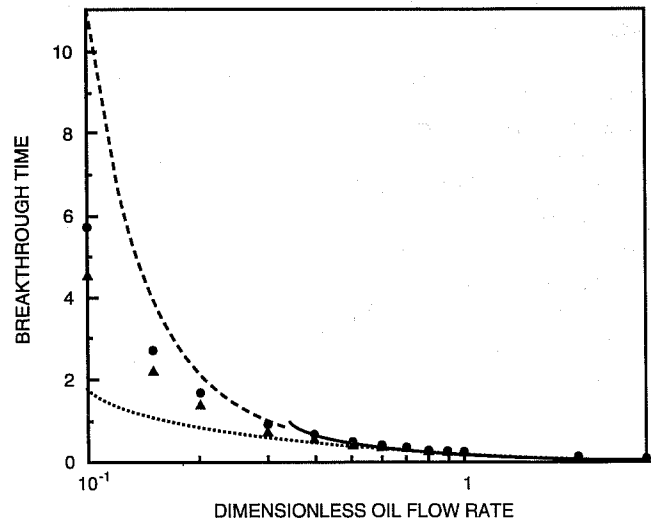


Fig. 5 Comparison of breakthrough times between simulation and solutions of Ref. 7 for horizontal wells. ----, Fit of fast Fourier transform solution (Eq. 17). —, gravity equilibrium solution (Eq. 16)., constant pressure solution (Eq. 14). ●, simulation of horizontal well at the bottom. ▲, simulation of horizontal well 8 ft above the bottom.

The critical coning and cresting rates were estimated from the simulations. It is then possible to produce the reservoir at a higher rate obtained by a fixed factor increase in the corresponding critical rates for horizontal and vertical wells, respectively. Results for the wells at the bottom of the reservoir are shown in Fig. 6, where a significant advantage of horizontal wells in postponing the breakthrough of gas into the well is clearly observed. For example, a factor of about 50 is obtained in extending the breakthrough time with the horizontal well producing at a rate of 9.3 times its critical rate. In this case, gas breakthrough occurs at 721 d for the horizontal well, whereas it only takes 15 d for the breakthrough in the vertical well at the same relative flow rate condition. This implies a hypothetical condition of a vertical well of almost zero length flowing at 9.3 times its critical rate.

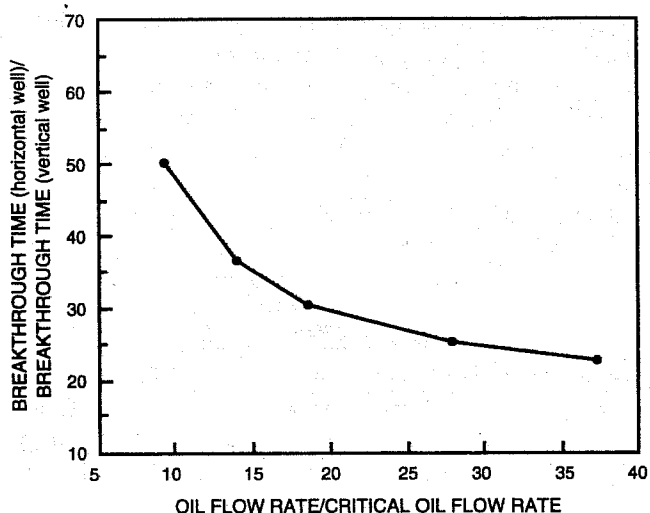


Fig. 6 Comparison of breakthrough times for horizontal and vertical wells at various supercritical rates from simulations. —●—, simulation data.

Conclusions

The analytical solution of Wheatley³ appears to give accurate values for the critical coning rates of vertical wells. For the gas coning example studied, the Wheatley solutions for the critical rates are within 5% of the corresponding simulation results. The analytical solutions for the critical cresting rates for horizontal wells give a wide range of predictions. Joshi's method² is less restrictive on the location of the horizontal well; although it overestimated the simulation results by as much as a factor of 2.5, it might be regarded as the preferred method over the other analytical solutions. The solutions of Guo and Lee⁶ for both horizontal and vertical wells predict much higher critical rates than the simulation results and the other analytical methods. For instance, their method predicts a critical rate of 2759 STB/d for the base problem with the horizontal well at the bottom, whereas the simulation gives a critical rate of 148 STB/d.

It is concluded that the important cresting property for horizontal wells is not so much their critical rate but rather their delayed breakthrough time. This trait of horizontal wells becomes more significant as the well spacing becomes longer.

References

1. Annual Report, *Productivity and Injectivity of Horizontal Wells*, Contract No. DE-FG22-93BC14862, October 1, 1992–September 30, 1993.
2. S. D. Joshi, *Horizontal Well Technology*, pp. 285-292, Pennwell Books, Tulsa, Okla., 1991.
3. M. J. Wheatley, An Approximate Theory of Oil/Water Coning, paper SPE 14210 presented at the SPE 60th Annual Meeting, Las Vegas, Nev., Sept. 22–25, 1985.
4. H. L. Meyer and A. O. Garder, Mechanics of Two Immiscible Fluids in Porous Media, *J. Appl. Phys.*, 25(11): 1400-1406 (November 1954).
5. I. Chaperon, Theoretical Study of Coning Toward Horizontal and Vertical Wells in Anisotropic Formations: Subcritical and Critical Rates, paper SPE 15377 presented at the SPE 61st Annual Meeting, New Orleans, La., Oct. 5–8, 1986.
6. B. Guo and R. L-H. Lee, A Simple Approach to Optimization of Completion Interval in Oil/Water Coning Systems, *SPE Reserv. Eng.*, 8(4): 249-255 (November 1993).
7. P. Papatzacos et al., Cone Breakthrough Time for Horizontal Wells, *SPE Reserv. Eng.*, 6(3): 311-318 (August 1991).

DETAILED EVALUATION OF THE WEST KIEHL ALKALINE-SURFACTANT-POLYMER FIELD PROJECT AND ITS APPLICATION TO MATURE MINNELUSA WATERFLOODS

Contract No. DE-AC22-93BC14860

Surtek, Inc.
Golden, Colo.

Contract Date: Jan. 7, 1993
Anticipated Completion: Sept. 30, 1994
Government Award for FY94: \$165,148

Principal Investigator:
Malcolm J. Pitts

Project Manager:
Thomas Reid
Bartlesville Project Office

Reporting Period: Jan. 1–Mar. 31, 1994

Objectives

The objectives of this research are to (1) quantify the incremental oil produced from the West Kiehl alkaline-surfactant-polymer (ASP) project by classical engineering and numerical simulation techniques, (2) quantify the effect of chemical slug volume on incremental oil in the two swept areas of the field, (3) determine the economics of the application of the ASP technology, (4) forecast the results of injecting an ASP solution to mature waterfloods and polymer floods, and (5) provide the basis for independent operators to book additional oil reserves by using the ASP technology.

Summary of Technical Progress

Geological and Reservoir Engineering Evaluation

A geological study of 72 Minnelusa fields surrounding the West Kiehl is complete. Of the 72 fields, 35 were studied in detail. Current and estimated ultimate oil recovery data were developed for each of the 35 fields using decline curve analysis.

From this list of 35 fields, 2 fields [Simpson Ranch (polymer flood) and Prairie Creek South (waterflood)] were selected for numerical simulation. A series of geologic maps and cross sections have been prepared, and reservoir simulation models will be run on both of these fields.

The remaining 33 fields were also subjected to reservoir analysis. Each of these fields has been mapped in a slightly less rigorous manner than West Kiehl, Prairie Creek South, and Simpson Ranch. Pore volumes and oil saturations were calculated. The production histories were subjected to decline analysis to determine ultimate primary and secondary oil recoveries. From the primary performance characteristics, reservoirs with a water drive, a partial water drive, and no water drive were defined. A table of information about each field, an isopachous map, and a plot of the oil production, oil cut, and injection rate was developed for each of the 35 fields.

Laboratory Study

Two linear corefloods and seven radial corefloods were completed. Relative permeability analysis indicated that the Minnelusa Lower B sand is water-wet, and the mobility ratio for water-displacing West Kiehl oil averages 2.2. Oil saturation shifts were from 0.788 to 0.343 pore volume (PV), for a recovery of 56.5% of the initial oil saturation by coreflooding. Injection of polymer (Pusher 700) after the waterflood recovered no additional oil. Injection of 0.8 wt % sodium carbonate (Na_2CO_3) plus 0.1 wt % Petrostep B-100 plus Pusher 700 reduced the oil saturation to 0.207 PV for an additional recovery 0.136 PV of incremental oil or 39.7% of the waterflood residual oil. Dynamic retention of chemical from the linear corefloods averaged 72,966 lb/acre-ft for Na_2CO_3 , 5,123 lb/acre-ft for Petrostep B-100, and 723 lb/acre-ft for Pusher 700 injected with Na_2CO_3 plus Petrostep B-100, and

314 lb/acre-ft when injected dissolved in Fox Hills water prior to ASP solution. When Pusher 700 dissolved in injection water was injected after the ASP solution, an additional 49 lb/acre-ft was retained by the Minnelusa sand. On the basis of resistance factor and chemical retention data of these linear corefloods, the injection concentration of 1,050 mg/L Pusher 700 is considered to be sufficient for mobility control if 1 PV of polymer were injected.

Chemical oil recoveries of the radial corefloods using 4-in. radial disks are summarized in Table 1. The chemical floods were performed with no waterflood prior to chemical injection with the exception of two corefloods.

The average polymer flood performed no better than the average waterflood, 42.8% S_{oi} vs. 46.6% S_{oi} , respectively. However, injection of 0.8 wt % Na_2CO_3 plus 0.1 wt % Petrostep B-100 plus 1,050 mg/L Pusher 700 recovered 15% S_{oi} . Additional oil was recovered when 30% PV or more of ASP slug was injected. Reduction of the volume of ASP slug injected to 13% PV lowered the incremental oil production to 6.2% S_{oi} .

TABLE 1

Chemical Oil Recoveries of the Radial Coreflood with 4-in. Radial Disks

Chemical injected	Waterflood recovery, % S_{oi}	Chemical flood recovery, % S_{oi}	Combined recovery, % S_{oi}
Waterflood followed by 37% PV ASP	45.4	12.6	58.0
Waterflood followed by 13% PV ASP	47.7	5.5	53.2
29% PV ASP-10% PV polymer	-	61.2	-
13% PV ASP-26% PV polymer	-	52.7	-
94% ASP-no polymer	-	65.9	-
43% polymer	-	40.0	-
35% polymer	-	45.7	-

Note: S_{oi} , initial oil saturation. ASP, alkaline-surfactant-polymer.

Numerical Simulation of the West Kiehl Field

A history match was done to calibrate the chemical option of the numerical simulator for three radial corefloods. These matches included waterflood to residual oil saturation (ROS) followed by Na_2CO_3 -Petrostep B-100 Pusher solution injection; Na_2CO_3 plus Petrostep B-100 plus Pusher 700 injection; and Pusher 700 injection.

The initial West Kiehl reservoir model has been designed. The chemical flood model parameters defined in the corefloods history matches have been incorporated into the numerical simulator. The oil production rate and water cut history match of the West Kiehl are shown in Fig. 1. No ASP, polymer flood, or waterflood forecasts have been performed.

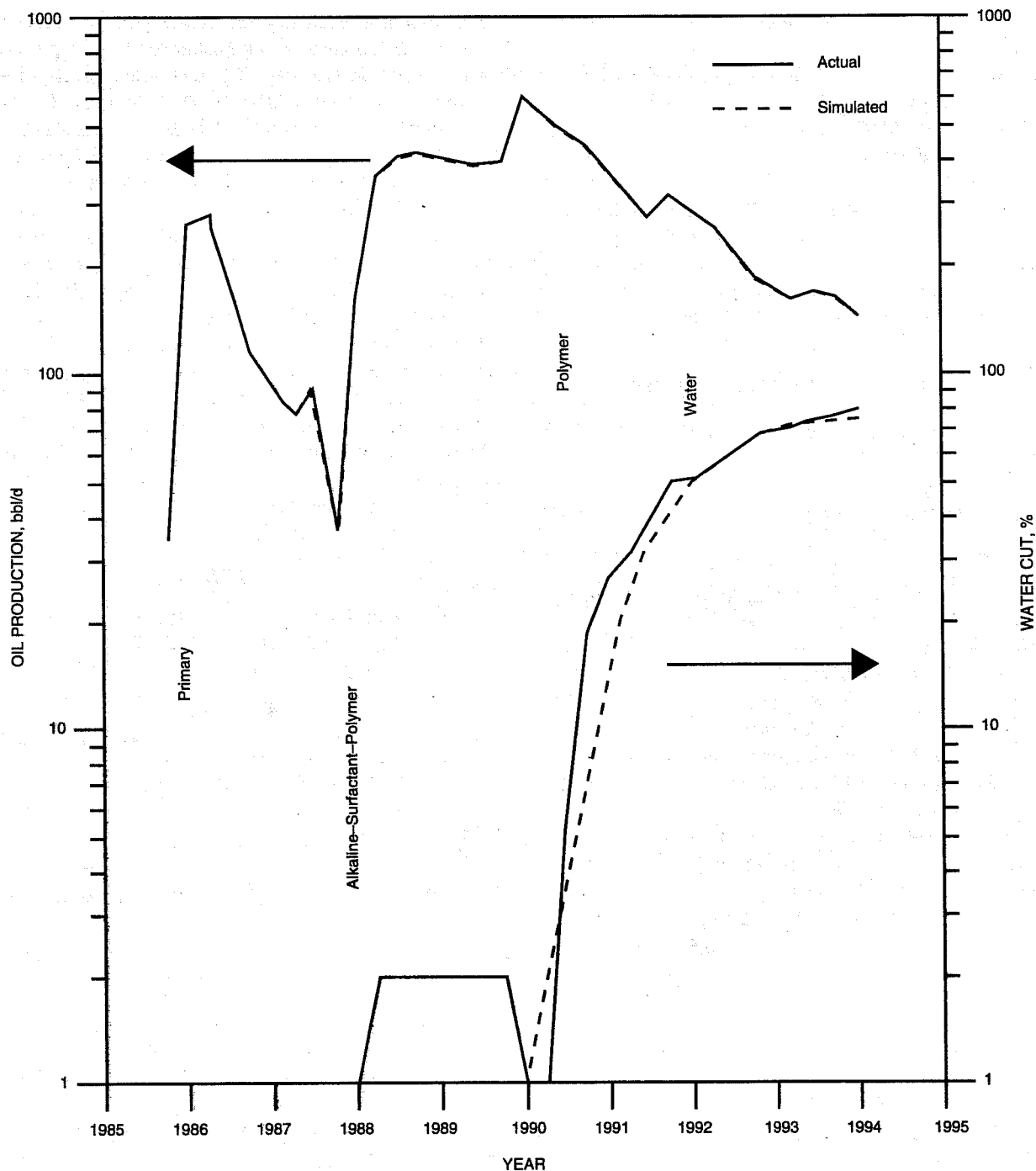


Fig. 1 Oil production rate and water cut history match of West Kiehl.

Simulation Analyses Application to Waterflooded Minnelusa Fields

The grid systems have been designed and the initial reservoir properties interpolated for the Prairie Creek South and the Simpson Ranch reservoir models. History matches have not been achieved.

References

1. S. R. Clark, M. J. Pitts, and S. M. Smith, Design and Application of an Alkaline-Surfactant-Polymer Recovery System to the West Kiehl Field, *SPE Adv. Technol. Ser.*, 1(1): 172-179 (April 1993).
2. J. J. Meyers, M. J. Pitts, and K. Wyatt, *Alkaline-Surfactant-Polymer Flood of the West Kiehl, Minnelusa Unit*, paper SPE 24144 presented at the SPE/DOE Eighth Symposium on Improved Oil Recovery, Tulsa,

THERMAL RECOVERY— SUPPORTING RESEARCH

***STUDY OF HYDROCARBON MISCIBLE
SOLVENT SLUG INJECTION PROCESS
FOR IMPROVED RECOVERY OF HEAVY
OIL FROM SCHRADER BLUFF POOL,
MILNE POINT UNIT, ALASKA***

Contract No. DE-FG22-93BC14864

**University of Alaska
Fairbanks, Alaska**

Contract Date: Dec. 1, 1992

Anticipated Completion: June 30, 1996

Total Project Cost:

DOE Funding for FY94	\$200,000
Contractor	129,726
Total	\$329,726

**Principal Investigator:
G. D. Sharma**

**Project Manager:
Thomas Reid
Bartlesville Project Office**

Reporting Period: Jan. 1–Mar. 31, 1994

Objectives

The ultimate objective of this 3-yr research project is to evaluate the performance of the hydrocarbon miscible solvent slug process and to assess the feasibility of this process for improving recovery of heavy oil from Schrader Bluff reservoir. This will be accomplished through measurement of pressure–volume–temperature (PVT) and fluid properties of Schrader Bluff oil, determination of phase behavior of Schrader Bluff oil solvent mixtures, asphaltene precipitation tests, slim-tube displacement tests, coreflood experiments, and reservoir simulation studies. The expected results include determination of optimum hydrocarbon solvent composition suitable for hydrocarbon miscible solvent slug displacement process, optimum slug sizes of solvent needed, solvent recovery factor, solvent requirements, extent and timing of solvent recycle, displacement and sweep efficiency to be achieved, and oil recovery.

Summary of Technical Progress

During this quarter more displacement experiments in slim-tube and miscible coreflood experiments were conducted. Also, work has been initiated to match the slim-tube displacement results with the use of GEM, a compositional simulator developed by the Computer Modeling Group.

Slim-Tube Experiments

Three experimental displacement runs were conducted in the slim-tube apparatus. Solvents used for these tests were carbon dioxide (CO₂) and various enrichments of CO₂ with natural gas liquids (NGLs).

1. *100% CO₂ at 1300 psia and 72 °F.* This run was conducted with the use of 100% CO₂ as solvent at 1300 psia and 72 °F. This run resulted in recovery of 71% at 1.2 pore volume (PV) injection (Fig. 1). This shows that there is no development of miscibility. Sight glass observations also showed the presence of two phases. Figure 2 shows that solvent breakthrough occurred around 67% PV injection.

2. *90% CO₂ and 10% NGLs at 1300 psia and 72 °F.* This run was conducted by enriching CO₂ with 10 mol % NGL. Oil recovery at 1.2 PV injection improved to 86% (Fig. 3). This increase in recovery was caused by the presence of intermediates in the solvent, but sight glass observations indicated the presence of two phases. Figure 4 shows that solvent breakthrough occurred after 85% of PV injection.

3. *85% CO₂ and 15% NGLs at 1300 psia and 72 °F.* This run was conducted by enriching CO₂ with 15 mol % NGL at 1300 psia and 72 °F. Oil recovery after the injection of 1.2 PV increased to 96% (Fig. 5). Sight glass observations did not indicate the presence of phases. Thus it was inferred that miscibility was developed in this experiment. Figure 6 shows that solvent breakthrough occurred after 99% PV injection.

Coreflood Experiments

After initial unsteady-state waterflood experiment, further experiments were conducted to study the effect of miscible slug size on recovery. Three experiments with slug sizes of 5, 10, and 20% PV were conducted. The miscible solvent used in these experiments was a mixture of 50% NGLs and 50% Prudhoe Bay natural gas, which is miscible with Schrader Bluff oil. Results of these experiments are shown in Figs. 7 to 15.

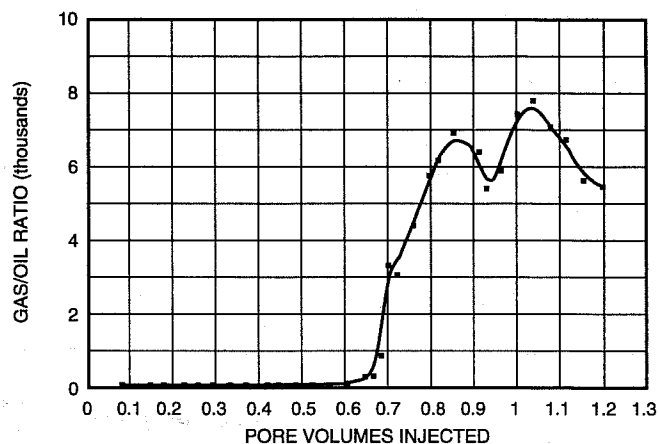


Fig. 2 Illustration showing gas/oil ratio vs. pore volumes injected (solvent, 100% carbon dioxide).

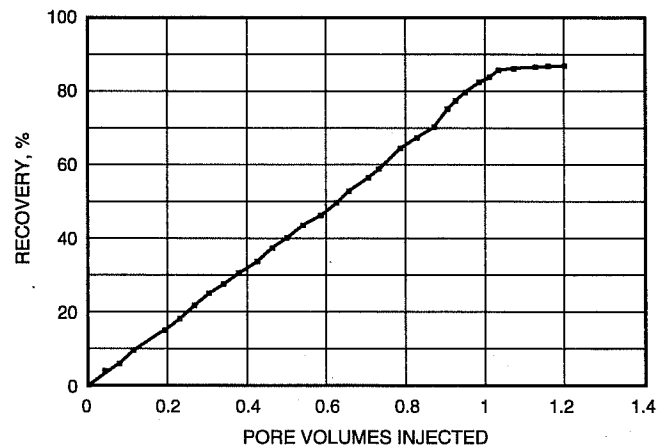


Fig. 3 Illustration showing recovery vs. pore volumes injected (solvent, 90% carbon dioxide and 10% natural gas liquids).

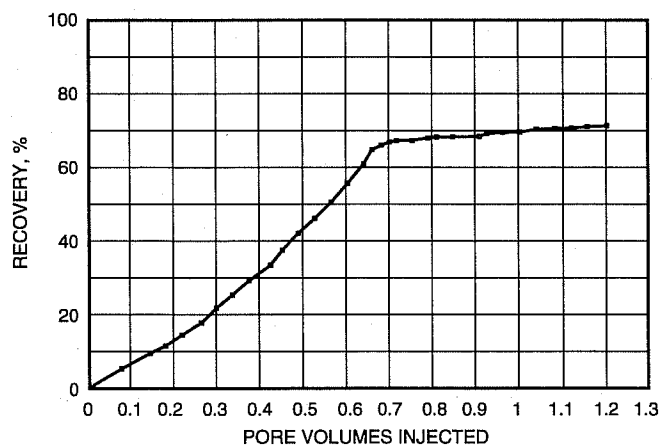


Fig. 1 Illustration showing recovery vs. pore volumes injected (solvent, 100% carbon dioxide).

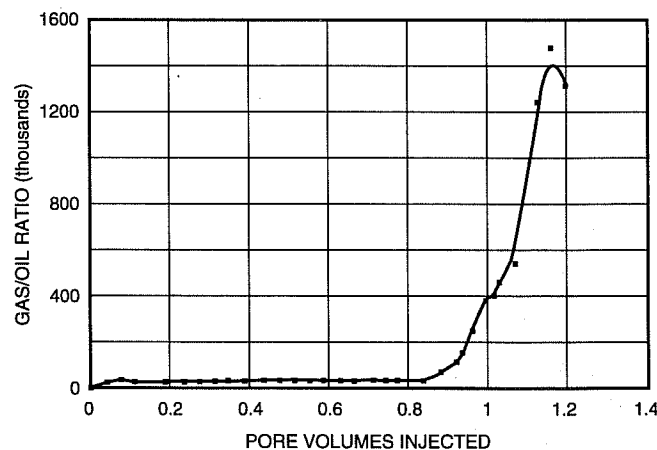


Fig. 4 Illustration showing gas/oil ratio vs. pore volumes injected (solvent, 90% carbon dioxide and 10% natural gas liquids).

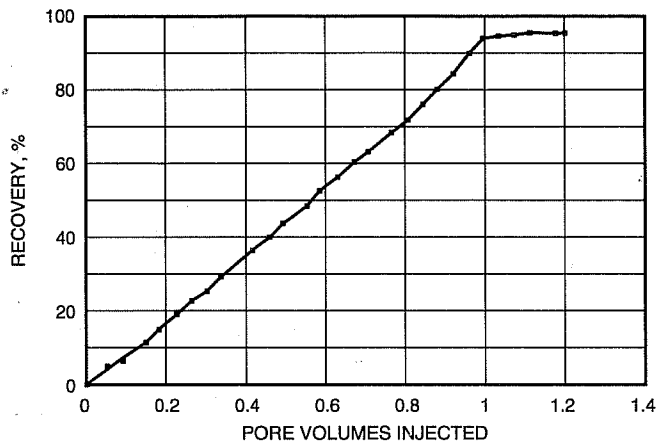


Fig. 5 Illustration showing recovery vs. pore volumes injected (solvent, 85% carbon dioxide and 15% natural gas liquids).

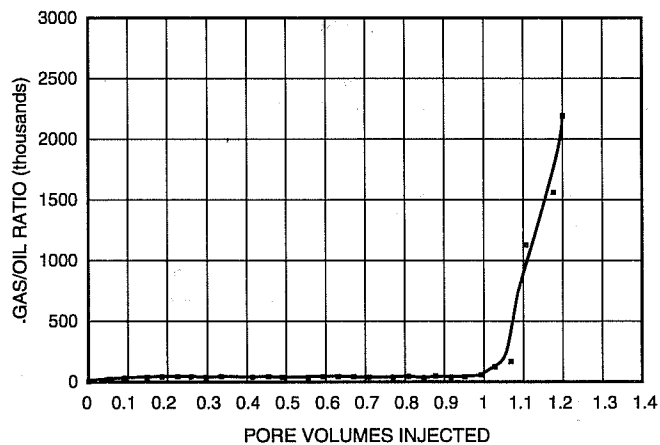


Fig. 6 Illustration showing gas/oil ratio vs. pore volumes injected (solvent, 85% carbon dioxide and 15% natural gas liquids).

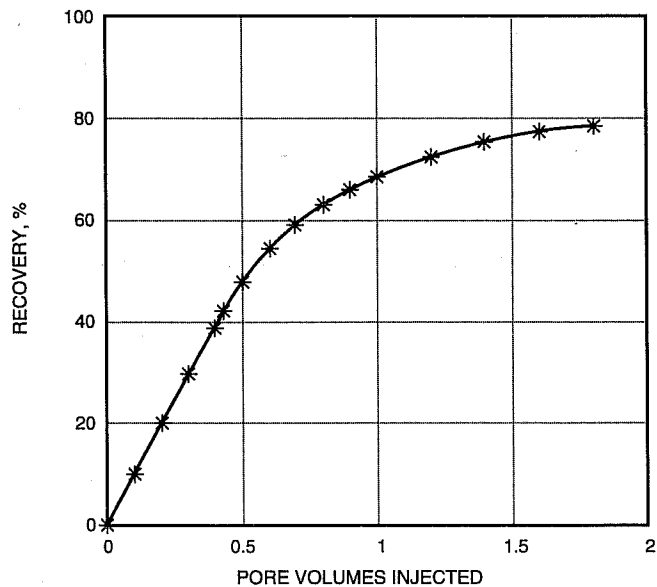


Fig. 7 Illustration showing recovery vs. pore volumes injected (slug size, 0.05 pore volume). —*, oil recovery.

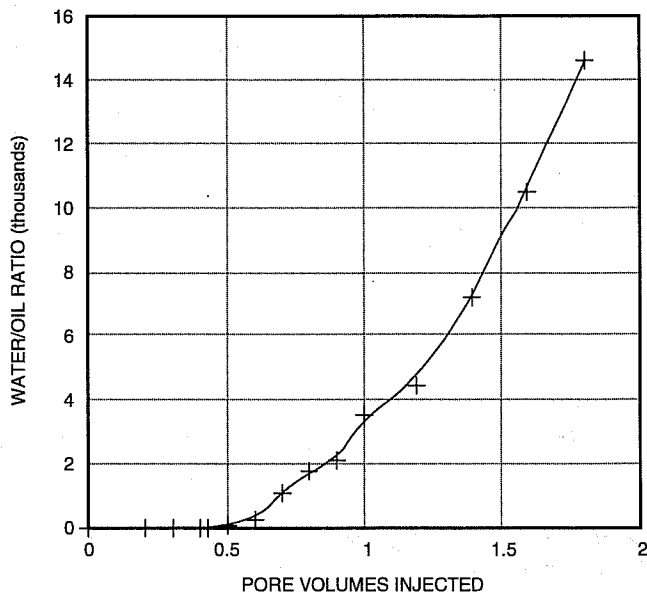


Fig. 8 Illustration showing water/oil ratio vs. pore volumes injected (slug size, 0.05 pore volume). +, water/oil ratio.

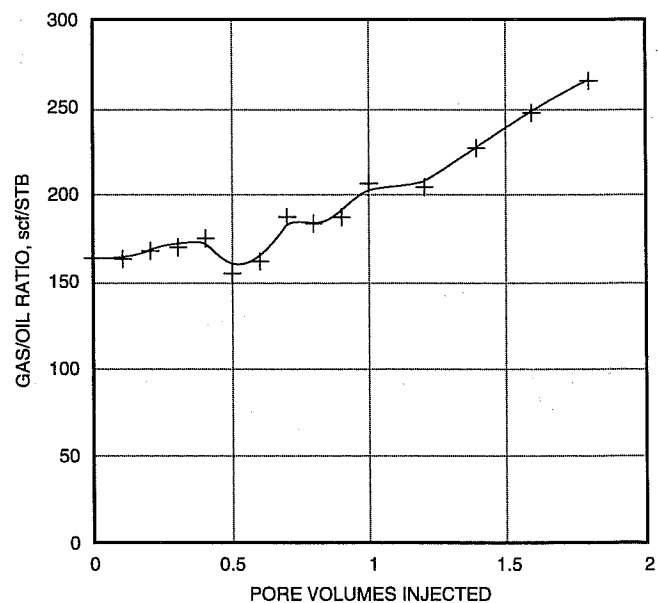


Fig. 9 Illustration showing gas/oil ratio vs. pore volumes injected (slug size, 0.05 pore volume). +, incremental gas/oil ratio.

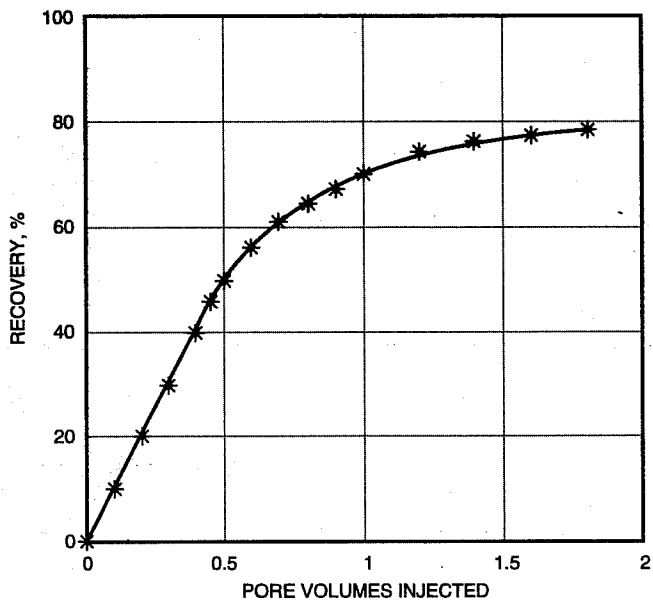


Fig. 10 Illustration showing recovery vs. pore volumes injected (slug size, 0.1 pore volume). —*—, oil recovery.

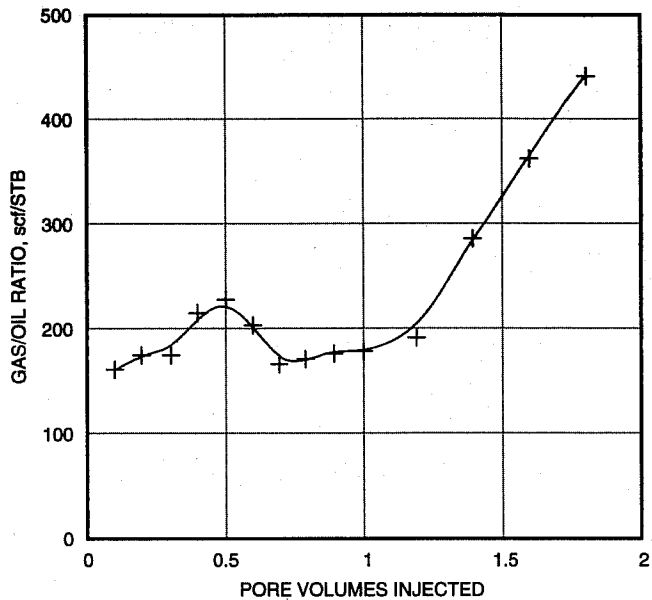


Fig. 12 Illustration showing gas/oil ratio vs. pore volumes injected (slug size, 0.1 pore volume). +, incremental gas/oil ratio.

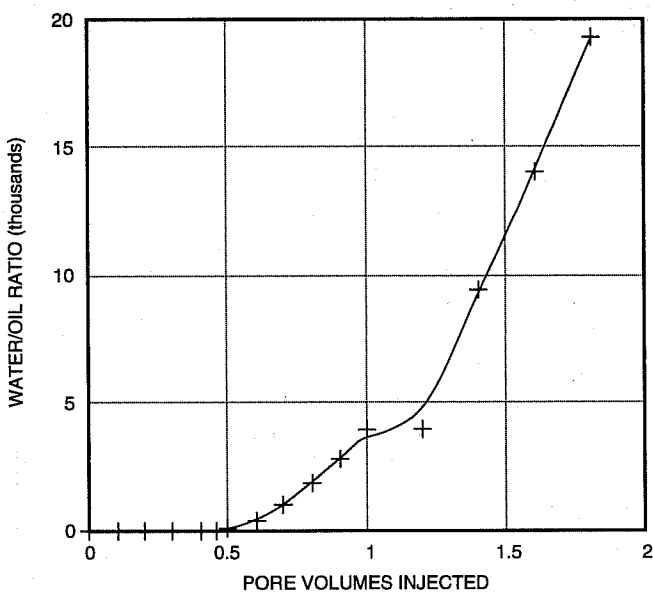


Fig. 11 Illustration showing water/oil ratio vs. pore volumes injected (slug size, 0.1 pore volume). +, water/oil ratio.

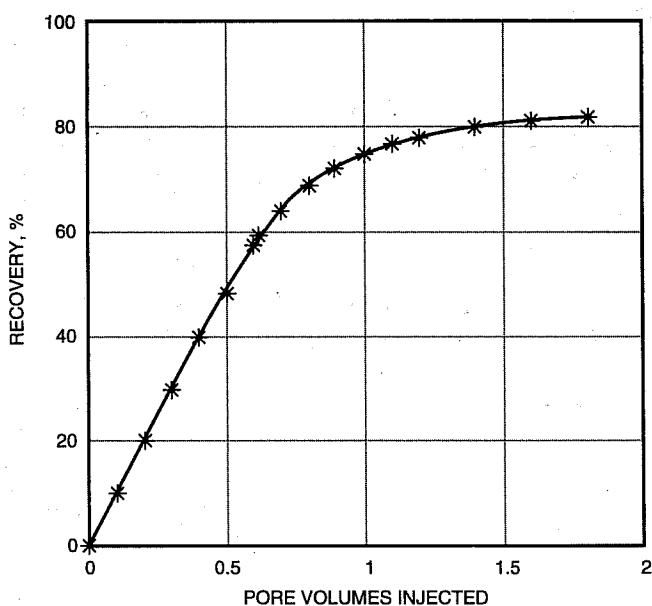


Fig. 13 Illustration showing recovery vs. pore volume injected (slug size, 0.2 pore volume). —*—, oil recovery.

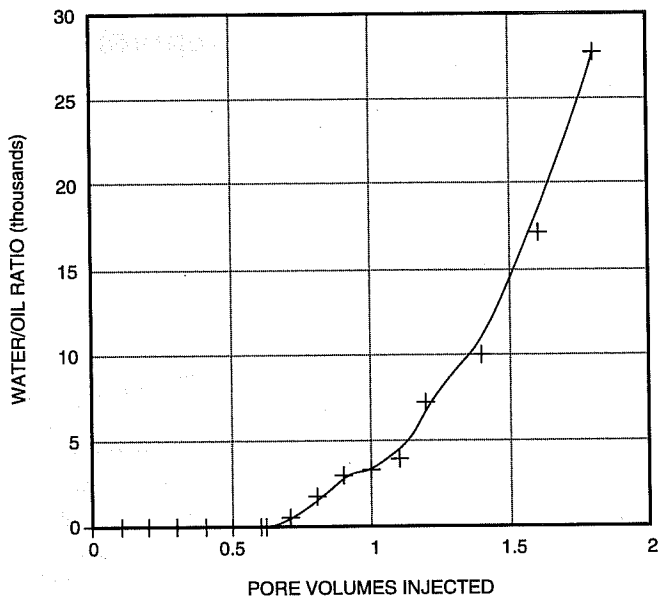


Fig. 14 Illustration showing water/oil ratio vs. pore volumes injected (slug size, 0.2 pore volume). +, water/oil ratio.

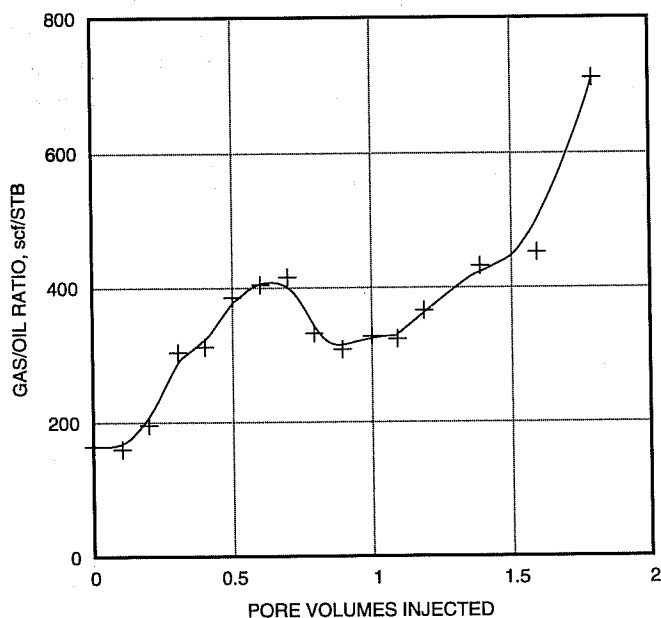


Fig. 15 Illustration showing gas/oil ratio vs. pore volumes injected (slug size, 0.2 pore volume). +, incremental gas/oil ratio.

**MODIFICATION OF RESERVOIR
CHEMICAL AND PHYSICAL FACTORS
IN STEAMFLOODS TO INCREASE
HEAVY OIL RECOVERY**

Contract No. DE-FG22-90BC14899

University of Southern California
Los Angeles, Calif.

Contract Date: Feb. 22, 1993

Anticipated Completion: Feb. 21, 1996

Government Award: \$150,000

(Current year)

Principal Investigator:

Yanis C. Yortsos

Project Manager:

Thomas Reid

Bartlesville Project Office

Reporting Period: Jan. 1-Mar. 31, 1994

Objectives

The objectives of this research are to continue previous work and to conduct new fundamental studies in areas of interest for thermal oil recovery: displacement and flow properties of fluids involving phase change (condensation-evaporation) in porous media; flow properties of mobility control fluids (such as foam); and the effect of reservoir heterogeneity on thermal recovery. The specific projects address the need to improve heavy oil recovery from typical reservoirs as well as from less-conventional fractured reservoirs producing from vertical or horizontal wells.

Thermal methods, particularly steam injection, are currently recognized as the most promising for the efficient recovery of heavy oil. Despite significant progress, however, important technical issues remain unresolved. Specifically, knowledge of the complex interaction between porous media and the various fluids of thermal recovery (steam, water, heavy oil, gases, and chemicals) is still inadequate. Also, the interplay of heat transfer and fluid flow with pore- and macro-scale heterogeneity is largely unexplored.

Summary of Technical Progress

Vapor-Liquid Flow

Work has continued on the modeling of vapor-liquid flow in porous media. During this quarter gravity was added to the pore network simulator, which accounts for the growth of the vapor phase by heat transfer in a single-component system. The analysis of the effect of heat convection on the growth of

the vapor phase continued. A study of the resulting curve of heat flux vs. degree of superheat continued, and for the first time, the effects of porous media were included. A technical paper was completed on the problem of bubble growth driven by an applied superheat.¹ Work is continuing on the development of a steam displacement simulator and on the extension of the problem to a three-phase system involving oil, water vapor, and water liquid under conditions that simulate steam displacement of oil.

Heterogeneity

During this quarter a Ph.D. thesis on visualization and simulation of displacements in fractured systems with the use of micromodels was completed.² Drainage, imbibition, and steam injection were studied. A pore network simulation of the experiments of drainage and imbibition (both primary and secondary) was conducted to support the experimental results. The simulation of the steam injection experiments, however, must await further progress in the pore network simulation of steam injection.

Additional work on heterogeneity addressed effects of correlations and viscous gradients on immiscible displacement. A study on the effect of pore-size correlations on slow drainage was completed.³ The theory developed shows how the spectral analysis of the saturation profile reveals the correlation structure of the underlying pore-size distribution. Numerical (and some experimental) results support the theory of both uncorrelated and correlated percolation processes. The results of this study are applicable to the identification of the correlation of permeability from saturation measurements. Work was also conducted to model the effect of viscous forces during immiscible displacements with gradient percolation.⁴ Except for very unfavorable mobility ratio, the process leads to a novel form of gradient percolation, where the gradient of the percolation probability vanishes at the percolation threshold. The scaling of the front width with the capillary number of the displacement was also determined. In parallel, the idea of a critical path⁵ was used to develop a scaling theory for the determination of the permeability of a disordered system of a large standard deviation.

Finally, work on the use of transverse flow equilibrium (TFE) [also known as vertical flow equilibrium (VFE)] to simulate displacement processes in porous media continued. In addition to the theory, numerical simulations of the full problem with the use of high resolution showed that TFE is reached when the relevant parameter R_L is large. Under the latter conditions, a boundary effect associated with viscous fingering in the presence of no-flow boundary (but not with periodic boundaries) was identified.⁶ Work is in progress to

identify the limitations of TFE and also to use TFE to rigorously derive simpler, viscous fingering models to replace the existing empirical ones. Work on the optimization of recovery processes with the use of optimal control methods is also in progress.

Chemical Additives

In the area of chemical additives, work on the behavior of non-Newtonian fluid flow and displacement in porous media continued. A Ph.D. thesis⁷ was completed on the flow and displacement of power-law fluids and Bingham plastics in porous media. Visualization experiments and pore network simulations involving the displacement of various fluids were conducted. For power-law fluids, a phase diagram for drainage processes similar to that for Newtonian was constructed. For Bingham Plastics, new patterns were identified. Results of experiments and simulations were in good agreement. The results indicate that Bingham Plastics, in particular, are applicable to the displacement of some heavy oils.

In the area of foam flow, work continued in the development of a pore network simulator. The gas displacement of a wetting phase in the presence of a surfactant, which allows for the formation of lamellae by a snap-off mechanism at various pore throats, as dictated by the aspect ratio, was modeled. This approach leads to a model invasion process, which is intermediate between invasion percolation and the process that models displacement by a Bingham plastic. The aspect ratio is a parameter that controls the extent of the continuous gas phase, the relative permeability of which can now be determined. Significantly, this approach does not rely strictly on percolation rules, which are typically used in other studies. Instead, the advancement of interfaces is determined by calculating a path of minimum resistance. The resulting values for the minimum pressure gradient are consistent with published experimental values.

References

1. C. Satik and Y. C. Yortsos, *Pore Network Models for Boiling and Bubble Growth in Porous Media*, to be submitted (1994).
2. M. Haghghi, Ph.D. Thesis, University of Southern California, May 1994.
3. C. Du, D. Salin, and Y. C. Yortsos, *Correlation of Drainage Saturation Profiles*, to be submitted (1994).
4. B. Xu, D. Salin, and Y. C. Yortsos, *A Study of Displacement Fronts in Porous Media at Low Rates*, to be submitted (1994).
5. C. Shah and Y. C. Yortsos, A Note on the Permeability of Strongly Disordered Systems, *Water Resour. Res.*, submitted for publication (1994).
6. Z. Yang and Y. C. Yortsos, *Effects of No-Flow Boundaries on Viscous Fingering in Porous Media*, to be submitted (1994).
7. C. Shah, Ph.D. Thesis, University of Southern California, May 1994.

OIL FIELD CHARACTERIZATION AND PROCESS MONITORING USING ELECTROMAGNETIC METHODS

Lawrence Livermore National Laboratory
Livermore, Calif.

Contract Date: Oct. 1, 1984
Anticipated Completion: Oct. 1, 1994
Government Award: \$350,000

Principal Investigator:
Mike Wilt

Project Manager:
Thomas Reid
Bartlesville Project Office

Reporting Period: Jan. 1–Mar. 31, 1994

Objective

The objective of this project is to develop practical tools for geophysical characterization of oil strata and monitoring of in situ changes in the electrical conductivity during enhanced oil recovery (EOR) operations in a developed field. Crosshole and surface-to-borehole electromagnetic (EM) methods are being applied to map oil field structure and to provide images of subsurface electrical conductivity changes.

Summary of Technical Progress

Activities this quarter have been focused on field projects at the Lost Hills oil field and at the University of California (U.C.) Richmond Field Station. A complete set of both crosshole and surface-to-borehole EM data was collected at Lost Hills oil field for monitoring the development of an EOR steamflood. These new data were collected four and one-half months after the initial baseline measurement and five months after the onset of steam injection and indicate that significant changes have occurred in the deeper parts of the target sands.

The borehole-to-surface EM measurements for saltwater injection monitoring at the U. C. Richmond Field Station that were completed during this time period are being reduced and prepared for interpretation. These high-density multicomponent measurements indicate a good sensitivity to the injected saltwater slug and a generally high-quality data set. The data will be interpreted in summer 1994 and presented to the industrial sponsors in fall 1994.

EM Monitoring at Lost Hill No. 3

Steamflooding activities began in late September 1993; during October and November 1993, a set of crosshole and surface-to-borehole EM data was collected for steamflood

monitoring. In March and April 1994, both crosshole and surface-to-borehole data sets were remeasured for the purpose of monitoring the progress of the flood.

Figure 1 displays 5-kHz crosshole EM profiles collected before and after steaming. The profiles are for one receiver fixed at a depth of 65 m in one observation borehole and for more than 100 transmitter positions from depths of 30 to 130 m in the other observation hole which is located 54 m from the receiver hole. The steam injection borehole, located midway between the observation wells, is completed for steam injection into oil sands at depths of 60, 80, and 95 m. The crosshole plots in Fig. 1 show only small changes at transmitter depths within the upper 65 m but significant changes below these depths. A maximum decrease of more than 25% amplitude and 20° phase is observed in the newly acquired data compared to the baseline data set. The greatest changes occur at transmitter depths below 80 m, which is typical of other crosshole data for the two surveys. The March 1994 data are consistently lower than the November 1993 data in both amplitude and phase for transmitter depths below 65 m but show little change above this level. These

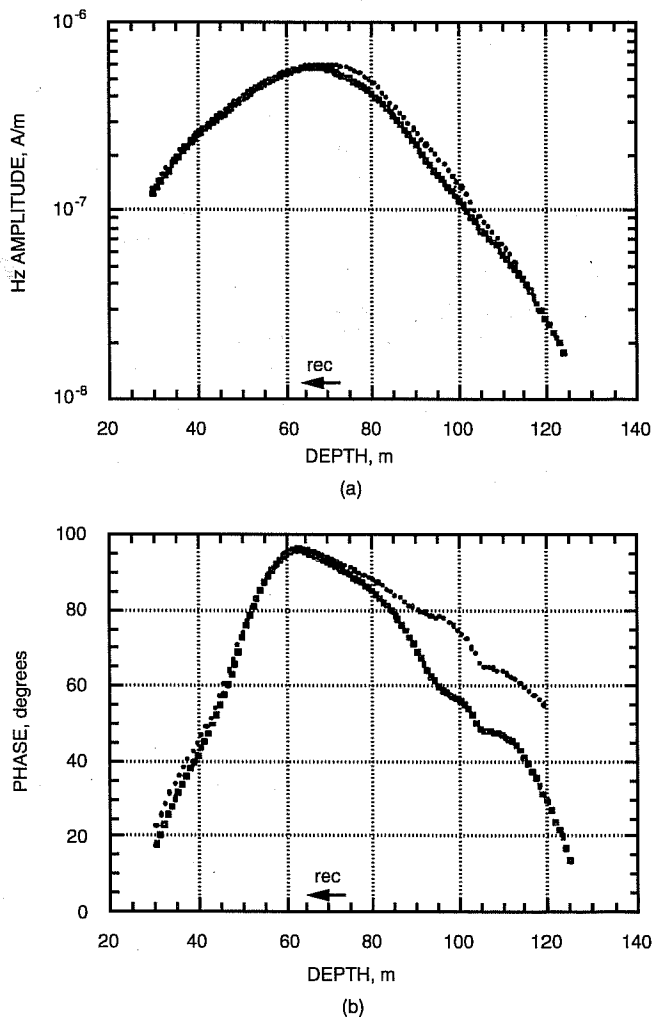


Fig. 1 Crosshole electromagnetic (a) field amplitude and (b) phase before and after steamflooding. ■, 3/94. ●, 11/93.

observed changes are consistent with a decrease in the resistivity of the formation because lower resistivity tends to absorb more of the EM energy and reduce the amplitude and phase of the observed EM fields. These changes are well above the 2% repeatability error and bode well for interpretation of these data and delineation of the zone of changed resistivity.

Resistivity decreases of up to 50% have been observed in other fields undergoing steamflooding.^{1,2} The principal cause of the resistivity decline is thought to be the temperature increase in the sands and confining shale layers affected by the steaming. The changes in pore fluid from heavy oil to hot saline water and steam are considered significant contributors to the resistivity decline.² In general, however, delineating the zone of decreased resistivity will identify the high-temperature zone associated with the steam sweep.

A two-dimensional inversion code developed by Schlumberger-Doll Research (SDR) is being applied to interpret crosshole data. This code, also used on baseline data, will allow mapping of the resistivity distribution after steam injection. It also allows the identification of steam zone location by taking a difference of the two resistivity images.³

In contrast to the crosshole results, the 1-kHz surface-to-borehole data over the steamflood show much smaller differences before and after steam injection. The maximum observed differences are 5 to 10% amplitude decreases at depths greater than 80 m (Fig. 2). Although these results suggest changes in the lower sands, the observed changes are too small and data quality too poor for definitive modeling. This is consistent with earlier modeling which indicated that the 1-kHz data would probably be inadequate if the process was occurring at depths greater than 70 m. For this reason surface to-borehole data were collected at 5 kHz. Unfortunately these higher frequency 5-kHz data collected are affected by surface cultural features such as pipelines, which channel the high-frequency EM signal into local electrical wires and well casings, and thus distort the observed field. This distortion, which does not occur at the lower frequency, degrades the quality of the high-frequency data for transmitter stations over the steamflood to the point that these data may not be used

for definitive modeling. As the steamflood intensifies, a larger anomaly in the 1-kHz data should be observed, and modeling can then be applied to these data.

Both crosshole and surface-to-borehole data will be collected every three to six months at both the lower and higher frequencies. An attempt is being made to reduce the sensitivity of the high-frequency surface-to-borehole data to external noise and cultural features. Note that the crosshole 5-kHz data are much less affected by surface culture since the tools are positioned in the borehole, well away from the distributing features. These data typically repeat at the level of 1 to 3%.

Surface-to-Borehole Experiment at Richmond Field Station

As part of the Lawrence Berkeley Laboratory (LBL)/Lawrence Livermore National Laboratory (LLNL)/industrial sponsors EM consortium, a field exercise at U.C. Richmond Field Station was undertaken beginning in December 1993. Saltwater injection was monitored by applying a variation of the borehole-to-surface EM technique. A borehole transmitter was deployed in the injection well, and several other observation holes and horizontal and vertical component magnetic fields were collected on the surface using a densely sampled grid. A complete survey was done before and after saltwater injection.

The baseline data were collected in December 1993, and the saltwater was injected during the Christmas holidays. Postinjection data were collected during the last week of December and early January 1994. Early analysis of these data showed significant distortion as a result of a ground loop from the transmitter supply cable into the local ground. This was subsequently repaired, and new data were collected in January 1994 and later in March 1994 after saltwater withdrawal. With the exception of a few stations near the transmitter borehole the data quality for the experiment is very high.

The observed data show a consistent amplitude and phase change in both field components as a result of the saltwater injection. The data will be interpreted by applying a combination of established two- and three-dimensional codes as well as some simpler codes for delineation of the subsurface resistivity and mapping of the underground saltwater plume. With these data the problem of sampling density and image resolution with the borehole-to-surface method will be addressed.

Conferences and Presentations

During this quarter two presentations^{5,6} were made at two conferences in Venezuela.

References

1. J. J. Justice et al., Recent Developments in Geophysics for Reservoir Characterization, *Expanded Abstracts of the Society of Exploration Geophysicists Annual Meeting*, Dallas, Texas, pp. 549-550, 1989.
2. A. J. Mansure, R. F. Meldau, and H. V. Weyland, *Field Examples of Electrical Resistivity Changes During Steamflooding*, paper SPE 20539

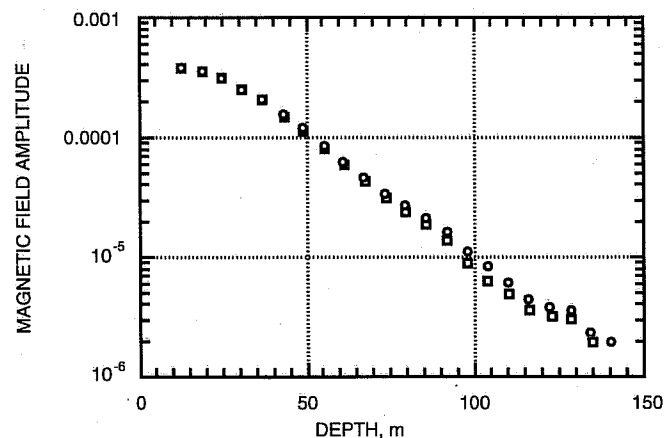


Fig. 2 Surface-to-borehole results before and after steamflood.

- presented at the 65th Annual SPE Technical Conference and Exhibition, New Orleans, Louisiana, Sept. 23–26, 1990.
3. C. Torres-Verdin and T. Habashy, An Approach to Nonlinear Inversion with Application to Crosswell EM Tomography, *Expanded Abstracts of the Society of Exploration Geophysicists Annual Meeting*, Washington, D.C., pp. 351-354, 1993.
 4. M. J. Wilt, *Quarterly Progress Report for Project FEW6038 in "Activities of the Oil Implementation Task Force"*, DOE Report Number DOE/BC/94-1, 1993.

5. M. J. Wilt, *Crosshole Electromagnetic Imaging for Reservoir Definition and Monitoring*, paper presented at the II SOVG/SEG International Symposium on Reservoir Characterization, Los Teques, Venezuela, 1994.
6. M. J. Wilt, *Thermal Front Tracking and Reservoir Characterization*, paper presented at the Semi-Annual DOE/INTEVEP Annex IV Meeting on Enhanced Oil Recovery, Los Teques, Venezuela, 1994.

MULTIFREQUENCY ELECTROMAGNETIC INDUCTION

**Lawrence Livermore National Laboratory
Livermore, Calif.**

**Contract Date: Oct. 1, 1993
Anticipated Completion: Oct. 1, 1994
Government Award: \$200,000**

**Principal Investigator:
Mike Wilt**

**Project Manager:
Thomas Reid
Bartlesville Project Office**

Reporting Period: Jan. 1–Mar. 31, 1994

Objective

The objective of this research is to develop and apply the high-resolution multifrequency electromagnetic (EM) induction technique to oil field characterization. In collaboration with Schlumberger–Doll Research (SDR) and Lawrence Berkeley Laboratory (LBL), instrumentation is being constructed, and software for high-resolution, subsurface resistivity imaging is being developed.

Summary of Technical Progress

Progress was made in two areas during this quarter. First, at LBL a frequency-Q-domain transform code was successfully developed and tested. The code shows that an effective Q-domain transform may be made with as few as 10 frequencies. In a second development the hardware design for the multifrequency soil was finalized, and the purchase order

was issued for the tool construction. Tool completion is scheduled for September 1994.

Research Updates

Interpretation of the data is a crucial element in the program. The collaboration with LBL is critical for the development of the frequency-Q-domain transform to allow full interpretation of these data.

Lee and Xie¹ demonstrated that very high resolution imaging is possible with crosshole EM if data are collected as a transient pulse and mathematically transformed into a wave-like field (Q-domain). Equivalently, EM data may be collected over a range of frequencies (the Fourier equivalent of a pulse) and transformed to Q-domain. In practice, field data are collected at only a few frequencies, which suggests that the Q-domain transform must be adapted to allow for the collection of imperfect field data.

During this quarter, the frequency-Q-domain data transformation procedure was successfully completed. From tests of the transform code using synthetic data sets, it was found that it is possible to achieve a stable Q-domain waveform with as few as 10 frequencies.² Although the transform yielded superior waveforms when 100 or more frequencies were used, it is not a large improvement over the 10 frequency transforms. This new development is several months ahead of schedule and allows application of this code when the new crosshole system is tested this fall.

Hardware Development: New Coil

A purchase order has been issued to Electromagnetic Instruments Inc. (EMI) for the construction of a multifrequency borehole transmitter. The tool will be made in accordance with design criteria established at Lawrence Livermore National Laboratory with assistance from SDR and engineering help from EMI. The tool will have a maximum moment of 1000 at a current of 10 amps, operate at 16 frequencies, be switchable from the surface, and be made compatible

with the SDR three-component borehole receiver tool. Construction activities will begin in June 1994. The tool is scheduled for completion in September 1994, as shown in Fig. 1.

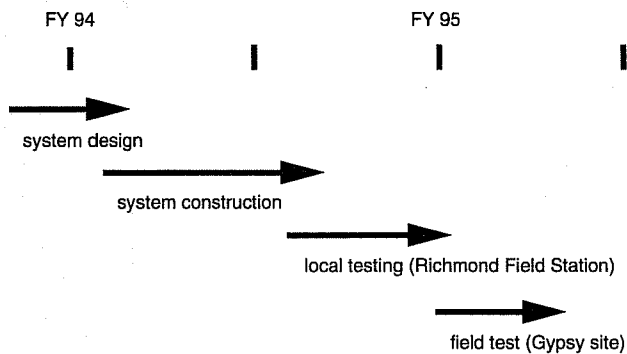


Fig. 1 Construction timetable for multifrequency borehole transmitter.

Multifrequency EM

Hardware and software tools for this project are designed for the application of the Q-domain wave field imaging technique.¹ Because of physical or temporal constraints, however, it may be impossible in some cases to collect a sufficiently complete suite of frequency data for the Q-domain transform waveform to be stable. In these cases, it is more effective to interpret the data set in the frequency domain. Even without the Q-domain transform, improved resolution over single-frequency data can be achieved.

In Fig. 2, a synthetic dual-block inversion³ was used to compare two block targets (a one-frequency inversion and a five-frequency inversion) using the same sampling locations. The results clearly show that the multifrequency inversion provides superior resolution.

A practical problem in the inversion of multifrequency data sets is the proper weighting of data so that all are used without one frequency dominating the inversion. This difficult problem is being addressed by researchers at LBL, SDR, and Sandia laboratories.

References

1. K. H. Lee and F. Q. Xie, A New Approach to Imaging with Low Frequency Electromagnetic Fields, *Geophys.*, 58(6): 780-796 (1993).
2. K. H. Lee, *Multifrequency Crosshole EM Imaging for Reservoir Characterization*, Quarterly Progress Report Lawrence Berkeley Laboratory Contract ESD-38, Enhanced Oil Recovery Progress Review No. 78, DOE Report Number DOE/BC-94/2, 1994.
3. C. Torres-Verdin and T. M. Habashy, *Rapid 2.5-D Forward Modeling and Inversion via a New Nonlinear Scattering Approximation*, Schlumberger-Doll Research Report EMG-001-94-06, 1994.

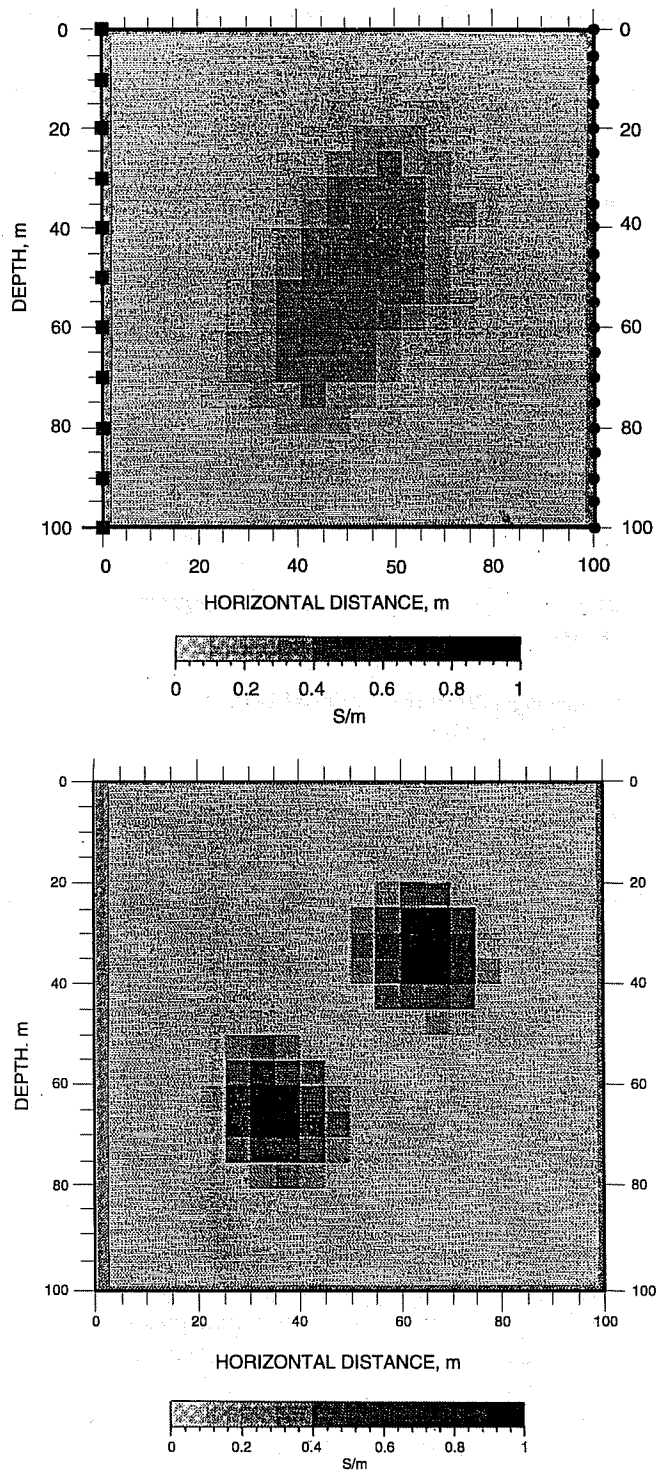


Fig. 2 Comparison of single-frequency crosshole electromagnetic inversion (upper) with multifrequency inversion (lower) for a synthetic dual-block inversion. [From Torres-Verdin and Habashy, 1994 (Ref. 3)].

GEOSCIENCE TECHNOLOGY

INTERDISCIPLINARY STUDY OF RESERVOIR COMPARTMENTS

Contract No. DE-AC22-93BC14891

**Colorado School of Mines
Golden, Colo.**

**Contract Date: Sept. 29, 1993
Anticipated Completion: Sept. 30, 1996
Government Award: \$753,266**

**Principal Investigator:
Craig W. Van Kirk**

**Project Manager:
Robert Lemmon
Bartlesville Project Office**

Reporting Period: Jan. 1–Mar. 31, 1994

Objective

The objective of this research project is to document the integrated team approach for solving reservoir engineering problems. A field study integrating the disciplines of geology, geophysics, and petroleum engineering is the mechanism for

documenting the integrated approach. The goal is to provide tools and approaches that can be used to detect reservoir compartments, reach a better reserve estimate, and improve profits early in the life of a field.

Summary of Technical Progress

Four research tasks either began or were ongoing during first quarter 1994. Theme 1 (Reservoir/Outcrop Selection/Evaluation) is being investigated in two aspects: reservoir selection and evaluation and experimental investigation.

Reservoir Selection and Evaluation

Reservoir Selection and Data Gathering

The Hambert field was selected for the integrated study during this quarter, and data gathering began. It is estimated that approximately 35% of the data has been gathered. One objective of the data gathering phase is to develop an integrated set of databases that is consistent and can be used by each of the reservoir study disciplines.

The basic well and production data used in the Hambert study were derived from Dwight's well history and production CD-ROMs. The Dwight's front end is limited in its selection and sorting capabilities, and it contains a few bugs that prevent selecting wells using certain combinations of selection criteria. Thus these data were downloaded into

Microsoft EXCEL for WINDOWS spreadsheets to enable design of selection and sorting criteria to suit any situation. Subsequently, the data were ported to Exploration Data Manager (EDM), a program designed specifically to manage such data with a user-friendly interface. EDM is designed to import CD-ROM data directly from production and scout ticket CD-ROM disks and merge the two files into one database. The use of two very distinct data sets has proven to be the most difficult obstacle with regard to data management. One of the first tasks for this project was to plot a base map of wells in the Hambert field with associated oil and gas production using an XYZ format. Importing the data into mapping programs (Rockware) provided additional problems because of format.

Geologic Reservoir Characterization

The Hambert field in Colorado produces oil and gas from the Cretaceous Terry Sandstone (or Sussex Sandstone). Characteristics of the reservoir were defined on the basis of

outcrop, core, and log analysis and correlations to obtain an internal architecture description.

The core analysis and correlation work done on the Hambert field was studied in relation to analogous fields. Faulting and compartmentalization are indicated as key components for reservoir characterization in the Hambert field.

Seismic Analysis

The three-dimensional (3-D) seismic data are being loaded onto a workstation for processing.

Experimental Investigation

The experimental procedure for permeability measurements was designed to include pressure decay profile permeameter measurements; core plug cutting; porosity, permeability, and compressibility measurements; relative permeability measurements; and capillary pressure measurements.

APPLICATION OF ARTIFICIAL INTELLIGENCE TO RESERVOIR CHARACTERIZATION: AN INTERDISCIPLINARY APPROACH

Contract No. DE-AC22-93BC14894

**University of Tulsa
Tulsa, Okla.**

**Contract Date: Oct. 1, 1993
Anticipated Completion: Sept. 30, 1996
Government Award: \$312,407**

**Principal Investigator:
B. G. Kelkar**

**Project Manager:
Robert Lemmon
Bartlesville Project Office**

Reporting Period: Jan. 1–Mar. 31, 1994

The main challenge of the proposed research is to automate the generation of detailed reservoir descriptions honoring all the available soft and hard data, which range from qualitative and semiquantitative geological interpretations to numeric data obtained from cores, well tests, well logs, and production statistics. In this sense, the proposed research project is truly multidisciplinary. It involves a significant amount of information exchange between researchers in geology, geostatistics, and petroleum engineering. Computer science and AI provide the means to effectively acquire, integrate, and automate key areas of expertise in the various disciplines represented in a reservoir characterization ES. Additional challenges are the verification and validation of the ES because much of the interpretation of the experts is based on extended experience in reservoir characterization.

The project plan to design the system to create integrated reservoir descriptions begins by initially developing an AI-based methodology for producing large-scale reservoir descriptions generated interactively from geology and well test data. Parallel to this task is a second task that develops an AI-based methodology that uses facies-biased information to generate small-scale descriptions of reservoir properties, such as permeability and porosity. The third task involves consolidation and integration of the large-scale and small-scale methodologies to produce reservoir descriptions honoring all available data. The final task will be technology transfer. This plan carefully allocates and sequences the activities involved in each of the tasks to promote concurrent progress toward the research objectives. Moreover, the project duties are divided among the faculty member participants, and graduate students will work in teams with faculty members.

The results of the integration are not limited merely to obtaining better characterizations of individual reservoirs.

Objectives

The objectives of this research project are to use novel techniques from artificial intelligence (AI) and expert systems (ES) to capture, integrate, and articulate key knowledge from geology, geostatistics, and petroleum engineering to develop accurate descriptions of petroleum reservoirs. The ultimate goal is to design and implement a single powerful ES for use by small producers and independents to exploit reservoirs efficiently.

They have the potential to significantly impact and advance the discipline of reservoir characterization itself.

Summary of Technical Progress

Decomposition of System

The overall system development has been decomposed into smaller component parts to allow focusing on the expert knowledge required for each component. In addition, the decomposition facilitates the implementation of the system and its validation and verification. The three component systems will be representative of how each of the experts in geology, geostatistics, and engineering characterizes the reservoir. Figure 1 describes a model for this breakdown. The

concurrent development of these component systems fits into the development of the large- and small-scale aspects of the system as originally stated in the proposal. In Fig. 1, each component system in the model is depicted as interfacing (through the bidirectional links) with a central repository of reservoir descriptions. Although portions of these descriptions will essentially be passed from component to component as more information is gathered (as shown by the bidirectional links in Fig. 2), the model of a central repository is an accurate account of how the components are integrated (i.e., the final descriptions in the repository are consistent with all the information given by the component systems). This system model allows the development of the system with an AI technique called a *blackboard system*, in which information is centrally located (i.e., on a blackboard), and experts take their turn to update, change, and correct the information on the blackboard. A small prototype in KAPPA-PC is being developed to gain an understanding of the representation issues in order to provide each system with the information that it needs, either as raw input or as feedback information from another system.

Figure 2 shows a more detailed decomposition of Fig. 1 and includes the current raw input information that is being examined (designated by double arrows). The bidirectional links indicate where feedback will occur between systems when more information is learned and inconsistencies in descriptions are discovered.

Stochastic methods have gained widespread acceptance as a promising methodology for enhancing the ability to describe the spatial distribution of reservoir properties. Conditional simulation, because of its ability to honor the sample data and create multiple equiprobable reservoir descriptions if required, has been selected as the stochastic method to be used for this study.¹ Specifically, the conditional simulation algorithm to be used is the simulated annealing method.² This method was selected because of its robustness and the facility and flexibility of incorporating conditioning data.

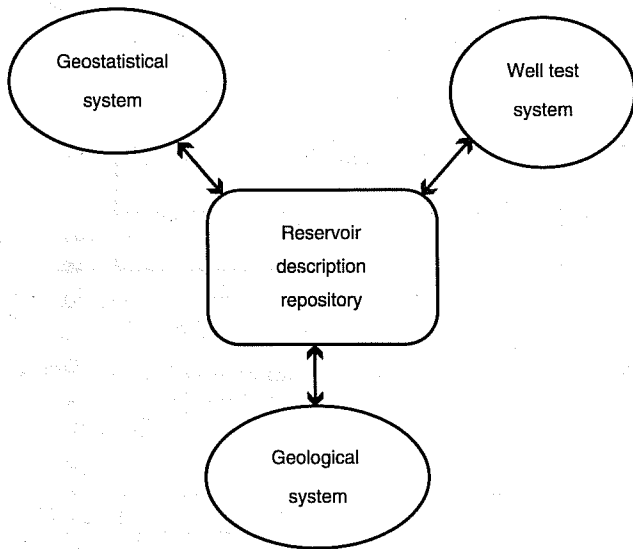


Fig. 1 Expert system decomposition.

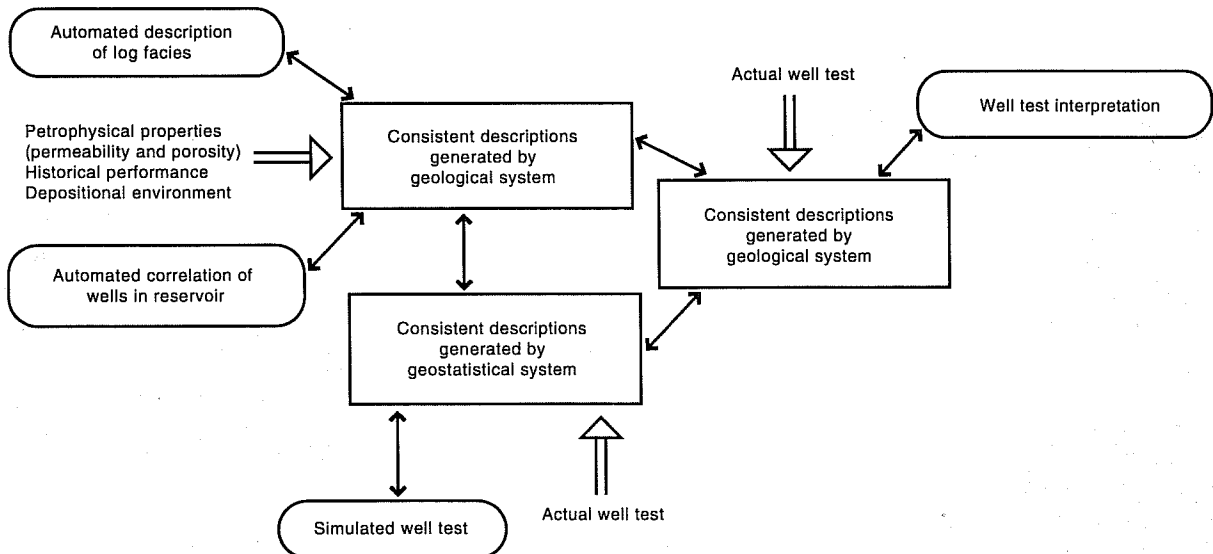


Fig. 2 Detailed decomposition of the system.

Traditionally, only static constraints, such as core and log data, have been used in the simulated annealing process. Although the inclusion of dynamic constraints, such as well test and production data, is considered desirable, practical considerations prevented their use in large-scale projects. One major impediment has been the required computational expense for using a dynamic constraint.

The primary objective of this work is to develop a methodology for incorporating dynamic constraints, such as well test and production data, into the simulated annealing algorithm. Improved reservoir description can be obtained for the following reasons:

- Uncertainties in describing reservoirs can be minimized by adding more constraints. In addition, the description will also be closer to the truth case as more information is added. This implies that the description approaches a closer approximation of the reservoir being studied.
- Dynamic constraints (e.g., production and pressure data) provide the only observable response that is representative of reservoir-scale behavior as well as in situ information. Other available data, including log and core data, represent reservoir data that are limited to the near-wellbore region.
- This work can eventually be combined with geological constraints to create a truly integrated reservoir description.

This approach involves the coupling of a numerical flow simulator to the simulated annealing algorithm. The flow simulator constitutes a dynamic constraint as part of the simulated annealing objective function, which consists of a variogram constraint and a flow simulation constraint.

Simulated annealing is an example of adaptive heuristics for multivariate or combinatorial optimization. The implementation requires, among other parameters, the definition of an objective function that represents a measure of the difference between an input model and the fit of that model. Thus the goal of the algorithm is to determine the configuration of independent variables—for example, permeability values—that minimize the objective function. When the objective function is comprised of more than one model, an attempt is made to minimize the sum of the differences.

The Laplace transform finite difference (LTFD) method is used for the flow simulation. This method is based on solving the single-phase flow equations in Laplace space. It has the advantage of using only one time step between the initial time and the time of interest. As a result, this method is far less computationally expensive than other numerical methods.

The annealing method has been modified so that the perturbations of the permeability field are no longer random but radiate outward from the well location(s). This modification was performed after the observation that, especially in early times, the near-wellbore conditions had a significant effect on the production response.

The first phase involved testing the performance of the LTFD numerical simulator against a commercial simulator (ECLIPSE was used). The results of this successful test are shown in Fig. 3. This figure shows a comparison of the output

pressures for a heterogeneous reservoir from ECLIPSE and the LTFD simulator at different times for a two-well system, with each well producing at a variable rate.

In the second phase, a synthetic permeability distribution was generated and used to test the performance of the algorithm. Conditioning data (permeability values) at two well locations and a cumulative distribution function representing the synthetic input data were included in the input constraints.

One of the tests executed compared the production behavior of the reservoir model obtained with both constraints with the results obtained with only the variogram constraint. The results showed a dramatic improvement (see Figs. 4 and 5) in the agreement with the synthetic input data when the simulator constraint was included.

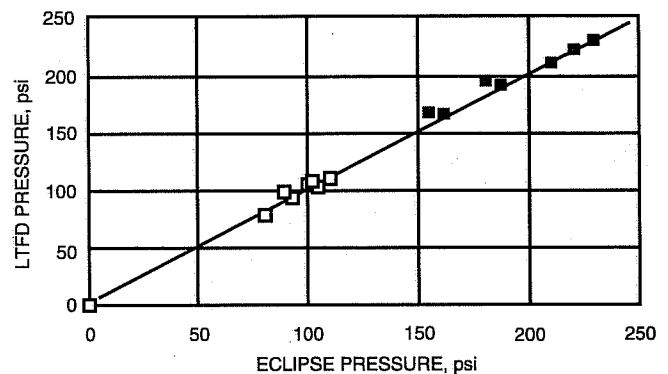


Fig. 3 Comparison of Laplace transform finite difference (LTFD) and ECLIPSE output pressures. ■, well No. 1. □, well No. 2.

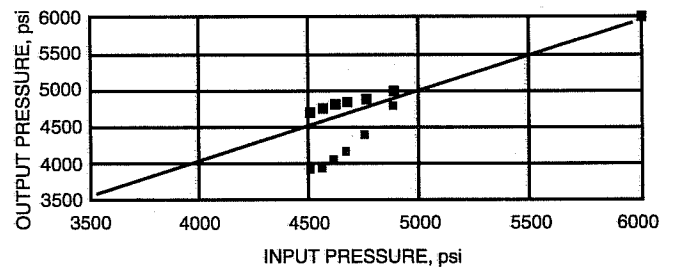


Fig. 4 Comparison of results for well No. 1 with both constraints and with variogram constraint only. ■, both constraints. □, variogram only.

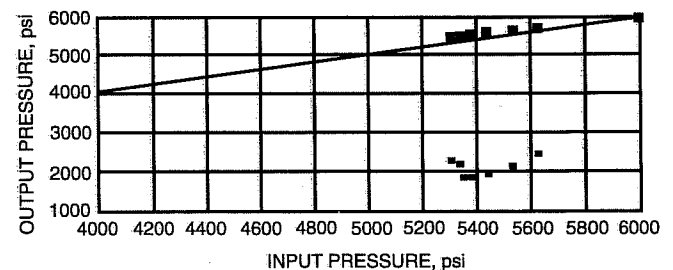


Fig. 5 Comparison of results for well No. 2 with both constraints and with variogram constraint only. ■, both constraints. □, variogram only.

Although the results are encouraging, the algorithm remains computationally demanding. Additional work is needed to include the effect of convergence tolerances on the final solution. Further optimization of the matrix solving routines or sourcing of better routines is needed. In addition, the code needs to be streamlined and optimized. Eventually, the integration of this program with other routines to include known geological constraints would be desirable.

Well-Test Interpretation System

In addition to the research described previously, for a more traditional ES approach a well-test interpretation is being developed. The development of such a system involved gathering knowledge from petroleum engineering experts to determine the appropriate model and to apply the associated equations of that model. Transient testing is a major source of vital information about reservoir parameters, such as permeability, reservoir pressure, wellbore conditions, reservoir discontinuities, and other information considered essential for reservoir studies. The accuracy of these properties estimated from well tests depends on previous identification of a model that describes the reservoir accurately. This model is known as the well-test interpretation model.

The procedure for finding an appropriate model can be quite complex. It usually resides in the mind of the expert. The failure of mathematical models to solve the problem can be attributed to the nature of the problem itself because the procedure is not completely quantitative and relies on experience.

A computerized well test involves interpreting the various forms of the time vs. pressure data, in addition to other well data, to determine the well model and calculate the various parameters. Basically, this interpretation can be grouped into two parts: qualitative analysis and quantitative analysis. Qualitative analysis deals with selecting the appropriate well model from the input data. Quantitative analysis involves calculating various well parameters, such as permeability and skin factor (if applicable). The estimation of well properties depends on the selection of the right model, which makes qualitative analysis a crucial part of the problem.

The ES being developed for well-test interpretation consists of rules and facts for buildup test analysis. The initial rules simulate the reasoning process used by the experts to identify the appropriate interpretation model for a well test. Within this approach, the ES is designed to use a description of the shapes of different graphs of test data, particularly the derivative plot. When needed, the system seeks information in addition to test data from relevant sources, such as known reservoir and fluid properties, production statistics, well logs, and geological data.

The ES architecture consists of three main components: (1) a knowledge base consisting of facts and rules, (2) a database consisting of supplied data and model parameters, and (3) a control strategy to determine when to use the expert rules in the knowledge base. Although knowledge is the most

important part of the knowledge base, the control problem is a critical component in the design of the system. Simulating the reasoning process of the human expert requires control strategy to organize the reasoning steps and domain knowledge to achieve an efficient way of constructing a solution to a problem.

Figure 6 describes the flow of information through the system and shows the different modules in the system. The first module takes in the time vs. pressures data and the derivative data. In the absence of the derivative data, this module may be used to calculate the derivative data from the existing time and pressure data. The graph-drawing module is used to plot the graph. This module is required to apply smoothing techniques and eliminate the noisy data. The sketch algorithm by Allain and Horne³ extracts a set of consecutive log-log segments from a potentially noisy derivative. A hybrid neural network-based scheme was presented by Houze and Allain.⁴ The algorithm chosen for this module should be able to draw a smooth plot and eliminate noisy data. Although the system concentrates on the derivative plot, other plots may be required. This is especially true because the derivative plot is more sensitive to noise. The other plots used to confirm the results include the semi-log plot, the log-log plot, and the Horner plot.

The graph analysis module would take the graph plotted in the previous step, identify flow region, and look for typical characteristics in the graph. The derivative plot is well suited for this purpose because it intensifies the response of each flow regime. Basically a limited number of signatures on the derivative curve can be attributed to each flow region. These signatures include maxima, minima, stabilization

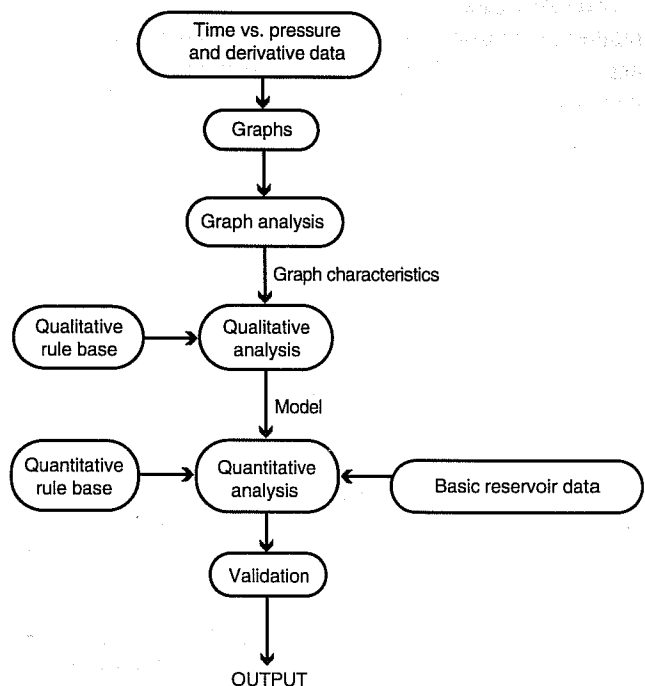


Fig. 6 Well test expert system model.

(flattening), and upward and downward trends. Shape recognition algorithms are used for this purpose.

The signatures identified in the preceding module are given to the qualitative analysis module. This module is responsible for the model selection on the basis of the flow regions and the corresponding signatures. This module would have to access the qualitative rule base, which consists of rules for selecting the models on the basis of the plot trends. In the absence of a flow region (incomplete data) or the inability to select a model on the basis of the incomplete graph data, this module would use the available geological data. In addition, the user can provide a preference over model selection.

The quantitative analysis module is used to calculate the reservoir parameters once the model is selected. This module would have to access a rule base containing the equations used by different models. It would also need basic reservoir data supplied by the user.

The verification module is used to verify the deduced model. This module may also be used to select between models when more than one model is obtained. The verification method would use the interpretation model reservoir parameters (e.g., permeability, skin, etc.) as initial estimates in an automatic history matching algorithm.⁵

The initial input to the system consists of pressure vs. time data, basic fluid properties (compressibility, viscosity, and density), and basic rock properties (porosity and fluid saturations). This input is used by the system to generate the diagnostic plots. Later in the process, the system will seek other relevant data when needed.

In a complete well test analysis, the expert often uses diverse information sources to find the applicable interpretation model. These knowledge sources are shown in Fig. 7.

The first category shown in Fig. 7 comprises the data related to the response of the physical properties of the well and the reservoir. These include pressure and flow data, well data, fluid data, and field data (which include interpreted geological data). The second category is the expertise or the

expert's knowledge. This category forms the critical part of the knowledge base because it affects the whole reasoning process. The third category contains mathematical models and other data to simulate the known reservoir behavior. This category is used to validate and confirm the interpretation obtained from the knowledge base.

The model recognition process will be carried out by first dividing the plot into flow regions. The well test interpretation model can be partitioned into three components: (1) the reservoir behavior, (2) the behavior at the inner boundaries, and (3) the behavior at the outer boundaries. Each of these is associated with a well-defined flow region in the well test data. These regions are the early-time, middle-time, and late-time regions. The early-time region is associated with the wellbore and near-well conditions; the middle-time region is associated with the reservoir behavior; and the late-time region is associated with the outer boundary conditions.

The system would identify the time intervals spanned by the flow regions before attempting to identify the interpretation model segments. Figure 8 shows the different regions and the different conditions and behavior recognized by the system in each region.

The available expert's knowledge is used for separating the flow regimes and interpreting the responses of the flow regimes on the derivative curve. The change from one flow regime (behavior) to another produces a distinct change in the shape of the curve. The procedure, based on the *left-to-right* visual inspection of the derivative curve, will be fully automated. The system would start by selecting a marker point (e.g., a point of inflection). The recognition process then proceeds by expanding around the marker and describing the characteristic shapes that precede or succeed the marker zone. User interaction may be taken at this stage to select the marker if required. The process ends when all the regions have been defined. The system may conclude that one or more regions are missing, a situation that arises because of incomplete well data.

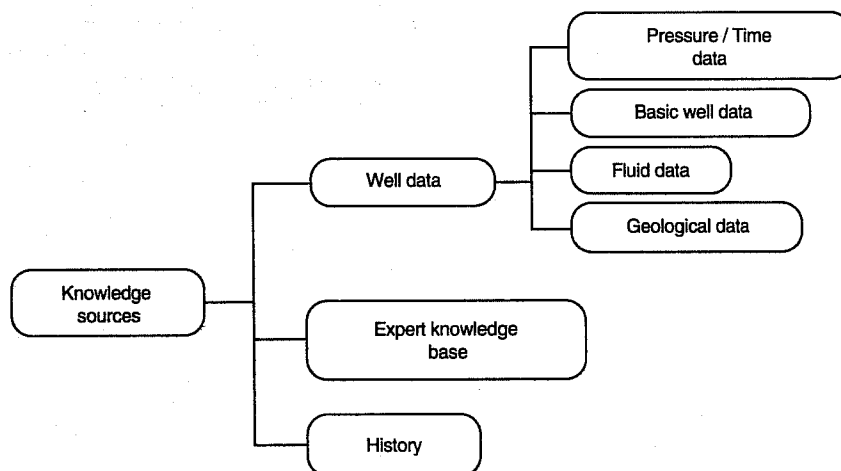


Fig. 7 Expert system knowledge sources.

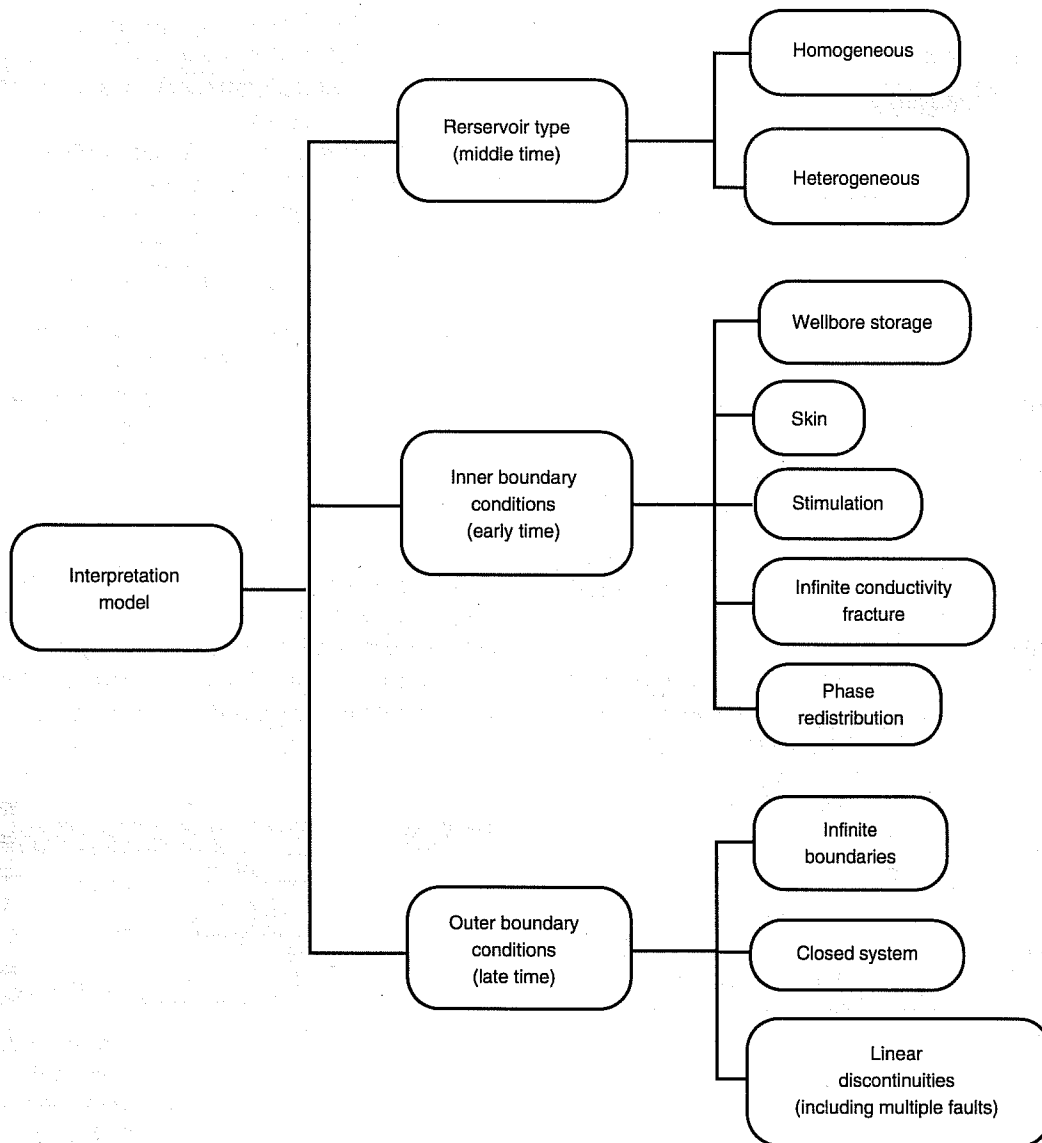


Fig. 8 Conditions and behavior recognized by each region.

Determination of the interpretation model will begin with defining the reservoir type (middle-time region) to see whether the reservoir is homogeneous or heterogeneous. Once the reservoir type is defined, the system will proceed to check the early-time region of the graph, where the system determines the inner boundary conditions. The system will be able to distinguish the following inner boundary conditions: wellbore storage, skin, stimulation, infinite conductivity fracture, finite conductivity fracture, and phase redistribution. The well can show any logical combinations of these conditions. The last segment the system would resolve is the late-time region. The system will be able to differentiate between three outer boundary conditions: (1) an infinite acting reservoir, (2) a completely closed reservoir, and (3) linear discontinuities. The system will allow any logical combinations of these outer boundary conditions.

At the end of the session, one or more segments may not be resolved because of incomplete data, or inconsistent conclusions may be reached because of incorrect data. In this case, the system will seek help from information sources other than the test data, such as well reports and geological information. Also, the system may identify more than one possible solution for a segment of the interpretation model. In such cases, both of the solutions will be considered for the rest of the analysis. Final selection will be based on the verification process or the user's choice. The output given by the system is the final selected model and the calculated reservoir properties, such as permeability and skin.

The interpretation model is identified by focusing on individual flow regions. The system starts by identifying the reservoir model with the use of the middle-time region characteristics of the derivative plot. The rules required in this step

are those which determine whether the reservoir model is homogeneous or heterogeneous. A typical rule for identifying the reservoir model is as follows:

- If** the derivative plot has a minimum
- And** minimum is V-shaped
- And** the semi-log plot shows two parallel straight lines
- Or** the semi-log plot shows a flat line (transition) followed by a straight line
- And** the log-log plot shows a slope change
- Then** the reservoir model is heterogeneous.

The log-log plot and the semi-log plot are used to confirm the observations from the derivative plot. The middle-time region of the plot without a minimum indicates a homogeneous model. Trends in the plot may sometimes indicate the possibility of two different models.

- If** Minimum is observed in the middle-time region of the derivative plot
- And** minimum has open U-shape
- And** semi-log plot shows evidence of two straight lines with possible slope doubling
- And** log-log plot indicates slope change
- Then** the reservoir model is heterogeneous
- Or** the reservoir model is homogeneous with possible linear discontinuity (fault).

The preceding rule leads to the identification of two models: (1) heterogeneous model and (2) homogeneous model with linear discontinuity. Both models produce similar test data plots.

After the reservoir model is identified, the system then looks at the early-time region of the plot. Rules in this step identify wellbore storage, skin, stimulation, infinite conductivity fracture, phase redistribution, etc. The following trends suggest typical inner boundary conditions:

- If** Plot shows a unit slope line
- And** plot shows a hump
- Then** indicates presence of wellbore storage.
- If** plot has a 1/4 slope line
- Then** indicates presence of finite conductivity fracture.
- If** plot has a 1/2 slope line
- Then** indicates presence of infinite conductivity fracture.

The preceding trends may be confirmed by looking at the semi-log and the log-log plot. After the inner boundary conditions are identified, the system will look at the late-time region in the graph to identify the outer boundary conditions. This includes identifying infinite boundary conditions, closed systems, and linear discontinuities (including multiple faults). Typical rules in this step are as follows:

- If** the derivative plot is horizontal
- And** semi-log plot is a single straight line
- And** the log-log plot shows one line (no inflection point)
- Then** the reservoir is infinite acting.

- If** the derivative plot shows an upward increase followed by stabilization
- And** the upward increase is preceded by stabilization
- And** there is evidence of second straight line on the semi-log plot with doubling of slope
- Then** linear discontinuity exists in a homogeneous system
- Or** a heterogeneous system is infinite acting.

In cases where more than interpretation is possible, geological information and well test results from wells in the same area may provide further information and help in the selection of a model. Model verification through history matching also can confirm a particular selected model.

Geological System

The geological system is further decomposed into two subsystems as depicted in Fig. 2. Some of the functionality of the system in KAPPA-PC has been implemented in an effort to determine a frame-based representation of the system and its information. Screen printouts of the KAPPA-PC program are shown in Fig. 9.

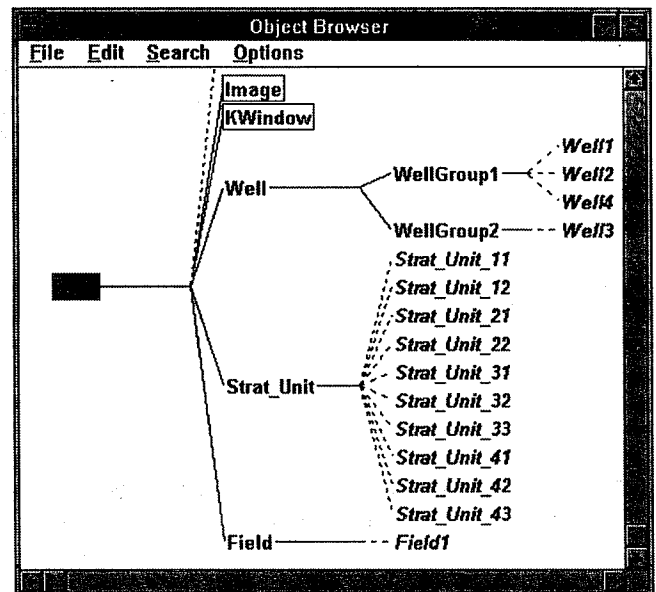


Fig. 9 Frame-based representation of reservoir.

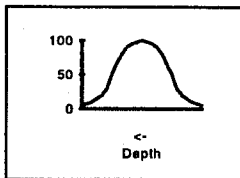
Log Facies Description System

The initial development of the log facies description system concentrates on gamma-ray logs only. An artificial log is being examined at first to determine the location of sand bodies, and then the corresponding logs will be drawn. Initial experiments have been limited to five different wells. The drawings will then be digitized and stored in Microsoft Excel. Excel is used to automate the normalization of the data, as

shown by the 0 to 100 scale on the x-axis of the following illustrations, and to correlate the data. Once implemented in KAPPA-PC, the system will use specific functions to directly interact with Excel to use the previously derived information. The ES portion will include rules similar to the following rules to classify the log facies.

Symmetrical Rule

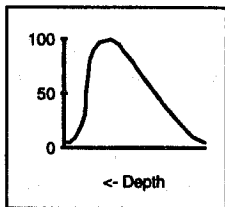
If $(|D_{l10} - D_{u90}|) = (|D_{l90} - D_{u10}|)$
Then the curve is symmetrical.



If the absolute value of the lower **Depth** of the curve at **10** (D_{l10}) minus the **upper Depth** of the curve at **90** (D_{u90}) is equal to the absolute value of the lower **Depth** of the curve at **90** (D_{l90}) minus the **upper Depth** of the curve at **10** (D_{u10}), then the curve is symmetrical.

Bell Rule

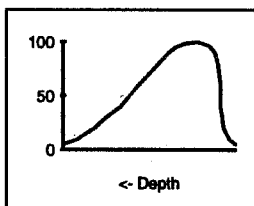
If $(|D_{l10} - D_{l90}|) < (|D_{u90} - D_{u10}|)$
Then the curve is bell shaped.



If the absolute value of the lower **Depth** of the curve at **10** (D_{l10}) minus the lower **Depth** of the curve at **90** (D_{l90}) is less than the absolute value of the **upper Depth** of the curve at **90** (D_{u90}) minus the **upper Depth** of the curve at **10** (D_{u10}), then the curve is bell shaped.

Funnel Rule

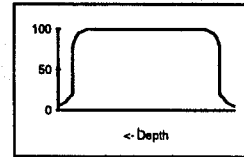
If $(|D_{l10} - D_{l90}|) > (|D_{u90} - D_{u10}|)$
Then the curve is funnel shaped.



If the absolute value of the lower **Depth** of the curve at **10** (D_{l10}) minus the lower **Depth** of the curve at **90** (D_{l90}) is greater than the absolute value of the **upper Depth** of the curve at **90** (D_{u90}) minus the **upper Depth** of the curve at **10** (D_{u10}), then the curve is funnel shaped.

Blocky Rule

If $(|D_{l10} - D_{l90}|) = (|D_{u90} - D_{u10}|)$
Then the curve is blocky.



If the absolute value of the lower **Depth** of the curve at **10** (D_{l10}) minus the lower **Depth** of the curve at **90** (D_{l90}) is equal to the absolute value of the **upper Depth** of the curve at **90** (D_{u90}) minus the **upper Depth** of the curve at **10** (D_{u10}), then the curve is blocky.

Correlation System

Once the log facies for each well have been classified, the information in the wells must be correlated across the reservoir. The initial development of this module of the ES has begun by identifying specific expert rules for correlation and then determining an appropriate representation of the reservoir information within KAPPA-PC. Stratigraphic correlation means the determination of equivalent depositional units prevalent throughout a reservoir under consideration. The types of equivalency include *lithostratigraphic*, referring to similarities in sedimentary rock types using lithologic criteria; *biostratigraphic*, referring to similarities in fossil content; and *chronostratigraphic*, referring to similarities in the time of deposition. The wireline log data are used extensively to determine the equivalency between various stratigraphic units.

Given that $dt1$ and $dt2$ are the depths from the marker bed to the top of the first sand in wells 1 and 2, respectively, some basic rules for well-to-well correlation are:

If $dt1 = dt2$ or nearly so
Then probably the units marked 1 in the two wells are correlatable.

If the log facies of both units are similar
Then it is even more likely that the two stratigraphic units are correlatable.

If the log facies of both units are not correlatable
Then the two units are discontinuous in the middle and they are not stratigraphically equivalent. Move to the next units in sequence.

These rules are translated into a KAPPA-PC function designated as **divide**.

The **divide** function operates on the initial frame-based representation of the reservoir. A frame-based representation is used in the AI system to combine the advantages of object-oriented system with rule-based reasoning techniques. KAPPA-PC offers such a frame-based representation. The representation of the reservoir is shown in Fig. 9.

In Fig. 9 the class units designate wells, stratigraphic units, and oil fields. The information derived graphically from the class unit represents the instances of the class; for example, in the figure, there are four well instances. The stratigraphic unit instances can be recognized as being numbered (by the last number) within a well (by the first number). At this time in the computation, the **divide** function has been executed to separate the wells into correlatable (WellGroup1) and undetermined (WellGroup2).

Once it has been determined that the wells are possibly correlatable, the next step is to find the correlation coefficient between the two units. A high correlation coefficient would indicate that they are correlatable. The correlation coefficient should be computed taking into account the expansion index between the two units under comparison.

In addition, the ES tries to match other evidences, such as drill cutting analysis, side-wall core analysis, and fossil content. The more closely the parameters are related, the more the system increases its certainty in the stratigraphic equivalency.

The following rules pick the next stratigraphic units in the two wells and repeat the preceding procedures.

If $dt1$ is less than $dt2$
Then either the 1st sand on well1 is a pinch out or it is thinning toward well2.

If there is strong evidence of similarities between log features, drill cuttings, sidewall cores, or fossil contents

Then probably unit 1 of well1 is thinning toward well2
Else it is probably a pinch out.

If unit 1 of well1 is a pinch out
Then correlate second unit with the first of well2.

If unit 1 of well1 is thinning toward well2
Then move to the second stratigraphic units on both the wells and start correlation.

If $dt1$ is greater than $dt2$
Then either the 1st sand on well2 is a pinch out or it is thinning toward well1.

If there is strong evidence of similarities between log features, drill cuttings, sidewall cores, or fossil contents

Then probably unit 1 of well2 is thinning toward well1
Else it is probably a pinch out.

If unit 1 of well2 is a pinch out
Then correlate second unit with the first of well1.

If unit 1 of well2 is thinning toward well2
Then move to the second stratigraphic units on both the wells and start correlation.

The KAPPA-PC function **correlate** performs the correlation represented by the preceding rules.

References

1. G. Perez, *Stochastic Conditional Simulation for Description of Reservoir Properties*, Ph.D. dissertation, The University of Tulsa, Tulsa, Okla., 1991.
2. S. Kirkpatrick, C. D. Gelatt, Jr., and M. P. Vecchi, Optimization by Simulated Annealing, *Science*, 671-680 (May 13, 1983).
3. O. F. Allain and R. N. Horne, Use of Artificial Intelligence in Well-Test Interpretation, *J. Pet. Technol.*, 42(3): 342-349 (March 1990).
4. O. P. Houze and O. F. Allain, *A Hybrid Artificial Intelligence Approach in Well Test Interpretation*, paper SPE 24733 presented at the SPE 67th Annual Technical Conference, Washington, D.C., October 4-7, 1992.
5. A. T. Watson and W. J. Lee, *A New Algorithm for Automatic History Matching Production Data*, paper SPE 15228 presented at the SPE Unconventional Gas Technology Symposium, Louisville, Ky., May 18-21, 1986.

ANISOTROPY AND SPATIAL VARIATION OF RELATIVE PERMEABILITY AND LITHOLOGIC CHARACTER OF TENSLEEP SANDSTONE RESERVOIRS IN THE BIGHORN AND WIND RIVER BASINS, WYOMING

Contract No. DE-AC22-93BC14897

**University of Wyoming
Laramie, Wyo.**

**Contract Date: Sept. 15, 1993
Anticipated Completion: Sept. 14, 1996
Government Award: \$258,359**

**Principal Investigator:
Thomas L. Dunn**

**Project Manager:
Robert Lemmon
Bartlesville Project Office**

Reporting Period: Jan. 1-Mar. 31, 1994

Objectives

The objectives of this multidisciplinary study are to provide improvements in advanced reservoir characterization techniques. They are to be accomplished through (1) an examination of the spatial variation and anisotropy of relative permeability in the Tensleep sandstone reservoirs of Wyoming; (2) the placement of that variation and anisotropy into paleogeographic, depositional, and diagenetic frameworks; (3) the development of pore-system imagery techniques for the calculation of relative permeability; and (4) reservoir simulations testing the impact of relative permeability anisotropy and spatial variation on Tensleep sandstone reservoir enhanced oil recovery (EOR).

Concurrent efforts are aimed at understanding the spatial and dynamic alterations in sandstone reservoirs caused by fluid-rock interaction during carbon dioxide (CO₂) EOR processes. The work focuses on quantifying the interrelationship of fluid-rock interaction with lithologic characterization in terms of changes in relative permeability, wettability, and pore structure and with fluid characterization in terms of changes in chemical composition and fluid properties. This work will establish new criteria for the susceptibility of Tensleep sandstone reservoirs to formation alteration that results in change in relative permeability and in wellbore-scale damage. This task will be accomplished by flow experiments with the use of core material, examination of regional trends in water chemistry, examination of local water chemistry trends at field scale, and chemical modeling of the reservoir and experimental systems to scale up the experiments to reservoir conditions.

Summary of Technical Progress

Regional Frameworks

This research will associate spatial distributions and anisotropy of relative permeability with the depositional subfacies and zones of diagenetic alteration found within the Tensleep sandstone. The associations between depositional lithofacies, diagenetic alteration, and pore geometry will strongly link relative permeability with the distinct and measurable dimensions of lithofacies and authigenic mineral facies. Effects of the depositional processes and burial diagenesis will be investigated.

Two geologists were hired to work on the regional frameworks task: one on database development and construction of the regional and field-scale maps and cross sections and the other on construction of the regional depositional and lithofacies frameworks and on field work.

Compilation of existing literature, maps, and cross sections is complete. In addition, field data from more than 60 fields producing from the Tensleep in the Bighorn and Wind River Basins have been compiled. The construction of the regional database continues. The Dwight's database contains data on approximately 14,000 wells in the area of interest. Input files are being built and edited for the Production Analyst software. A structure map of the two basins showing

the Tensleep fields has been constructed; it will serve as a base map for portions of the program results.

Relative Permeability Measurements

The focus of this task is to obtain quantitative laboratory data on the magnitude and variability of relative permeability anisotropy and spatial variation of the dominant reservoir and boundary surface lithologies of the Tensleep sandstone. Existing data will be collected, compiled, and placed within the regional frameworks constructed. Laboratory measurements will be performed in the Petroleum Engineering Department at the University of Wyoming. The unsteady-state technique will be used to measure relative permeability. An additional objective of this study is to provide algorithms for calculating relative permeability from quantitative pore imagery data.

The engineering effort continues to focus upon laboratory apparatus setup. The constant-rate fluid pump has been installed. The apparatus is nearing completion. A search of the published literature revealed only a few relative permeability analyses for the Tensleep. Enlargement of the compilation will be attempted through contacts with the industrial advisor/mentors. Conventional core analyses of the Tensleep sandstone were obtained from 68 wells during the quarter. These data are being prepared for input into the database. The decision to purchase production data for the Tensleep is pending.

CO₂ Flood—Formation Alteration and Wellbore Damage

The work of this task is to establish criteria for the susceptibility of Tensleep sandstone reservoirs to formation alteration that results in a change in absolute or relative permeability and possible wellbore scale damage during CO₂ EOR. This advanced reservoir characterization technology will be used to optimize recovery efficiency. This task includes (1) flow experiments on core material to examine the effects of CO₂ flooding on the alteration of the fluid and rock system; (2) examination of regional trends in water chemistry; (3) examination of local water chemistry trends at field scale; and (4) chemical modeling of both the reservoir and experimental systems in order to scale-up the experiments to reservoir conditions.

More than 1500 formation water analyses were obtained from the Wyoming State Geological Survey during the quarter. Approximately 90 of these waters are from the Tensleep sandstone reservoirs. These data are being prepared for input to the database. Some additional temperature information on each water, required in order to fully utilize this dataset in the water modeling, is being collected.

Project Management and Technical Transfer

This task incorporates efforts to achieve a high level of success in this interdisciplinary project. This administrative task provides for effective coordination and integration of the

project's research tasks. The program manager is responsible for ensuring that the task workers meet on a frequent and regular basis to exchange information and discuss results. The program manager is responsible for the coordination and timely reporting of results to its industry advisor/mentors, the U.S. Department of Energy, and the scientific and engineering communities.

The resulting research will integrate various geophysical and hydrological methods and apply them at a well-calibrated and characterized site, where their use can be assessed. This cooperation will allow techniques developed for waste storage and geothermal energy to be adapted for use in heterogeneous and fractured reservoirs. The work will be coordinated with the cross-well electromagnetic (EM) research and development (R&D) Project and the LBL/Morgantown Energy Technology Center (METC) reservoir performance definition project.

Summary of Technical Progress

Hydrologic-Related Work

Two tasks related to the hydrological inversion of the pilot-site well tests were carried out this quarter. Visualization of pilot-site hydrogeology continued with 3D-Rock, an integrated database and visualization package tailored to geologic media. Cross-validation studies of the lower sand channel pressure transients were completed.

Visualization of Pilot-Site Hydrogeology

Visualization can be used not only to represent the finished product of reservoir characterization but also to help develop understanding during the characterization process; this illustrates how different kinds of information add to that understanding. The starting point for development of a subsurface model is usually borehole-based, with information derived from core samples and well logs. Well-test analysis can be used to infer connectivity between high-permeability zones (or equivalently, continuity of low-permeability zones), and geophysical imaging can provide more detail on the extent of such zones. Visualization of each stage shows the current understanding of the subsurface, and a series of visualizations increases understanding incrementally as each type of information is added. Through this process the most useful characterization tools are determined.

Previous visualizations of the Gypsy pilot site showed lithology (inferred from cores and well logs such as gamma ray and neutron density) and hydrologic connectivity (inferred from well-test data) at wellbore locations. Figure 1 extends this visualization work to draw in surfaces representing the low-permeability clay layers separating the sand channels within the Gypsy formation. The Gypsy-Tallant contact and the dense red clay layer are inferred to be continuous low-permeability layers based on the well-test analysis (i.e., the lower sand channel behaves like a confined aquifer and does not communicate with the upper or middle sand channels). The upper clay is known to be discontinuous over the well-field scale from well-test analysis and by its absence in wells 5-7 and 8-7. At present, its extent can only be conjectured. One possibility is shown somewhat schematically in Fig. 1. This figure is the first in a series. As more information is added from further hydrologic inversion of the upper and middle sand channels and information is incorporated from the cross-well seismic surveys, a greater understanding of

LAWRENCE BERKELEY LABORATORY/ INDUSTRY HETEROGENEOUS RESERVOIR PERFORMANCE DEFINITION PROJECT

Lawrence Berkeley Laboratory
University of California
Berkeley, Calif.

Contract Date: Apr. 1, 1992
Anticipated Completion: September 1995
Government Award: \$275,000
(Current year)

Principal Investigators:

J. C. S. Long
E. L. Majer
L. R. Myer

Project Manager:

Robert Lemmon
Bartlesville Project Office

Reporting Period: Jan. 1-Mar. 31, 1994

Objectives

The purpose of this work is to validate geophysical and hydrological techniques for characterizing heterogeneous reservoirs in the most optimal (economic) manner. The overall objective of the project is to develop a methodology that can be used by the petroleum industry in a variety of heterogeneous regimes for characterizing and predicting the performance of petroleum reservoirs.

This objective will be accomplished through a cooperative research program between Lawrence Berkeley Laboratory (LBL), British Petroleum, Inc. (BP), and the University of Oklahoma (OU), which is focused on the characterization of heterogeneous reservoirs in a meander-belt porous-medium formation. BP has done characterization and data integration at several test facilities. The present program will continue BP's multiyear efforts at the Gypsy site in northeastern Oklahoma.

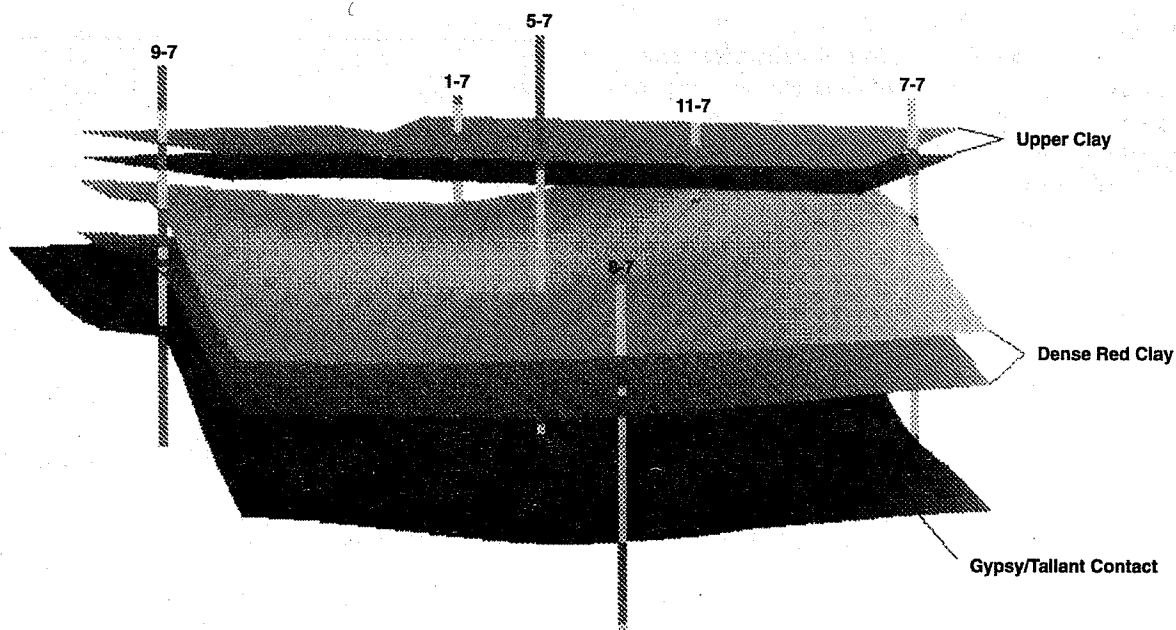
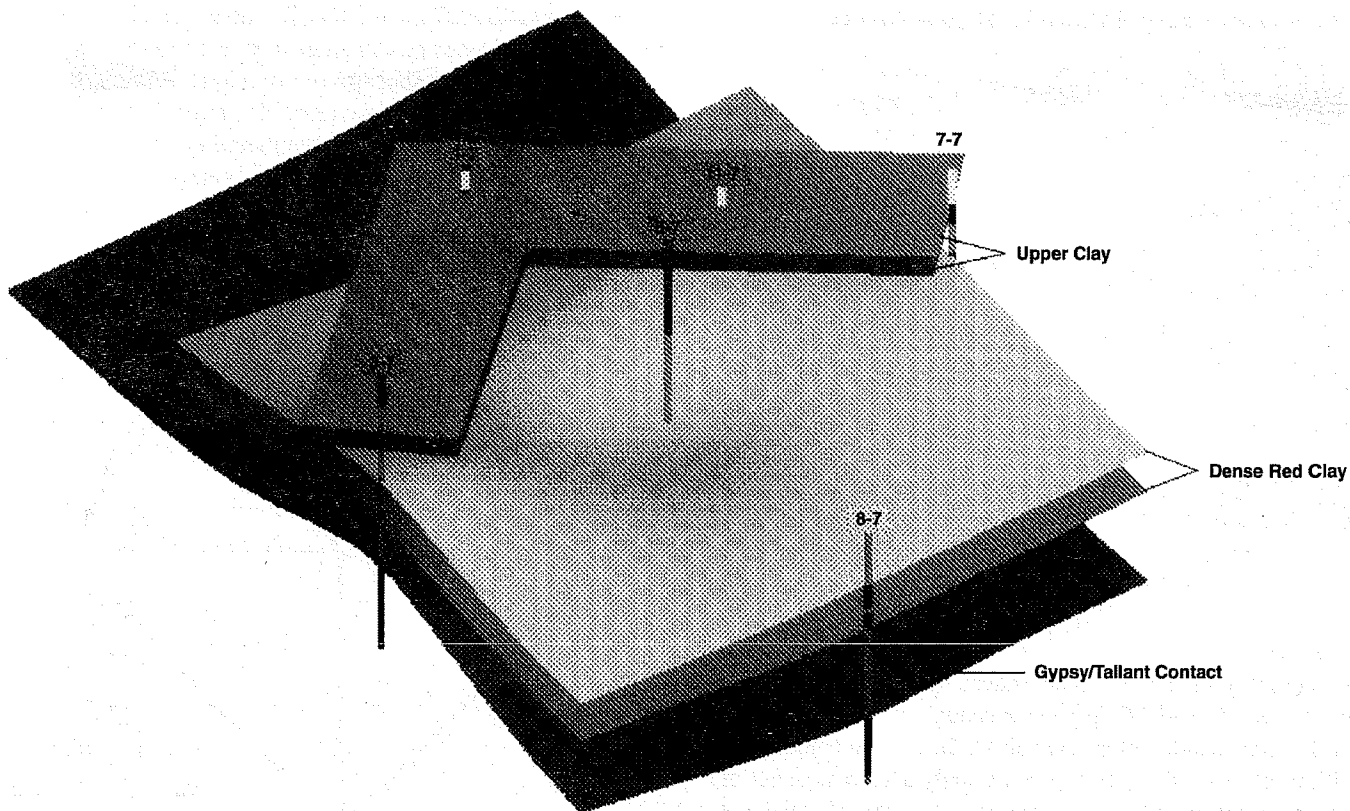


Fig. 1 Two views of the Gypsy pilot site with the top and bottom surfaces of two prominent clay layers shown. The Gypsy-Tallant contact and borehole lithologies (light is sand, dark is clay) are also shown. Vertical scale is stretched by a factor of 4. The location of the upper clay layer is just conjectured; as more analyses are done its location should become more certain.

the system will be reflected via a more detailed visualization. Other kinds of information may enhance understanding as well; for example, dipmeter logs were taken for several of the pilot-

site wells. It may be possible to extrapolate the dip of the upper and lower surfaces of a clay lens to estimate the location where it pinches out.

Lower Sand Channel Cross-Validation Studies

Cross-validation may be used to assess how well a hydrologic inversion is working and to judge how much and what kind of information is contained in the well-test data. In cross-validation, only some of the available data are used in the inversion process, and the inferred hydrological model is subsequently used for matching. If the model cannot match the held-out data, it suggests that there is a significant amount of new information in that data that is not contained in the original observations used to develop the model.

Figure 2 shows a schematic diagram of the lower sand channel well-test data. Five tests were conducted, each using a different well as the pumping well. The test in which the sixth well, well 9-7, was the pumping well is suspected of experiencing packer failure, so no data from that test are considered. There are 12 observed pressure transients for which both the pumping well and observation well were screened in the lower sand channel; each is shown in Fig. 2 as a curve connecting the appropriate pumping and observation wells. Only two of the tests, 90/S4/T1 and 90/S3/T1, provide pressure transients that are complete enough for independent inversions. Two other tests, 90/S1/T1 and 89/T2, provide enough partial information (early time pressure transients only) to be used in conjunction with other tests. Test 89/T1 provides only a short segment of early time data from one observation well and probably will not add much to the analysis.

The following sequence of inversion studies has been carried out for the lower sand channel well tests as a cross-validation exercise:

1. Repeated inversions of test 90/S4/T1 yield similar patterns of transmissivity for the region between the pumping and observation wells (the upper half of the well field) but highly variable results for transmissivity outside that region (the lower half of the well field). Repeated inversions of test 90/S3/T1 show comparable behavior, which suggests that neither of these tests alone provides adequate information to characterize heterogeneity throughout the well field.

2. Repeated co-inversions of tests 90/S4/T1 and 90/S3/T1 yield similar patterns of transmissivity throughout the well field. Figure 3 shows the transmissivity distribution for one such inversion. The key features to note are the high transmissivity region in the lower left quadrant, medium transmissivity values in the lower right, and generally low transmissivities in the upper half, with the lowest values in the upper left. These features recur in each inversion and can be traced to specific features in the pressure transients for the two tests that were co-inverted.

3. The transmissivity distribution shown in Fig. 3 is then used to model all the well tests individually. The returned energies are compared with the energies obtained with a model that uses a single uniform value of transmissivity. The energy provides an overall value for the mismatch between the observed and calculated pressure transients for a given model. The results are summarized in Table 1, which also shows the results of the best individual inversion of each well test.

Both tests 90/S3/T1 and 90/S4/T1 show much lower energies for the co-inversion model than for the uniform medium model. This is expected because information from each of these tests was used in the co-inversion. The true cross-validation check is to compare energies for the other tests. Both tests 89/T2 and 90/S1/T1 show an energy decrease of nearly a factor of 2 for

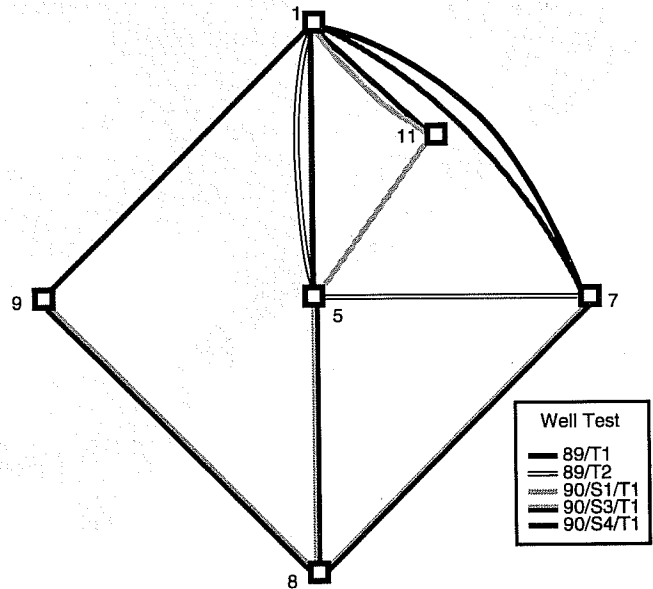


Fig. 2 Gypsy pilot-site lower sand channel well-test schematic.

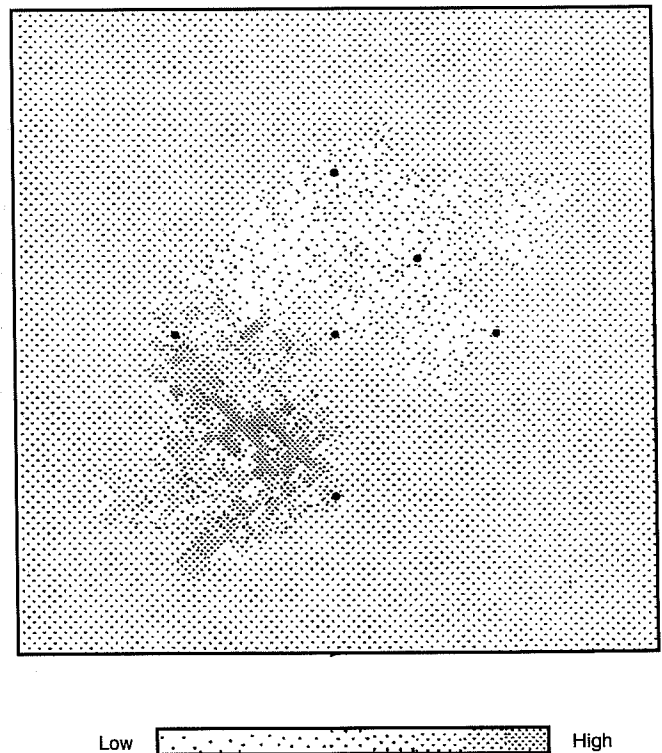


Fig. 3 Transmissivity distribution inferred from the co-inversion of tests 90/S3/T1 and 90/S4/T1. BP33, E = 2.29.

TABLE 1
Modeled Well Tests Energies

Test	Uniform medium model	Model based on co-inversion of 90/S3/T1 and 90/S4/T1	Best individual inversion
90/S4/T1	10.0	2.8	2.0
90/S3/T1	13.7	2.0	2.7
90/S1/T1	17.3	9.6	1.3
89/T2	50.0	25.4	-
89/T1	0.6	4.3	-

the co-inversion model compared with the uniform medium model. Test 89/T1 shows an increase in energy, but so few observed data are available for this test that the overall conclusion remains that the cross-validation exercise is successful.

4. An individual inversion of test 90/S1/T1 yields a much lower energy than does the co-inversion model, which suggests

that there is extra information to be gained by a co-inversion of all three of (90/S4/T1, 90/S3/T1, and 90/S1/T1). Test 89/T2 shows rather odd, flattened pressure responses that suggest instrumentation problems, so it has not been included in further analysis. A co-inversion of the three 1990 tests has been done with the previous co-inversion model as its starting point. The initial energy is $E = 3.8$ (the energy is normalized by the number of observed data points); there are about twice as many observed pressures for tests 90/S4/T1 and 90/S3/T1 as there are for test 90/S1/T1, so $E = \{[2(2.0 + 2.8) + 9.6]/5 = 3.8\}$. At the end of the inversion, the energy has been reduced to $E = 2.4$. The resulting transmissivity distribution is shown in Fig. 4, and the 90/S1/T1 portions of the pressure transients are shown in Fig. 5. The main difference in the calculated pressure transients between the start and end of the inversion is that the response is smaller at well 5-7 when well 11-7 is pumped. This difference is reflected in the transmissivity distribution around well 5-7 by the extension of the low transmissivity region between wells 5-7 and 11-7.

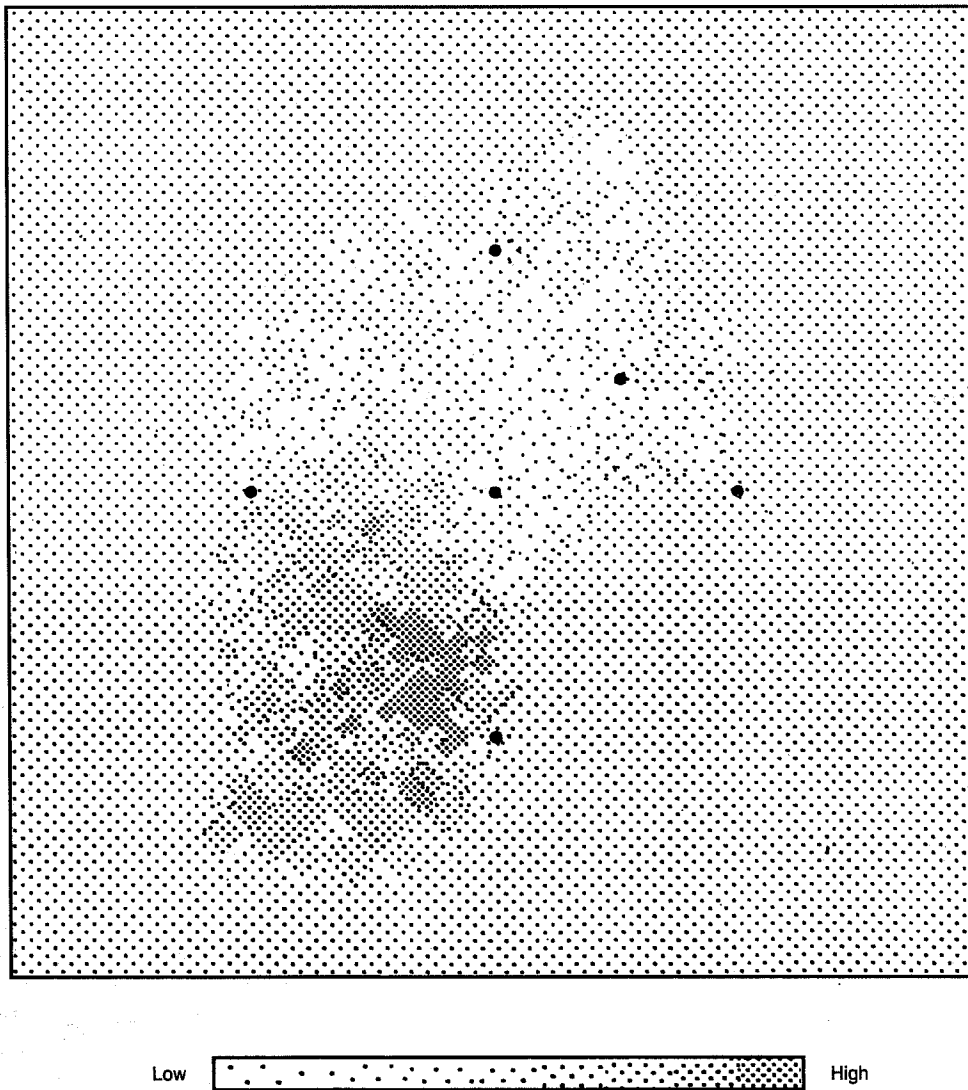


Fig. 4 Transmissivity distribution inferred from the co-inversion of tests 90/S1/T1, 90/S3/T1, and 90/S4/T1. BP45, $E = 2.39$.

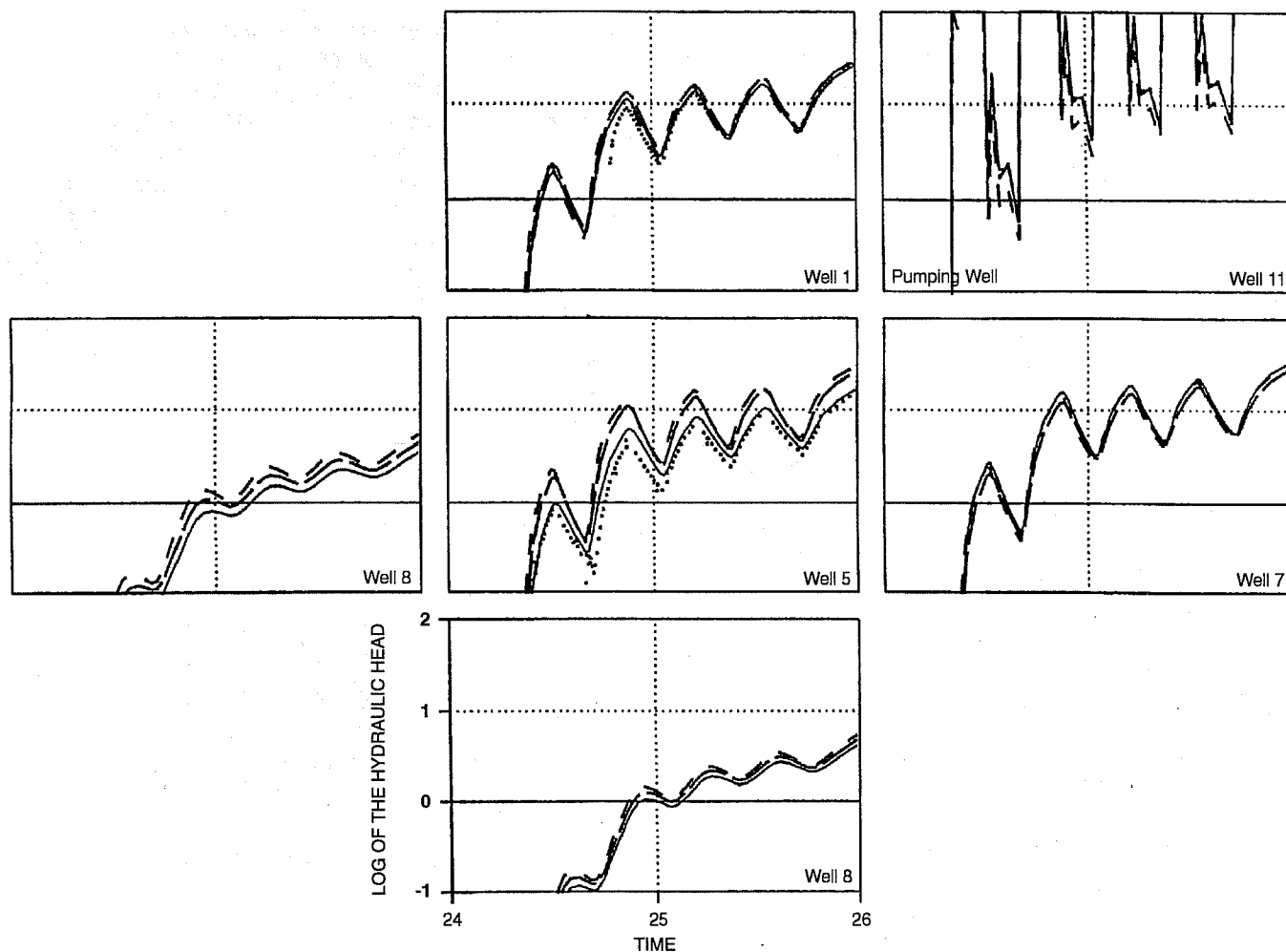


Fig. 5 Pressure transients for the co-inversion of tests 90/S1/T1, 90/S3/T1, and 90/S4/T1. BP45. ●, observed. ---, uniform medium. — — —, start of inversion. —, end of inversion.

This procedure of sequential model building, in which the well tests with the most observed data available are inverted individually first, then co-inverted together, then co-inverted with additional information to fine tune the transmissivity distribution, appears to be successful. Because the computational effort of the calculations increases dramatically as more tests are added to the co-inversion, it makes sense to first try to infer the major features of the transmissivity distribution with the minimum number of tests possible and then use this distribution as a starting point for further inversions.

Seismic-Related Work

Three tasks related to seismic imaging were carried out this quarter:

1. Development of seismic inversion techniques continued with examination of the nature of local minima found by optimization algorithms used in travel-time tomography.

2. Outcrop-site cross-well seismic data collected in 1993 were assessed.

3. Pilot-site cross-well seismic data received on OU's first Gypsy compact disc (CD) were examined.

The Nature of Local Minima Found by Travel-Time Tomography

It is often stated that local minima exist in nonlinear inverse problems. The exact nature of such local minima has not been satisfactorily explored. A synthetic travel-time tomography problem has been used to examine how local minima arise. The geometry of the cross-borehole tomography problem is identical to that of one of the Gypsy experiments. The model consists of a grid of 63 constant velocity blocks between two boreholes. Local minima appear when constraints are introduced (i.e., when penalty terms are included in the inversion). Examples of penalties are model parameter norm and model parameter roughness. The attempt has been made to characterize the local minima through the generation of a large set of

models fitting the data and satisfying the associated penalties. A conjugate gradient algorithm was used to construct a suite of 1123 models. A random number generator was used to produce a starting model to initialize the conjugate gradient sequence. The Parallel Virtual Machine (PVM) software enabled generation of the models in parallel on a network of workstations.

The models that fit the data and satisfy the penalties are found to cluster into a number of distinct groups (Fig. 6). For a determination of the number of local minima present, the number of clusters must be deduced and the models grouped into clusters. Algorithms for such declustering have been implemented and are currently being tested on the ensemble of acceptable models. One goal is to determine the exact number of clusters, or local minima. The number of clusters may be estimated by plotting the intercluster distance (the sum of the squares of the distances in parameter space between each model and the nearest cluster center) against the number of clusters (Fig. 7). When the intercluster distance is not significantly changed as a new cluster is introduced, that cluster is not necessary. The members of the ensemble tend to cluster into approximately 80 local minima. The minima tend to share common features and to resemble the model used to generate the synthetic data. The clustering methods will be applied to the actual Gypsy travel-time data set.

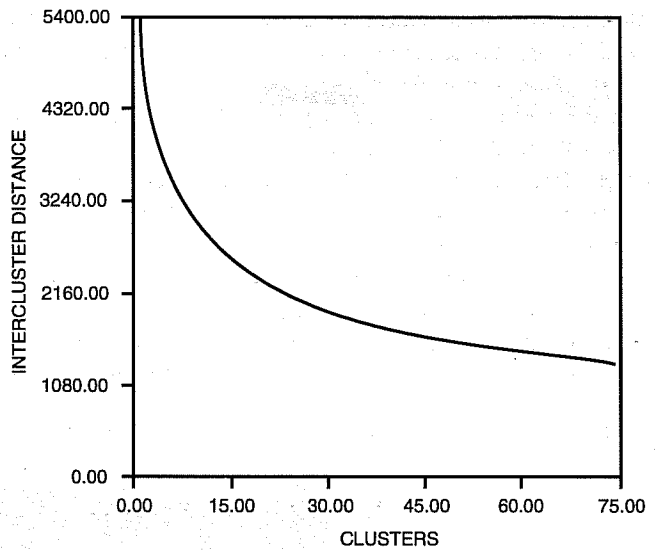


Fig. 7 Intercluster distance (sum of the squares of the distances in parameter space between each model and the nearest cluster center) as a function of the number of clusters.

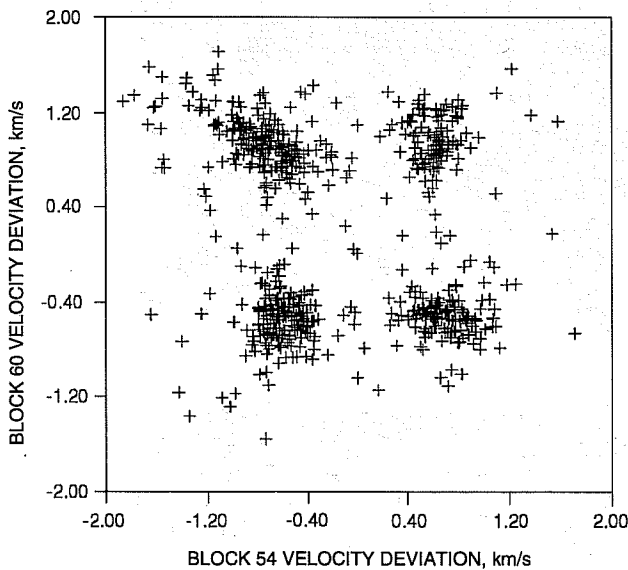


Fig. 6 Values of velocity deviation for two blocks for the ensemble of models that fit the data and satisfy the imposed penalties. In the two-dimensional parameter space shown, the models cluster into four local minima.

Assessment of Outcrop-Site Cross-Well Seismic Data

Figure 8 shows the boreholes used for the outcrop-site cross-well seismic surveys run in 1993. Data from the A-4,

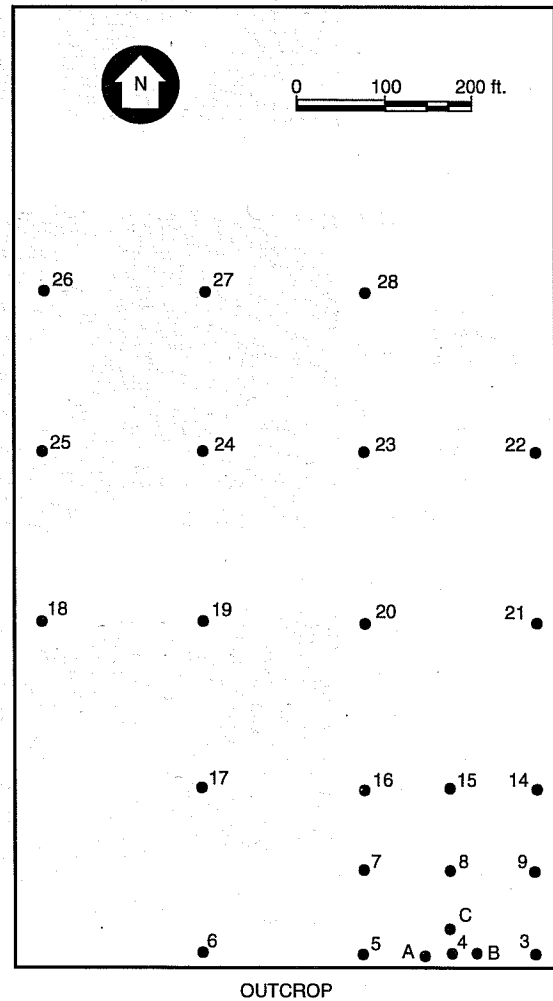


Fig. 8 Plan view of the boreholes at the Gypsy outcrop site. Cross-well seismic profiles were taken between borehole pairs A-4, B-4, C-4, and A-C.

B-4, and C-4 tests (source in borehole 4, receivers in boreholes A, B, and C, respectively) have been examined. The single source–multiple receiver plots show large attenuation (no signal at all at any receiver) when the source is above a depth of about 12 m (39 ft). This corresponds to most of the Gypsy interval. Thus any information to be gained from the outcrop-site cross-well data will be limited to the lowermost region of the Gypsy interval.

When the source depth is between 12 and 13 m, there is a weak signal for receivers in the depth range 14 to 19 m. When the source is below 13 m, there is a strong signal for receivers in the depth range 14 to 19 m. Figure 9 shows a sample of the traces

for the A-4 profile; the B-4 and C-4 profiles look comparable. This response implies that there is a high-velocity, low-attenuation layer at depths of about 14 to 19 m. According to the borehole lithologies, these depths correspond to the bottom of the lowest sand channel (composed of mud-clast conglomerate at 13 to 15 m), floodplain deposits (15 to 17 m), and the top of the Tallant marine sandstone (17 to 19 m). From the seismic response it is inferred that, in order to form a continuous high-velocity layer, these lithofacies must be continuous between the boreholes.

Comparison of the seismic response to gamma logs and lithology helps further interpret the seismic data. Gamma

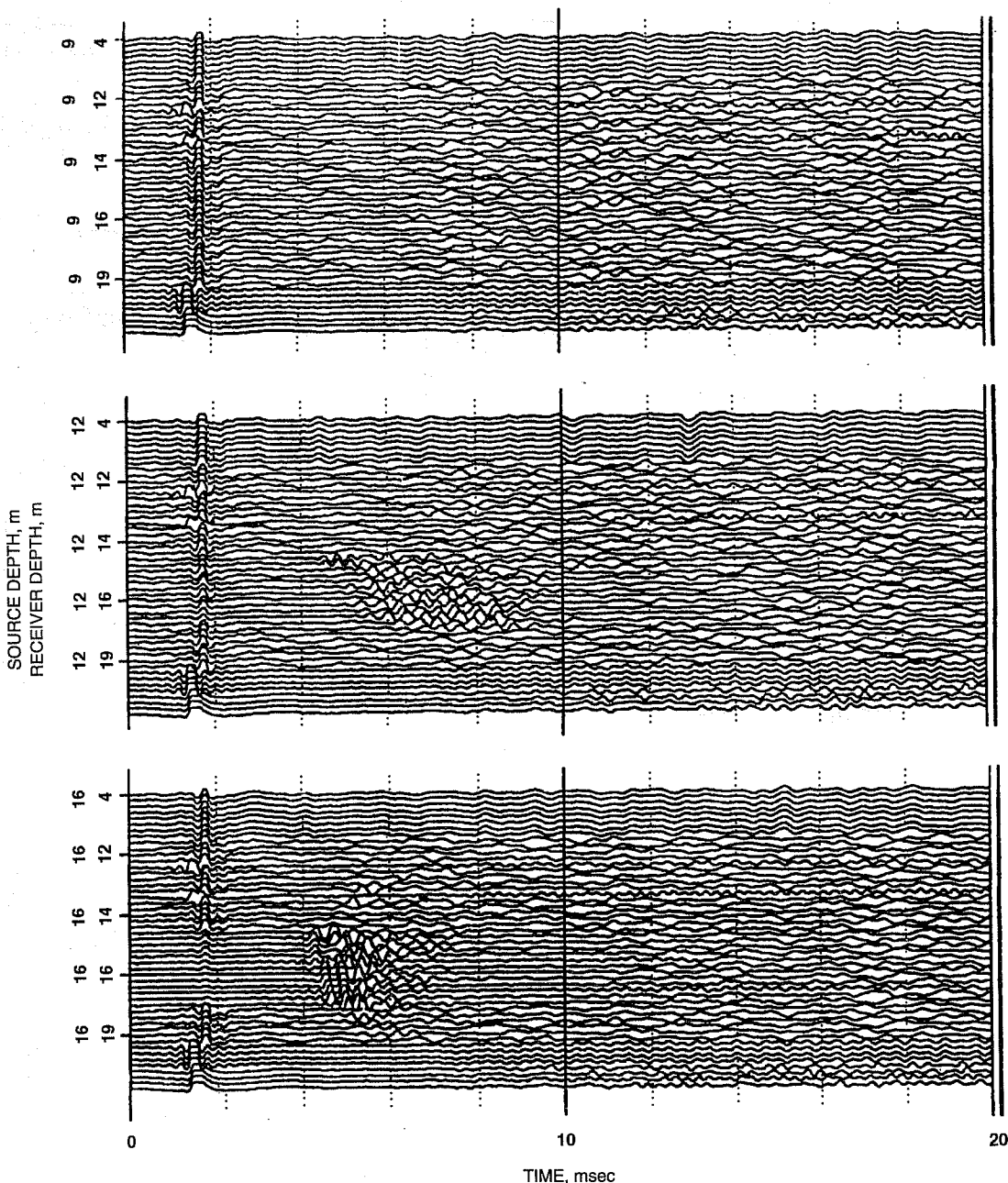


Fig. 9 Single source–multiple receiver plots for Gypsy outcrop-site borehole pair A-4.

logs (Fig. 10) for boreholes 3, 4, and 5 show a larger response in the lowest Gypsy interval and a smaller response above it, following the same trend as the cross-well seismic response; lithologies for boreholes 3, 4, and 5 show predominantly sands above 11 to 14 m (36 to 46 ft). In contrast, in borehole 8 there is a moderate gamma response over most of the borehole depth, and the lithology for borehole 8 shows a mixture of sands and muds, which is consistent with this response. Note that borehole C is part way between borehole 4 and borehole 8. The fact that the seismic response for the C-4 profile looks very similar to that of the A-4 and B-4 profiles suggests that the distinct sand-mud lithological character of borehole 8 does not extend as far as borehole C.

Preliminary Assessment of Pilot-Site Cross-Well Seismic Data

Preliminary assessment of the pilot-site cross-well seismic data set, which was received on OU's first Gypsy CD, has begun. Single source-multiple receiver traces for well pairs 5-7 and 1-7 have been plotted; an example is shown in Fig. 11. The data quality looks good. In contrast to the outcrop-site cross-well seismic data, there is a strong signal at all receivers for all source depths throughout the Gypsy interval. Significant variations in arrival times as well as multiple reflections should make interesting interpretations

possible; detailed interpretations will begin soon. For the creation of travel-time tomograms, the first arrival times need to be picked off all the traces. With approximately 100 receiver depths and 100 source depths of interest, there are at least 10,000 traces for each of three well pairs, which means that picking will be a significant effort. Picked-first arrival times were not included in the Gypsy CD, but tomograms based on these times have been published.¹ Rather than duplicating the picking work, an attempt will be made to obtain this information.

Information Transfer

Southwest Research Institute is using the Gypsy site to study the relationship between attenuation of seismic energy and permeability; they are using air permeability as measured in core samples. The advantage of using permeability inferred from well-test analysis (it gives an effective value averaged over the well-field scale) was discussed, and some of the transmissivities quoted in the BP well-test summary reports were converted to permeabilities to compare with the core-sample values. For the lower sand channel, the core-sample permeability (780 to 1400 mD) appears to be somewhat lower than the well-test permeability (1500 to 2300 mD). Such a scale dependence of permeabilities is not uncommon and illustrates the importance of doing field-scale characterization studies.

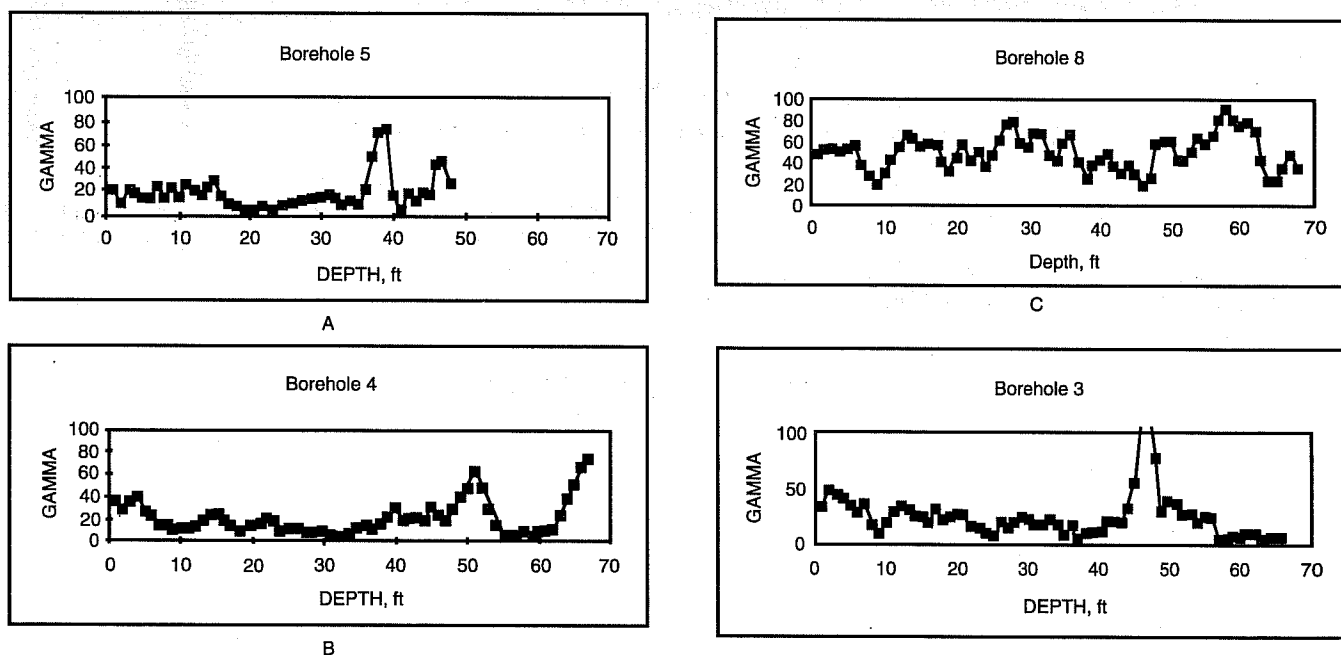


Fig. 10 Gamma logs for boreholes 3, 4, 5, and 8. The arrangement of the plots follows the locations of the borings; the locations of borings A, B, and C are shown schematically.

RESOURCE ASSESSMENT TECHNOLOGY

**CONTINUED SUPPORT OF THE
NATURAL RESOURCES INFORMATION
SYSTEM FOR THE STATE OF
OKLAHOMA**

Contract No. DE-FG22-92BC14853

**Oklahoma Geological Survey
University of Oklahoma
Norman, Okla.**

**Contract Date: May 18, 1992
Anticipated Completion: May 17, 1994
Government Award: \$350,000
(Current year)**

**Principal Investigators:
Charles J. Mankin
Terry P. Rizzuti**

**Project Manager:
R. Michael Ray
Bartlesville Project Office**

Reporting Period: Jan. 1-Mar. 31, 1994

Objective

The objective of this research program is to continue developing, editing, maintaining, using, and making publicly available the Oil and Gas Well History File portion of the Natural Resources Information System (NRIS) for the state of Oklahoma. This contract funds that ongoing development work as a continuation of earlier contract numbers DE-FG19-88BC14233 and DE-FG22-89BC14483. The Oklahoma Geological Survey (OGS), working with Geological Information Systems (GIS) at the University of Oklahoma Sarkeys Energy Center, has undertaken the construction of this information system in response to the need for a computerized, centrally located library containing accurate, detailed information on the state's natural resources. Particular emphasis during this phase of NRIS development is being placed on computerizing information related to the energy needs of the nation, specifically oil and gas.

Summary of Technical Progress

The NRIS Well History File contains historical and recent completion records for oil and gas wells reported to the Oklahoma Corporation Commission (OCC) on Form 1002-A.

entire county had been copied and sent, and received to be recopied, coded, keyed, and entered into the Well History File. Forms from the first shipment of Osage records were reviewed to ascertain how many different form layouts were used to report well completions. It was determined that five layouts would require new keying formats, reformatter programs, and processing job streams. The five layouts were reviewed to identify what data elements were unique to the Osage forms. As a result of this review, 62 labels were identified and added to the data dictionary. Coding procedures for these data elements and formats were established, and coding began. Data-entry keying formats, reformatter programs, and processing streams were developed and tested, and data entry began early in the current quarter.

It is expected that 400,000 forms will be on file by the close of the contract. The processing of the Osage County records is proceeding at approximately half the pace as processing of the 1002-A forms because of the increased amount of data recorded on the Osage forms. However, a no-cost extension has been requested of the U.S. Department of Energy (DOE) through September 1994, at which point it is estimated that approximately 375,000 forms will be on the file. The remaining 38,000 forms will require additional funding, so discussions will be initiated with DOE to identify funding options for completing Osage County data transfer.

Efforts to standardize the formation names on the Well History File are continuing. A personal computer (PC)-based program uses a conversion table to standardize spellings and allows the user to interactively build new entries for the conversion table as new spelling variations are encountered. In the southeast, southwest, and northwest regions, over 99% of the reported names have been standardized. Efforts to standardize formation names in the northeast region are complete, with 97% standardized. Efforts on the north-central region were resumed, with 95% of the region standardized. This formations-editing process is further enhanced by the addition of a table to determine the standard Franklized abbreviation for each reported name following the convention with which industry users are familiar.

One goal of the NRIS system involves efforts to assign leases and wells to fields on the basis of the official field outlines as designated by the Midcontinent Oil and Gas Association's Oklahoma Nomenclature Committee (ONC). Some areas exist in which significant field extension drilling has taken place, but the ONC has had insufficient resources to update the field boundaries accordingly. To assist the ONC in updating their field outlines, information packages are produced from the NRIS system for selected areas; these packages include well data listings and well spot maps. On the basis of this input, the ONC began by first updating several gas-field boundaries; emphasis has shifted to oil-field boundaries as work proceeds on a separate DOE project involving the identification and evaluation of Oklahoma's fluvial-dominated deltaic reservoirs. Overall, unassigned gas production comprises 13% of the annual average production, and unassigned oil production comprises 20%.

During the previous quarter, 28 new data elements were added to accommodate the new 1002-A completion report forms for 1992. A new reformatter program was written as well as a processing job stream. Keying of the forms began this quarter and is proceeding smoothly. Initial efforts for the January 1994 data release were completed this quarter also, and all new data elements (definitions and coding instructions) will be documented in the NRIS Data Manual. It is anticipated that the 92 new data elements for the 1992 forms and the Osage County records will be included in the July 1994 data release.

Public Data Release

Since early 1991 efforts have been made to disseminate NRIS information through meetings, workshops, OGS annual reports, and mass mailings to numerous individuals, companies, and organizations. As a result, a dramatic response to the release of NRIS data began during the summer of 1991 and has continued. Feedback from the public continues to reflect excitement about this new resource for the oil and gas industry in Oklahoma. Data and analyses have been provided that would not have been feasible before construction of the NRIS system.

One commercial firm subscribes to the Well History File, and several inquiries are received each quarter from small companies and independents who typically acquire NRIS subsets to evaluate within their specific computer systems before committing to larger data acquisitions.

Also, as previously reported, NRIS well data have been made available through the Oklahoma City Geological Society Library with positive results. The high level of interest by library members has led to the acquisition of several thousand records by several members as well as constructive feedback on user-detected data anomalies. Also, the Library, which is cataloging its extensive well-log collection and tying each log to the corresponding NRIS well record, will be able to provide a listing of logs for which no NRIS records are on file. This should enhance efforts to locate missing well records.

OGS is establishing a computing facility to promote user access to the NRIS data, initially by staff and eventually by the public. A PC-level relational database management system called Advanced Revelations is being used to develop a menu-driven retrieval system customized to NRIS data. A large digitizer, large plotter, and desktop scanning equipment enhance the capabilities available through GeoGraphix and Radian CPS/PC contour mapping software as well as through ARC/INFO, a Geological Information Systems (GIS) spatial analysis tool.

The NRIS data are a significant factor in several projects. One such project, completed in conjunction with the Geography Department, involved the creation of a GIS database of oil and gas pipelines for the Oklahoma Ad Valorem Task Force in which four Oklahoma counties were used as a pilot study. The NRIS well data were included as related data layers. Another, a DOE project, involves the study of Oklahoma's

fluvial-dominated deltaic reservoirs. A third project, which involves cooperative research with the School of Civil Engineering and Environmental Science, is the creation of a GIS database (with a wellhead protection component) containing

current and potential waste sites located on Oklahoma's Cheyenne/Arapaho tribal lands. A fourth involves a secondary gas recovery project with the Texas Bureau of Economic Geology.

**ASSIST IN THE RECOVERY OF
BYPASSED OIL FROM RESERVOIRS
IN THE GULF OF MEXICO**

Contract No. DE-AC22-93BC14831

**Louisiana State University
Baton Rouge, La.**

**Contract Date: Feb. 18, 1992
Anticipated Completion: Mar. 18, 1994
Government Award: \$2,025,755**

**Principal Investigator:
Phillip A. Schenewerk**

**Project Manager:
Gene Pauling
Metairie Site Office**

Reporting Period: Jan. 1-Mar. 31, 1994

Objectives

The objective of this research is to assist the recovery of noncontacted oil from known reservoirs on the Outer Continental Shelf (OCS) in the Gulf of Mexico. Mature offshore reservoirs, declining oil reserves, declining production, and other natural forces are accelerating the abandonment of offshore oil resources and production platforms. As these offshore wells are plugged and the platforms are abandoned, an enormous volume of remaining oil will be permanently abandoned. Significant quantities of this oil could be recovered with advanced technologies now available if the resource can be identified. Project research will proceed under three broad phases: data analysis, supporting research, and technology transfer.

The Tertiary Oil Recovery Information System (TORIS)-level data will be collected on the major fields located in the piercement salt dome province of the Gulf of Mexico OCS. Representative reservoirs will be studied in detail to evaluate undeveloped and attic oil reserve potential. These detailed investigations will be used to calibrate the TORIS-level predictive models. The recovery potential of advanced secondary and enhanced oil recovery (EOR) processes and the exploitation of undeveloped and attic oil zones for salt dome reservoirs in the Gulf of Mexico will be assessed.

Supporting research will focus on the modification of public domain reservoir simulation models to accurately simulate the conditions encountered in the piercement salt dome province of the Gulf of Mexico. Laboratory research will focus on the development of fluid relationships that will be used in the simulation of miscible and immiscible processes in the project area.

A significant effort is planned to transfer the results of this project to potential users of the technology. Technology transfer activities will also provide feedback channels that will help keep the analysis and supporting research focused on the most important problems associated with this project.

Summary of Technical Progress

Data Analysis

A report on the simulation work performed on Reservoir 3 of Field 2 (U-8 reservoir) was completed as a master's thesis.¹ This Gulf of Mexico oil reservoir was placed on initial production in November 1982. With initial oil in place (OIP) estimated at 17.3 million stock tank barrels (MMSTB), the reservoir was expected to produce a significant quantity of hydrocarbons during the primary phase of production. However, after 11 years and 3 production wells, the reservoir had produced only 1.8 MMSTB of oil (10% of the estimated OIP) and 7 billion cubic ft (bcf) of gas. The wells also produced 879 thousand bbls (Mbbbl) of water.

The U-8 reservoir is located on the north side of a large salt tongue that has risen diagonally through surrounding sediments, creating an extremely complex fault pattern. The reservoir lies on the northeast side of a major fault that radiates out from the salt. Several minor faults that splay out from this major fault form the boundaries of the reservoir block. These minor faults partially isolate portions of the reservoir block and create long migration pathways from sections of the reservoir to the producing wells.

Two major oil companies, or producers, have penetrated the U-8 sand with four producing wells. One producer controls the northern portion of the reservoir, while the other has been developing the southern section of the block. One well in the northern portion penetrated the reservoir but was not completed. The other three wells have been productive.

Early interpretations of the reservoir were based on two-dimensional (2-D) seismic lines shot in the 1970's and 1980's. The original structural interpretation of the area showed a

saddle-shaped structure with an anticlinal feature at each end (Fig. 1). The three producing wells were placed to produce from the crest of the northern anticline and from an area just south of the low point on the saddle.

As the area was developed, additional information was gathered and three dimensional (3-D) seismic surveys were run. The data were collected and seismic workstations were utilized to interpret the new data. The results showed a much more complicated picture than was originally envisioned. The first 3-D interpretation is shown in Fig. 2. The major faults surrounding the reservoir have been reinterpreted and the internal structure of the sand is shown as much more complex. The anticlinal features are much less obvious. However, the production from the southern portion of the reservoir did not match any pattern that would have been predicted based on the initial geologic interpretation made.

The sand was subdivided into three layers (A, B, and C) with two intervening shale zones. The top layer was a relatively uniform blanket sand, between 12 and 15 ft thick. A shale zone isolated this unit from the underlying B sand, a much thicker but more irregular sand body. The upper unit appears to be completely oil-saturated at all of the penetration points. It is not known if it waters out at some downdip point, but the production and pressure data imply that the entire layer

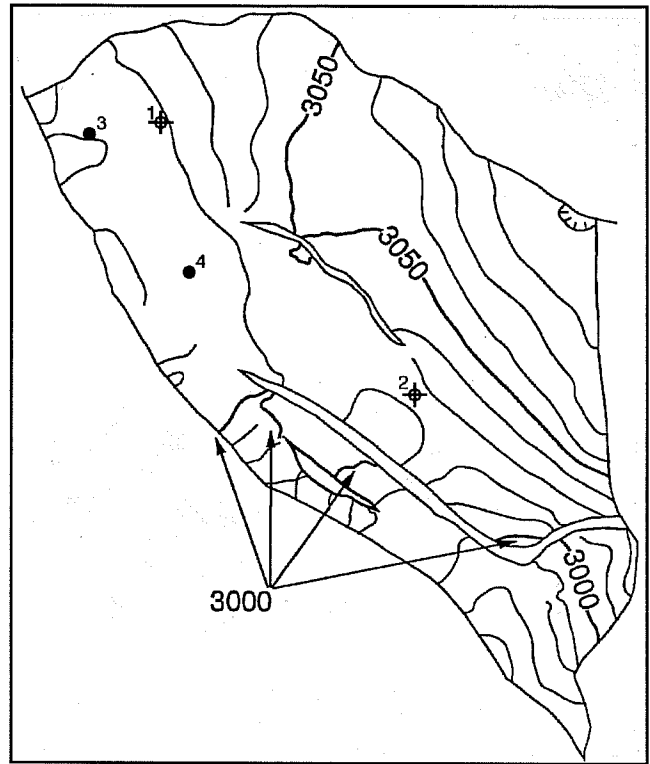


Fig. 2 Initial U-8 sand 3-D seismic interpretation.

may be oil-filled. The B layer shows a relatively shallow oil-water contact. The total capacity of this layer is much greater than that of the A layer, but much of this is filled with water.

The deepest zone, the C layer, is also very thick. It has an oil-water contact, showing that the deeper sections are water-filled. The C layer is also irregular in thickness. The isopach data for the B and C layers suggest that they were deposited during a period of active fault movements. The sand appears to pile up against the main fault boundaries.

The shale zones between the layers are thin, but they have apparently formed effective barriers to the fluid migration, as demonstrated by the differing oil-water contacts in each of the layers.

Figure 3 shows the latest 3-D seismic structural interpretation of the U-8 sand. The data has been further refined, and better picks have been made on some of the reflectors. Potential migration have been revised. Analysis of reflection patterns and strength on the southern high suggest that there is very little oil potential in this area. This revised structural map and the isolation of the southwestern portions of the reservoir were factored into the new reservoir model.

The primary, contiguous area of the reservoir was split into three layers and laid out in a custom-designed grid pattern to account for local reservoir properties. A number of parameters, such as structural position, thickness, porosity, and permeability, were determined for each block. The geologic and engineering data were used in concert to produce a model and a production scenario that best fit the actual history of the reservoir.

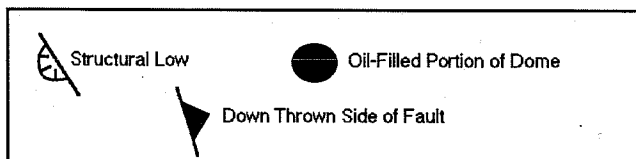
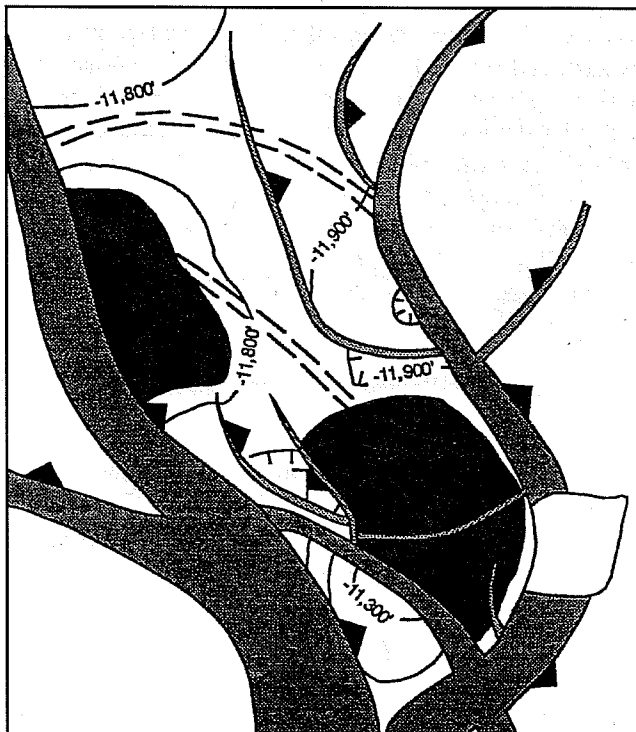


Fig. 1 Original U-8 sand reservoir interpretation.

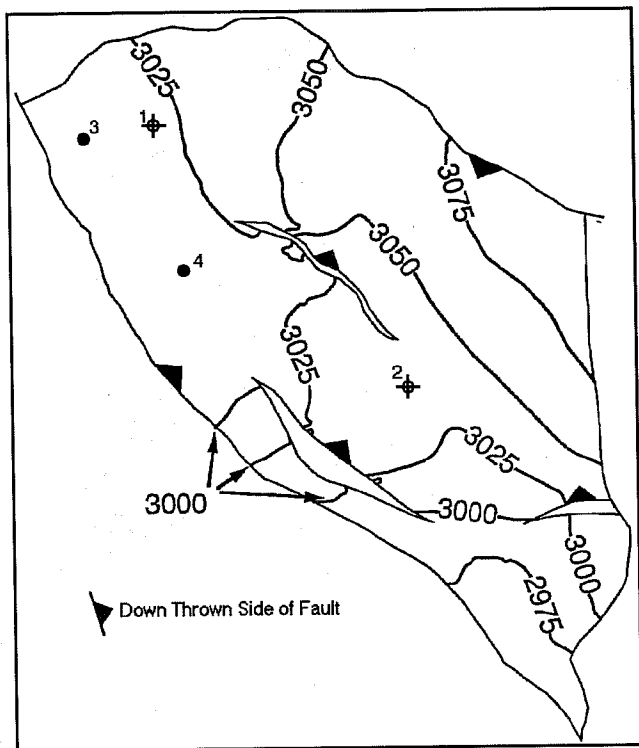


Fig. 3 Current U-8 sand 3-D seismic interpretation.

Material balance estimations were carried out by the U-8 sand's producer using an in-house material balance software package. A pressure-volume-temperature (PVT) correlation software package was also provided by the operator to generate PVT data for the entire U-8 reservoir.

Upon completion of the history match of the reservoir and several predictive runs, the following conclusions were drawn:

1. Evidence indicates that layers A and B of the U-8 sand are in communication.
2. The given reservoir relative permeability data were not appropriate for the U-8 sand reservoir, and the relative permeabilities were modified to enable a history match to be obtained.
3. The vertical permeability (K) values were found to be within the accepted range for the Gulf of Mexico ($0.1K_x < K_z < 0.5K_x$, with $K_x = K_y$) at $0.4K_x$.
4. Based on industry's desired design (water injection of 5100 bbl/d), the best possible production scenario is in the northeastern portion of the reservoir.
5. If the water injection rate is doubled to 10,200 STB/d, the additional oil recovery may be increased by 33% (1214 MSTB) in the vertical well scenario and by 37% (1320 MSTB) in the horizontal well scenario.
6. By converting the production wells to water injection wells and drilling a horizontal production well in the

north-central portion of the reservoir, the production obtained is approximately 90% of the production obtained from the northeastern portion of the reservoir at the same field injection rate.

TORIS Predictive Modeling

Predictive models for undeveloped oil and immiscible and miscible processes continued. The design of the miscible and updip displacement models as well as the design of the economic and timing models also continued. Data validation, map measurements, model development, and supporting cost data collection continued. Maps collected at the Minerals Management Service (MMS) were processed to reduce each reservoir to a polar coordinate segment for analysis in the bypassed oil model under development. Updip and downdip limits and penetrating and completed well locations were input for each reservoir using a digital technique. A Quality Assurance/Quality Control (QA/QC) check is currently under way. A second set of production data magnetic tapes (with all required data intact) were received from the MMS and translated into ASCII data files for integration with other databases. This data is currently being reduced for input into the production database.

Conceptual work continued on the development of the models required to access unrecovered oil, continued primary recovery of existing mapped oil, updip attic oil recovery, and miscible and immiscible recovery. The literature was searched to find supporting references for model assumptions regarding radial faulting around piercement salt structures, log-normal distribution of fault block sizes, and data supporting average rock properties.

Efforts continued to supplement existing TORIS data with drilling, workover, and facility costs related to past enhanced oil recovery efforts in the offshore Gulf of Mexico area.

Critical Process Parameter Laboratory Experiments

Critical Process Parameter Laboratory Experiments have been completed. Computer simulations of the experimental work has also been completed. Write-ups in the form of a master's thesis are currently being prepared.

References

1. George J. Koperna, Jr., *Reservoir Characterization and Performance Predictions for the U-8 Sand Reservoir*, Master's Thesis, Department of Petroleum and Natural Gas Engineering, College of Mineral and Energy Resources, West Virginia University, Morgantown, West Virginia, June 1994.

MICROBIAL TECHNOLOGY

**THE USE OF INDIGENOUS MICROBES
TO SELECTIVELY PLUG
THE MORE POROUS ZONES
TO INCREASE OIL RECOVERY
DURING WATERFLOODING**

Contract No. DE-FC22-94BC14962

**Hughes Eastern Corporation
Jackson, Miss.**

**Contract Date: Jan. 1, 1994
Anticipated Completion: June 30, 1999
Government Award: \$508,835**

Principal Investigators:

**Lewis R. Brown
Alex A. Vadie**

Project Manager:

**Edith Allison
Bartlesville Project Office**

Reporting Period: Jan. 1-Mar. 31, 1994

Objective

The objective of this work is to demonstrate the use of indigenous microbes as a method of profile control in water-

floods [i.e., microbial enhanced oil recovery (MEOR)]. It is expected that, as the microbial population is induced to increase, the expanded biomass will selectively block the more permeable zones of the reservoir and thereby force injection water to flow through the less permeable zones, which will result in improved sweep efficiency.

This increase in microbial population will be accomplished by injection of a nutrient solution into four injectors. Four other injectors will act as control wells. During Phase I, two wells will be cored through the zone of interest. Special core analyses will be performed in order to arrive at the optimum nutrient formulation. During Phase II, nutrient injection will begin, the results will be monitored, and adjustments to the nutrient composition will be made, if necessary. Phase II will also include the drilling of three wells for postmortem core analysis. Phase III will focus on technology transfer of the results. One outcome expected of this new technology is a prolongation of economical waterflooding operations (i.e., economical oil recovery should continue for much longer periods in the producing wells subjected to this selective plugging technique).

Summary of Technical Progress

Planning and Analysis

The concepts for this new technology are considered to be scientifically sound and have been proven to be effective in laboratory experiments. Laboratory tests on live cores from the reservoir of interest must be performed nevertheless. Two

wells will be drilled for this purpose, and special core analyses will be conducted in order to determine the exact concentration of and schedule for additions of nutrients to the injection water.

Whereas the main purpose for drilling the two wells is to obtain cores suitable for use in the laboratory work, a secondary purpose is to obtain production data that will indicate the sweep efficiency of the existing waterflood. The two core wells ultimately will be converted to injection wells if this project is successful and the program is expanded. At the conclusion of Phase I, a specific feeding regime will have been formulated for each of the injection wells. Because the injection wells vary in terms of years of service, differences in channeling are anticipated and a different feeding regime may be needed for each well.

The work for Phase I of the project has been divided into seven tasks: (1) drilling two new injection wells for the acquisition of cores and other data, (2) on-site handling of cores, (3) core analysis to determine MEOR requirements, (4) microbial analyses of cores, (5) laboratory waterflooding test of live cores, (6) acquisition of baseline data, and (7) analysis of baseline data.

Of the seven Phase I tasks, only two tasks were scheduled for completion during the present quarter of the project. The

initiation of drilling activities was slow because of wet weather in February 1994, but as of March 31, 1994, the first well, NBCU 34-6 No. 3, had been drilled and cased and awaited completion for production. The well was a geological success, encountering 20 net feet of Carter reservoir sand. Because of the overbalanced drilling condition in the subnormally pressured reservoir, however, no increase in drilling rate occurred in the sand and the core point was missed. From this experience the customary method of selecting core point was changed on the second well. That well is to be cored strictly on the basis of where in the geologic section the sand should occur without the necessity of actually having an increase in drilling rate to indicate penetration of the sand. The second well's site construction was completed March 13, 1994, but actual drilling did not start until April 5, 1994.

The feeding regime to be employed in Phase II will be formulated on the basis of the data generated in the laboratory waterflooding test of live cores. Determination of the microbial population of the cores will begin when the samples are received. Waterflooding tests of live cores will begin when the cores are received. Chemical and microbiological analyses of injection water and production fluid have begun. The analysis of baseline data will begin when the data are collected.

FIELD DEMONSTRATIONS

**APPLICATIONS OF ADVANCED PETROLEUM
PRODUCTION TECHNOLOGY AND WATER-
ALTERNATING-GAS INJECTION FOR
ENHANCED OIL RECOVERY—MATTOON OIL
FIELD, ILLINOIS**

Contract No. DE-FC22-93BC14955

**American Oil Recovery, Inc.
Decatur, Ill.**

**Contract Date: Dec. 29, 1992
Anticipated Completion: Dec. 31, 1994
Government Award: \$702,091
(Current year)**

**Principal Investigator:
Michael R. Baroni**

**Project Manager:
Gene Pauling
Metairie Site Office**

Reporting Period: Jan. 1–Mar. 31, 1994

Objectives

The objectives of this project are to continue reservoir characterization of the Cypress Sandstone; identify and map facies-defined waterflood (FDW) units; and design and implement water-alternating-gas (WAG) oil recovery utilizing carbon dioxide (CO₂). The producibility problems are permeability variation and poor sweep efficiency. Phase 1 of the project focuses on the development of computer-generated geological and reservoir simulation models that will be used to select sites for the demonstration and implementation of CO₂ displacement programs in Phase 2. Included in Phase 1 is the site selection and drilling of an infill well, coring of the Cypress interval, and injectivity testing to gather information used to update the reservoir simulation model. Phase 2 involves field implementation of WAG. Technology transfer includes outreach activity, such as seminars, workshops, and field trips.

Summary of Technical Progress

Relative Permeability Curve at Saturation Pressure of 500 psig

Determination of experimental relative permeability curves for Cypress core plugs from American Oil Recovery

(AOR)—Seaman well No. 15 was continued during this report period. The same experimental procedures described in the fourth quarterly report for the determination of relative permeability curves at 1000 psig were followed. The Mattoon crude oil, however, was saturated with CO₂ at 500 psig instead of 1000 psig.

The following runs were conducted with results shown in tables and figures as noted: brine displacing CO₂-saturated Mattoon crude oil (Table 1; Fig. 1); CO₂-saturated Mattoon crude oil displacing brine (Table 2; Fig. 2); CO₂ displacing CO₂-saturated Mattoon crude oil (Table 3; Fig. 3); and CO₂-saturated Mattoon crude oil displacing CO₂ (Table 4; Fig. 4).

TABLE 1

Relative Permeability of Brine Displacing CO₂-Saturated Mattoon Oil at 500 psig

Water saturation	Experimental data		Regressed data	
	K _{ro}	K _{rw}	K _{ro}	K _{rw}
37.34	0.2560	0.0000	0.2560	0.0000
40.00			0.2143	0.0041
45.00			0.1430	0.0163
50.00			0.0821	0.0314
52.84	0.0475	0.0379	0.0528	0.0409
54.58	0.0388	0.0407	0.0371	0.0469
58.00	0.0128	0.0511	0.0124	0.0594
61.16	0.0000	0.0720	0.0000	0.0714

Note: Initial water saturation, 37.34. K_{ro}, relative permeability of oil. K_{rw}, relative permeability of water.

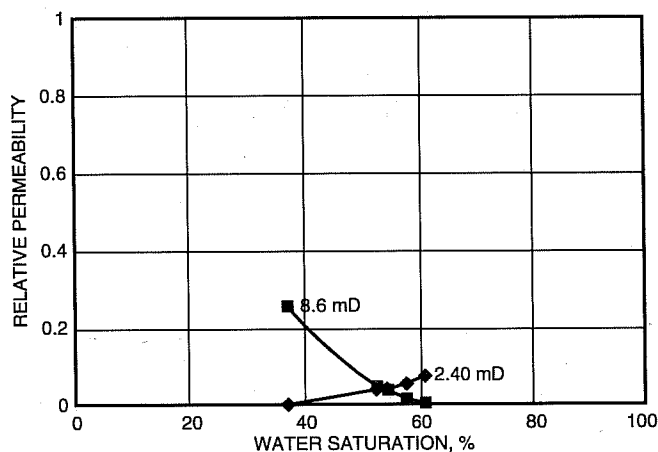


Fig. 1 Brine displacing CO₂-saturated oil at 500 psig using Mattoon Cypress Sandstone core plug.

Water/Cypress Rock Compatibility Tests

Two Cypress Sandstone core samples from the E interval of the AOR—Seaman well No. 15 were tested for compatibility with Mattoon city water. Mattoon city water was under consideration as the supply for the WAG injection program in the Sawyer Unit.

TABLE 2

Relative Permeability of CO₂-Saturated Mattoon Oil Displacing Brine at 500 psig

Oil saturation	Experimental data		Regressed data	
	K _{rw}	K _{ro}	K _{rw}	K _{ro}
38.84	0.0719	0.0000	0.0719	0.0000
45.00			0.0448	0.0000
50.00			0.0267	0.0002
55.00			0.0120	0.0066
57.00			0.0074	0.0201
59.00			0.0035	0.0544
60.00			0.0020	0.0861
61.13	0.0040	0.1480	0.0006	0.1411
61.30	0.0035	0.1780	0.0005	0.1519
62.66	0.0000	0.2150	0.0000	0.2150

Note: K_{rw}, relative permeability of water. K_{ro}, relative permeability of oil.

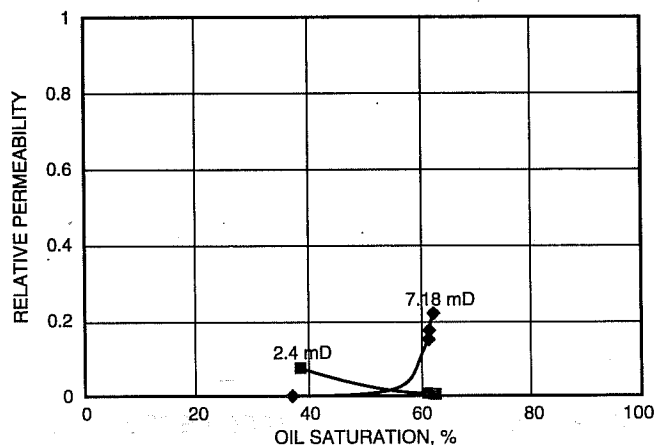


Fig. 2 CO₂-saturated oil displacing brine at 500 psig using Mattoon Cypress Sandstone core plug.

TABLE 3

Relative Permeability of CO₂ Displacing CO₂-Saturated Mattoon Oil at 500 psig

Gas saturation	Experimental data		Regressed data	
	K _{ro}	K _{rg}	K _{ro}	K _{rg}
37.34	0.2682	0.0000	0.2682	0.0000
39.06	0.2065	0.0016	0.2268	0.0032
39.87	0.1916	0.0020	0.2090	0.0039
42.58	0.1494	0.0036	0.1550	0.0055
45.06	0.1160	0.0054	0.1138	0.0067
47.00	0.0922	0.0069	0.0868	0.0075
52.00			0.0362	0.0093
55.00			0.0176	0.0102
60.00			0.0023	0.0115
61.40	0.0000	0.0125	0.0000	0.0125

Note: K_{ro}, relative permeability of oil. K_{rg}, relative permeability of gas.

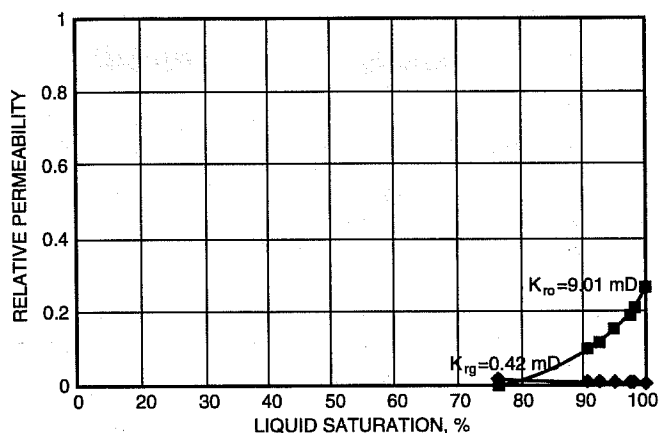


Fig. 3 CO₂ displacing CO₂-saturated oil at 500 psig using Mattoon Cypress Sandstone core plug. K_{ro} , relative permeability of oil. K_{rg} , relative permeability of gas.

TABLE 4

Relative Permeability of CO₂-Saturated Mattoon Oil Displacing CO₂ at 500 psig

Liquid saturation, S_w and S_o	Experimental data		Regressed data	
	K_{rg}	K_{ro}	K_{rg}	K_{ro}
77.20	0.0730	0.0000	0.0730	0.0000
83.60			0.0591	0.0119
88.60			0.0260	0.0673
92.95	0.0134	0.1395	0.0108	0.1501
92.63	0.0001	0.1656	0.0091	0.1668
93.94	0.0000	0.3041	0.0000	0.3041

Note: S_w , water saturation. S_o , oil saturation. K_{rg} , relative permeability of gas. K_{ro} , relative permeability of oil.

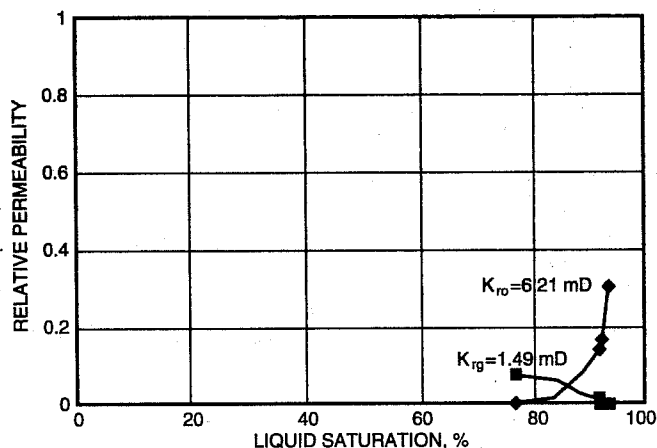


Fig. 4 CO₂-saturated oil displacing CO₂ at 500 psig using Mattoon Cypress Sandstone core plug. K_{ro} , relative permeability of oil. K_{rg} , relative permeability of gas.

The tests were performed in a Hassler-type core holder at an injection rate of 1 cm³/min with a back pressure of 100 psi and a confining pressure of 1000 psi. In the first test, water contain-

ing 2% sodium chloride (NaCl) was injected; this was followed by the city water. The initial 2% NaCl brine injected into the core represented the saline aqueous environment existing in Cypress reservoirs. A minimum of 20 pore volumes (PV) of each water sample was injected before changeover, and the permeability of the core plug to each water sample was also measured (Table 5). The result shows that the core sample permeability was decreased by 6.5% by Mattoon city water. Subsequently, brine containing 2% potassium chloride (KCl) was injected to stabilize freshwater-sensitive clays in the core sample. During this time, permeability reduction stopped; however, it resumed when city water was reinjected. Permeability reduction continued because the first injection of fresh water may have already affected water-sensitive clays and dislodged clay particles, which migrated and caused permeability reduction. Altogether, an 11.1% reduction in permeability occurred by the end of the experiment because of the use of Mattoon city water.

The protocols for the second and third tests included injection of brine containing 2% KCl prior to the injection of the Mattoon city water. The purpose of these tests is to investigate whether the injection of brine containing 2% KCl, acting as a clay-stabilizing agent, would prevent permeability reduction. The results show that, within the limits of experimental error, permeability reduction did not occur (Tables 6 and 7). These

TABLE 5

Compatibility Testing of Sample MA 1752.4,* AOR-Seaman Well No. 15, Cypress Sandstone, Mattoon Field, Coles County, Illinois

Fluid injected	Permeability, mD
Air	60.7
2% sodium chloride	36.8
City water	34.4
2% potassium chloride	34.8
City water	32.7

*Inside diameter, MA1752.4; length, 4.838 cm; diameter, 2.540 cm; and porosity, 18.5%.

TABLE 6

Compatibility Testing of Sample MA1754,* AOR-Seaman Well No. 15, Cypress Sandstone, Mattoon Field, Coles County, Illinois

Fluid injected	Permeability, mD
Air	34.4
2% potassium chloride	22.5
City water	22.5

*Inside diameter, MA1754; length, 4.464 cm; diameter, 2.540 cm; and porosity, 18.5%.

TABLE 7

**Compatibility Testing of Sample
MA 1751.7,* AOR-Seaman Well
No. 15, Cypress Sandstone,
Mattoon Field, Coles County,
Illinois**

Fluid injected	Permeability, mD
Air	36.8
2% sodium chloride	22.9
2% potassium chloride	22.2
City water	22.5

*Inside diameter, MA1751.7; length, 5.204 cm; diameter, 2.540 cm; and porosity, 16.7%.

experiments show that clays within the Cypress Sandstone at Mattoon field are freshwater-sensitive and will be affected if contacted with fresh water, such as the city water. However, injection of a clay-stabilizing agent prior to freshwater injection may prevent permeability reduction caused by clay swelling, dislodgment, and migration.

Reservoir Simulation of Sawyer Unit

The reservoir simulation model of the Sawyer Unit, previously developed, was updated with production and pressure data during the reporting period. Figure 5 shows the historical and predicted oil production from the Sawyer Unit. The predicted cumulative oil production increases with the number of producing wells. For instance, up to 40,000 additional barrels of oil can be recovered in four years with the recompletion of five more oil producing wells (W. Brining No. 13, V. Strohl No. 1, M. Sawyer community 1 No. 1, Sawyer community 1 No. 1, Sawyer community 2 No. 2) in the E interval (Fig. 6).

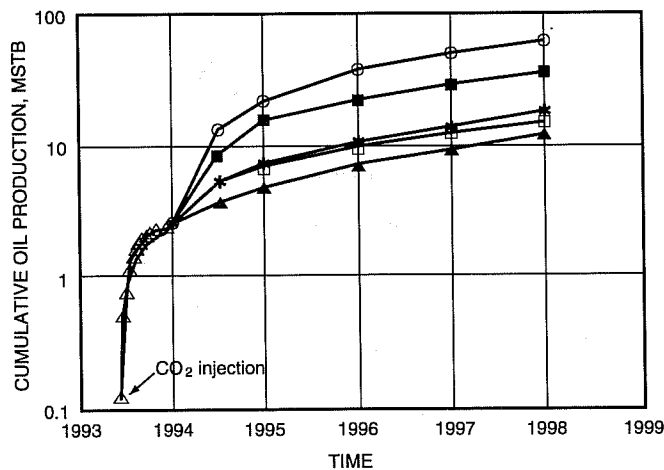


Fig. 5 Historical and predicted oil production of Sawyer Unit. Δ , field data. —, simulator calculated result. Δ , waterflood after 1994 (2 producers). *, water alternating gas (WAG) 1:1 (3 producers). \square , waterflood only after 1994 (3 producers). \circ , WAG 1:1 (8 producers). \blacksquare , waterflood only after 1994 (8 producers).

Field Testing

Sawyer Unit

Natural gas produced from the new infill well AOR-Seaman No. 15 was sampled on March 11, 1994, and analyzed in the Illinois State Geological Survey (ISGS) laboratory. The produced gas contained 13.22% CO_2 (Table 8). Since the original solution gas in Mattoon crude oil contained less than 1% CO_2 , the result indicated that the injected CO_2 from Sawyer community 3 No. 1 has arrived at AOR-Seaman well No. 15. Oil production from AOR-Seaman well No. 15 during the reporting period averaged 4.3 bbl oil/day (BOPD).

Pinnell Unit

Cyclic CO_2 Injection in Pinnell-Uphoff Well No. 14.

One hundred eighty-four (184) tons of CO_2 were injected into Pinnell-Uphoff well No. 14 from December 20 to December 21, 1993. After a soak period of 12 days, the wellhead pressure decreased from the postinjection pressure of 600 to 325 psig. Average oil production rate between January 3, 1994, and February 28, 1994, was 4.0 BOPD.

Pressure Testing of Pinnell Unit. Two thousand tons of liquid CO_2 were injected into Pinnell well No. 3-W in December 1993 to verify the existence of a permeability barrier between the injector well Pinnell No. 3-W and the producer well Pinnell-Uphoff No. 1. Pressure response observed in Pinnell-Uphoff well No. 1 was minimal during the injection period. However, oil production increased from the pre-injection rate of 1 BOPD to an average of 4.3 BOPD during January but has since decreased to below 3 BOPD. This result shows that there may be favorable oil production response from Pinnell-Uphoff well No. 1 if water is injected into Pinnell well No. 3-W (A interval).

Technology Transfer

A presentation entitled "Enhanced Recovery Opportunities in Illinois Basin Using Carbon Dioxide" was presented at the Illinois Oil and Gas Association (IOGA) Annual Meeting, Evansville, Ind., March 2-4, 1994. The history of the progress of this demonstration project, problems encountered, lessons learned, and advantages of CO_2 applications were discussed. The presentation also provided opportunities for consultations with independent oil operators.

A paper entitled "Laboratory Experiments and Reservoir Simulation Studies in Support of a CO_2 Injection Project in Mattoon Field, Illinois, USA" was accepted for presentation at the 45th annual technical meeting of the Canadian Petroleum Society of the Canadian Institute of Mining in Calgary, June 12-15, 1994. The abstract accompanying the preprint follows:

This paper describes the results of rock and fluid property measurements and the results of integrated reservoir modeling associated with Phase I of a demonstration of CO_2 -assisted oil recovery in the Cypress Sandstone reservoirs at Mattoon Field, Illinois. The objectives of the project are to characterize the Cypress Sandstone through

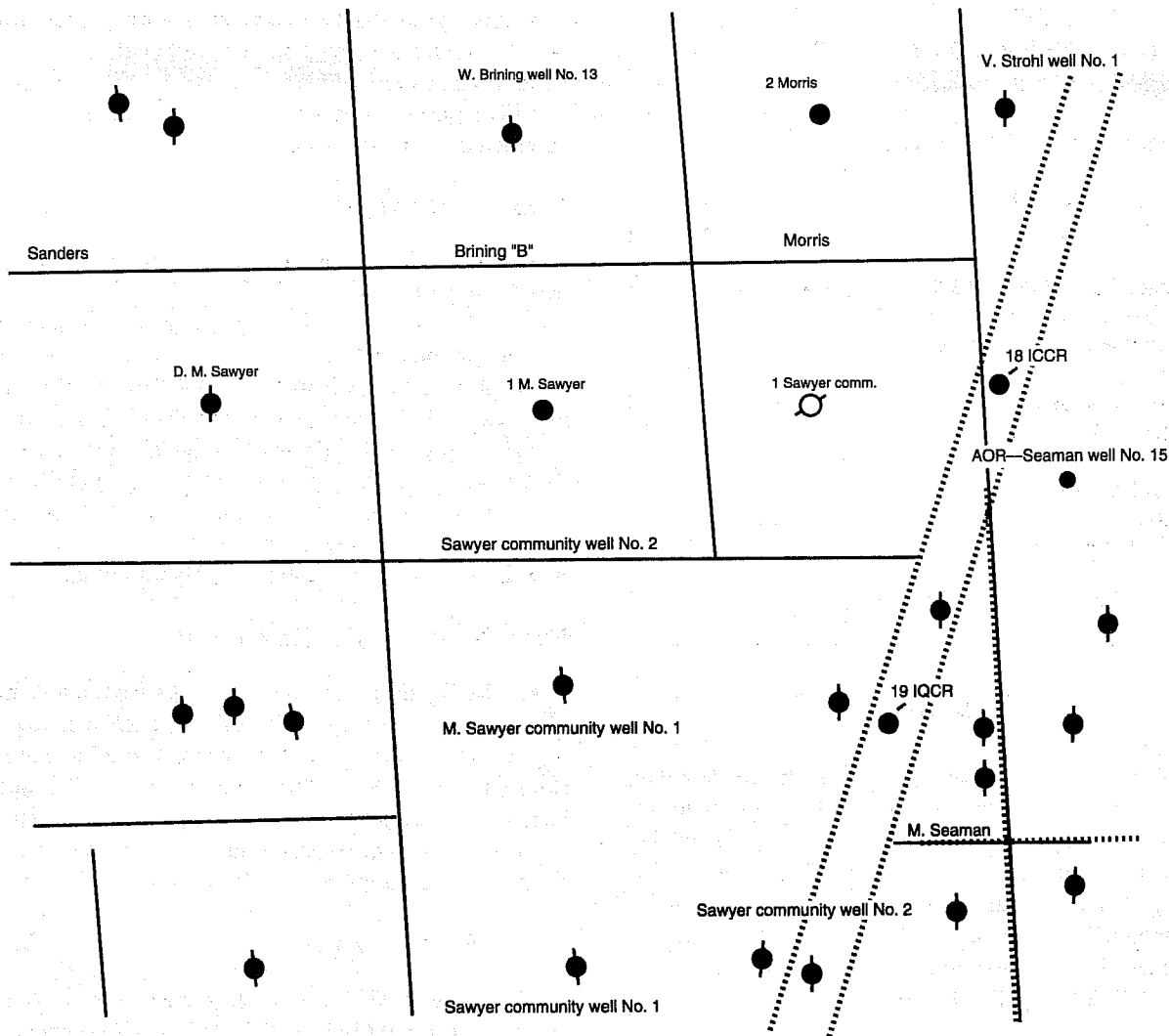


Fig. 6 Location map of Sawyer CO₂ injection unit.

an integrated geologic and engineering approach; to identify facies-defined waterflood units; to design and implement an enhanced oil recovery program utilizing CO₂; and to transfer technology to oil and gas operators.

Although results from slim-tube displacement experiments show that implementation of a miscible flood may not be possible, phase behavior experiments show that the effects of dissolved CO₂ on oil swelling and viscosity reduction are significant even at pressures below miscible conditions. Results from coreflood tests indicate that oil recovery from immiscible displacement of reservoir crude oil with carbon dioxide will increase with displacement pressure.

Reservoir simulation studies and injectivity tests on the Pinnell Unit of the project area indicate poor inter-well communication and limited areal extent of the producing interval of this unit. Inefficient displacement of reservoir crude by the injected CO₂ is also indicated from production tests.

Injectivity tests on the Sawyer Unit of the project area show good inter-well communication. Results from analyses of core samples from a newly drilled infill well within this unit confirm the isolation of the target E sandstone interval from the extensively waterflooded lower B and C sandstone intervals. Reservoir simulation results indicate that a significant amount of additional oil can be recovered by the implementation of a water-alternating-gas (WAG) injection program utilizing eight or more oil producers.

TABLE 8

Gas Chromatography Analysis of AOR—Seaman Well No. 15, Cypress Sandstone, Coles County, Illinois*

	Vol. % (normalized)
Carbon dioxide (CO ₂)	13.22
Oxygen/argon (O ₂ + Ar)	0.19
Nitrogen (N ₂)	3.79
Methane (CH ₄)	30.40
Ethane (C ₂ H ₆)	10.08
Propane (C ₃ H ₈)	23.94
Isobutane (I-C ₄ H ₁₀)	2.81
N-Butane (N-C ₄ H ₁₀)	9.91
Isopentane (I-C ₅ H ₁₂)	ND
N-Pentane (N-C ₅ H ₁₂)	0.01
Hexanes +	5.66
BTU/ft ³ dry @ 60 °F and 14.7 psia: Total	1794
Specific gravity: calculated	1.30

*Sampled, 3/11/94; analyzed, 3/18/94. ND = not detected.

DYNAMIC ENHANCED RECOVERY TECHNOLOGIES

Contract No. DE-FC22-93BC14961

**Columbia University
New York, N.Y.**

**Contract Date: July 5, 1993
Anticipated Completion: Oct. 30, 1995
Government Award: \$7,742,000**

**Principal Investigator:
Roger N. Anderson**

**Project Manager:
Edith Allison
Bartlesville Project Office**

Reporting Period: Jan. 1–Mar. 31, 1994

Objectives

The objectives of this project are to test the concept that the growth faults in a Gulf of Mexico field are conduits through which the producing reservoirs are charged and the proposal that enhanced production can be developed by producing from the fault zone. The field demonstration will be accomplished by drilling and production testing of growth fault systems associated with the Eugene Island Block 330 (EI 330) operated by Pennzoil in federal waters off Louisiana.

Summary of Technical Progress

Management Start-Up and Technology Transfer

Management start-up and technology transfer activities are continuing in accordance with project objectives. Accomplishments of the present quarter include:

- Global Basins Research Network (GBRN) meeting was held on 1/31/94–2/1/94 to discuss the results of the field demonstration experiment and ongoing science related to this project.
- Pennzoil and partners are considering drilling another fault zone amplitude anomaly in the EI 330 area in the summer of 1994.
- Pennzoil is whole-coring EI 316 as a result of the whole-coring success of the Pathfinder well.
- Pennzoil and partners of EI 330 are drilling a joint lease line well with Texaco/Chevron, owners of EI 338, as a direct result of the GBRN meeting with all involved parties searching for the optimum Pathfinder target.

- Conoco and GBRN will meet in April 1994 to discuss a possible scientific extension of a well drilled in their Jolliet field (Green Canyon 184).

- Five publications or abstracts for presentations were completed during this quarter.¹⁻⁵

Database Management

- A computer algorithm was generated to correlate well logs from the EI 330 area.
- All field demonstration experiment well data have been loaded into the database.
- Coding of 12 Advanced Visual Systems, Inc. (AVS) modules to meet data visualization needs is complete.
- Hyperedge software was ported to Solaris Operating System on Sparc10 at Louisiana State University (LSU).
- HyperMedia and LSU developed user-interface components to enter information and results automatically from AKCESS.BASIN simulations into Hyperjournals.

Field Demonstration Experiment

- A display of the actual whole cores from the Pathfinder well was available for viewing at the GBRN meeting.
- All whole cores were shipped from Core Laboratories in Houston, Texas, to the GBRN core repository at Pennsylvania State University (PSU).
- Core Laboratories performed core analysis on selected plugs from the Pathfinder whole cores.

Reservoir Characterization

- Mapping the GA sand and adjacent stratigraphic units in three-dimensional (3-D) seismic data sets is complete.
- Preliminary structure, isopach, and electrofacies distribution maps have been prepared.
- Work on integration of the dipmeter and 3-D seismic data of the GA sand and stratigraphically equivalent sands in Blocks 338 and 339 began.
- The pressure measurements obtained from the Pathfinder well were integrated with pressures derived from porosity data to produce pressure maps.
- A speech to Chevron employees on the modern Fraser Delta and its use as a modern analog to interpret deltaic deposits such as the GA sands was presented.
- Temperatures of well No. A-20ST at the EI 330 A platform were measured.

Modeling

- EI 330 geologic interpretation was converted and entered into the Minibasin scale, and, as a result, several new utilities were added to the preprocessor.
- Several heuristic sections were constructed to illustrate erosion, salt diapirism, and faulting.
- Visual inspection of the revised 3-D flat files was performed at LSU and no errors were found in the four profiles.

- The software programming to enter 3-D geologic data into 3-D AKCESS.BASIN is complete.
- The Pathfinder digital logs were transferred to Cornell and, with the use of the procedures developed last quarter, were processed to predict porosity.
- The 25-block South Eugene Island (SEI) interpretation based on two-dimensional (2-D) seismic profiles and well logs was completed.
- Example cases for the Ageohist preprocessor were developed and tested at LSU to ensure compatibility with AKCESS.BASIN.
- Additions to the AKCESS.BASIN include hydrocarbon maturation models developed at Cornell and fault venting models developed at LSU.
- The calculation of 3-D venting on a parallel computer was demonstrated.
- Diapirism and compaction FORTRAN algorithms were completed in 2D.
- The physical property fabric theory algorithm was completed and evaluated against other methodologies.
- A one-dimensional (1-D) finite-difference model of sedimentation and maturation was developed.
- Two modeling workshops were held at LSU (February and March) to train 10 researchers on the AKCESS.BASIN modeling system.

Geochemistry

- Petrography
 - a. Four hundred samples have been taken from the whole core for various analyses by both academic and industry researchers.
 - b. Laser particle size analysis has been performed on 12 samples.
 - c. Computerized axial tomography (CAT) scanning of the whole core was performed by Exxon Production Research and Shell Oil Company Bellaire Laboratory.
 - d. A large amount of rock property data was collected, such as porosity, permeability at overburden stress and atmospheric pressure, capillary entry pressure, V_p/V_s [velocity of "P" (compressional wave) versus velocity of shear wave] measurements, bulk density, particle size analysis, and Coulomb failure criteria.
- Eight thin selections from sidewall cores were examined under the cathode-ray apparatus.
- Eighteen core plugs were analyzed for major element oxides, sulfur, and several major elements.
- Major element analytical work and iodine-129 dating were completed on 22 brine samples.
- Oil Analysis
 - a. Analyses of oils recovered from the Pathfinder well were completed, including whole oil-gas chromatograms, percentage alkanes:aromatics:asphaltenes, gas and gasoline range hydrocarbon compositional analyses, and gas and oil isotopic analyses.

- b. Hydrous pyrolysis experiments were conducted on several rocks believed to be similar to Eugene Island oils source rock.
- c. Whole oil-gas chromatograms and gasoline range hydrocarbon compositional analyses were completed on 45 oil samples from EI 330 area.

References

1. U. T. Mello, G. Karner, and R. Anderson, Salt Restrains Maturation in Subsalt Play, *Oil Gas J.*, 92(5): 101-107 (January 31, 1994).
2. R. N. Anderson, Field Demo Confirms Deep Potential, *Am. Oil Gas Report.*, 37(2): 62-67 (February 1994).
3. U. T. Mello, G. Karner, and R. Anderson, A Physical Explanation for the Positioning of the Depth to the Top of Overpressure in Shale-Dominated Sequences in the Gulf Coast Basin, United States, *J. Geophys. Res.*, 99(B2-10): 2775-2789 (February 1994).
4. L. M. Cathles, R. N. Anderson, J. Nunn, and The Global Basins Research Network, *Sedimentation, Salt Diapirism, Fluid Flow, and Hydrocarbon Migration in an Area of Very Active Sedimentation Offshore Louisiana, Gulf of Mexico*, paper to be presented at the Margins Session of the American Geophysical Union Annual Meeting, Baltimore, Md., May 25-27, 1994.
5. B. S. Eiche et al., *AVS Techniques for Well Log Analysis for the Eugene Island Field Track: Oil and Gas Exploration and Production*, paper to be presented at the AVS 94 Convention, Boston, Mass., May 2-9, 1994.

GREEN RIVER FORMATION WATERFLOOD DEMONSTRATION PROJECT, UINTA BASIN, UTAH

Contract No. DE-FC22-93BC14958

**Lomax Exploration Company
Salt Lake City, Utah**

**Contract Date: Oct. 21, 1992
Anticipated Completion: Oct. 20, 1995
Government Award: \$1,304,000**

**Principal Investigators:
John D. Lomax
Dennis L. Nielson
Milind D. Deo**

**Project Manager:
Edith Allison
Bartlesville Project Office**

Reporting Period: Jan. 1-Mar. 31, 1994

Objectives

The objectives of this project are to understand and demonstrate improved oil recovery techniques in fluvial-deltaic reservoirs. Three distinct units were targeted in this study, the Monument Butte Unit, the Travis Unit, and the Boundary Unit. All three units are located in the Uinta Basin in east-central Utah. The Green River formation in Utah's Uinta Basin consists typically of low-permeability reservoirs that yield only about 5% of the oil in place in primary production. The waterflood recovery at the Monument Butte Unit has already exceeded the primary production. The project goals are to understand the recovery mechanisms of the Monument Butte waterflood so that the technology can be transferred to similar reservoirs operated by Lomax Exploration Co. and other operators.

Summary of Technical Progress

Field Drilling and Production Results

The Monument Butte Unit No. 10-34, which was put on production in the last quarter of 1992, had produced 10,119 bbl of oil and 12,614 Mcf of gas as of Mar. 31, 1994. Monument Butte No. 9-34, drilled and completed in December 1993, had produced a total of 6,418 bbl of oil and 3,957 Mcf of gas. Travis No. 14a-18 was completed in the last quarter of 1992. Even though the primary sand target when drilling and completing Travis No. 14a-28 was the Lower Douglas zone, commercial D-sands were identified by advanced logging methods. Owing to the success of No. 14a-28, wells 14-28 and 10-28 in Travis were also completed in D-sands. No. 14a-28 produced 7,953 bbl of oil and 23,045 Mcf of gas before it was converted into an injector in October 1993. After recompletion, No. 14-28 had produced 9,012 bbl of oil and 53,098 Mcf of gas, and No. 10-28 had produced 5,071 bbl of oil and 14,569 Mcf of gas. The cumulative water injection in No. 14a-28 (D-sands) at the end of March 1994 was 16,430 bbl, and the cumulative injection in No. 15-28 (Lower Douglas Creek) after it was restarted at a lower rate (March 1993) was 91,947 bbl. The total cumulative injection in No. 15-28 at the end of this reporting period was 408,166 bbl. Injection into the Lower Douglas Creek was begun in Travis No. 3-33 in October 1993, and the cumulative injection by Mar. 31, 1994, was 45,134 bbl.

Near-Wellbore Effects

Numerous studies have recognized formation cooling in oil reservoirs that are on continued cold-water injection. This could have serious consequences, particularly for light oil reservoirs containing significant amounts of paraffins in the oil. The formation cooling reduces waterflood oil recoveries by adversely affecting the oil-water fractional flow behavior and by causing paraffin precipitation in the vicinity of the wellbore, thereby reducing injectivity and eventually the reservoir sweep. Heat-transfer calculations have established the distinct possibility of paraffin wax formation in the vicin-

ity of the wellbore. In the case of Monument Butte, field and geologic data and extensive reservoir simulations have shown that the production from the unit is limited by the injectivity of the injectors and that the reservoir sands are not being swept uniformly. The reservoir contains light (gravity, 35 °API), but highly paraffinic, oil (with a pour point of about 100 °F) at a reservoir temperature of 140 °F. About 2.5 million bbl of cold water at around 55 to 60 °F has been injected into the formation to date. The belief is that continued injection of cold water into the reservoir has cooled the wellbore and the formation around the wellbore and has precipitated high-molecular paraffins from the oil in the immediate vicinity of the wellbore. The effect of continued cold-water injection on wax formation in the vicinity of the wellbore and its impact on oil recoveries in paraffinic crude reservoirs has been explored.

The Wellbore Model

The wellbore model used in this study is a modification of the models proposed by Ramey¹ and Pratt.² The temperature of injected fluids in the wellbore as a function of depth and time is given by

$$T(z, t) = az + b - aA + (T_0 + aA - b) e^{z/A} \quad (1)$$

where

$$A = \frac{Wc[k + r_1 U f(t)]}{2\pi r_1 U k} \quad (2)$$

The terms in the equations are explained in the nomenclature. U is the overall heat-transfer coefficient and considers the net resistance to heat flow offered by the fluid inside the tubing, the tubing wall, fluids in the annulus, the casing wall, and the cement. Figure 1 is a schematic of the thermal resistances to heat flow. The time function $f(t)$ is estimated from

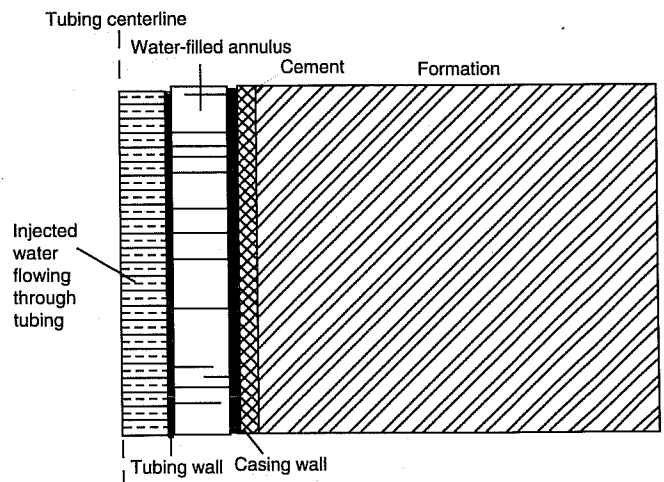


Fig. 1 Schematic of thermal resistances to heat flow in an injection well.

solutions for radial heat conduction from an infinitely long cylinder. The general form of U is given by

$$\frac{1}{U} = \frac{1}{h_t} + \frac{r_1 \ln(r_2/r_1)}{k_i} + \frac{r_1}{r_3 h_c} + \frac{r_1 \ln(r_4/r_3)}{k_o} + \frac{r_1 \ln(r_5/r_4)}{k_c} \quad (3)$$

The function $f(t)$ for large values of time is calculated with the use of the following approximation:

$$f(t) = 0.403 + 0.5 \ln(t_D) \quad (4)$$

The argument t_D is given by

$$t_D = \frac{\alpha t}{r_5^2} \quad (5)$$

Results and Discussion

The procedure described was used to calculate the temperature profiles in the Monument Butte injectors. A sample temperature profile is shown in Fig. 2. The parameters used in the calculation are tabulated in Table 1. The sample calculation was performed with an injection rate of 300 STB/d, which can be considered a middle of the range for the Monument Butte Unit. Figure 2 shows that the temperature of the water entering the perforations after about 1 yr of injection is 83.8 °F for the parameters used in this calculation. For smaller injectors (100 STB/d), the injected water reaches the perforations at 109 °F, whereas for the larger injectors (500 STB/d), the injected water reaches the formation at 76 °F.

Continued injection of cold water does not change these results significantly; for example, after 10 yr of injection, the temperature of the injected water for the base case (300 STB/d) at the perforations was 82.3 °F. Note that the thermal resistance of cement dominates these calculations. The effect of surface injection temperatures on temperatures at the perforations for the base case was also explored. Maintaining the temperatures of the injected water (entering the formation) at or above the cloud point of the oil (approximately 125 °F) would be desirable. For the base-case calculations, the surface injection temperatures would have to be around 150 °F to achieve this goal. For an injection rate of 500 STB/d, a surface injection temperature of 138 °F was adequate to maintain the temperature of the injected fluid above the oil cloud point at the perforations.

In the Travis Unit, about 1000 STB/d of water was injected into well No. 15-28. The predicted temperature profile of the injected fluid in this well after 1 yr of injection is shown in Fig. 3. As shown in this figure, the injected water reaches the perforations at a temperature of 71.9 °F. Other temperature effects are expected to be analogous to those observed and discussed for the Monument Butte Unit.

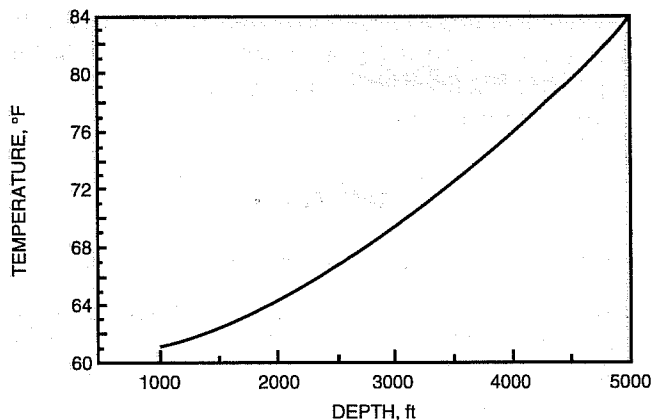


Fig. 2 Temperature profile in a typical Monument Butte injector. Profile after 1 yr. Injection rate, 300 bbl/d.

TABLE 1

Parameters Used in Calculating the Temperature Profiles in Injection Wells

Surface temperature, °F	60
Geothermal gradient, °F/ft	0.016
Reservoir temperature at 5000 ft, °F	140
Water injection temperature, °F	60
Tubing, outside diameter, in.	2.875
Tubing, inside diameter, in.	2.441
Casing, outside diameter, in.	5.5
Casing, inside diameter, in.	4.892
Cement, thickness, in.	0.5
Thermal conductivity, steel, Btu/(d · ft · °F)	600
Thermal conductivity, earth, Btu/(d · ft · °F)	34
Thermal conductivity, cement, Btu/(d · ft · °F)	12
Thermal diffusivity, earth, ft ² /d	1

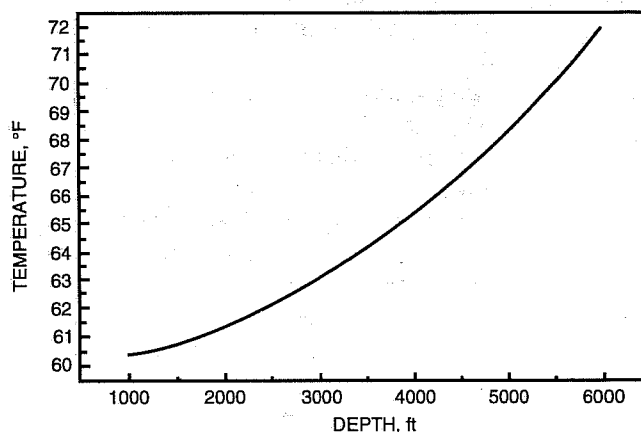


Fig. 3 Temperature profile in an injector in Travis Unit. Profile after 1 yr. Injection rate, 1000 bbl/d.

In summary, the near-wellbore calculations have established that formation cooling is caused by continued injection of cold water into the formation in Monument Butte and Travis Units. The bottomhole injection temperatures predicted by the model

raise the distinct possibility of paraffin precipitation in the vicinity of the wellbore. The model was also used to calculate surface injection temperatures necessary to alleviate the paraffin deposition problem for various injection rates.

References

1. H. J. Ramey, Jr., Wellbore Heat Transmission, *J. Pet. Technol.*, 14: 427-440, April 1962.
2. M. Pratt, *Thermal Recovery*, Monograph Volume 7, Society of Petroleum Engineers, Henry L. Doherty Series, 1982.

Nomenclature:

A	Factor used in temperature profile calculations (defined in the text), ft
a	Geothermal gradient, °F/ft
b	Surface temperature, °F
c	Specific heat of injected fluid, Btu/(lb · °F)
f(t)	Transient heat conduction time function for earth, dimensionless
h_t	Heat-transfer coefficient for the fluid inside the tubing, Btu/(d · ft ² · °F)
h_c	Heat-transfer coefficient for the fluid inside the casing, Btu/(d · ft ² · °F)
k	Thermal conductivity of the earth, Btu/(d · ft · °F)
k_i	Thermal conductivity of the tubing material, Btu/(d · ft · °F)
k_o	Thermal conductivity of the casing material, Btu/(d · ft · °F)
r_1	Inside radius of the tubing, ft
r_2	Outside radius of the tubing, ft
r_3	Inside radius of the casing, ft
r_4	Outside radius of the casing, ft
r_5	Outside wellbore radius inclusive of cement, ft
T(z,t)	Temperature of the injected fluid in the wellbore, °F
T_0	Surface injection temperature, °F
t	Time from start of injection, d
t_D	Dimensionless time defined in the text.
U	Overall heat-transfer coefficient based on the inside tubing diameter, Btu/(d · ft ² · °F)
W	Mass injection rate, lb/d
α	Thermal diffusivity of the earth, ft ² /d

VISUAL DISPLAY OF RESERVOIR PARAMETERS AFFECTING ENHANCED OIL RESERVOIRS

Contract No. DE-AC22-93BC14892

Michigan Technological University
Houghton, Mich.

Contract Date: Sept. 29, 1993
Anticipated Completion: Sept. 30, 1996
Government Award: \$272,827

Principal Investigator:
James R. Wood

Project Manager:
Robert Lemmon
Bartlesville Project Office

Reporting Period: Jan. 1–Mar. 31, 1994

Objective

The objective of this project is to provide the small- to medium-size oil-field operators with the tools necessary for an enhanced oil recovery (EOR) evaluation of the same quality and sophistication that only large international oil companies have been able to afford to date.

Summary of Technical Progress

Project Administration and Management

The Spatial Database Manager

A geologically oriented relational database manager (TECHBASE by MINEsoft Ltd.), which integrates many basic data entry and transfer protocols (including digitization); computational abilities, such as statistical analysis, data transformation, and data modeling; data plotting and graphing options; and mapping functions, including one-dimensional (1-D), two-dimensional (2-D), and three-dimensional (3-D) capabilities and cross sections, has been identified and examined. This software has been heavily used in the mining and engineering industries and has recently entered the oil and gas market. Initial contracts have been made with the vendor to obtain copies for evaluation. This software is available on PC-, Macintosh-, and UNIX-based systems.

A state-of-the-art Macintosh-based 3-D visualization software system available from Spyglass, Inc., has been evaluated, and a recommendation to purchase the system has been made. Spyglass visualization software allows data entry in formats common to most database management systems. The visualization capabilities of the system will be tested on data

from the Pioneer Anticline. As a first step, surface topographic data for the Pioneer area are being ported into Spyglass from a U.S. Geological Survey (USGS) database. If tests prove successful, the Spyglass files will be transferred to the PC by year-end when a PC-based version of the software will be available.

Investigators met with Reservoir Characterization and Research Consultants Inc. (RC²) to examine their software capabilities for geostatistical analysis of reservoir properties, discuss the potential to port their software from workstation to PC-based systems, and review opportunities to incorporate their technology into the project. RC² is a new company formed by former Chevron employees who developed the GEOLITH software package, which has become an industry standard for geostatistical analysis and reservoir evaluation. Their newly designed software was written from scratch and represents a significant upgrade from GEOLITH. The new software is designed to treat vertically oriented and spatially distributed data, such as well-log data, with the use of state-of-the-art geostatistical techniques to develop a spatial variability model for interwell interpretation of reservoir properties. Interpolation models can be developed with the use of well data, seismic data, or both in combination. The system has been developed on UNIX-based workstations and is being combined with state-of-the-art licensed 3-D visualization software.

This software provides the last necessary link to translate geologic information into quantitative engineering terms for ready use by reservoir engineers. It can be used to optimize design of oil and gas recovery systems and to maximize resource recovery and economic return. RC² is building a module to provide their interpreted data model as gridded data that can be exported directly to 3-D black oil simulators.

With the new generation of Pentium-based systems, users will soon be able to port this software to the PC environment. RC² plans to produce a PC-based version of the software and is interested in the possibility of using a project such as this one to test and demonstrate their software.

Database initialization. Individual databases were set up in LOTUS spreadsheets by Michigan Technological University (MTU) personnel to archive and display x-ray diffraction (XRD) Fourier transform infrared spectroscopy (FTIR), and mineralogical data. Macros and templates were developed to display data in LOTUS graphs and charts. Data from analysis of samples from the Gary Drilling Co., KLC 44, Well No. 315 in Pioneer field were used to develop and test the programs.

Database management. Every manager and site has a high-end PC (486-based computer or better) with which to access the database and run the visualization applications programs. These computers are in the process of being networked and linked to a common server at MTU. A machine has been dedicated to serve as a bulletin board at MTU, and test files were successfully transferred from La Habra, Calif., to MTU in Houghton. An MTU undergraduate student has been successful in designing and implementing this system.

Organization and Management

Project coordination. Three formal meetings were held during this quarter:

- During January and February 1994, two investigators spent about a week at MTU working on the project. During this time, procedures for linking the off-site computers to MTU were finalized, construction of a multimedia presentation shell to display project data and results in interactive tutorial format was begun, and many issues regarding project plans and staff members' responsibilities were decided.

- On Feb. 16 and 17, 1994, the same investigators visited Digital Petrophysics Inc. (DPI) in Bakersfield and reviewed the extensive log and core data set from Union McKittrick Front Well No. 418 in Cymric field which was loaned MTU by UNOCAL for use in calibrating the Pioneer Anticline logs.

- On Feb. 22, 1994, project managers met with the U.S. Department of Energy (DOE) Program Manager Robert Lemmon in Bakersfield, Calif., for a project overview meeting. The investigators also met with an employee of Chevron and were introduced to TECHBASE, a database management program that is being considered for the project.

Data Collection

Well Logs and Well Data

During this reporting period the Munger maps covering the Pioneer Anticline were scanned into the Canvas (Deneba) drafting program, digitized into several layers, and preliminary results were incorporated into the project hypermedia database. Surface geology will be added as an additional layer.

The reservoir interval to be characterized in detail will be confined to a zone that extends from about 300 ft above the top of the Miocene to the base of the Monterey reservoir facies. Although reservoir characterization studies will focus on the Monterey reservoir, this interval includes the Etchegoin sandstone reservoir as well. This is evidence that most of the Pioneer Anticline structure contains heavy oil in the Monterey formation.

Log database management. During the first quarter of FY 1994, Digital Petrophysics, Inc. (DPI) staff constructed a Quattro Pro spreadsheet to collect well location and depth, well-log, and sample data during the interim period until a database management system is chosen. Data can be easily exported from this Quattro Pro inventory file to the database manager of choice. Log digitization is proceeding more slowly than planned because of increased business opportunities for DPI; so there was little activity in this subtask during the present quarter. This problem has been addressed in two ways: a digitizing station has been set up at MTU to relieve DPI of some digitizing tasks, and DPI has been asked to meet a June 1 deadline for submission of some critical digitized logs.

Log digitization. The DPI staff is responsible for log digitization. Digitization of logs from Union McKittrick Front Well No. 418 in Cymric field began. This well has a complete modern log suite and it will be used as the template to which all logs from Pioneer Anticline will be calibrated. Digitization of logs from the 13 wells that penetrate the Monterey formation in the immediate area around Pioneer field has fallen behind schedule because of a heavy workload of other projects at DPI.

Core and Sample Acquisition

Core and cuttings. Sidewall core and cuttings samples recovered from one of the 13 Pioneer field wells were shipped to MTU in December 1993 for petrographic, petrophysical, and geochemical analysis. During this quarter the uncleaned bagged samples were examined, and a preliminary lithological examination of the cleaned samples was performed. The XRD and FTIR analyses were performed on selected samples. Spreadsheets and macros were constructed to store, reduce, and plot the data.

An extensive rock properties data set collected on a long core from Union McKittrick Front Well No. 418 was acquired from UNOCAL.

ARCO core. Project members will approach ARCO to acquire additional core and cuttings samples from several ARCO wells in the vicinity of Pioneer field. As wells elsewhere on the Pioneer Anticline are inventoried, other operators will also be contacted. The DPI will approach ARCO and/or Western Geophysical to request access to several seismic lines shot over the Pioneer Anticline. If access can be arranged, picks on the top of the Miocene and on other stratigraphic markers will be used to further improve control on the structure of the anticline for the visualization package.

Data Analysis and Measurement

Petrophysics

Extensive petrophysical data were acquired from UNOCAL on the long core from Union McKittrick Front Well No. 418.

FTIR spectra. FTIR analyses were performed on selected samples of sidewall core and cuttings from Gary Drilling, KLC 44, Well No. 315.

Petrology

XRD. XRD analyses were performed on selected samples of sidewall core and cuttings from Gary Drilling, KLC 44, Well No. 315.

Scanning Electron Microscope Image Analysis

Image analysis work began on cuttings from one of the Pioneer wells. The Institute of Mineral Processing plans to purchase a camera for making slides and prints directly from video images.

Log Calibration

A modern log suite and conventional core data were acquired from Union McKittrick Front Well No. 418 from UNOCAL. This information will be used to calibrate well-log data to rock properties in Pioneer field. The core is currently stored in the UNOCAL Research Center in Brea, Calif., and will be examined and sampled in April 1994.

Data preparation. Well-log data for the initial 13 wells in the Crocker Petrolog program will be entered, depths will be corrected for well deviation, all logs will be printed out at the same scale, and the reservoir intervals between wells will be correlated. Because of the heavy workload at DPI, the logs have not been digitized, and this work has not yet begun.

Model selection. After calibration of these logs to the Cymric core, the Crocker Petrolog program will be used to calculate additional parameters, such as porosity, oil saturation, percent clays, and matrix properties, from the Pioneer well-log suite. These parameters are critical to reservoir evaluation. This work, planned for the third and fourth quarters of FY 1994, will result in logs of calculated parameters that will be adjusted to the same scale and used to zone the reservoir. This information will be primary input to the reservoir visualization program.

Modeling

Geochemical Modeling

The geochemical modeling program CHILLER will be used to model fluid-rock interaction. This has practical significance because of active steamflooding of the Monterey and Etchegoin formations elsewhere in the southern San Joaquin Valley. Geochemical modeling is scheduled to begin in late FY 1995. A new Windows interface is complete, data input are being simplified, and work on a graphical output interface for rapid visual display of output is in process.

Technology Transfer

Two investigators attended an organizational meeting of the Petroleum Technology Transfer Council (PTTC) of the Independent Petroleum Association of America (IPAA) in Bakersfield, Calif., on February 16, 1994. They later volunteered to serve on the Technology Committee of the national organization.

The MTU and DPI plan to present current project results at a booth in the exhibition hall at the 1994 American Association of Petroleum Geologists (AAPG) National Meeting in Denver in June 1994. Poster displays describing the project and computer demonstrations of the visualization, log evaluation, and multimedia software will be used.

A prototype multimedia-based shell using MacroMind Director was designed and developed. This shell will be used as a technology transfer mechanism. The concept is to provide the user with a CD ROM containing all project data, reports,

maps, etc., in a multimedia presentation format that will allow the user to selectively access the information in a tutorial mode. Knowledgeable users will be able to directly access reports and data tables, and less knowledgeable users will be able to select

different levels of support, depending on their level of understanding. Help manuals and tutorials on how to access and interpret each type of information will be integrated. The prototype version will be demonstrated at the AAPG meeting.

**ENHANCED OIL RECOVERY UTILIZING
HIGH-ANGLE WELLS IN THE FRONTIER
FORMATION, BADGER BASIN FIELD,
PARK COUNTY, WYOMING**

Contract No. DE-FC22-93BC14950

**Sierra Energy Company
Reno, Nev.**

**Contract Date: July 10, 1993
Anticipated Completion: Dec. 31, 1994
Government Award: \$1,124,127
(Current year)**

**Principal Investigators:
Richard G. Formann
Jerome P. Walker**

**Project Manager:
Edith Allison
Bartlesville Project Office**

Reporting Period: Jan. 1-Mar. 31, 1994

Objective

The objective of this study of the Frontier Formation in Badger Basin Field, Park County, Wyo., is to use three-dimensional (3-D) seismic and core data to analyze the diagenetic history, rock properties, and the natural fracture system. This analysis will provide the basis for increasing recovery with slant and horizontal wells to intersect oil-bearing fractures.

Sierra Energy Co. has significantly revised its targeted goals for this Cooperative Agreement because of its sale of the producing wells in Badger Basin field in the first quarter of 1994 to The Rim Companies. Sierra Energy has not assigned its interest in the Cooperative Agreement to Rim.

However, Rim has an exclusive option until Apr. 30, 1994, to accept assignment, subject to approval of the U.S. Department of Energy (DOE).

Sierra Energy, in consultation with Rim, concluded that additional work was needed on the interpretation of the 3-D seismic data, which includes the use of a workstation to locate the surface and subsurface positions for the slant and horizontal wellbores. Although this goal had been reached, more work is needed for plotting maps and seismic sections. Furthermore, an additional look at the amplitude distribution in the Frontier sands would benefit the interpretation.

Summary of Technical Progress

Interpretation of Acquired 3-D Seismic Data

Interpretation of the 3-D seismic survey was reviewed on a Sun Sparcstation 10 workstation (UNIX based) using Landmark Graphics' latest version of Seisworks 3D software. After the picks for the three Frontier horizons were edited on a 10 by 10 (inline by crossline) grid, it was necessary to rerun the autopicking routine (ZapIII) for the Frontier sands. These new horizontal interpretations were edited with the Horizons—Areal Delete capability in Seisworks 3D. A smoothing procedure was performed, with the crossline and inline filters both equal to two. Then, fault-exclusion polygons were picked for each Frontier horizon after the normal and reverse faults were edited. Horizon picks for the first, second, and third Frontier sands were converted to map points in a northwest-southeast (i.e., crossline) direction with an increment of five. The fault polygons were then appended to the map-point files for the three Frontier horizons. The map points were gridded with the use of the following parameters: (1) x-grid interval = y-grid interval = 400 ft and (2) search radius = 1000 ft. The grid was contoured with two smoothing passes. The computed contour map was converted to manual contours, where editing for the final time-structure contour map occurred.

Additionally, amplitude extraction was performed on the three Frontier horizons. Finally, maps (Figs. 1 and 2) for the three Frontier horizons were plotted; the time–structure contours were combined with a color-coded amplitude display.

Seismic displays of crossline (i.e., northwest-southeast) No. 121 (Fig. 3) and inline (i.e., southwest-northeast) No. 100 (Fig. 4) were plotted of the section between the Cody marker and the Lakota conglomerate. The high-angle reverse fault, which cuts up through the Frontier and Cody sections, is best displayed by inline No. 100. The northeast-trending normal faults are best seen on crossline No. 121, which shows a complex faulting pattern. The first Frontier horizon is broken by two faults. One (the main normal fault) has offset down into the Mowry shale, whereas the fault to the southeast dies out before penetrating the second Frontier. Both the second and third Frontier horizons are cut by the main normal fault and a fault to the northwest, which has offset down through the Lakota.

Displays of amplitude for the Frontier horizons show well-defined high- and low-amplitude trends cutting across

the axis of the anticline in a northeasterly direction as well as paralleling the hinge line of the main anticline and a subsidiary nose plunging to the south from the southeast end of the main structure. This amplitude pattern is most prominently displayed by the first Frontier. It is also easily seen in the third Frontier. However, because of the low-quality reflector associated with the second Frontier, this pattern can be more difficult to demonstrate.

An attempt was made to correlate productivity of individual wells to trends of low amplitude. There are numerous examples of better productivity correlated to low amplitude [e.g., No. 7 and No. 9 Badger Basin Field Unit (BBFU) wells and the No. 3 BBFU—the best well in the field, if the bottomhole location of the well deviated southeasterly to a total depth just on the downthrown side of the main normal fault] (Fig. 5). There are also examples of poor wells in low-amplitude areas (e.g., No. 10 BBFU). However, a common situation is to find both good and poor producers in an area with no well-defined amplitude trend, particularly for the third Frontier.

Two possible causes may explain these observations if there is a relationship between low amplitude and productive

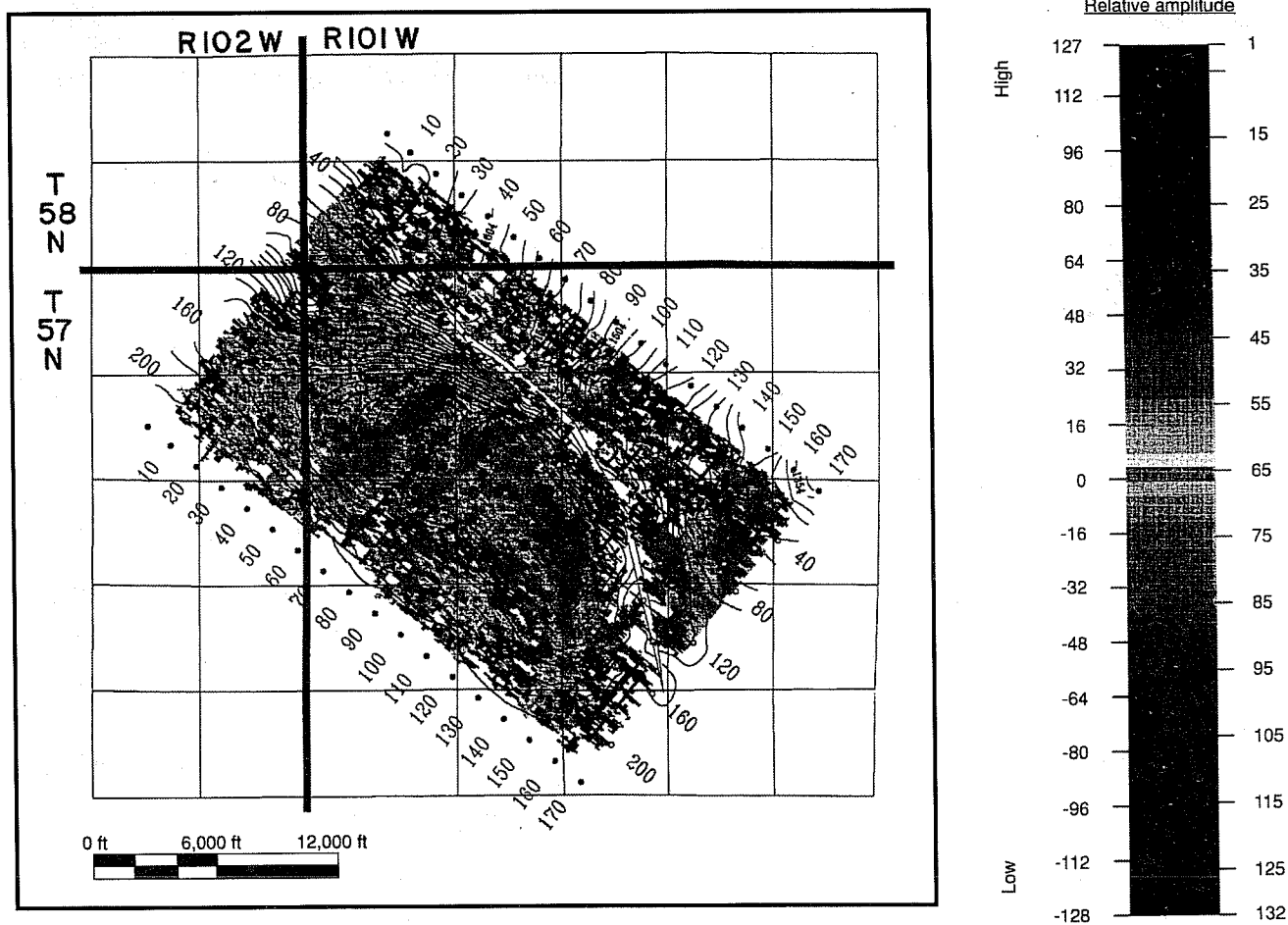


Fig. 1 Amplitude and time–structure map of the first Frontier horizon, Badger Basin Field, Park County, Wyo. Note: The bottomhole location for the Badger Basin Field Unit (BBFU) No. 3 is an estimate based on expected dips and absence of normal faulting in the Cody shale or Frontier Formation well No. 3. C.I., 10 ms [Hz: Amp2_Kf1 (1.00, 131.88)].

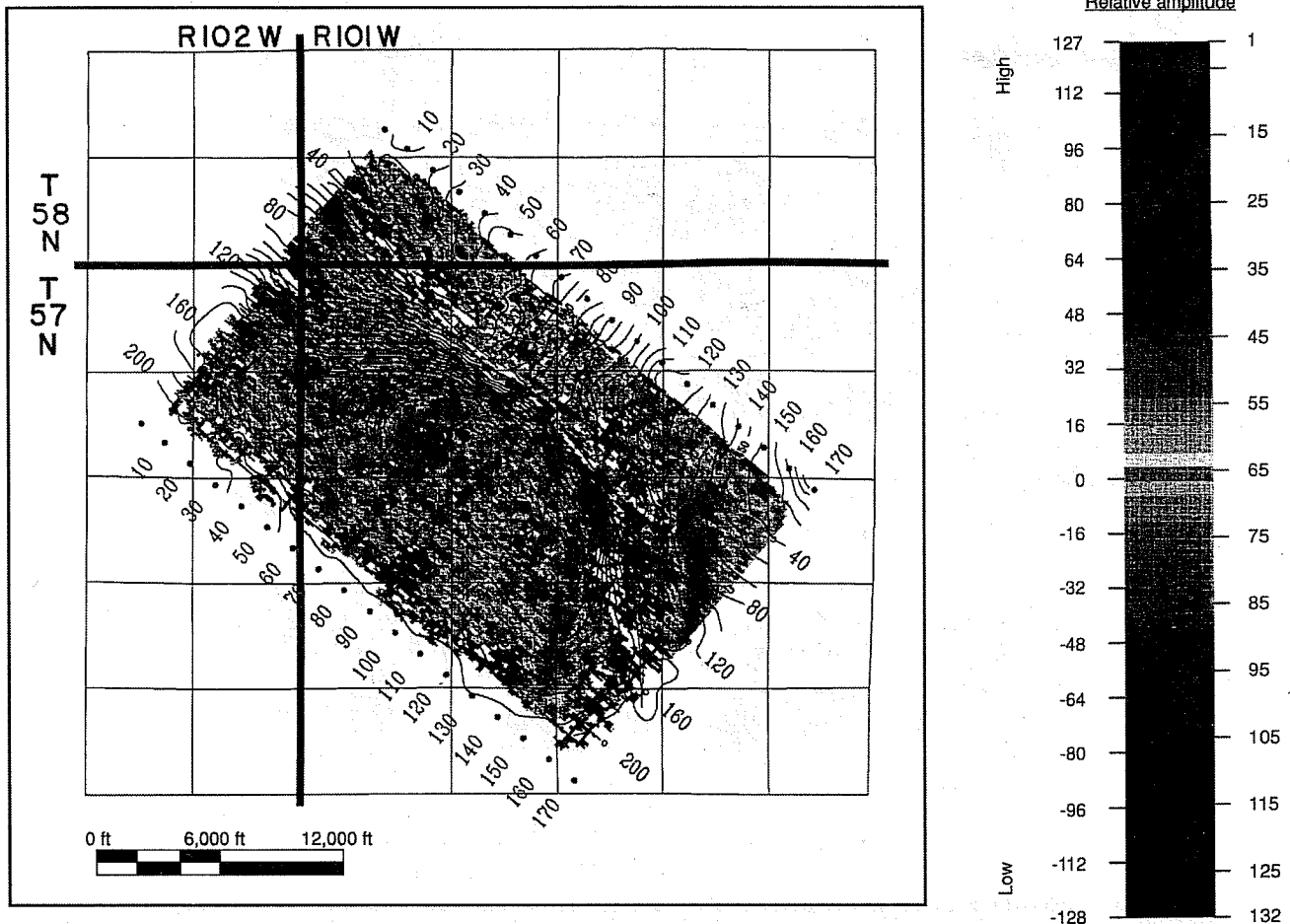


Fig. 2 Amplitude and time-structure map of the third Frontier horizon, Badger Basin Field, Park County, Wyo. Note: The bottomhole location for the Badger Basin Field Unit (BBFU) No. 3 is an estimate based on expected dips and absence of normal faulting in the Cody shale or Frontier Formation well No. 3, C.I., 10 ms [Hrz: Amp2-Kf3 (1.00.132.62)].

fractures. First, the less than full correlation of low amplitude and productivity may be due to the difference in *scale* between seismic and well data. The 3-D seismic survey has a horizontal resolution that is based on the bin size of the subsurface points. The bin dimension in a northwest-southeast direction, perpendicular to the normal faults, is 165 ft. It is believed that these northeasterly trending normal faults and associated fractures are the features providing permeability in the reservoir. Thus the seismic can only resolve horizontal features that are at least 165 ft apart. A wellbore through the Frontier is normally drilled with a 7 $\frac{7}{8}$ -in. bit. The direction of any stimulation (e.g., hydraulic fracturing) is controlled by the local stress field, which also controls the direction of the open, permeable fractures and thus causes stimulations to propagate in a direction parallel to the fracture set. Thus stimulation will not significantly increase the number of open fractures that the wellbore has encountered. Productivity of an individual well is first of all a function of the open fractures penetrated during drilling (and possible stimulation) and subsequently of the extent to which the penetrated fracture is connected with an extensive fracture

system. It is conceivable that a poor well in a low-amplitude zone may not have encountered any open fractures. Likewise, a good well in a mixed area of amplitude trend may have drilled into a narrow fracture zone that is well connected to a fracture network.

The second possible reason for the imperfect correlation of low amplitude and productivity may be due to *completions in multiple Frontier sands* by both open-hole and cased wellbores. Evidence for high productivity can be shown for all three Frontier sands. However, only the amplitude maps of the first and third Frontier display clear patterns. An example of the interpretational problem this situation may cause would be a well with significant production from the second Frontier but associated with high amplitude in the third. Unfortunately, producing practices did not allocate the amount of production to individual zones.

The most recent work on the 3-D seismic survey supports the locations for the slant and horizontal wellbores selected by Sierra Energy in December 1993, but reasonable arguments can be made for alternate locations. A final decision on which location to drill has not been made.

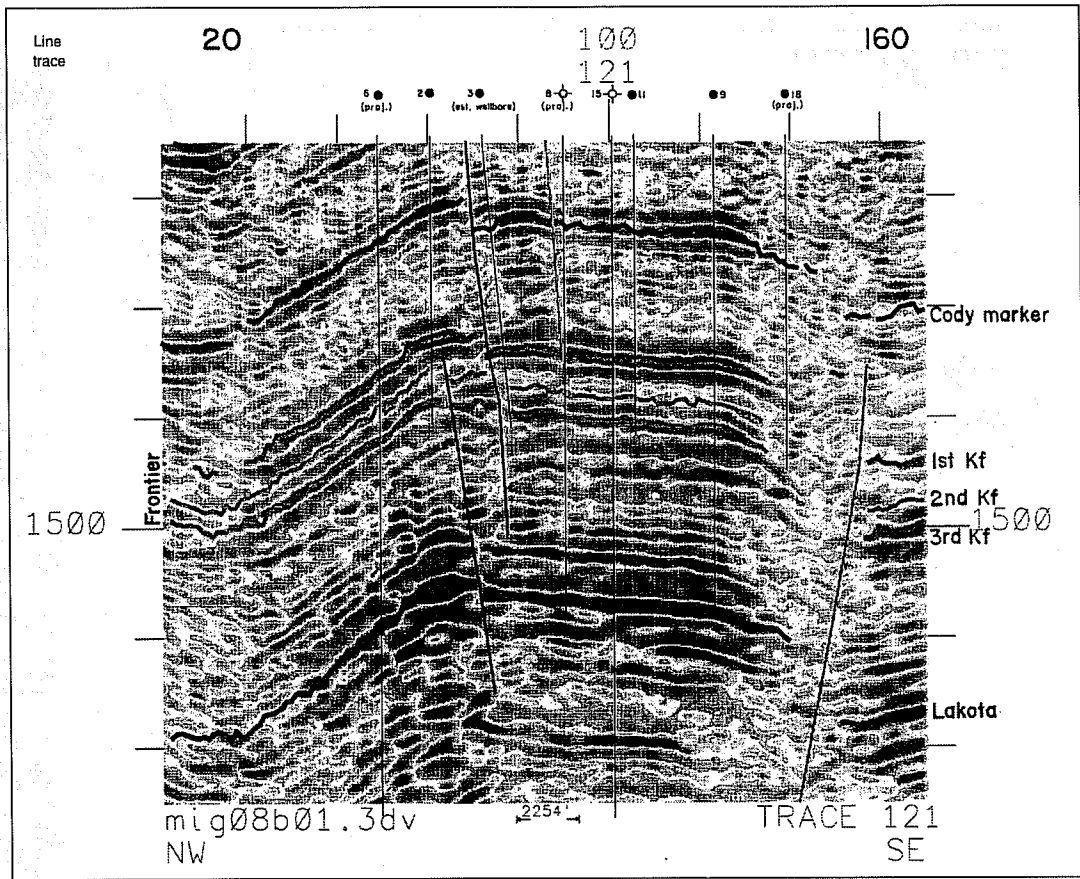


Fig. 3 Northwest-southeast seismic panel of crossline (trace) 121 between the Cody marker and the Lakota conglomerate, Badger Basin Field, Park County, Wyo. Note: The wellbore path for the Badger Basin Field Unit (BBFU) No. 3 is an estimate based on expected dips and absence of normal faulting in the Cody shale or Frontier Formation well No. 3. C.L., 10 in./s.

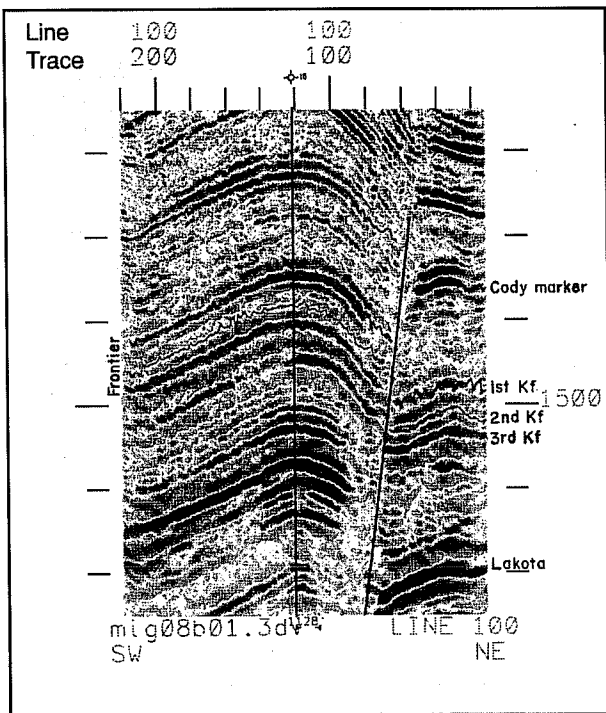


Fig. 4 Southwest-northeast seismic panel of inline (line) 100 between the Cody marker and the Lakota conglomerate, Badger Basin Field, Park County, Wyo.

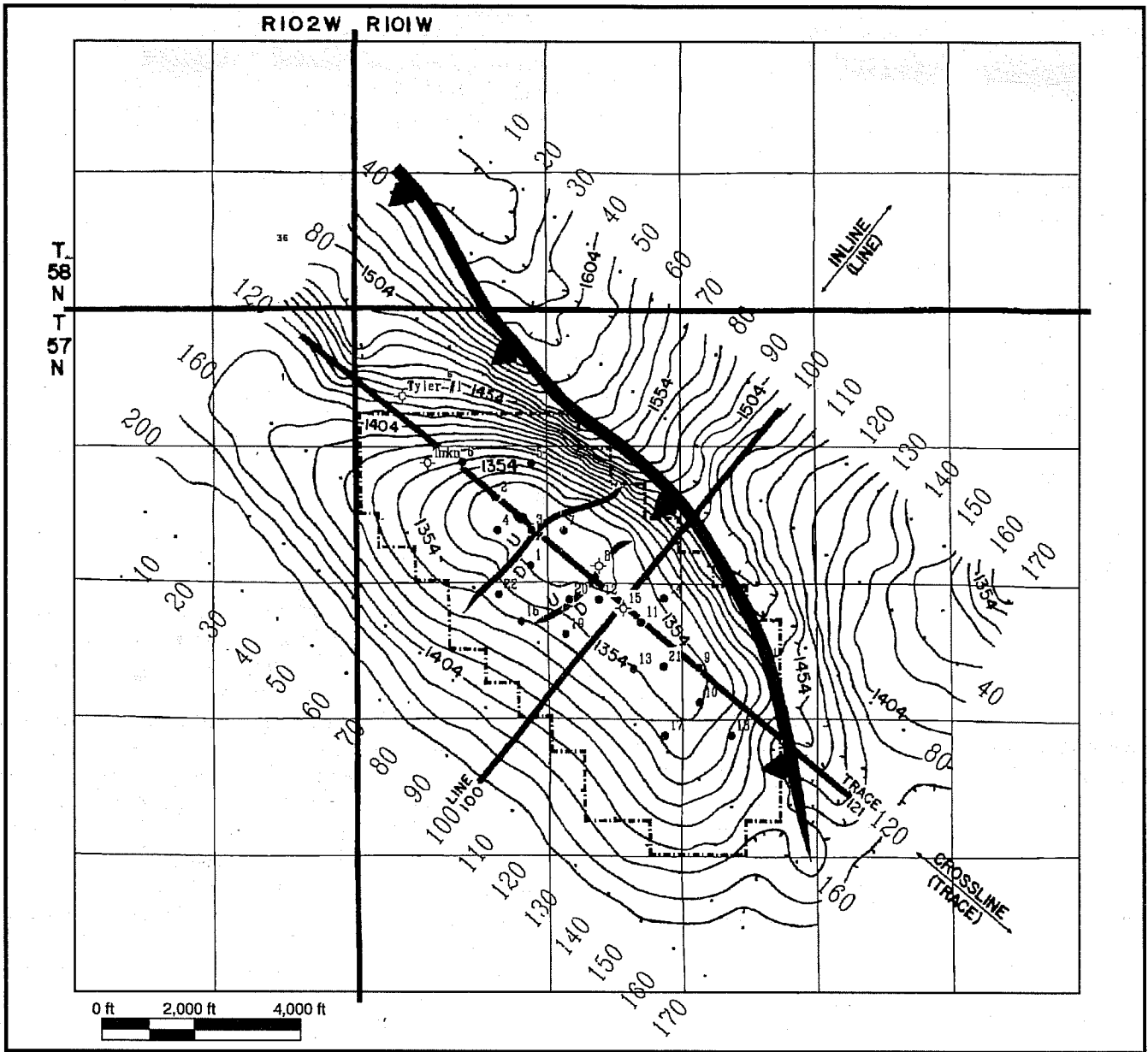


Fig. 5 Time-structure map of the first Frontier horizon showing location of seismic panels, Badger Basin Field, Park County, Wyo. Note: The bottomhole location for the Badger Basin Field Unit (BBFU) No. 3 is an estimate based on expected dips and absence of normal faulting in the Cody shale or Frontier Formation well No. 3, C.I., 10 ms.

POSTWATERFLOOD CO₂ MISCIBLE FLOOD IN LIGHT OIL, FLUVIAL-DOMINATED DELTAIC RESERVOIR

Contract No. DE-FC22-93BC14960

**Texaco Exploration and Production, Inc.
New Orleans, La.**

**Contract Date: June 1, 1993
Anticipated Completion: Dec. 31, 1997
Government Award: \$3,424, 258
(Current year)**

**Principal Investigator:
Darrel W. Davis**

**Project Manager:
Chandra Nautiyal
Bartlesville Project Office**

Reporting Period: Jan. 1–Mar. 31, 1994

Objectives

The overall objective of this project is to integrate research on petroleum reservoir characterization and process monitoring funded by the U.S. Department of Energy (DOE). Specific objectives this quarter include (1) improving the reservoir model by incorporating new grid, (2) establishing CO₂ injection into the horizontal well and production from the remaining producers, and (3) modifying CO₂ injection patterns to allow for optimum CO₂ use by incorporating a standard water-alternating-gas (WAG) injection process if necessary.

Summary of Technical Progress

Production resumed from the Port Neches carbon dioxide (CO₂) project on December 6, 1993, after a 75-day shut-in period. Since that date production has continued to improve on various wells that responded to CO₂ injection. Current production is averaging 325 bbl of oil per day (BOPD) from three wells. This represents a fourfold increase from the production level before commencing CO₂ injection. Texaco Exploration and Production, Inc., continues to purchase an average of 4.3 million cubic feet per day (MMCF/D) of CO₂ from Cardox. The reservoir pressure increased with CO₂ injection from 2460 psi in September 1993 to 3328 psi in January 1994. However, the reservoir pressure has declined slightly since then to 2730 psi in March 1994 because of reservoir imbalance caused by downtime at the CO₂ source. Currently, CO₂ is being injected in three wells in the reservoir, including the horizontal well drilled specifically for this purpose.

Texaco is continuing the transfer of this technology to other operators by presenting two papers at the Society of Petroleum Engineers (SPE)/DOE symposium that will be held April 17–20, 1994, in Tulsa, Okla. Subjects discussed will be design¹ and the development of the screening model.² The screening model, scheduled for public release in 1994, will be a useful screening and design tool for the industry. A topical report covering the environmental regulations and constraints related to the implementation of similar projects is being prepared.

Reservoir Model

The reservoir model was updated on the basis of the three-dimensional (3-D) seismic survey evaluation. A fault was placed in the center of the reservoir. The grid was rotated to accommodate this change, and a finer 29 × 72 × 1 grid system (shown in Fig. 1) was reconstructed. The reservoir volumetrics did not change. The original oil in place (OOIP) and original gas in place (OGIP) are 10.4 million stock tank barrels (MMSTB) and 4.5 billion cubic feet (bcf), respectively. Several runs were made to history match the reservoir primary production. The results clearly indicate the need of aquifer support to match the reservoir production and pressure. The highest oil saturation is present in the updip portion of the reservoir. This is supported by the high rate of oil production from well No. 15-R, which is attributed mostly to movable oil present in the reservoir.

Simulation runs made with the presence of an aquifer influx resulted in a cumulative primary production of 5.08 MMSTB of oil, 5.87 MMSTB of water, and 4.12 bcf of gas. This is below the actual reservoir production, which required an adjustment of permeability data and aquifer strength. The prediction runs indicate higher recovery than that actually observed in the field. To improve the current reservoir model, Texaco intends to develop a strata model based on 3-D seismic and other pertinent reservoir data and to use the results of the strata model to improve the current compositional model.

Horizontal Injection Well

The horizontal CO₂ injection well (Marginulina Area 1, No. 1-H) was drilled and completed in the subject reservoir, and CO₂ injection has been established in the well. The 250-ft horizontal section is capable of taking the entire 4300 thousand cubic feet per day (MCFPD) of CO₂ available for injection. However, the rate has been restricted to an average of 1500 MCFPD to distribute the CO₂ volume evenly in the reservoir.

Production response to date has been slightly higher than anticipated as a result of the CO₂ and water injection. The average initial reservoir yield, estimated at 100 bbl of oil/MMCF, is consistent with the performance of other projects conducted in similar sandstone reservoirs. The yield will be recalculated when a new software that is capable of accurately

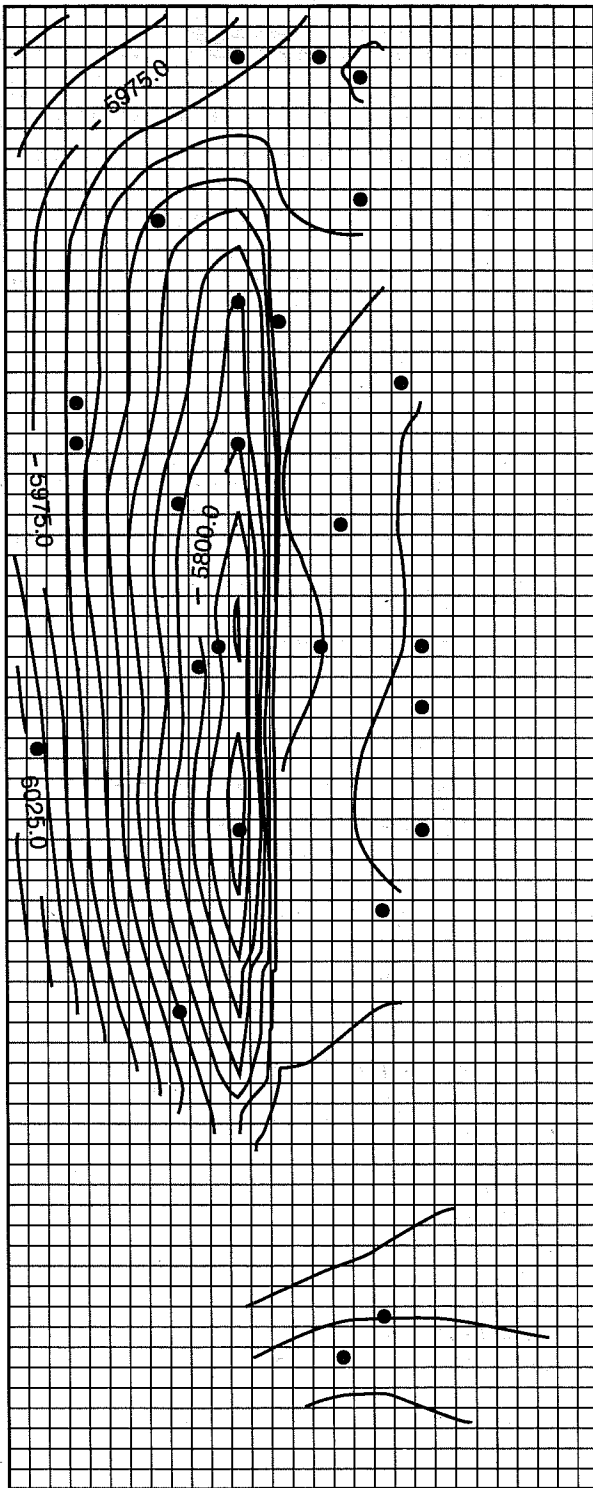


Fig. 1 Upgraded grid system.

measuring gaseous CO₂ production is installed in the field. This software is being developed by the supplier to handle a wider range of gas density that will cover CO₂. The actual and the forecasted production vs. time are shown in Fig. 2. This production trend is expected to continue with continuing CO₂ injection.

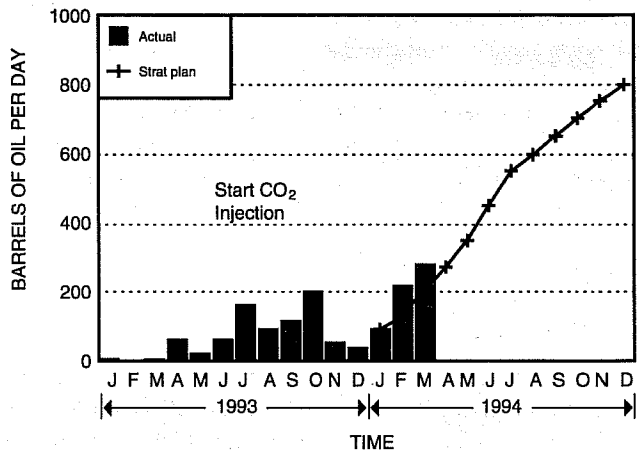


Fig. 2 Port Neches CO₂ Project allocated production.

Injection Patterns

The injection of CO₂ and water continued into the Port Neches (Marginulina Area 1) at a quarterly average rate of 2716 MCFPD and 753 bbl of water per day. This reduced CO₂ rate was caused by downtime at the Dupont plant during the month of February 1994 and repairs done on the water injection pump. The CO₂ was injected into well Nos. 7, 10, 36, and 1-H (Fig. 3), whereas water injection continued in well

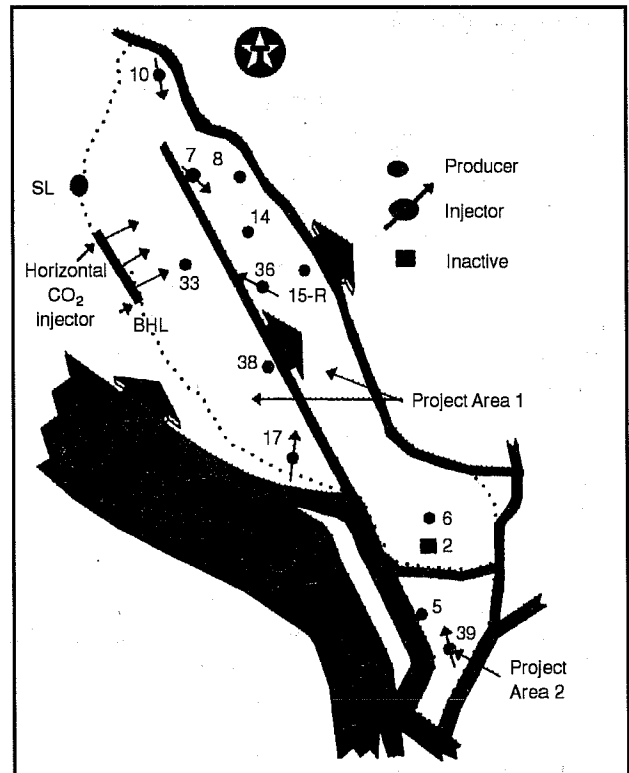


Fig. 3 Map of CO₂ Project area, Port Neches Field, Orange County, Tex. Map not to scale.

No. 17 only. Texaco is attempting to maintain high reservoir pressure to maximize production. The need to install additional pumping capacity to handle high water production rates will be evaluated, including the conversion of well No. 10 to water injection because well No. 17 will be unable to take all the produced water at the higher reservoir pressure. The conversion of well No. 10 to an injector will allow the containment of CO₂ in the inner portion of the reservoir near the producing wells.

Results

Field Implementation

The Port Neches project implementation phase is nearly complete, including facilities installation, workovers, and drilling of new wells. Exceptions to this are the drilling and workover of two wells in project area 2 that were delayed until early 1995. CO₂ and water injection are progressing as scheduled to achieve and maintain a reservoir pressure at or above the minimum miscibility pressure (MMP) of 3300 psi. A reservoir pressure of 3328 psi was reached in January 1994. This pressure, however, has declined slightly since then to 2730 psi in March 1994 because the reservoir withdrawal rate exceeded the injection rate. This situation was remedied once the CO₂ source was back on line. On the basis of project performance, additional steps may be needed to increase the water injection capacity.

Table 1 lists results of the most recent well tests performed on April 5, 1994, for all producing and injection wells.

Other wells are anticipated to respond to CO₂ injection as the reservoir continues to fill with CO₂. Peak performance is anticipated by early 1995, as predicted by various reservoir models.

TABLE 1
Well Test Results*

Well No.	BOPD	BWPD	MCFPD	CK	TBG
Producing Wells					
Khun No. 15-R	252	1686	3492	35/64	600 lb
Khun No. 38	57	320	154	18/64	140 lb
Khun No. 33	4	48	7	12/64	210 lb
Stark No. 8	14	146	730	12/64	710 lb
Injection Wells					
Marginulina Area 1					
No 1-H			2197	14/64	1090 lb
Stark No. 7			2769	48/64	1094 lb
Khun No. 36			2586	8/64	1092 lb
Khun No. 17		1343		OL.	1910 lb

*BOPD, barrels of oil per day; BWPD, barrels of water per day; MCFPD, million cubic feet per day; Choke (CK), Tubing Pressure (TBG).

Technology Transfer

In addition to Texaco releasing a screening and design program for CO₂ projects, other technology transfer work is

being conducted by Louisiana State University (LSU) and Science Applications International Corporation (SAIC). With the use of Louisiana's Office of Conservation database, LSU is collecting production and reservoir data on fluvial-dominated deltaic reservoirs; with the use of the data and Texaco's reserves estimation method, they are able to estimate recoverable tertiary reserves from such reservoirs. SAIC is working on a topical report to address the environmental regulations and constraints facing projects of this type, some of which occurred during the Port Neches project implementation.

References

1. D. W. Davis, *Project Design of a CO₂ Miscible Flood in a Waterflood Sandstone*, paper SPE 27758 presented at the SPE/DOE Ninth Symposium on Improved Oil Recovery, Tulsa, Okla., April 17-20, 1994.
2. J. K. Dobitz and J. Prieditis, *A Stream Tube Model for the PC*, paper SPE 27750 presented at the SPE/DOE Ninth Symposium on Improved Oil Recovery, Tulsa, Okla., April 17-20, 1994.

IMPROVED OIL RECOVERY IN FLUVIAL-DOMINATED DELTAIC RESERVOIRS OF KANSAS—NEAR TERM

Contract No. DE-FC22-93BC14957

**University of Kansas
Lawrence, Kans.**

**Contract Date: June 18, 1993
Anticipated Completion: Dec. 31, 1998
Government Award: \$2,007,450**

Principal Investigators:

**Don W. Green
G. Paul Willhite**

Project Manager:

**Rhonda Lindsey
Bartlesville Project Office**

Reporting Period: Jan. 1-Mar. 31, 1994

Objective

The objective of this project is to address waterflood problems of the type found in Cherokee Group reservoirs in southeastern Kansas and in Morrow sandstone reservoirs in southeastern Kansas. Two demonstration sites operated by different independent oil operators are involved in the project. The Nelson Lease (an existing waterflood), located in Allen

County, Kans., in the northeastern Savonburg field, is operated by James E. Russell Petroleum, Inc. The Stewart field (on the latter stage of primary production), located in Finney County, Kans., is operated by Sharon Resources, Inc.

Topics to be addressed include (1) reservoir management and performance evaluation; (2) waterflood optimization; and (3) the demonstration of recovery processes involving off-the-shelf technologies that can be used to enhance waterflood recovery, increase reserves, and reduce the abandonment rate of these reservoir types.

The reservoir management portion of the project will involve performance evaluation and will include such work as (1) reservoir characterization and the development of a reservoir database; (2) identification of operational problems; (3) identification of near-wellbore problems; (4) identification of unrecovered mobile oil and estimation of recovery factors; and (5) identification of the most efficient and economical recovery process.

The waterflood optimization portion of the project involves only the Nelson Lease. Optimization will be based on the performance evaluation and will involve (1) design and implementation of a water-cleanup system for the waterflood; (2) application of well remedial work, such as polymer gel treatments, to improve vertical sweep efficiency; and (3) changes in waterflood patterns to increase sweep efficiency.

Finally, plans are to implement an improved recovery process, possibly polymer-augmented waterflooding, on both field demonstration sites.

Summary of Technical Progress

Savonburg Field Project

Engineering and Geological Analysis

The computer database has been modified with the following information: new geological picks for two productive sandstones identified as B2 and B3 and a revised version of net sandstone that has a possible dead oil sand removed. Draft cross sections have been modified on the field. Several meetings were conducted to merge geological and engineering analyses. The productive sandstones B2 and B3 have been identified and mapped. New volumetric calculations have been conducted on selected patterns to determine the high potential areas.

Water Plant Development

Several meetings were held to discuss water quality in the field. The air flotation device was selected as the major water-cleanup equipment to be installed. The water was evaluated for the potential of suspended solids in oil with flotation chemicals. The flotation unit was ordered.

Pattern Changes and Wellbore Cleanup

The investigation of potential five-spot patterns continued. Possible workover-wellbore cleanup techniques are being investigated.

Field Operations

Normal field operations have included (1) monitoring wells on a daily basis; (2) repairing water plant, piping, and wells as required; (3) collecting daily rate and pressure data; and (4) solving any other daily field operational problem that might occur. In January 1994, seven producing wells were serviced and the pump was changed in the water supply well. In February 1994, three producing wells were serviced. Oil production in January 1994 was 30.8 bbl/d; in February 1994, it was 30.9 bbl/d; and in March 1994, it was 30.3 bbl/d.

The current chemical treatment program has not been altered; neither have there been any waste materials generated beyond that associated with the production of crude oil.

Stewart Field Project

Geological and Engineering Analysis

On the basis of seismic interpretation, two development wells were drilled on the eastern end of the field to assist in defining the limits of the Morrow reservoir. On the Bulger Lease wells Nos. 7-8 and 7-10, the reservoir volume was extended to 15 and 27 ft of net pay, respectively. With this additional reservoir volume, the discrepancy between material balance calculations and volumetric mapping of the net sand was narrowed. Large differences still exist, however, and the resolution of this issue remains a major objective associated with the reservoir simulation.

Independent simulation studies were undertaken by Sharon Resources and the University of Kansas. Sharon Resources simulation efforts consist of two phases: a two-dimensional (2-D) study of radial and linear models to examine sensitivities to reservoir characteristics and a three-dimensional (3-D) study to history match the Morrow production in the Stewart field. The 2-D study is complete, and the 3-D simulation is in the early stages. Results of the 2-D simulation indicate that

- Some external pressure source is required to match production and hydraulic fracturing history.
- Layering in the reservoir is detrimental to flood performance, whereas crossflow (vertical permeability) between the layers establishes a more uniform flood.
- Larger values of vertical permeability make the model less sensitive to the number of layers.
- Permeability ordering is not an influencing factor when using a favorable mobility ratio. Similar ultimate recoveries occur with different orderings; however, there is significant difference in the time associated with water breakthrough.
- Capillary pressure effects are not significant.
- Wells communicated to the St. Louis formation are suitable producers and may be shut in with no crossflow of the flood into the St. Louis.
- First-line producers should be shut in shortly after water breakthrough.

Reservoir simulation conducted by the University of Kansas is 3-D for the entire Stewart field. To avoid complexity and large computational run times, the reservoir was divided into four sections, each having no-flow boundaries. Each section is simulated separately to match the primary production. The simulation of two of the four sections is complete. The following changes to the original reservoir description were made to obtain the production history match:

- Permeability of the reservoir was increased by a factor of 2 from values based on permeability–porosity cross-plots.
- Reservoir volume was added to the northern portion of the first section simulated.
- Outside pressure support is required to match production and reservoir history.

Porosity and resistivity log data (foot by foot) have been cross-plotted on log–log paper (Pickett plot) keeping track of depth trends. The three primary zones in the Morrow form distinct clusters of points on these plots, which indicate that the zonation identified thus far nicely groups the levels of heterogeneity. Although most of the field is above the oil–water contact, several wells in the western half of the field indicate a transition zone and water leg.

Wettability tests, petrographic data, and standard core analysis have been compared as series of plots with log analysis results to define correlations. In particular, relationships between bulk volume water (water saturation and porosity) and relative permeability data, grain size and sorting, and mineral composition (clays) were sought.

Permeability is being estimated with different relationships with the use of porosity and water saturation. One method being investigated is the Timor relationship. To date, this empirical relationship has provided only fair results when comparing measured core permeability with estimated permeability.

Geological analysis is continuing in an attempt to identify the outside pressure source(s) to the Morrow reservoir. Well logs and drill stem test data from locations adjacent to the field have been estimated. A complete collection of well logs from areas adjoining the field has been assembled.

The possibility of open fractures in the Morrow reservoir is being evaluated through three potential sources of information:

1. 4-arm dipmeters from the reservoir to examine for borehole breakouts to establish minimum horizontal compressive stress direction.
2. Paleomagnetic measurements of core samples to orient the cores to define directions of any open fractures that might be present.
3. Sherman No. 3 oriented core examinations.

The presence and characterization of fractures may help to define any anisotropy in the reservoir in addition to the influence of sedimentary structures on fluid flow.

Laboratory Testing

Laboratory tests were conducted on preserved cores from the Stewart field. The tests consisted of a fluid–rock linear core study in which reservoir fluids were used to determine the relative permeability characteristics. The mercury injection method was used to determine capillary pressure. The linear corefloods also defined the initial and residual oil saturation (ROS), effective and absolute permeability, fractional flow, wettability of the reservoir rocks, and the mobility ratio between water and oil. The capillary pressure tests' results were used to calculate the pore-size distribution and saturation data.

The average initial oil saturation from three linear corefloods using Scott 4-8 core was 71%, and the average waterflood ROS was 44%. The average oil recovery was 38% original oil in place (OOIP). The average initial saturation in the laboratory for two relative permeability determinations was 0.67 pore volume (PV), and the waterflood was 0.48 PV for a recovery of 35% OOIP. The mobility ratio averaged 1.0 with the use of end-point permeability and saturation values for water displacing crude oil. This indicates that water is a good fluid for displacing crude oil.

Fractional flow data from the two relative permeability tests indicate that the producing water/oil ratio will be approximately 3.5 after water breakthrough. The average oil saturation at water breakthrough would be 0.62 for 7.5% OOIP recovery at breakthrough. If an economic limit of 99% water is assumed, the average ROS would be 0.509, or a total of 24% OOIP recovered economically by waterflooding. The total waterflood recovery in coreflood two was 40.6% OOIP and in coreflood three was 30.1% OOIP for an average recovery of 35.4% OOIP. This indicates that approximately 11.4% of this waterflood oil cannot be recovered economically.

Mercury injection capillary pressure curves generated on the Meyer No. 10-1 and Sherman No. 3 cores suggest that the average initial nonwetting phase saturation would be 76% of the PV. If the imbibition curve is used, the change in oil saturation by both primary production and waterflooding processes will be about 31%. Pore-throat radius data indicate that pore throats with radii greater than 1 μm make up an average 64% of the total PV.

Unitization

Regular meetings and correspondence took place between the technical committee members and Working Interest Owners (WIO). The two wells drilled on the easternmost lease of the field provide additional information to help WIOs assess equity values in the unit net pay map. The Unit Agreement and Unit Operating Agreement were prepared and are being negotiated between WIOs. Negotiations concerning the selection of the Unit Operator were initiated. Equity issues necessary for unitization continue to be debated.

The current chemical treatment program has not been altered; neither have there been any waste materials generated beyond those associated with the production of crude oil.

**REVITALIZING A MATURE OIL PLAY:
STRATEGIES FOR FINDING
AND PRODUCING UNRECOVERED OIL
IN FRIO FLUVIAL-DELTAIC
RESERVOIRS OF SOUTH TEXAS**

Contract No. DE-FC22-93BC14959

**University of Texas
Bureau of Economic Geology
Austin, Tex.**

**Contract Date: Oct. 21, 1992
Anticipated Completion: Dec. 31, 1994
Government Award: \$817,911**

**Principal Investigator:
Noel Tyler**

**Project Manager:
Edith Allison
Bartlesville Project Office**

Reporting Period: Jan. 1-Mar. 31, 1994

Objectives

Project objectives are divided into three major phases: The first phase, reservoir selection and initial framework characterization, consisted of the initial tasks of screening fields within the play to select representative reservoirs that have a large remaining oil resource and are in danger of premature abandonment and performing initial characterization studies on selected reservoirs to identify the potential in untapped, incompletely drained, and new pool reservoirs. The second phase will involve advanced characterization of selected reservoirs to delineate incremental resource opportunities. Subtasks include the volumetric assessments of untapped and incompletely drained oil along with an analysis of specific targets for recompletion and strategic infill drilling. The third and final phase of the project will consist of a series of tasks associated with technology transfer and the extrapolation of specific results from reservoirs in this study to other heterogeneous fluvial-deltaic reservoirs within and beyond the Frio play in South Texas.

Summary of Technical Progress

Work during this project quarter consisted of continuation of identifying and delineating incremental recovery opportunities in selected Frio fluvial-deltaic sandstone reservoirs. The focus has been on defining interwell stratigraphic heterogeneity of individual reservoir zones in Rincon field through detailed stratigraphic correlations and analysis of abundant wireline core data.

A digital database for Rincon field consisting of log curves for over 200 wells has been refined and updated to include production data and reservoir tops; log facies type; thicknesses; net sandstone; percentage sandstone; and core porosity, permeability, and water saturation for individual reservoir zones. Digitized log data have been depth-adjusted to correspond with core analysis values. Maps illustrating distribution of oil production, initial potential, net sandstone thickness, percentage sand, and permeability thickness have been generated for several separate reservoir zones.

Characterization of Rincon Field Reservoirs

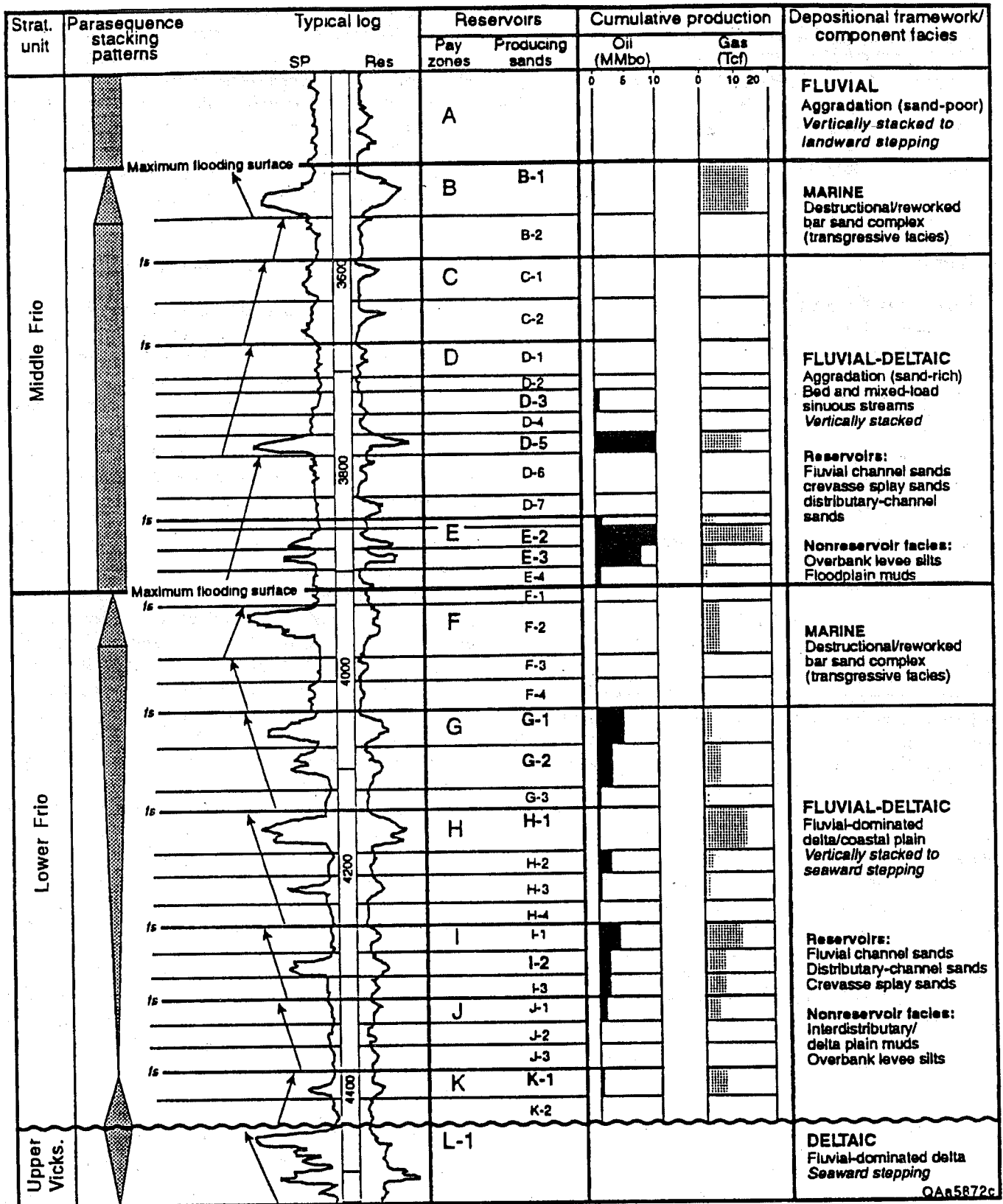
The stratigraphic positions of important reservoir units in Rincon field within the context of the larger scale genetic stacking sequence were evaluated to assess the importance of reservoir stratigraphy for hydrocarbon production, recovery efficiency, heterogeneity style, and the potential for compartmentalization of additional oil resources. Oil reservoirs in Rincon field represent deposition in aggradational fluvial channels, mixed aggradational-progradational fluvial and distributary channels, and progradational deltaic facies. The differing stratigraphic context of these reservoirs results in different engineering attributes and degrees of internal heterogeneity that affect reservoir quality, hydrocarbon recovery efficiency, and their potential for additional recovery. Further integration of past reservoir production behavior with detailed studies of geologic facies heterogeneity within individual reservoir units is being used to identify the location of significant additional reserves in unproduced reservoir compartments. Details of the reservoir stratigraphic framework, the current distribution of hydrocarbon production, and summarized petrophysical attributes for Rincon field oil reservoirs are provided in this report.

The stratigraphic subdivisions between upper Vicksburg, lower Frio, and middle Frio reservoirs are identified on a representative log shown in Fig. 1. Wireline core data representing more than 1500 analyses from more than 100 wells in the Rincon field study area were assigned to individual reservoir subunits and evaluated to assess heterogeneity within each of the major reservoir units. A summary of reservoir attributes for each of the productive Frio reservoir sandstones is given in Table 1. Distributions of values for core porosity and permeability for reservoirs representing upper Vicksburg, lower Frio, and middle Frio are shown in Fig. 2.

Upper Vicksburg Reservoirs

Stratigraphic Framework and Reservoir Facies

Vicksburg reservoirs in Rincon field include the L sandstone unit shown at the base of the log interval illustrated in Fig. 1. These reservoirs consist of thick, progradational (seaward-stepping), deltaic sandstone deposits that occur in packages 50 to 150 ft thick and are separated by 50- to 200-ft-thick intervals of mudstone. Primary reservoir facies are channel-mouth-bar sandstones that are interbedded with



QA65872c

Fig. 1 Representative log from Rincon field illustrating general stratigraphy, reservoir nomenclature, and the stratigraphic distribution of oil and gas production of individual producing units in the Frio fluvial-deltaic sandstone play productive reservoir interval.

prodelta mudstone and siltstone. Individual, upward-coarsening channel-mouth-bar deposits are generally less than 50 ft thick

and stack to produce repetitive cycles that can reach 150 to 200 ft in thickness.

TABLE 1

Summary of General Reservoir Attributes for Individual Productive Frio Sandstone Zones Within Rincon Field

Zone	Depositional environment and Sandstone geometry	Depth (subsea)*	Pay	Mean porosity, † %	Mean permeability, † mD	Net sand*	Percent sand*	Cumulative production,* MMCF	Cumulative production,* MBO	Total oil, %	Abandoned zones, ‡ %
Middle Frio Aggradational Reservoirs											
Frio B	Strike-elongate bar sands	3164	Gas	27.0	62.9	12.9	13	11,774	138	0.4	81
Frio C	Thin narrow channels	3248	Oil	n/a§	n/a	2.5	3	1,558	124	0.4	100
Frio D	Broad dip-elongate fluvial channel system	3350	Oil	25.3	56.9	21.1	27	14,126	8,311	24.7	95
Frio E	Dip-elongate fluvial channel system	3449	Oil	26.6	67.6	18.2	22	29,103	14,066	41.9	85
	Interval totals			—	—	47.6	13	56,561	22,639	70.6	—
Lower Frio Mixed Aggradational-Progradational Reservoirs											
Frio F	Strike elongate bar sands minor dip-elongate channels	3517	Gas	24.7	25.8	25.5	0.18	6,647	96	0.3	
G zone	Dip-elongate channels	3633	Oil	27.4	96.9	18.4	0.17	10,457	5,356	15.9	86
H zone	Broad dip-elongate channels	3712	Oil and gas	27.9	55.6	16.8	n/a	14,840	873	2.6	100
I zone	Thin dip-elongate channels	3852	Oil	25.6	30.8	13.0	n/a	1,285	2,057	6.1	94
J zone	Narrow channel sands	3928	Oil	24.7	89.1	16.1	n/a	3,051	645	1.9	100
K zone	Strike-elongate bar sands	3969	Oil	26.9	62.5	9.0	n/a	21,433	421	1.3	100
	Interval totals			—	—	98.4	25%	68,713	9,448	29.4	—

*Mean reservoir depth, net and percent sand, and cumulative production data for study area (see location map).

†Mean porosity and permeability values based on wireline core analyses.

‡Percent of abandoned zones calculated from total completions and remaining active (producing and shut-in) zones as of 1991.

§Values listed as n/a reflect limited data available.

Reservoir Attributes

Deltaic reservoirs from upper Vicksburg have distinctly lower porosity and permeability [mean porosity (ϕ) = 20.3%, median permeability (k) = 8.2 mD] than Frio reservoirs (Fig. 2, Table 1), probably reflecting the interbedded sandstone-mudstone alternations characteristic of these stacked progradational units. These reservoirs are responsible for 21% of the total oil production from Rincon field.

Vicksburg reservoirs in Rincon field are not targets for resource delineation and additional recovery because their deposition was strongly influenced by faulting associated with the development of the Vicksburg Fault Zone.¹ Correlations necessary to document depositional heterogeneity and stratigraphic compartmentalization in these reservoirs are difficult. The present reservoir studies focus on the structurally uncomplicated Frio reservoir interval, which has a better potential for identifying lateral facies heterogeneity and stratigraphic compartmentalization and much more available data.

Frio Reservoirs

Stratigraphic Framework and Reservoir Facies

Subdivisions within main Frio reservoir-producing zones are illustrated in Fig. 1. Also shown are cumulative oil and gas production for each zone and the relative position of each reservoir within a genetic stratigraphic stacking hierarchy

developed for the Rincon field section. Low-resistivity shale markers separate the primary reservoir sandstone zones. Two significant low-resistivity markers interpreted to represent maximum flooding surfaces have been identified at the top of a transgressive bar sandstone complex (B and F units). Each transgressive sandstone complex that occurs below a major flooding surface (B and F units) produces mostly gas and is not an important oil reservoir. Aggradational channel sandstones (e.g., D, E, and G units) located below each transgressive unit are primarily oil reservoirs; the most significant accumulations occur in the sands immediately below the main gas reservoir. This observation suggests that these flooding surfaces may act as important subregional seals.

The Frio G–J (lower Frio) reservoir interval corresponds to an interval of mixed progradational and aggradational sedimentation, whereas the Frio C–E sandstone zones (middle Frio) represent deposition in a purely aggradational setting. The F shale marker marks the boundary between these two contrasting styles of deposition. Reservoir facies in the lower Frio interval are interpreted to represent predominantly delta-plain distributary-channel sandstones. Distributary channels are distributed as elongate, dip-parallel belts. Individual, upward-fining channel sandstone packages range from 5 to 20 ft thick and commonly stack to produce amalgamated units that have vertical thicknesses of 10 to 50 ft. These stacked sandstone packages commonly display an upward-thickening trend. Sandstone body continuity is generally less than in

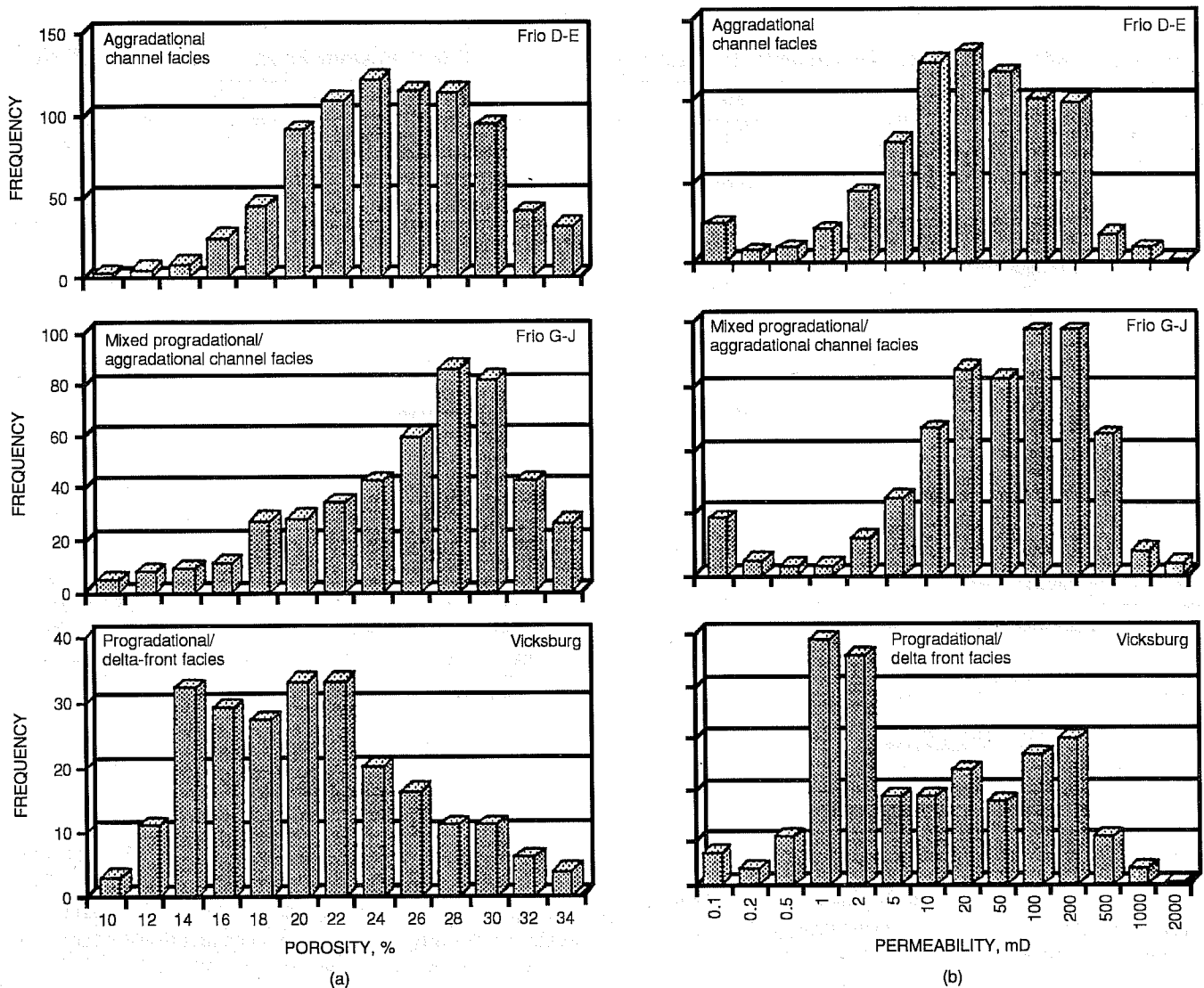


Fig. 2 Frequency distributions for values of core porosity (a) and permeability (b) from various fluvial-deltaic reservoir groups within the productive Frio-Vicksburg stratigraphic interval.

middle Frio fluvial channels, (distributary channel-fill sandstones are narrower and are flanked laterally by sand-poor interdeltic facies). Low-permeability mudstone facies locally encase and compartmentalize or isolate individual reservoir sandstones. These reservoir compartments are primary targets for additional oil recovery in the lower Frio interval.

Middle Frio reservoir facies consist primarily of dip-elongate, fluvial channel-fill sandstones and are separated by non-reservoir facies that include levee siltstones and floodplain mudstones. Productive middle Frio reservoirs in Rincon field occur both as individual, narrow, channel-fill units isolated vertically and laterally by low-permeability overbank and floodplain facies and as large channel complexes with multiple sandstone lobes that combine into a single large communicating reservoir. Sandstones have individual thicknesses ranging from 5 to 30 ft but are commonly stacked into composite units with gross thicknesses between 20 and 60 ft.

Low-permeability subfacies within the channel fill are responsible for the development of multiple reservoir compartments that may represent significant opportunities for additional recovery.

Reservoir Attributes

Distinct distributions of reservoir porosity and permeability are illustrated by core data from lower and middle Frio reservoir units in Fig. 2. Channel sandstone reservoirs in the mixed progradational-aggradational lower Frio interval exhibit higher porosity and permeability values (mean $\phi = 27.1\%$, median $k = 85$ mD) than their counterparts in the aggradational middle Frio (mean $\phi = 25.7\%$, median $k = 38$ mD). In addition, the porosity and permeability values of middle Frio reservoirs appear normally distributed, whereas the distribution of values in lower Frio units is not. Different frequency distributions for reservoir attributes have been documented that have important

implications in estimates of recovery efficiency when average values of non-normally distributed data are used to calculate reservoir volumes.³

Core porosity and permeability values were cross-plotted to identify variability within individual Frio reservoir zones. Examples of these data from a middle Frio aggradational channel sandstone (Frio E), a transgressive bar sandstone (Frio F), and a lower Frio mixed aggradational channel sandstone (Frio G) are shown in Fig. 3. Core data measured from sands in Frio E and Frio G dip-oriented channel oil reservoirs exhibit a greater range of values from the Frio F gas reservoir. This may reflect the greater variability of depositional facies present within the fluvially dominated reservoir zones and may also be partly an artifact of slightly higher textural maturity of the reworked bar

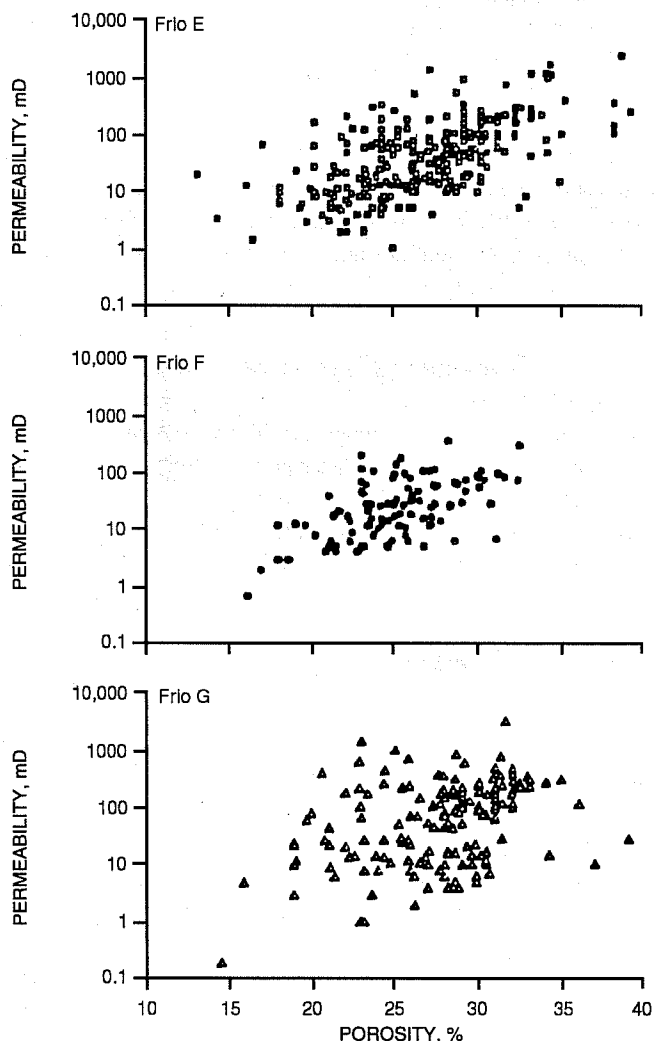


Fig. 3 Cross-plots of porosity and permeability values measured from wireline cores in representative Frio reservoirs in Rincon field. Dip-elongate channel sandstone oil reservoirs from the E and G units represent deposition in middle and lower Frio intervals, respectively. The F unit is a strike-elongate transgressive unit that exhibits significantly less variability in porosity and permeability values than the E and G channel reservoir facies above and below it. The F sandstone is a minor gas reservoir and is shown for comparison purposes only.

sandstone units. The lower Frio G sandstone unit exhibits greater variability and a weaker relationship between porosity and permeability than the Frio E sandstone unit, its channel counterpart in the middle Frio interval.

Production Behavior

Production histories for the most important Frio oil reservoirs in Rincon field were examined to identify relationships between the stratigraphic position and porosity and permeability characteristics of Rincon reservoirs and their ability to produce hydrocarbons. Evaluation of production data, including a reservoir's response to waterflooding and overall recovery efficiency, will be used in conjunction with studies of facies architecture to identify zones with the highest potential for containing compartments with unproduced oil.

The Frio E sandstone, the most prolific reservoir zone in the field, has produced nearly 12 million stock tank barrels (MMSTB) of oil since production began in 1940. Secondary waterflooding in the Frio E reservoir zone has accounted for 2.5 MMSTB, or nearly 21% of total E zone production. With the use of average reservoir values of 26.5% porosity and 37.5% water saturation, Frio E reservoirs have been estimated to have an overall recovery efficiency of 34%.

The reservoir attributes of Frio D sandstones are similar to those of Frio E (average porosity, 25.2%; water saturation, 40.5%; and estimated original oil in place (OOIP), approximately 35 MMSTB), but the recovery efficiency is lower (28%). Frio D reservoirs have produced nearly 10 MMSTB of oil since 1940. Waterflooding attempts in this reservoir zone accounted for secondary recovery amounting to only 2% of total D production. These disappointing results were attributed in part to the heterogeneous nature of the D sandstone interval.

The Frio G reservoir zone also began production in 1940 and has produced a total of 5.4 MMSTB of oil to date. Unsuccessful waterflooding in Frio G accounted for less than 2% of total production. Mean porosity and permeability values of G sandstones (27.4% and 96.9 mD, respectively) are greater than those of Frio D and E sands. In Fig. 3, G sandstones exhibit the greatest variability in porosity and permeability. Approximately 29% of the OOIP has been recovered from the G reservoir zone.

Further Studies

The Frio D, E, and G reservoirs in Rincon field are the current focus of more detailed studies to characterize the heterogeneity of the various productive reservoir facies. Detailed mapping of the internal physical architecture of individual reservoir flow units should explain why these reservoir zones have produced differently and may identify the location of untapped and incompletely drained reservoir compartments that may have significant potential for additional oil recovery. In conjunction with these efforts, studies of whole core from the D and E reservoir zones in Rincon field will begin during the next project quarter. Evaluation of the production data and identification of heterogeneity style in selected reservoir zones from Tijerina-Canales-Blucher (TCB) field are also continuing.

References

1. J. Coleman and W. E. Galloway, Petroleum Geology of the Vicksburg Formation, Texas: *Gulf Coast Assoc. Geol. Soc., Trans.*, 5(40): 119-130, (1990).
2. J. Coleman and W. E. Galloway, Sequence Stratigraphic Analysis of the Lower Oligocene Vicksburg Formation of Texas, in Sequence Stratigraphy as an Exploration Tool: Gulf Coast Section, Society of Economic Paleontologists and Mineralogists Research Conference, J. W. Armentrout and R. F. Perkins, (Eds.), pp. 99-112, 1991.
3. M. H. Holtz, L. E. McRae, and N. Tyler, *Identification of Remaining Oil Resource Potential in the Frio Fluvial-Deltaic Sandstone Play, South Texas: The University of Texas at Austin, Bureau of Economic Geology, Topical Report Prepared for the U.S. Department of Energy, Bartlesville Project Office, Under Contract: No. DE-FC22-93BC14959, Report DOE/BC/14959-8, 1994.*

INTEGRATED APPROACH TOWARD THE APPLICATION OF HORIZONTAL WELLS TO IMPROVE WATERFLOODING PERFORMANCE

Contract No. DE-FC22-93BC14951

**University of Tulsa
Tulsa, Okla.**

**Contract Date: Jan. 1, 1993
Anticipated Completion: Dec. 31, 1996
Government Award: \$250,973**

**Principal Investigator:
Balmohan G. Kelkar**

**Project Manager:
Rhonda Lindsey
Bartlesville Project Office**

Reporting Period: Jan. 1-Mar. 31, 1994

Objectives

The overall objective of the project is to improve secondary recovery performance of a marginal oil field through the use of a horizontal injection well. The location and direction of the well will be selected on the basis of detailed reservoir description using an integrated approach. With the use of this method, a recovery of 2 to 5% of original oil in place (OOIP) is expected. This should extend the life of the reservoir by at least 10 yr.

The project work is divided into two stages. In Stage I, part of the Glenn Pool field (William B. Self Unit) will be selected, and additional reservoir data will be collected with cross-borehole-tomography surveys and formation-microscanner logs through a newly drilled well. Analogous outcrop data will also be used. A detailed reservoir description will be

developed on the basis of an integrated approach by the combination of the state-of-the-art data and conventional core and log data. After extensive reservoir simulation studies have been conducted, the location and direction of a horizontal injection well will be selected. The well will be drilled on the basis of an optimized design, and field performance will be monitored for at least six months. If the performance is encouraging, the project will continue.

Stage II, the second budget period of the project, will involve selection of part of the same reservoir (Berryhill Unit, Tract 7), development of the reservoir description with the use of only conventional data, simulation of flow performance with the use of the developed reservoir description, selection of a location and direction of a horizontal injection well, and implementation of the well followed by monitoring of reservoir performance.

Comparison of the results obtained during the two budget periods will allow evaluation of the utility of collecting additional data with state-of-the-art technology. The application of horizontal wells in improving secondary recovery performance of marginal oil fields can also be evaluated.

A successful completion of this project will provide new means of extending the life of marginal oil fields using easily available technology. It will also present a methodology to integrate various qualities and quantities of measured data to develop a detailed reservoir description.

Summary of Technical Progress

The report of technical progress is divided into three sections: (1) preliminary geological description of Self No. 82 which was drilled in the Self Unit, (2) preliminary results based on the cross-borehole seismic surveys, and (3) additional results of the Well No. 54 well test and comparison of well-test permeability with core-permeability data from Well No. 82.

Geological Description

A vertical test well (Self No. 82) was drilled for advanced-technology data collection and for evaluation of subsurface mapping completed prior to drilling. The subsurface maps consisted of facies and net-sand isopach maps for each of seven discrete genetic intervals (DGI).

A total of 153 ft of core was recovered in three core runs. The core was cut from 1420 to 1575 ft, but the bottom 2 ft of the Glenn Sandstone was not recovered in core run No. 3. Well site observations noted that oil was bleeding from discrete stratigraphic intervals of 1 to 6 ft thick in DGI A, C, D, and E. The core was archived and is being processed at Amoco Research Laboratory, Tulsa, Okla.

As the core was being processed and prepared for subsampling, a detailed core description was made and stored in a computer graphics software file used by Amoco. A final description will follow the completion of core-plug sample processing.

Core plugs from the Glenn Sandstone were cut with the use of two spacing schemes and different orientations. The upper

46 ft of mudstone and lower 41 ft of sandstone largely depleted of hydrocarbons were plugged at about 3-ft intervals. The interval of greatest interest for the project, the upper 46 ft of mudstone, was also plugged at about 1-ft intervals. Orientations of plugs in this interval were horizontal, vertical, and 45° inclined to the core axis; these oriented samples are of particular interest to the geophysical studies. Plugs cut in the sandstone were horizontal and vertical to the core axis at each sampled interval. Core plug measurements include porosity, permeability, velocity, grain density, and mineralogy.

A microresistivity log (FMI) was successfully acquired in Self No. 82 through the Glenn Sandstone. The data have been processed by Amoco Production Company well-log services group in Houston, Tex. The processed log will be examined and analyzed after completion of the final core description and photography tasks. The microresistivity log will be evaluated at Amoco Research Laboratory, Tulsa, Okla.

Drilling of Self No. 82 provided an opportunity to assess the predictive quality of the reservoir architecture maps developed prior to drilling. Overall, the expected thicknesses were within the 5-ft contour interval used in the working facies and net-sand isopach maps for each DGI. Evaluation of the success of facies predictions is pending the final core description. The prediction of the presence of DGI B at the location of Self No. 82 was not validated by the results of Self No. 82; DGI B is markedly truncated by erosion prior to deposition of the channel-fill facies of the overlying DGI A. It is hoped that the interwell position of the termination of DGI B can be refined in the cross-well tomographic images. In addition, the greater thickness and higher-than-expected oil saturations found in DGIs D and E have resulted in a reassessment of the correlation of these two DGIs.

Interpretation of Geophysical Data of Full-Field Survey

The full cross-well survey was completed in early 1994. The preliminary survey resulted in high-quality data, but the second encountered high ambient noise. The noise levels were high enough to prohibit first-arrival picking over in much of the data. Analysis of the data from the second survey shows that tube waves are emanating from the perforated interval in the receiver well. This is interpreted to be fluid-flow or circulation noise through the perforations, even though the well was not flowing fluid at the surface.

Although this image plane was important for characterization of the reservoir, the survey was reshot by reversing sources and receivers in the two wells. The resulting high-quality data indicate that shooting direction can be an important acquisition factor.

In general terms, cross-well seismic imaging is a method capable of resolving very thin beds relative to conventional surface seismic methods. The main advantage of cross-well seismic over surface seismic methods is the notable difference of frequencies encountered (200 to 2000 Hz vs. 20 to 80 Hz, respectively) and the corresponding improve-

ment in resolution. The downhole vantage point allows tight integration with other borehole information. This can lead to inferences concerning reservoir properties such as porosity distribution and bed continuity.

The cross-well seismic objective at the Glenn Pool field is to create tomographic image planes to aid in reservoir characterization. Initial tomography results are discussed by Vassiliou et al.¹

Acquisition for the full cross-well work using well No. 82 involved Amoco's piezo-source and a proprietary 15-hydrophone receiver string developed by Conoco, Inc. Conoco supplied personnel, on-site data processing, and data editing services.

From early in the project the plan had been to use Self No. 82 as the cross-well seismic source well (see Fig. 1). This was considered the best plan to minimize risk of losing the expensive source downhole.

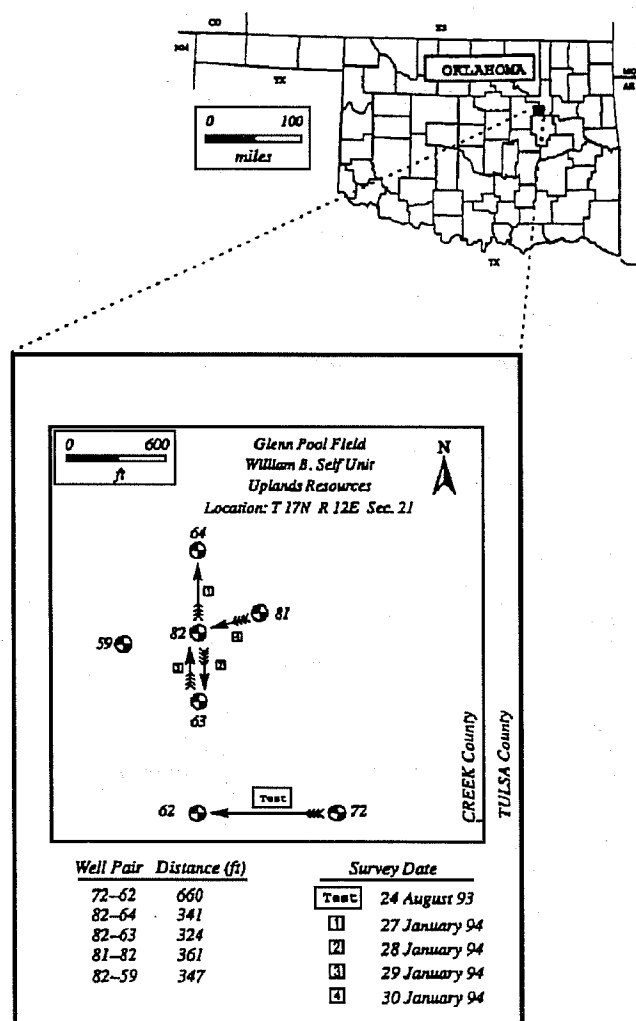


Fig. 1 Location and site map of Glenn Pool field, William B. Self Unit, uplands resources. Only those wells involved in the cross-well seismic work are shown. Arrows indicate cross-well shooting direction by pointing at the receiver well. Location, sec. 21, T. 17 N., R. 12 E.

The first full survey, 82 → 64, followed this plan and resulted in high-quality data. Figure 2 shows some features of the 82 → 64 survey, including geometry of selected common source gather (CSG) and common receiver gather (CRG). The CSG and CRG data are plotted in Fig. 3. Clear first breaks with good relief above ambient noise are evident on both.

After the success of the 82 → 64 survey, the acquisition team shot 82 → 63, labeled survey 2 in Fig. 1. The survey geometry is nearly identical to that shown in Fig. 2; Fig. 4 shows a CSG and CRG representative of the data. As shown in Fig. 4, the high ambient noise was surprising compared to the 82 → 64 data quality. In both surveys every precaution was taken to eliminate known sources of noise. Also, all information on well Nos. 63 and 64 indicated that they were nearly identical in drilling, completion, and production history.

On the CRG, ambient noise is strong before and after first-arrival times. This noise is incoherent on the CRG; on the CSG in Fig. 4, the noise is coherent and recognizable as tube-wave energy. Upgoing tube waves exist above 1500 ft and downgoing ones exist below this level. As suggested,² this is interpreted as fluid-flow noise associated with the perforated interval at 1460 to 1505 ft. It seems curious that such strong tube-wave energy should be generated by downhole (circulating?) fluid flow despite there being no fluid flow at the surface.

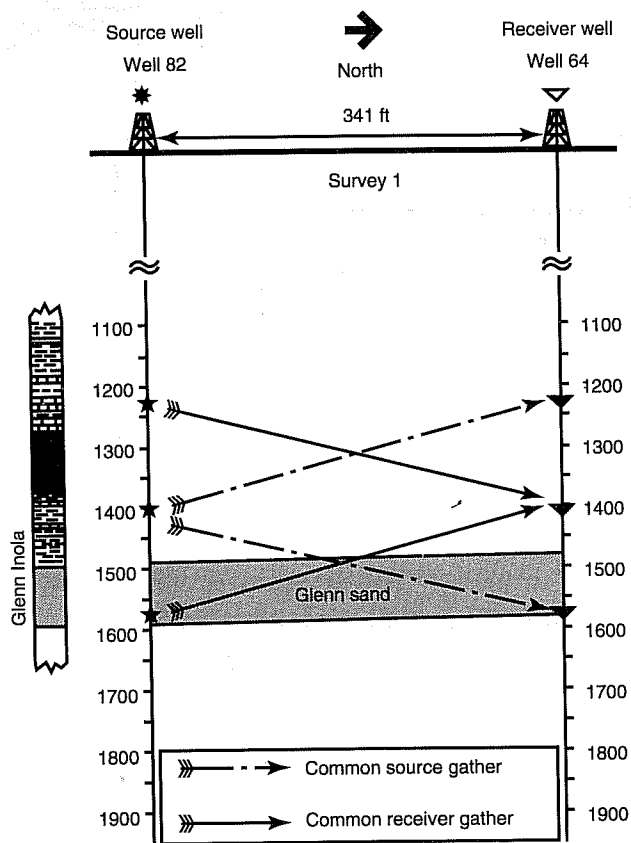


Fig. 2 Some features of the 82 → 64 survey, including generalized stratigraphic column and reservoir (Glenn sand). Also indicated are representative common source and common receiver gathers.

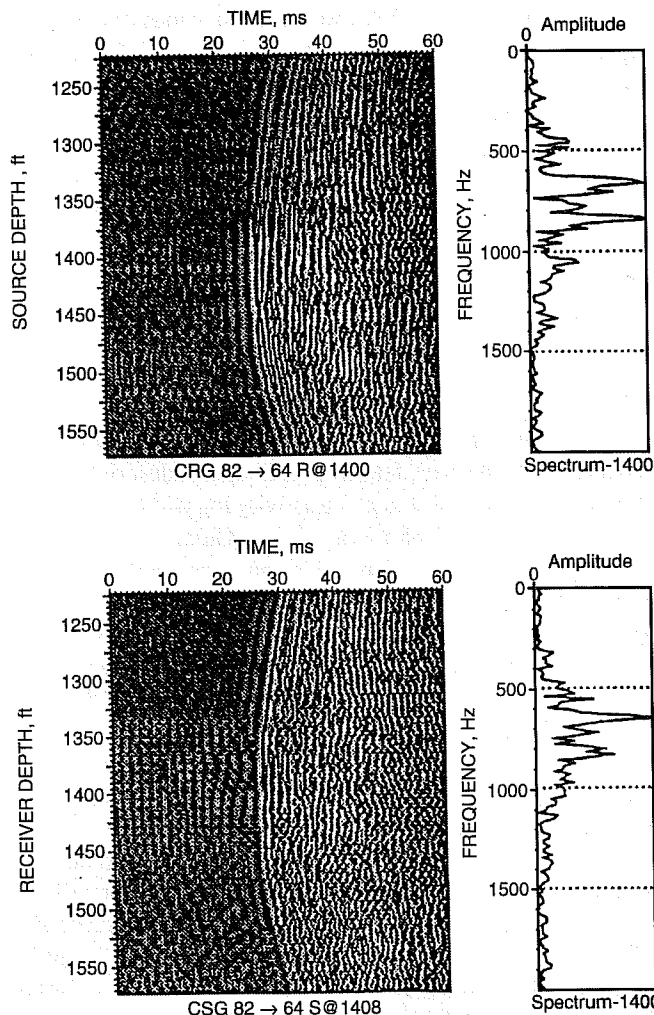


Fig. 3 Selected common receiver gather (CRG) and common source gather (CSG) data from the 82 → 64 survey. Beside each gather is a frequency spectrum for a trace near the center of the gather. The data quality is high, and first arrivals stand out well above ambient noise levels. The receiver well (No. 64) is perforated on the interval 1452–1473.

The ambient noise problem was serious enough that a significant portion of the wide-angle data could not be picked for first arrivals. Because picked-first arrivals are the raw data for cross-well tomography and because this image plane was deemed crucial to the characterization effort, it was decided to back-shoot the 82 → 63 survey as 63 → 82.

In an effort to enhance data quality for better characterization of the reservoir, the 82 → 63 survey was reshot with reversed source and receiver wells. In theory, the fluid-flow noise in the source well (No. 63) would radiate very little energy into the formation to appear as ambient noise in the receiver well (No. 82). In this way, the flow noise would be overwhelmed by the source signal.

Figure 5 shows CSG and CRG data over a common interval in the 63 → 82 survey. The data quality shown in Fig. 5 is greatly improved over that shown in Fig. 4. The data for this survey could be picked for first arrivals at all vertical offsets.

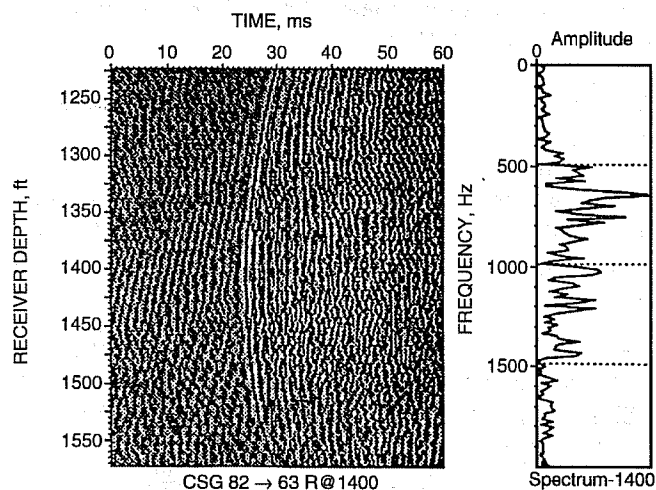
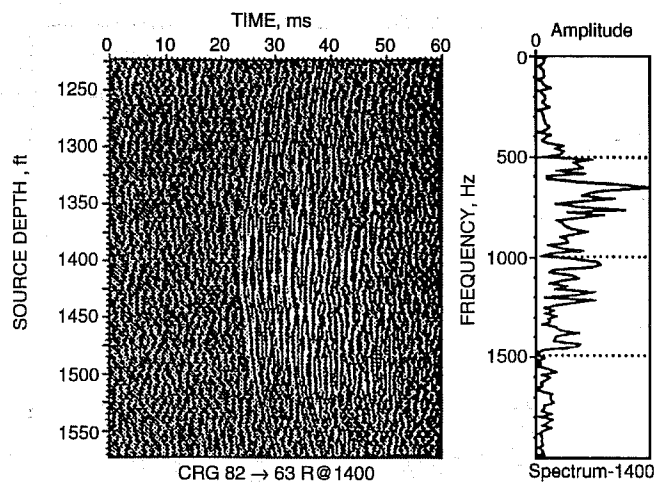


Fig. 4 Common receiver gather (CRG) and common source gather (CSG) data from the 82 → 63 survey. Note strong ambient, pre-first-arrival noise in the data. The CSG data show the noise to be coherent tube waves in receiver well (No. 63). The No. 63 well is perforated on the interval 1460–1505. It is interpreted that tube waves were generated by fluid flow in the perforated interval.

Shooting direction in a cross-well seismic experiment is usually based on operational issues, such as borehole condition and casing size relative to the seismic tools. Beyond these concerns, it is tempting to invoke the principle of reciprocity—the data will be identical if source and receiver positions are interchanged. Although reciprocity is a powerful principle known to be valid in arbitrarily complicated physical systems, the medium is assumed to be passive. If the medium is active (i.e., if it contains sources of energy), then reciprocity does not necessarily apply. Interchanging source and receiver in this case can give very different results. The experience reported with cross-well-seismic and fluid-flow noise is a simple example of this fact.

It has been shown that shooting direction can be a first-order concern on data quality. If a downhole source of noise exists in one well, it is best to use this as the source well.

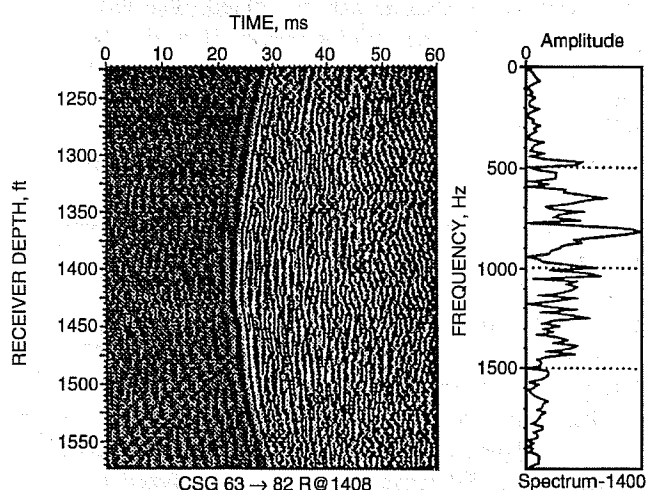
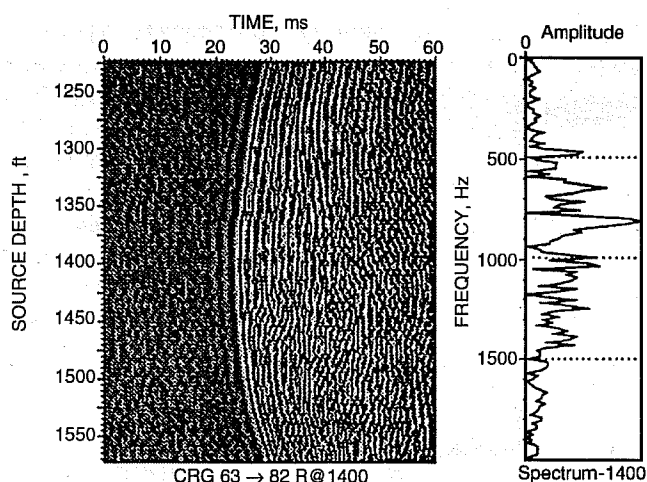


Fig. 5 Data from the 63 → 82 survey over the same range as shown in Fig. 4. By simply reversing the shooting direction, high-quality data have been acquired.

Unfortunately, it is often not known before the survey that such a downhole noise source exists.

The next step in working with the Glenn Pool cross-well seismic data is tomographic inversion. This requires the data to be picked for first-arrival times on all surveys to be inverted. This amounts to about 50,000 seismic traces. As of late March 1994, all data traces for surveys 82 → 64, 63 → 82, and 81 → 82 have been picked by Amoco.¹ Survey 82 → 63 was judged too noisy for reliable picking.

These picks are being forwarded to the University of Tulsa so that tomographic processing can begin with the use of the U.S. Bureau of Mines Tomography program (BOMTOM). Also, the picks will be used at Memorial University of Newfoundland to perform another tomographic inversion of the data. The three tomography sites are doing complimentary work by processing the data using different and increasing levels of complexity. Specifically, in the order of increasing complexity, the sites are University of Tulsa straight-ray

isotropic tomography with the use of BOMTOM, Memorial University of Newfoundland curved-ray isotropic tomography with the use of software developed at the University of Utah (courtesy G. Schuster), and Amoco curved-ray anisotropic tomography with the use of proprietary software. This multiple-processing exercise will result in information concerning how much effort is required to successfully image cross-well data in fluvial-dominated deltaic settings. In this way, one would be better able to judge both the viability of currently available software and hardware for processing of cross-well data and whether it is feasible for small- to medium-sized operators.

Engineering Description and Simulation

In the last quarterly report, the flow simulation results that led to drilling well No. 82 were presented.³ The details of the procedure used for description and the flow simulation can be found in Ref. 4. A preliminary comparison between observed oil saturation profile at well No. 82 and the simulated profile was reasonable.

One of the difficulties encountered in the reservoir description process is the limited permeability data. Very limited core data and no well-test data were available. Because well-test data provide permeability on a large scale, it was decided to conduct well tests with Ecometer. The result of one such well test is provided in this report.

A two-day pressure-buildup test was run on Self No. 54 (see Fig. 1). Before shut-in for pressure buildup, the well was producing 168 stock tank barrels (STB) of water per day and 2 STB of oil per day. Because the producing stream consisted of more than 95% water, the well was analyzed as a water producer. Relevant well and reservoir properties are summarized in Table 1.

The EPS PanSystem well-test analysis software was used to analyze the pressure buildup; final analysis results were refined with a nonlinear regression well-test analysis package developed at the University of Tulsa.

A log-log plot of the pressure and pressure-derivative data is shown in Fig. 6. Wellbore storage effects are exhibited at early times (i.e., 45° line in Fig. 6 for times less than 70 min); after these early time effects, the reservoir begins to influence the wellbore pressure response, and the pressure derivative goes to a maximum and then decreases. There is no radial flow (horizontal derivative data) evident in the

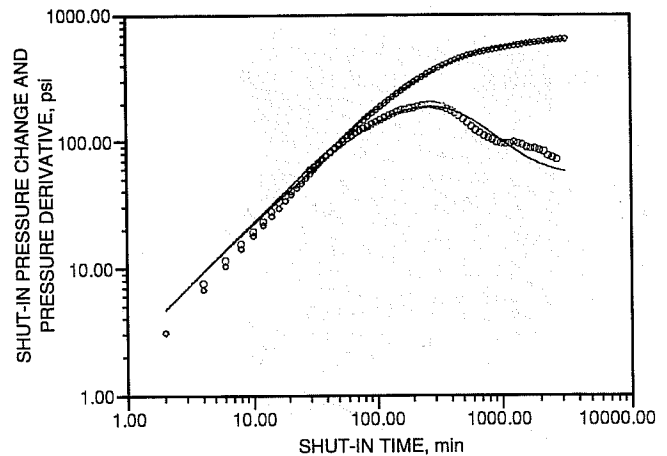


Fig. 6 Match between field data and type curves. Self well No. 54 buildup. \diamond , pressure data. \circ , pressure-derivative data. —, match from nonlinear regression analysis.

log-log plot, so semilog analysis is not strictly applicable. If semilog analysis were applied to the late-time data, estimates of the permeability to water would be low.

Two nonlinear regression analyses were done with the use of “well with skin and storage” type curve matching and automated type curve matching. The analyses were consistent with each other, and the results obtained were as follows:

Permeability to water, mD	5.5 ± 0.4
Wellbore storage coefficient, bbl/psi	0.049 ± 0.001
Skin factor	-1 ± 0.5
Radius of investigation, ft	700

The match from nonlinear regression analysis is shown in Fig. 6 as the solid curves. The reported permeability value represents an average permeability-thickness product over the A, B, and C producing sands in the well’s drainage area. This result compares favorably with core data on Self well No. 82, which indicates that the permeability in the A, B, and C sands varies between 0.02 mD and 20 mD (see Fig. 7). The slightly negative skin factor indicates that permeability in the near-well region is slightly higher than the average reservoir permeability. This could be due to a variety of reasons, such as formation pinching out far away from the well, degrading sand quality as distance from the well increases, and formation behind the casing washed out. Regardless of the reason for the negative skin, the well will not benefit from stimulation.

Plans are to collect additional well-test data on at least four more wells. This should allow a more extensive evaluation of the permeabilities used in four simulation studies, which are solely based on the limited core data. In addition, well No. 82 may allow a better description of the geological environment. Through the use of the revised geological description and the additional core and well-test data, the reservoir description will be improved and additional flow simulation studies will be conducted to better determine the ways to improve reservoir performance.

TABLE 1

Properties Used in Well Test Analysis

Well radius, ft	0.276
Net formation thickness, ft	31.
Sands encountered, A, B, C	
Total production rate, STB/d	170
Formation temperature, °F	100
Formation volume factor of water, bbl/STB	1.
Compressibility, psi^{-1}	376×10^{-6}

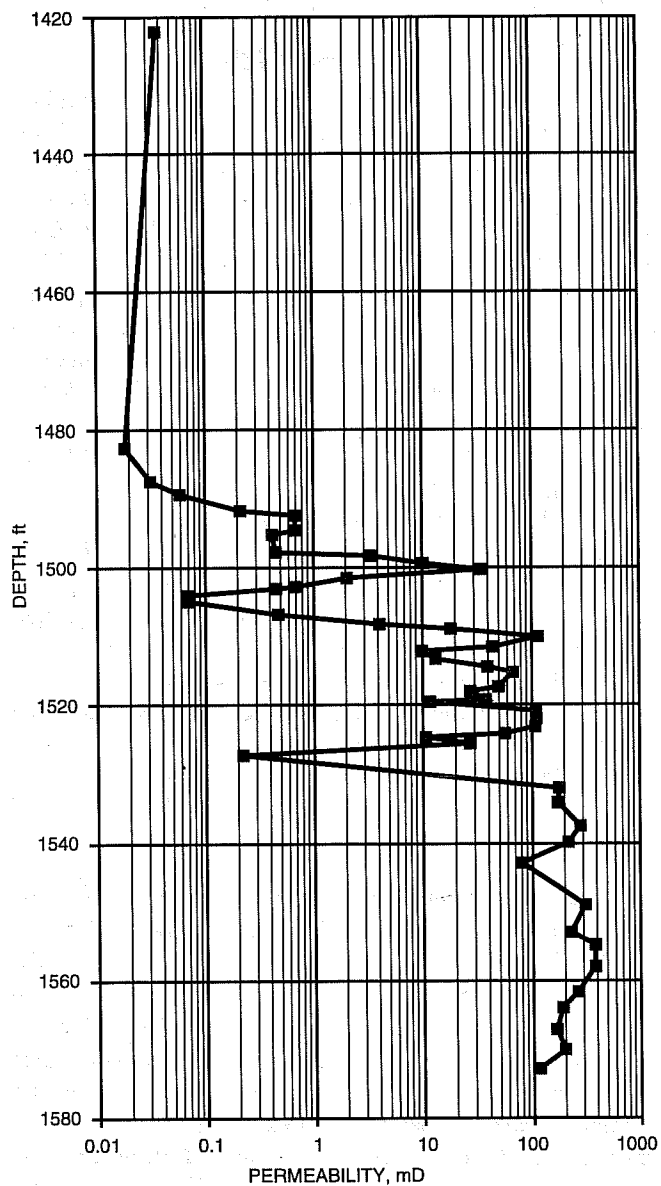


Fig. 7 Permeability of well No. 82.

References

1. A. A. Vassiliou, C. L. Liner, C. W. Savage, G. Bozkurt, and L. R. Lines, Glenn Pool Project: Initial Tomography Results, *Expanded Abstracts of the Society of Exploration Geophysicists Annual Meeting*, Los Angeles, Calif., October 23–27, 1994.
2. G. Bozkurt et al., Glenn Pool Project: Crosswell Seismic Data Acquisition Overview, *Expanded Abstracts of the Society of Exploration Geophysicists Annual Meeting*, Los Angeles, Calif., October 23–27, 1994.
3. *Quarterly Report, Integrated Approach Towards the Application of Horizontal Wells to Improve Waterflooding Performance*, Contract No. DE-FC22-93BC14951, Oct. 1–Dec. 31, 1994.
4. B. K. Ahuja, A. Bahar, D. R. Kerr, and B. G. Kelkar, *Integrated Reservoir Description and Flow Performance Evaluation of Self Unit*, Glenn Pool Field, paper SPE 27748 presented at the SPE/DOE Ninth Symposium on Improved Oil Recovery, Tulsa, Okla., April 17–20, 1994.

GEOLOGICAL AND PETROPHYSICAL CHARACTERIZATION OF THE FERRON SANDSTONE FOR THREE-DIMENSIONAL SIMULATION OF A FLUVIAL-DELTAIC RESERVOIR

Contract No. DE-AC22-93BC14896

Utah Geological Survey
Salt Lake City, Utah

Contract Date: Sept. 29, 1993
Anticipated Completion: Sept. 29, 1996
Government Award: \$321,042

Principal Investigator:
M. Lee Allison

Project Manager:
Robert Lemmon
Bartlesville Project Office

Reporting Period: Jan. 1–Mar. 31, 1994

Objective

The project objective is to develop a comprehensive, interdisciplinary, quantitative characterization of a fluvial-deltaic reservoir that will allow realistic interwell and reservoir-scale modeling to be used for improved oil field development in similar reservoirs worldwide. The geological and petrophysical properties of the Cretaceous Ferron sandstone in east-central Utah (Fig. 1) will be quantitatively determined. Both new and existing data will be integrated into a three-dimensional (3-D) representation of spatial variations in porosity, storativity, and tensorial rock permeability at a scale appropriate for interwell to regional-scale reservoir simulation. Results could improve reservoir management through proper infill and extension drilling strategies, reduce economic risks, increase recovery from existing oil fields, and provide more reliable reserve calculations. Transfer of the project results to the petroleum industry will be an integral component of the project.

Summary of Technical Progress

The technical progress reported is divided into several sections corresponding to subtasks outlined in the Regional Stratigraphy Task and the Case Studies Task of the original proposal. Other subtasks are dependent on field work that will begin in April 1994. The primary objective of the Regional Stratigraphy Task is to provide a more detailed interpretation of the stratigraphy of the Ferron sandstone outcrop belt from Last Chance Creek to Ferron Creek (Fig. 1). This regional

Collect and Interpret Existing Surface and Subsurface Data

The Utah Geological Survey (UGS) is continuing to collect and compile published and unpublished maps, measured sections, well logs, core descriptions, minipermeameter data, reports, and other data. Nine potential sources of basic geological and geophysical drill data on the Ferron sandstone (Table 1) have been identified. The largest data holder is the U.S. Department of the Interior, Bureau of Land Management (BLM), which has hundreds of drill records from coal exploration holes drilled by Consolidation Coal Company (CONSOL). Records indicate that 356 wells were drilled on the unleased federal lands in the study area.

Lithologic logs for 12 drill holes were obtained from the J. B. King mine area (formerly the Dog Valley mine). An attempt is being made to obtain drill-hole data from seven drill holes by CalMat on the Hidden Valley Coal Company (HVCC) mine property. This property is within the Ivie Creek case study area.

To date, the USG has acquired 101 geophysical logs from the 480 wells in the study area and 1880 feet (550 m) of core or core descriptions from the 405 wells cored as shown in Table 1. Information from 285 wells and core holes has been entered on data forms, with 156 of these also entered into ASCII files (Table 1).

Case Study Sites

Three case study sites have been selected and approved by the project team for detailed analysis of the major reservoir types: **Muddy Creek Canyon, Ivie Creek, and Willow Creek Wash** in the north, central, and southern parts, respectively, of the study area (Fig. 1). The entire Ferron section will be analyzed at the Muddy Creek Canyon site. In this area, the Ferron sandstone is composed of seven deltaic units. Some of these units are stratigraphically simple; others include a variety of facies and display abrupt lateral variations. The Ivie Creek site was selected for examination of the abrupt facies changes in the No. 1 delta-front unit. The basal unit is a thick, sandy parasequence pinching out to the west and is overlain by a thin, silty parasequence, which extends farther to the west. The Willow Creek Wash site is the largest of the study areas and was selected for the excellent 3-D aspect of exposures in the Willow Springs Wash and Indian Canyon areas. The focus of work at this site will be parasequences of the No. 1 delta-front unit.

Core Hole Locations

Eight core holes are planned in the Ivie Creek area (Fig. 1). These wells will be drilled downdip 200 to 1200 ft (60 to 365 m) from the Ferron outcrop. Cores and geophysical logs from these wells will provide data for 3-D morphology interpretation of individual lithofacies. Surface right-of-ways from Utah Division of State Lands and Forestry and the BLM are being obtained. A survey of current mineral lease ownership showed no active coal or other mineral holders. Staking and permitting procedures are being completed through the Utah

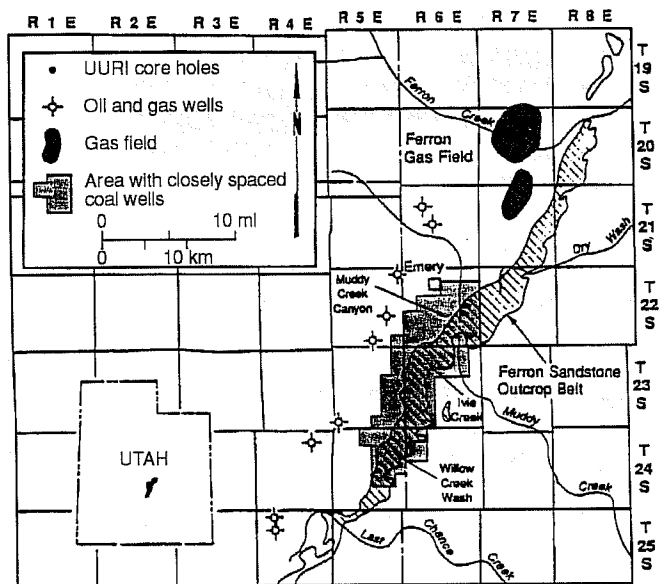


Fig. 1 Location map of the Ferron sandstone study area (cross-hatched) showing potential detailed case study sites.

study will include determination of the dimensions of each sandstone body, its depositional environment, and the nature of its contacts with adjacent rocks or flow units. The study will provide a basis for selecting optimal outcrops for detailed case studies of the major reservoir types (meander belt, mouth-bar complex, wave-dominated delta front, bar-finger sands, distributary channel, and tidal channels). The morphological framework established from the case studies will be used to generate subsequent flow models for the reservoir types.

The primary objective of the Case Studies Task is to develop, at a well-sweep or smaller scale, a detailed geological and petrophysical characterization of the primary reservoir lithofacies typically found in a fluvial-dominated deltaic reservoir. Sedimentary structures, lithofacies, bounding surfaces, and permeabilities measured along closely spaced traverses (both vertical and horizontal) will be combined with data from core drilling to develop a 3-D morphology of the reservoirs within each case study area.

Surface Mapping/Interpretation of the Outcrop Belt

Most of the Ferron sandstone outcrop belt within the study area (Fig. 1) will be obliquely photographed and photomosaics will be constructed. An initial test set of photographs was digitized and transferred to a compact disc (CD). Image-editing software has been purchased, and 48 photographs from the test set were reproduced from the CD without significant loss of resolution. These and future photographs will be assembled into reproducible photomosaics for annotation of lithofacies, measured sections, and other data in the field for both regional and case study analysis.

TABLE 1

Summary of Well, Geophysical Log, and Core Data in the Ferron Sandstone Study Area

Source of wells	No. of wells with geophysical logs	No. of logs obtained by the UGS*	No. of wells cored/ footage cored	Cored footage obtained by the UGS*	No. of wells entered on forms	No. of wells in ASCII format
Oil and gas						
UURI	2	2	2/800	800	0	0
ARCO	7	0	7/3,527	descriptions only	0	0
BP	5	5	5/1,000	1,000	0	0
Other	58	40	0	0	0	0
Coal						
CONSOL	356	40	356/unknown	descriptions only	285	156
USGS	33	14	29/1,402	descriptions only	0	0
BLM	0	0	6/1,156	descriptions only	0	0
JB King	12	0	0	0	0	0
HVCC	7	0	0	0	0	0
Total	480	101	405/7,885	1,800	285	156

*As of March 31, 1994.

Note: UGS, Utah Geological Survey; UURI, University of Utah Research Institute; ARCO, Atlantic Richfield Company; BP, British Petroleum; CONSOL, Consolidation Coal Company; USGS, United States Geological Survey; BLM, Bureau of Land Management; HVCC, Hidden Valley Coal Company.

Division of Oil, Gas, and Mining to drill and complete the core holes by the end of October 1994.

Interpretation

A large-diameter core (7 $\frac{7}{8}$ in.) from a University of Utah Research Institute (UURI) Ferron drill hole (the UURI No. 1) was logged, and important core segments were photographed. The core hole was drilled in the Muddy Creek case study area (Fig. 1) in 1991. The tops of lithologic and genetic units were noted, and the principal facies boundaries were interpreted. The geophysical log of the UURI No. 1 was interpreted and compared with the core description. This information, along with data from the cores to be taken later in the project, will be used to prepare strip logs, produce facies maps, and define type logs for the principal reservoir(s) in the case study area.

Databases

The UGS computer database has been modified for this study to integrate various geologic attributes of the Ferron sandstone to point-source locations. The formats for lithologic, paleocurrent, and core descriptions have been developed to standardize data collection. The database is designed so that geologic information, such as types and percentages of lithologies and sedimentary structures, can be incorporated into statistical models and exported into software programs to produce strip logs and lithofacies, percentage of lithofacies, and percentage of texture/fabric reservoir maps. Assigned stratigraphic rank of the various units measured in the field will be included in the database, and the thicknesses of these units will be calculated. A software package for 3-D visualization of these data has been evaluated, selected, and ordered.

INCREASED OIL PRODUCTION AND RESERVES FROM IMPROVED COMPLETION TECHNIQUES IN THE BLUEBELL FIELD, UINTA BASIN, UTAH

Contract No. DE-FC22-92BC14953

Utah Geological Survey
Salt Lake City, Utah

Contract Date: Sept. 30, 1993
Anticipated Completion: Sept. 29, 1998
Government Award: \$412,890

Principal Investigator:
M. Lee Allison

Project Manager:
Edith Allison
Bartlesville Project Office

Reporting Period: Jan. 1-Mar. 31, 1994

Objective

The objective of this project is to increase the oil production and reserves in the Uinta Basin by demonstration of improved completion techniques. Low productivity is attributed to gross production intervals of several thousand feet that contain perforated thief zones, water-bearing zones, and unperforated oil-bearing intervals. Geologic and engineering

characterization and computer simulation of the Green River and Wasatch formations in the Bluebell field will determine reservoir heterogeneities related to fractures and depositional trends. This will be followed by drilling and recompletion of several wells to demonstrate improved completion techniques based on the reservoir characterization. Transfer of the project results will be an ongoing component of the project.

Summary of Technical Progress

Outcrop Studies

No field work was done during the winter months. Detailed petrography has begun on thin sections of outcrop samples and core provided by Pennzoil Exploration and Production Co.

Subsurface Studies

Digitizing of geophysical well logs from the Bluebell field continues. Numerous ASCII files were sent to Halliburton Energy Services in Houston for trial input into their log-analysis system. Porosity analyses from core plug samples in the Bluebell field have been obtained from the U.S. Geologi-

cal Survey (USGS) and will be compared with log porosities of the same wells to develop appropriate corrections to log-derived porosity calculations throughout the field.

A structure contour map of the middle marker of the Green River formation was completed for the Bluebell field (Fig. 1). This map is the last in a series of eight maps on the oil and gas production of Bluebell field and is available from the Utah Geological Survey (UGS).¹

Stratigraphic cross sections were constructed for the Roosevelt Unit of the Bluebell field. Five zones of interest were correlated in a 4-mile² area. The porosity, oil, and water saturations were determined at 2-ft intervals for the entire thickness of each of the five zones. The data are being used to construct a preliminary engineering reservoir model. Detailed correlation and data gathering continue so that the model area can be expanded and include more zones.

Engineering Studies

A dual porosity-dual permeability, black-oil reservoir simulator is being used to model a four-section area in the eastern Bluebell field. The model includes a set of vertical fractures that were discontinuous between the producing

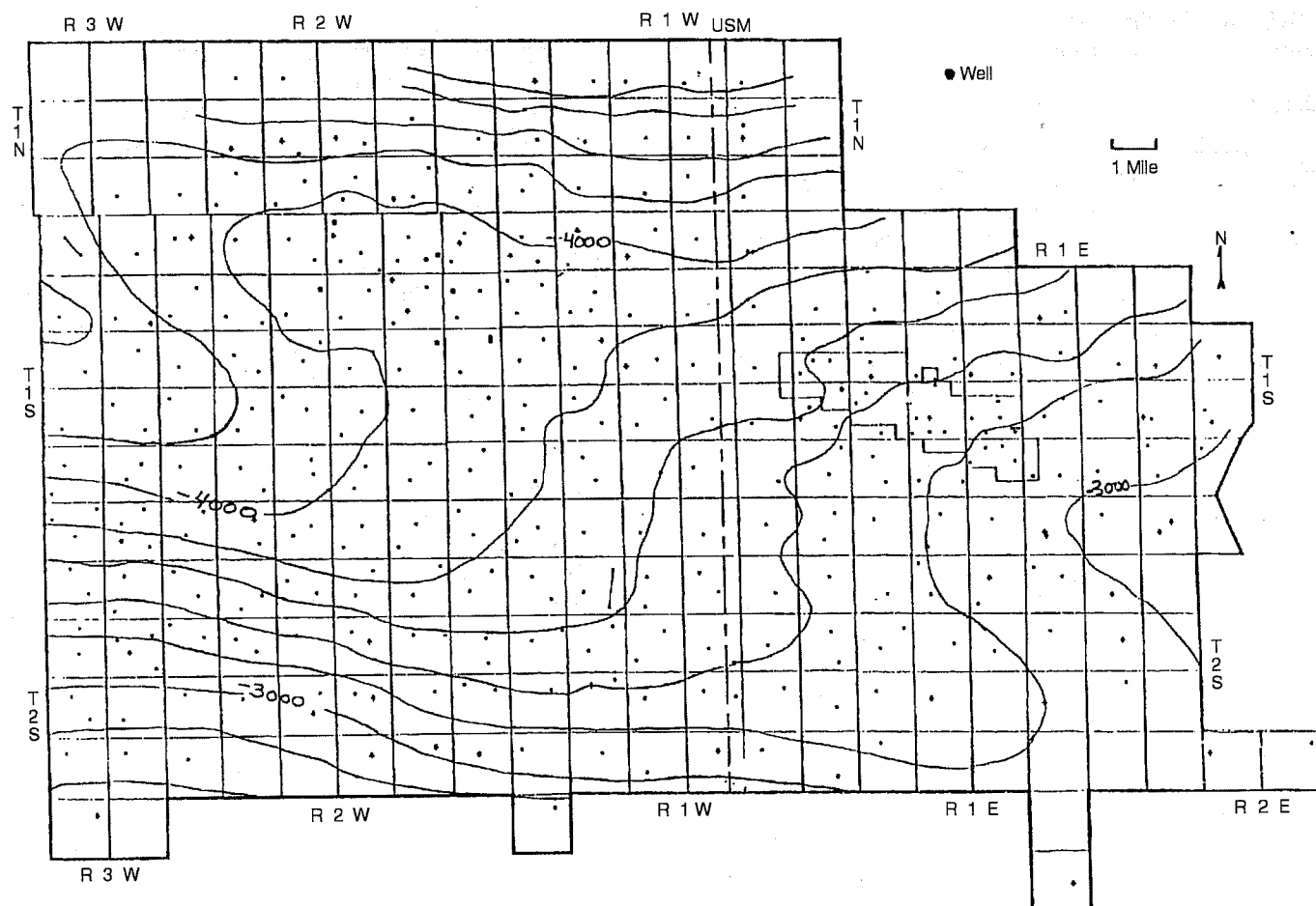


Fig. 1 Structure contour map of the middle marker of the Green River formation, Bluebell field, Duchesne and Uinta Counties, Utah. Contour interval 200 ft (modified from Ref. 1).

zones. Preliminary model predictions matched reasonably well with the actual oil and gas production from wells within the four-section area. The predicted oil and gas production was strongly dependent on the selection of grid-block size. The variable grid-block representation with a finer grid around the wells resulted in the best match with actual production histories.

Reference

1. C. D. Morgan, *Oil and Gas Production Maps of the Bluebell Field, Duchesne and Uinta Counties, Utah*, Utah Geological Survey Oil and Gas Field Study 15, 1994.

